Mads Damgaard

Dynamic Properties of Offshore Wind Turbine Foundations

Revised Version

PhD Thesis defended at Aalborg University,
Department of Civil Engineering

River Publishers

Dynamic Properties of Offshore Wind Turbine Foundations

Dynamic Properties of Offshore Wind Turbine Foundations

Revised Version

PhD Thesis
Defended in public at Aalborg University
24 November 2014

Mads Damgaard

Department of Civil Engineering,
The Faculty of Engineering and Science,
Aalborg University, Aalborg, Denmark

River Publishers

ISBN 978-87-93237-41-4 (e-book)

Published, sold and distributed by:
River Publishers
Niels Jernes Vej 10
9220 Aalborg Ø
Denmark

Tel.: +45369953197
www.riverpublishers.com

Preface

The present thesis "Dynamic Properties of Offshore Wind Turbine Foundations" is submitted as a partial fulfilment of the requirements for the Danish PhD degree. The work has been carried out in the period September 2011 to August 2014 at the Department of Civil Engineering, Aalborg University, Denmark, under the supervision of Prof Lars Bo Ibsen and Dr Lars Vabbersgaard Andersen.

The PhD thesis consists of two parts:

- **Part I** deals with full-scale testing of wind turbines installed on monopile, bucket and gravity base foundations. The dynamic properties in terms of natural frequencies and damping ratios are in focus based on so-called "rotor-stop" tests and operational modal identification techniques.
- **Part II** deals with the formulation and application of lumped-parameter models useful for fully coupled aero-hydro-elastic simulations. Gray box modelling based on the findings from Part I is used to evaluate to what extent the soil–foundation interaction influences the dynamic behaviour of the wind turbine.

The thesis is based on the following collection of scientific papers and reports written by the author of the present thesis and in cooperation with other authors:

- Damgaard, M. (2011). An introduction to operational modal identification of offshore wind turbine structures. DCE Technical Memorandum No. 13, Aalborg University.
- Damgaard, M., Ibsen, L. B., Andersen, L. V. and Andersen, J. K. F. (2012). Natural frequency and damping estimation of an offshore wind turbine structure. In *Twenty-Second International Offshore and Polar Engineering Conference*, Rhodes, Greece, pp. 300–306.
- * Damgaard, M., Ibsen, L. B., Andersen, L. V. and Andersen, J. K. F. (2013). Cross-wind modal properties of offshore wind turbines identified by full scale testing. *Journal of Wind Engineering and Industrial Aerodynamics* **116**, 94–108.
- * Damgaard, M., Ibsen, L. B., Andersen, L. V., Andersen, P. and Andersen, J. K. F. (2013). Damping estimation of a prototype bucket foundation for offshore wind turbines identified by full scale testing. In *5th International Operational Modal Analysis Conference*, Guimarães, Portugal, pp. 1–11.

- Damgaard, M., Ibsen, L. B., Andersen, L. V. and Andersen, J. K. F. (2013). Time-varying dynamic properties of offshore wind turbines evaluated by modal testing. In *18th International Conference on Soil Mechanics and Geotechnical Engineering*, Paris, France, pp. 2343–2346.

- * Damgaard, M., Andersen, L. V. and Ibsen, L. B. (2014). Assessment of dynamic substructuring of a wind turbine foundation applicable for aeroelastic simulations. *Wind Energy*. Early view.

- * Damgaard, M., Andersen, L. V. and Ibsen, L. B. (2014). Computationally efficient modelling of dynamic soil–structure interaction of offshore wind turbines on gravity footings. *Renewable Energy* **68**, 289–303.

- * Damgaard, M., Zania, V., Andersen, L. V. and Ibsen, L. B. (2014). Effects of soil–structure interaction on real time dynamic response of offshore wind turbines on monopiles. *Engineering Structures* **75**, 388–401.

- * Damgaard, M., Andersen, L. V. and Ibsen, L. B. (2014). Dynamic response sensitivity of an offshore wind turbine: A fully coupled time-domain approach for varying subsoil conditions. *Ocean Engineering*. In review.

- Damgaard, M., Andersen, L. V. and Ibsen, L. B. (2014). The importance of including dynamic soil–structure interaction into wind turbine simulation codes. In Group. Taylor & Francis (Ed). *8th European Conference on Numerical Methods in Geotechnical Engineering*, Delft, The Netherlands, pp. 1111–1116.

- Damgaard, M., Bayat, M., Andersen, L. V. and Ibsen, L. B. (2014). Assessment of the dynamic behaviour of saturated soil subjected to cyclic loading from offshore monopile wind turbine foundations. *Computers and Geotechnics* **61**, 116–126.

- * Damgaard, M., Andersen, L. V., Ibsen, L. B., Toft, H. S. and Sørensen, J. D. (2014). A probabilistic analysis of the dynamic response of monopile foundations: Soil variability and its consequences. *Probabilistic Engineering Mechanics*. In review.

Copies of all publications, marked with asterisk, are enclosed in the thesis. Parts of the papers are used directly or indirectly in the extended summary of the thesis. As part of the assessment, co-author statements have been made available to the assessment committee and are also available at the Faculty. The thesis is not, in its present form, acceptable for open publication but only in limited and closed circulation as copyright may not be ensured.

First and foremost, I would like to thank my supervisors, Prof Lars Bo Ibsen and Dr Lars Vabbersgaard Andersen. Their guidance, persistent encouragement and not least technical and moral support during the years are greatly appreciated. Further, gratitude is expressed to my industrial supervisor, Mr Jacob Karottki Falk Andersen, principal structural engineer, Statkraft (formerly Vestas Wind Systems A/S), for fruitful discussions and for an always positive attitude.

The PhD thesis has only been possible with the financial support from Vestas Wind Systems A/S and the Advanced Technology Foundation via the research project “Cost-Effective Monopile Design”. The funding is duly acknowledged. Special thanks should be directed to Mr Bjørn V.

Jønsson, director, Rambøll (formerly Vestas Wind Systems A/S), and Dr Lars Behrendt, director, Vestas Wind Systems A/S, for believing in me and making this research project possible.

Further, I wish to express my appreciation to the technical staff at Department of Civil Engineering, Aalborg University, for their assistance with the test set-up for the experimental work related to Part I. Dr Palle Andersen, Director, Structural Vibration Solutions, has assisted with the interpretation of the experimental test results based on operational modal analysis. His assistance is sincerely acknowledged.

Thanks are given to Dr Anders Melchior Hansen, Technical University of Denmark, Risø, for his help and support with the implementation of the consistent lumped-parameter model into the aeroelastic multi-body code HAWC2 according to Part II. I would also like to thank Dr Varvara Zania, Technical University of Denmark, for a good cooperation associated with Part II. Special thanks to Dr Henrik Stensgaard Toft and Prof John Dalsgaard Sørensen, Aalborg University, for their assistance and guidance offered during the probabilistic framework related to Part II.

Finally, I would like to thank my colleagues, friends and family for fruitful discussions, moral support and helpfulness during the course of the project.

Aalborg, September 2014 Mads Damgaard

Summary in English

Increasing oil prices and energy demands combined with a general acceptance that fossil fuels drive the climate changes justify the development of new sustainable energy solutions. Although offshore wind energy has proven potential to produce reliable quantities of renewable energy, there is a general consensus that offshore wind-generated electricity is still too expensive to be competitive with conventional energy sources. As a consequence, the overall weight of the turbine and foundation is kept to a minimum resulting in a flexible and dynamically active structural system—even at low frequencies. The highly variable and cyclic loads on the rotor, tower and foundation, caused by wind and wave loads as well as low-frequent excitations from the rotor blades, all demand special fatigue design considerations and create an even greater demand for a fuller appreciation of how the wind turbine ages structurally over its service life.

Well-covered in the field of earthquake engineering, the dynamic response of civil engineering structures is highly dependent on the impedance of the soil–foundation system. For offshore wind turbine applications, however, the hysteretical and geometrical dissipation effects in the soil are difficult to incorporate for time-domain simulations. Accurate assessment of the fatigue limit state requires simulations of several thousands of load cases, and the consequential high computational burden necessitates a structural model with few degrees of freedom that capture the most important effects of the dynamic wind turbine response. To overcome this, sequential or fully coupled aero-hydro-elastic simulations are often conducted where the soil–structure interaction is incorporated via the principle of an equivalent fixity depth or by a so-called Winkler approach with static springs along the foundation and soil damping applied as modal damping. The methods, however, do not account for the dynamic stiffness due to inertia forces, and a well-defined representation of the dissipation effects in the soil is neglected. This in turn forms the basis of the current thesis that examines the soil–foundation interaction and its influence on the natural and dynamic vibration characteristics of offshore wind turbines, and presents a novel, time-efficient coupled aero-hydro-elastic model of the wind turbine system accounting for the dissipation effects through wave radiation and material damping in the soil.

Modal properties in terms of natural frequencies and corresponding damping ratios of offshore wind turbines are investigated by full-scale modal testing and simple numerical quasi-static simulations. The analyses show distinctly time-varying inherent modal properties that, supported numerically, may be caused by moveable seabed conditions. In addition, “rotor-stop” tests and ambient vibration tests indicate the same level of damping related to the lowest damped cross-wind eigenmode. The tendency is caused by the fact that the hysteretic soil damping, caused by the slippage of grains with respect to each other, is high during “rotor-stop” tests with low contribution of aerodynamic damping. The opposite holds for normal wind turbine operations.

Although the dynamic soil–foundation response can be calculated rigorously based on three-dimensional elastodynamics with the coupled boundary element and finite element methods, these approaches are not applicable for coupled wind turbine simulations from a computational point of view. As a consequence, lumped-parameter models with frequency-independent real coefficients are applied in the thesis and successfully implemented into aeroelastic wind turbine codes. Time-efficient, semi-analytical solutions for the dynamic impedance functions of gravity base foundations and monopiles underlie the model calibration. Application of the fully coupled aero-hydro-elastic substructuring approach with deterministic and random linearised models of the soil indicates that the modal properties and cross-wind fatigue loads of offshore wind turbines are strongly affected by the interrelation effects between the foundation and subsoil.

Summary in Danish

Stigende oliepriser og energiefterspørgsel sammenholdt med en generel forståelse af fossile brændslers negative indvirkning på klimaet nødvendiggør udviklingen af nye bæredygtige energiløsninger. Til trods for at offshore-vindenergi har potentiale til at producere pålidelig vedvarende energi, er der bred konsensus om, at den genererede elektricitet er omkostningstung sammenlignet med konventionelle energikilder. Som følge heraf er vægten af vindmøllen og fundamentet forsøgt minimeret, hvilket resulterer i en fleksibel struktur, som agerer dynamisk – selv ved lave lastfrekvenser. Varierende cykliske laster fra bølger og vind samt harmoniske lavfrekvente lastpåvirkninger fra vingerne stiller store krav til udmattelsesdesignet af vindmøllen, og en god forståelse af den strukturelle opførsel gennem vindmøllens levetid er derfor påkrævet.

Studier inden for jordskælvsteori viser, at det dynamiske konstruktionsrespons i høj grad er påvirket af impedansen af jord–fundament–interaktionen. Desværre er de hysteretiske og geometriske dissipationseffekter i jorden svære at medtage for tidsdomæneanalyser af offshore vindmøller. En præcis vurdering af udmattelsesgrænsetilstanden betyder simuleringer af flere tusinde lasttilfælde, hvilket kræver en simpel beregningseffektiv model, som har få frihedsgrader, men stadig er i stand til at medtage de vigtigste effekter af vindmøllens respons. Dette klares ofte ved hjælp af sekventielle eller fuldkoblede aero-hydro-elastiske simuleringer, hvor jord–struktur–interaktionen inkorporeres via princippet om en ækvivalent indspændingsdybde eller ved brug af en Winkler model med statiske fjedre langs fundamentet, og jorddæmpning modelleres som modaldæmpning. Ingen af modellerne tager dog hensyn til den dynamiske stivhed grundet tilstedeværelsen af inertikræfter, ligesom en veldefineret beskrivelse af dissipationseffekterne i jorden er forsømt. Dette danner grundlag for nærværende afhandling, som undersøger jord–struktur–interaktionens indvirkning på havbaserede vindmøllers modale og dynamiske vibrationskarakteristikker, og som desuden præsenterer en ny beregningseffektiv aero-hydro-elastisk model af vindmøllesystemet, som tager bølgeudstrålingen og materialedæmpningen i jorden med i regning.

Offshore-vindmøllers modale egenskaber i form af egenfrekvenser og tilhørende dæmpningsforhold er undersøgt ved hjælp af fuldskalaforsøg og simple numeriske kvasistatiske simuleringer. Analyserne viser udpræget tidsvarierende modalegenskaber, som, underbygget af numeriske beregninger, forudsættes at være forårsaget af sedimenttransport af havbunden. Desuden indikerer "rotor-stop"-forsøg og forsøg med baggrundsvibrationer samme dæmpningsniveau relateret til den lavestdæmpede laterale egensvingningsform. Dette skyldes, at et "rotor-stop"-forsøg forårsager kraftig hysteretisk jorddæmpning og lav aerodynamisk dæmpning, mens det modsatte gør sig gældende for en havbaseret vindmølle i normal produktion.

Den dynamiske jord–struktur–interaktion kan bestemmes rigoristisk baseret på tredimensionelle elastodynamiske løsninger. Fra et beregningsmæssigt synspunkt er disse metoder dog særdeles tidskrævende og uegnet for koblede vindmøllesimuleringer. Med udgangspunkt heri gøres der i denne afhandling brug af lumped-parameter-modeller med frekvensuafhængige reelle koefficienter. Modellerne er med succes implementeret i aeroelastiske beregningsprogrammer. Semianalytiske løsninger for bestemmelse af gravitationsfundamenter og monopæles impedans er anvendt, hvilket sikrer en hurtig og effektiv kalibrering af lumped-parameter-modellen. Anvendelse af den fuldkoblede aero-hydro-elastiske fremgangsmåde med lineariserede deterministiske og stokastiske jordmodeller viser, at havbaserede vindmøllers modale egenskaber og laterale udmattelseslaster er stærkt påvirket af interaktionen mellem fundamentet og den omkringliggende jord.

Contents

CHAPTER 1
Introduction

Offshore wind energy is considered one of the most promising sources of energy towards meeting the European Union's commitment to reduce the consumption of fossil fuels. Even though the offshore wind turbine industry is one of the fastest growing maritime sectors, the technology is still young facing considerable political, economical and technical challenges. Reproducing the dynamic wind turbine response in the design process is a technical challenge but highly important from a fatigue point of view. In this regard, the soil–structure interaction may have a significant influence on the fatigue life but has, until now, been incorporated in a crude and uncertain manner. In this chapter, a brief overview and discussion of the engineering aspects of designing offshore wind turbine structures are given with emphasis on the dynamic behaviour of the wind turbine and support structure. The discussion is concluded with a brief overview of the present research, and a guide to the remainder of the thesis is given at the end of the chapter.

1.1 Offshore Wind — Challenges

Since the installation of the first ever commercial offshore wind farm in Vindeby, Denmark, 1991, offshore wind has become an important source of renewable energy. Influenced by the European renewable targets and the increasing reliability of the technology, offshore wind energy is a multi-billion Euro market involving many different disciplines within civil engineering and science. Many wind turbine technology projects have been completed successfully and new technology has emerged from these based on lessons learned in the field. Consequently, the tower heights, rotor diameters and rated powers of offshore wind turbines have increased during recent years in order to capture the more energetic winds that occur at higher elevations and to produce more energy per turbine installation. At this writing, however, the majority of wind turbines is located onshore due to lower installation cost. Nevertheless, the population density and existing buildings limit suitable wind turbine locations on land in many regions of the world. This justifies the development of offshore wind energy and indicates the potential of rapid growth of the market over the next decade. At the end of 2013, a total of 2080 wind turbines producing 6562 MW were installed in 69 offshore wind farms across Europe (EWEA 2013). As indicated in Fig. 1–1, the annual and cumulative offshore wind installations in Europe have increased significantly in recent years. Here, the UK has the largest amount of installed offshore capacity with 56% of all European installations, whereas Denmark follows with 19%. Today, the average turbine capacity is around 4 MW positioned within a average distance of 29 km from shore and located at positions with average water depths less than 16 m. However, the installation of several offshore wind turbines with capacities of up to 7 MW, distances to shore of up to 100 km and water depths of up to 60 m have been planned.

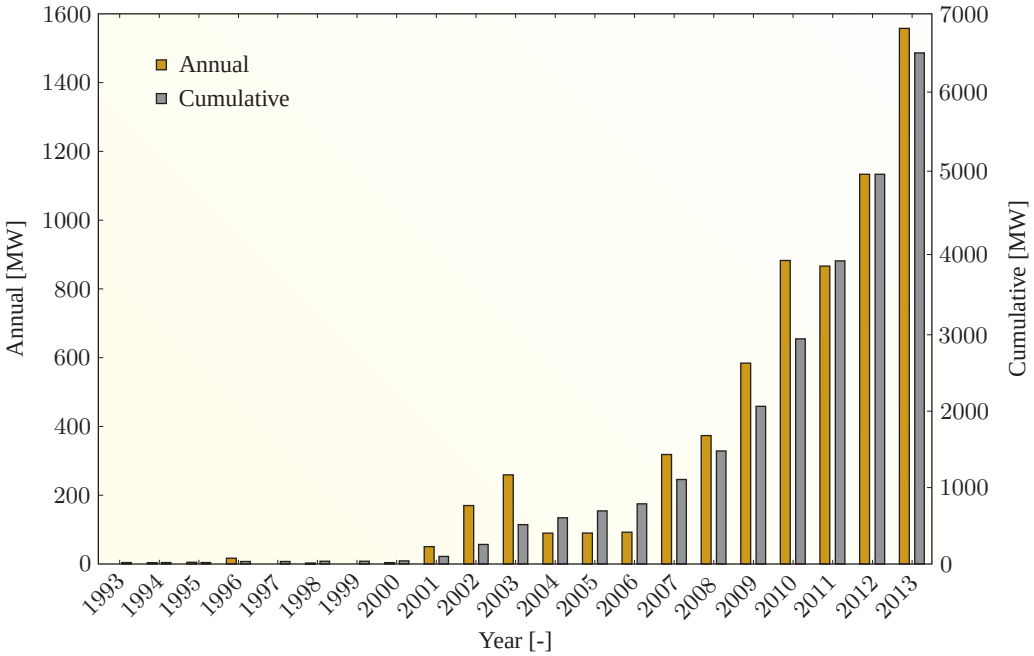

Figure 1–1 Annual and cumulative offshore wind installation in Europe. After EWEA (2013).

However, the high growth in the installed capacity of offshore wind turbines, mainly anchored by the ambitious energy and climate change objectives for 2020 by the European Union Committee (2008), causes many challenges within civil engineering and science, and the sector has still not made a definitive breakthrough. A plausible explanation is that the cost of offshore wind energy is higher compared to onshore wind energy and conventionally generated electricity. According to Engels *et al.* (2009), the cost of energy for onshore turbines is 0.04–0.05 €/kWh, whereas offshore energy is around twice as expensive, *i.e.* 0.08–0.10 €/kWh. The increased costs is mainly due to large costs in operation and maintenance which is twice as expensive offshore compared to onshore. In addition, offshore foundations may account for up to 35% of the installed cost (Byrne and Houlsby 2003). Evidently, the biggest challenge in the offshore wind industry is how to reduce the cost of energy. Three ways to achieve this are by a) increasing the availability and/or reducing the operational costs by predictive and customised maintenance programs and further automation and innovation of the wind turbine monitoring systems, b) lifetime extension of existing wind turbines due to conservative design approaches and, finally, c) improving the understanding of the interactive behaviour between the wind turbine and substructure in order to design the wind turbine converter exactly as strong as necessary but not more so. The last-mentioned option implies an accurate design methodology as well as a computational time-efficient model that takes the considerable interrelation effects between the dynamically active wind turbine and support structure into account. Consequently, a quasi-static design procedure does not apply since material fatigue plays a major role. Contrary to oil and gas platforms dominated by a huge self weight reducing the exposure to dynamic excitation, loading of offshore wind turbines is quite different. Strong cyclic loading originating from the rotor blades, wind and waves excite the structure. Offshore support structures within the oil and gas industry are all

characterised by the fact that the mass distribution is constant during time. The presence of rotor blades passing the flexible tower in a high altitude causes a time-dependent mass distribution for wind turbine structures. In addition, under the right circumstances wind turbines are affected by gyroscopic forces due to the rotating rotor. Evidently, the vibration behaviour has a high influence on the structural deformations, the internal stresses, the resulting ultimate and fatigue limit state as well as the operating life of the wind turbine.

The research work presented in this PhD thesis aims to improve the understanding of the dynamic vibration behaviour of offshore wind turbines based on full-scale testing and numerical investigations. Special focus on the dynamic soil–foundation interaction and its influence on the wind turbine response is addressed. The outcomes of the research work may directly or indirectly increase (or decrease) the economic feasibility of future offshore wind farms by reducing the uncertainties related to the interrelation effects between the wind turbine, the substructure and the subsoil.

1.2 Offshore Wind Turbine Structures

Advantageously, by moving offshore, larger wind turbine structures can be developed, less or no visual impact will occur, no human neighbours will be present and lower turbulent wind can be expected. However, environmental wind and wave loading on the larger structures lead to significantly greater forces than those that would occur onshore. Fig. 1–2 shows a classic three-bladed horizontal-axis offshore wind turbine installed on a so-called bucket foundation. Its dynamic response consists of an interactive behaviour between the rotor, tower, hub, nacelle, power train, control system and foundation. For the last-mentioned, different types of foundations can be used. There are major technical differences between the foundations that transfer the forces from the structure to the surrounding soil, and each type has its particular advantages depending on the prevailing environmental conditions. The following section gives a short introduction to some of the most important wind turbine components from a structural point of view. The sections are to a great extent based on National Research Council (1991), Spera (1994), EWEA (1999) and Lesny (2010).

Figure 1–2 A classic three-bladed horizontal-axis Vestas V90-3.0 MW offshore wind turbine installed on a bucket foundation.

1.2.1 Key Components of a Wind Turbine

As indicated in Fig. 1–3, the principal subsystems that make up the wind turbine converter include the rotor (hub and blades), power train, nacelle and tower. Despite of a few examples of vertical-axis wind turbines, the predominant configuration for large grid-connected wind turbines

consists of three rotor blades that rotate around a horizontal hub capturing the kinetic energy in the wind and transform it into the rotational kinetic energy of the wind turbine. The hub is connected to a gearbox and generator located inside the nacelle. Note that direct-drive generators may be used as well, meaning the gearbox is unnecessary. Basically, the stall or pitch regulated wind turbine with variable or fixed rotational speed control works on an aerodynamic lift principle where the difference in the pressure on either sides of the blade produces a lifting force causing the rotor to rotate. A yaw mechanism is built into the turbine in order to turn the wind turbine rotor against the wind. Typically, the turbine starts operating in mean wind speeds at hub height of 4 m/s and reaches its rated power output at around 13 m/s. At about 24 m/s, the wind turbine will shut down.

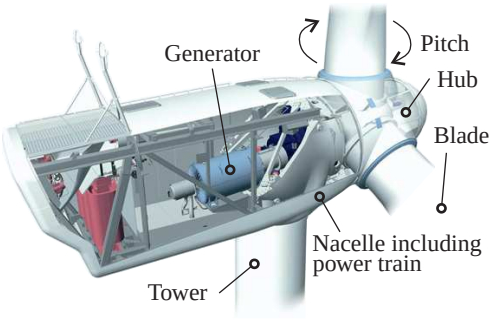

Figure 1–3 Key components of a wind turbine. After Vestas Wind Systems A/S (2011).

Rotor

The rotor subsystem consists of the hub that connects the turbine blades to the main shaft. The blades are commonly made of composite material in terms of glass fibre reinforced polyester or epoxy. They are shaped as airfoils to make the air flow faster on one side and slower on the other. Furthermore, a tapered and twisted geometry is chosen in order to provide the best possible energy capture. For a three-bladed wind turbine, the hub, typically made of ductile cast steel, rigidly connects the blades to one another and to the drive train. The cantilevered boundary conditions imply that the dynamic loads of the blades are transferred to the shaft. This also means that during yawing, each blade is exposed to a cyclic load, and the rotor thereby experiences a rigid-body motion. For a two-bladed wind turbine, the loading can be reduced by using a teetered hub (Burton *et al.* 2011). For a three-bladed rotor, the cyclic loads are much smaller than those produced by the two-bladed rotor since the cyclic loads combined together at the hub are nearly symmetric and balanced. Even though a one-bladed or two-bladed rotor offers potential reductions in both fabrication and maintenance costs, studies have shown that a three-bladed wind turbine is more efficient from an aerodynamic point of view. In turn, this explains the rare numbers of one-bladed rotors with counterweights and two-bladed rotors, despite of their technical feasibility. In addition, the disadvantages of one-bladed or two-bladed wind turbines are the visual intrusion—both when it comes to onshore and offshore wind turbines near the cost. In general, to avoid fatigue damage of the blades, the individual blade must be stiff and light enough to ensure that the frequency of the blade modes does not coincide with the frequency at which the blades pass the tower. For a 5.0 MW wind turbine with a hub height of 90 m and around 60 m blades, (a)symmetric flapwise and edgewise blade modes typically occur in the frequency range 0.6–2.0 Hz with corresponding damping well above 0.02 logarithmic decrement.

Drive train

The series of mechanical and electrical components in the wind turbine that convert the mechanical power from the rotor to electrical power is denoted as the drive train. It consists of a turbine

shaft (low-speed shaft), a generator shaft (high-speed shaft), a gearbox, brakes and a yaw drive as well as additional components for control, lubrication, and cooling functions. In general, the turbine shaft is a critical component of the drive-train since the rotor weight, torque and lateral forces all excite this component. Consequently, fatigue damage may occur, and the lifetime of the turbine shaft typically equals or exceeds that of the total system. The disk of the rotor brake is often mounted on the generator shaft. For pitch controlled turbines, the rotor brake is only used for emergency stops, parking conditions and maintenance. A speed-increasing gearbox and an induction generator are often used to convert the rotor torque to electrical power. During the years, however, failures with gears have been discovered which in turn has enabled the development of a direct-drive generator that eliminates the costly gearbox and corresponding failures. The drawback of the direct-drive is its slow shaft speed causing a heavy generator of 4–10 m in diameter.

The majority of today's wind turbines operates at variable speed. The control system regulates the rotor speed to keep the ratio of the blade tip speed to the wind speed more or less constant in order to make the wind turbine operate at maximum efficiency for all wind speeds between cut-in and cut-off. Often, the maximum output (rated power) occurs at rated wind speeds around 10–15 m/s. Above the rated wind speed, the control system for a variable speed turbine limits the rotational speed in order to keep the drive train torque constant. One of the most popular methods of limiting the rotor power is by changing the pitch angle of the blades. Typically, hydraulic cylinders are used to turn the entire blade about its longitudinal axis. Above the rated wind speed, the blades will pitch to reduce the lifting forces generated by the blade aerofoil section. Fig. 1–4 shows a typical power curve for a wind turbine with pitch-regulated power control. Another control strategy is based on stall regulation. The approach relies on the principle that for increasing wind speed, the airfoil angle of attack and lift as well as the power output will increase until the angle of attack reaches a point at which aerodynamic stall occurs. Without any change of the inherent rotor geometry, it follows from the stall-regulated procedure that the power is passive regulated by the loss of rotor efficiency as stall extends over the blade, *i.e.* the geometry of the rotor blades has been designed so that the rotational speed decreases for high wind speeds. Fig. 1–4 shows the phenomenon. As indicated, only a pitch-regulated system is able to have a constant power output above rated wind speed. Nevertheless, keep in mind that a stall-regulated system may be preferred since it does not have the same level of mechanical and operational complexity as a pitch-regulated turbine.

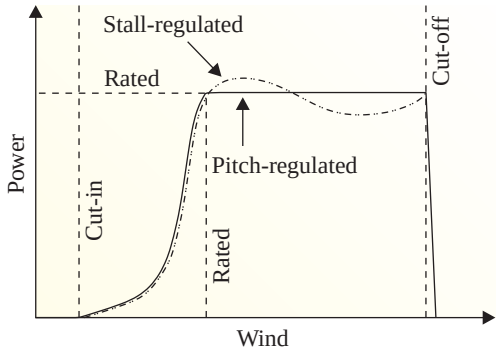

Figure 1–4 Power curve for a typical wind turbine with a pitch-regulated and stall-regulated system.

Nacelle and Tower

The nacelle structure is a combination of welded and bolted steel sections that protect the power train components mounted on a stiff steel bed plate. A yaw drive is used to turn the nacelle in order to keep the rotor shaft aligned with the wind. Based on a wind vane on top of the nacelle providing signals to the control system, the yaw drive reacts and aligns the wind turbine with the wind. A large bearing connects the bed plate to the tower. Normally, cylindrical and tapered

tubular shell towers are used, even though stepped tubular, lattice and cylindrical concrete towers are available. The tubular shape allows access from inside the tower to the nacelle. Internal devices such as a ladder and/or a powered lift for maintenance as well as cables for carrying power and control signals are often present. The towers are manufactured in sections of 20–30 m with flanges at both ends. The structural material damping related to the lowest eigenmode of the nacelle-rotor-tower system is typically assumed around 0.01 logarithmic decrement. However, experimental experiences from this thesis indicate damping values even below 0.01 logarithmic decrement.

1.2.2 Support Structures

Whereas the visual layout of the wind turbine tower and nacelle including drive train typically remains the same for different offshore locations, the actual selection of the support structure is governed by several factors like the water depth, the hydrodynamic conditions, the geotechnical site conditions and the wind turbine size. The substructure, here referred to as the entire structure from below the seabed level to above the splash zone, transfers the environmental and parametric harmonic wind turbine loads to the surrounding soil by having either one or more interfaces to the seabed. At the end of 2013, the most common wind turbine substructure used in Europe was the monopile foundation that accounted for 76% of all installed offshore wind turbines (EWEA 2013). The second most frequently used foundation was the gravity base foundation with 12% followed by the jacket and tripod support structures with respectively 5%. In addition, four floating substructures are in test phase in Europe. Finally, it should be noted that a research and development project at Aalborg University has proven the novel principle of the bucket foundation to be feasible in suitable soil conditions in water depth from near shore to approximately 40 m. In the following, the four most commonly used support structure configurations — gravity base, monopile, tripod and jacket — are presented, just like a short introduction to the bucket foundation is given, cf. Fig. 1–5.

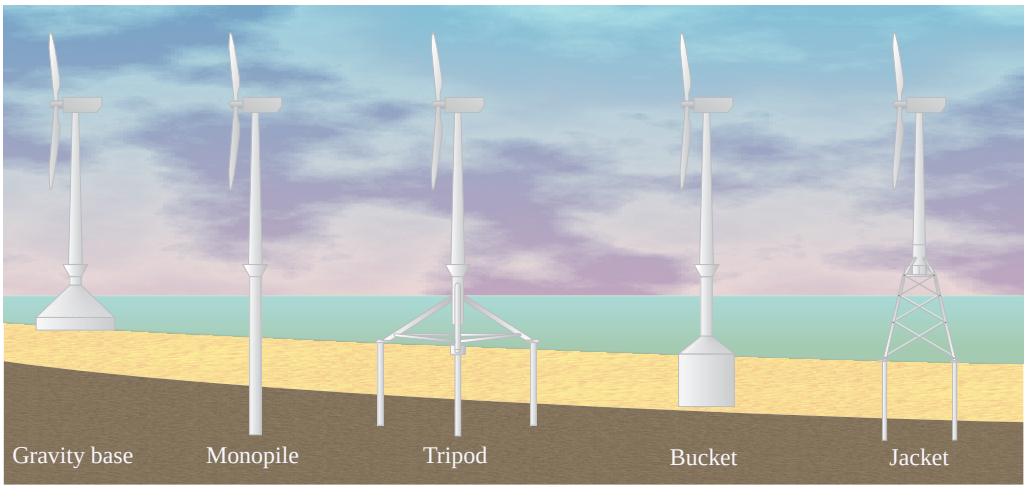

Figure 1–5 Typical substructure concepts for offshore wind turbines.

Monopods

Monopod substructures are defined as having a single interface to the seabed. As indicated in Fig. 1–5, a gravity base, a monopile and a bucket foundation all fulfil this requirement. Common for the foundation types is that the overturning load from wind and waves is applied directly to a single large foundation resisted by the horizontal and the vertical bearing capacity of the structure.

Gravity base foundations applied for offshore wind typically consist of caissons made of reinforced concrete or steel with and without small skirts that may increase the base shear resistance and reduce scour below the base, see Fig. 1–6. Due to its compact structure, the hydrodynamic loads may be very large. Consequently, the gravity base foundation is mainly erected for shallow water depths up to 30 m. The foundation type requires a great seabed area that must be prepared, *i.e.* any soft top layers should be removed prior to the installation as well as levelling of the seabed is required, in order to ensure proper contact at the base of the foundation. This is important since the loads are transferred to the seabed by means of normal and shear stresses at the base of the foundation. Tensile or uplift forces between the bottom of the support structure and the seabed should therefore be avoided. Hence, a large self-weight is necessary and additional ballast material like stones, sand, gravel or other material of high density is normally added after the installation. The pre-ballast ensures that the cellular shaped gravity base foundation can be floated to the site. Due to the shear size of the gravity base foundation required to stabilise the structure when subjected to horizontal forces, it nearly acts as a full (rigid) fixity in the seabed, *i.e.* the subsoil has almost no influence on the first structural eigenfrequency and corresponding damping. Nevertheless, as indicated in the present thesis and, in particular, in the conference paper by Damgaard *et al.* (2014), the second tower modes are affected by the soil–structure interaction that change the fatigue loading significantly. Middelgrunden (2001), Nysted (2003) and Thornton Bank I (2009) offshore wind farms are all examples of sites with gravity base foundations.

Figure 1–6 Gravity base foundation for the Thornton Bank I offshore wind farm. (Peire *et al.* 2008a)

Monopile foundations consist of a single large diameter steel pile drilled or driven into the seabed, typically 20–40 m, by use of a hydraulic or vibratory hammer. The installation technique is simple and contrary to the gravity base foundation concept, it does not usually require any preprocessing of the seabed. The wind turbine tower is bolted to a transition piece attached on top of the monopile. Based on high-strength grout injected into the annular gap between the transition piece and steel pile, the transition piece is fixed in place. The vertical and high-valued horizontal loads are transferred to the subsoil by means of vertical and lateral earth pressures acting on the monopile. Compared to the gravity base foundation, the monopile provides a more flexible foundation configuration. However, larger deformation of the soil also results in more material damping. As indicated by the present research and discussed later in the thesis, the monopile foundation including the subsoil is able to change the first eigenfrequency of the tower mode with

approximately 10% and more than doubling the corresponding damping ratio. This is contrary to the gravity base foundation that only slightly decreases the first eigenfrequency with 0.5% and increases the corresponding modal damping in terms of the logarithmic decrement with around 0.005. Examples of wind parks with monopile foundations are Horns Reef I (2002), Scroby Sands (2004), Kentish Flats (2005), Horns Reef II (2009), Thanet (2010) and Anholt (2013) offshore wind farms. Fig. 1–7 shows one of the monopiles used for the Horns Reef II offshore wind farm. The main advantage of the monopile is its simple and reliable technology that makes it possible to design the pile and transition piece with weights below 250 tons in water depths up to 25 m and with pile diameters of around 4–6 m. Hence, the structure is simple to handle, and standard jack-ups are sufficient for the installation. The disadvantage of the monopile concept is its sensitivity to formation of scour holes, and the grouting for the transition piece is difficult in cold conditions. The former also applies to the gravity base foundation. Further, the installation process is time-consuming when drilling of the monopile is required. Finally, even though wave loads scale drastically with the pile diameter, recent research (Scharff and Siems 2013a; Scharff and Siems 2013b) has shown that XL monopiles with diameters up to 10 m may be economically feasible for water depths above 40 m. However, it should be noted that both fabrication and installation techniques at this writing are bottlenecks, and the pile driving is, in general, a problem since explosives blast waves are generated. Pile driver cushions raise the installation costs.

Figure 1–7 Monopile foundation for the Horns Reef II offshore wind farm. (Doe Ringo 2014)

Suction caisson monopod foundations originate from the concept of suction anchors that has been applied for several offshore platforms to a great extent. However, research (Byrne 2000; Ibsen *et al.* 2003; Houlsby *et al.* 2005) shows that the concept is also suitable for offshore wind turbines located at sites with fine sands or clay material. Basically, the suction caisson monopod foundation — here denoted as the monopod bucket foundation — is a hybrid of a monopile and a gravity base foundation where the overturning moment caused by the wind and wave loads is accommodated by a combination of earth pressures on the bucket skirt and the vertical bearing capacity of the bucket. The structural stiffness is higher than that of the monopile foundation resulting in less soil material damping. This in turn makes the monopod bucket foundation suitable for greater water depths than the typical monopile foundation. According to Fig. 1–8, it consists of a large cylindrical monopod foundation constructed as a thin steel shell structure. The installation of the bucket foundation is conducted in two stages: an initial phase where the skirt penetrates into the seabed due to the self-weight of the structure, and a final phase where a combination of suction and water

Figure 1–8 Monopod bucket used as foundation for the Mobile Met Mast at Horns Reef II offshore wind farm. (Bakmar 2009)

injection at the skirt tip efficiently penetrates the skirt to the design depth. Hence, a silent installation process is obtained with no use of pile driving, just like expensive jack-ups and heavy cranes are avoided. Note that the installation process can be reversed when the design life is exceeded. Although straightforward to use, even for multi-foundations (Byrne and Houlsby 2003), the bucket foundation is a complicated structure to fabricate and more vulnerable compared to the monopile foundation. The thin shell structure compared to the diameter of the bucket makes it sensitive to buckling during installation (Madsen *et al.* 2013). Presently, four monopod bucket foundations have been installed: one onshore in Frederikshavn, Denmark, in 2004; one offshore for the Mobile Met Mast at Horns Reef II offshore wind farm in 2009; and two for the support meteorological masts at the Dogger Bank in 2013.

Multipods

Various types of multipod substructures based on either gravity base foundations, piles or buckets exist, even though the most common way of anchoring the structure to the seabed is by piles. Pre- and post-piled methodologies are possible. During pre-piling, templates are used to ensure the correct positions of the piles. Once the piles are inserted into the seabed, the substructure is lowered and fitted into the piles. On the other hand, post-piling follows the principle of the installation of piles through the sleeves located on legs of the lattice substructure. However, this piling methodology implies higher costs since the costs for the foundation installation and the piling operation are the same, *i.e.* the installations are done from the same heavy and costly lift vessel. For the pre-piling, a less expensive pre-piling spread can be used and, consequently, no downtime is present. In other words, pre-installation of piles removes the need for substructure pile sleeves ensuring a lighter structure, and the vertical installation of the piles helps to standardise the substructure design for mass production. As a consequence, the post-piling process has not been commonly adopted for use on offshore wind farms. Contrary to the monopods, the multipods are characterised by having more than one interface to the seabed. In turn, this makes them suitable for deep water depths where the large bending loads are divided into tension and compression parts before transferred into the ground. Typically, space frame structures originating from the oil and gas sector like the tripod or jacket foundation are used for the load transfer, cf. Fig. 1–5. Additional ballasting can be applied to minimise the critical tensile loading. In the following, only tripods and jackets with piled anchoring are presented.

Tripod foundations are three-legged, welded steel structures made of cylindrical steel tubes. Using diagonal braces and three supporting vertical or inclined sleeves with mud mats, the centre column is divided into a triangular frame of steel transition pieces. Through each sleeve, a pile is driven into the seabed and connected to the sleeve with concrete or grouting. The three penetrated piles and the relatively large base provide structural stiffness and stability which makes the tripod more suitable for larger water depths than the monopile foundation. However, large impact from wave forces as well as com-

Figure 1–9 Tripod foundations for the Alpha Ventus offshore wind farm with a pre-installed pile method. (Geniusstrande 2014)

plex joints with no experience of risk for fatigue damage imply that the jacket foundation often is preferred instead. As indicated in Fig. 1–9, the tripod foundation for offshore wind was used for the Alpha Ventus offshore wind farm in 2010. The test field consists of six tripods and six jackets.

Jacket foundations are latticework structures and consist of three or more main legs connected by slender tubular braces, see Fig. 1–10. Like the tripod, piles driven inside the sleeves are used to fix the jacket to the seabed. Due to a large base, the jacket foundation offers a large overturning moment resistance. Compared to the tripod foundation, the majority of the steel is located further away from the centre axis which results in significant material savings. Hence, a light construction is obtained with high structural stiffness that reduces the wave loads compared to the monopile foundation. A critical component of the jacket foundation is, however, the tubular joints which require many man-hours of welding, just like the maintenance and transportation costs are high. Several offshore wind farms make use of the jacket foundation concept, among these the Alpha Ventus (2010), Ormonde (2011), Thorton Bank II (2013) and Nordsee Ost (2013) offshore wind farms.

Figure 1–10 Jacket foundations for the Ormonde offshore wind farm. (Peire *et al.* 2008b)

1.3 System Dynamics of Offshore Wind Turbines

The design of offshore wind turbines requires that all situations likely to be experienced by the turbine in its service life must be checked for fatigue damage, structural collapse and allowable structural deformations. A mathematical model representing the reality as good as possible is needed that accounts for the acting loads as well as the mass, stiffness and damping (aerodynamic, structural, soil and hydrodynamic) properties of the wind turbine and its support structure. To limit the complexity to a level appropriate to engineering applications, different tools for evaluating the dynamic vibration response of onshore wind turbines have been developed during the years (Øye 1996; Bossanyi 2003; Jonkman and Buhl 2005; Larsen and Hansen 2007; Larsen *et al.* 2013), even though many of them have been extended to deal with the numerical challenges of taking the offshore environmental conditions into account. This section provides an overview of the most relevant environmental parameters affecting the dynamic behaviour of offshore wind turbines and deals with the physical modelling of the structures.

1.3.1 Excitation Range

Obviously, stochastic wind and wave loads as well as current loads and structural harmonic loads from the rotor and sea ice dictate the dynamic vibration response of an offshore wind turbine to some extent, cf. Fig. 1–11. Nevertheless, several meteorological and oceanographic

parameters affect some of these loads. The magnitudes of the wave loads are influenced by the sea level that fluctuates due to tides and storm surges. Short-term (local scour) and long-term (global scour) changes of the seabed level affect the wave loads and the structural dynamic properties in terms of the natural frequencies and damping ratios of the wind turbine. In addition, the determination of the atmospheric stability, wind shear and wind turbulence is governed by differences between water and air temperatures as well as temperature gradients. Finally, marine growth tends to increase the wave loading since the hydrodynamic drag and inertia forces are increased due to the increased roughness and diameter, respectively.

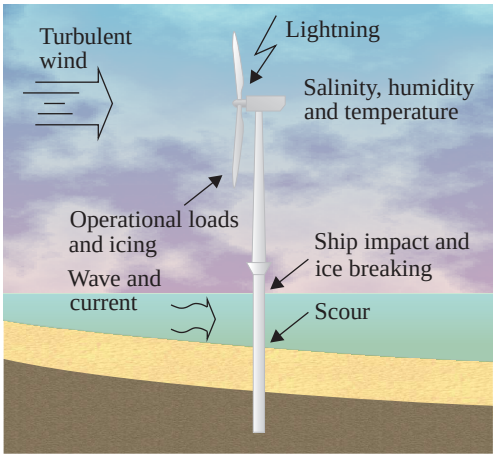

Figure 1–11 Environmental impact and structural loads of an offshore wind turbine.

Wind Loads

The incoming wind field in which the turbine must operate can be described by a superposition of a constant or slowly varying mean wind component with a stochastic varying perturbation on top, named the turbulence component. Normally, the long-term distribution of wind speeds is described by a Weibull distribution fitted to site specific measurement data. Compared to onshore, a greater annual mean wind speed is obtained for offshore locations, and the reduced surface roughness results in a steeper vertical wind profile and lower turbulence intensity. The wind profile is commonly expressed by an exponential relation between height over water and roughness according to IEC 61400-3 (2009). Based on the turbulence intensity, a three-dimensional stochastic wind field is generated, typically by use of the Mann model (Mann 1994). Here, the turbulent wind field is modelled in two spatial dimensions using a spectral density function describing the amount of variance in the wind at a particular frequency in connection with a coherence function defining the spatial correlation of the turbulence. The Kaimal spectrum (Kaimal *et al.* 1964) is often applied to represent the wind power spectrum that contains high energy at frequencies below 0.10 Hz.

The aerodynamic loads are, in general, derived from the fast and fairly accurate blade element momentum method (Burton *et al.* 2001). Detailed description of the theory is out of the scope of the current thesis. However, a short introduction to aerodynamic principles of a wind turbine blade may be relevant for the understanding of the wind loads. Wind turbine blades are shaped as airfoils to make the air flow faster on one side and slower on the other. This means that the pressure will be lowest on the curved side creating a lift force F_L perpendicular to the resulting flow direction and a drag force F_D parallel to the resulting flow direction, cf. Fig. 1–12. The rotation is assumed from right to left which induces a horizontal wind component F_M. Hence,

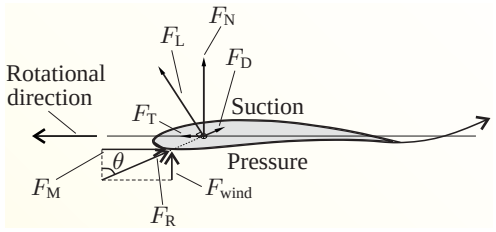

Figure 1–12 Aerodynamic principle for a wind turbine blade. After Larsen (2005).

an angle θ between the resultant wind component F_{R} and the incoming wind component F_{wind} appears. The wind flow generates a pressure and a suction on the different sides of the surface which initiates the lift force F_{L} and the drag force F_{D}. The two forces can be projected onto the tangential and normal direction. As long as the tangential force F_{T} is in the rotational direction, a positive torque is produced on the spinning axis for generating electricity. The normal force F_{N} and the tangential force F_{T} cause bending deformation in the flapwise direction and edgewise direction, respectively.

Wave and Current Loads

Wave loads originate from wind seas generated by local winds and swells arising from waves travelling over a long distance. For the North Sea, however, swell is less significant due to the topography. The frequency range of energy rich waves is typically in the range 0.05–0.50 Hz, whereas extreme waves typically occur in the range 0.08–0.14 Hz. Since the natural frequency of the lowest eigenmode of an offshore wind turbine often is in the range 0.20–0.30 Hz, waves of moderate height with high probability of occurrence are the most important from a dynamic point of view. A number of wave theories are available for the determination of the particle kinematics (Sarpkaya and Isaacson 1981). In case of small wave heights compared to the water depth, linear Airy wave theory may be used where the surface elevation and movement of particles along circular paths follow a sinusoidal shape. The theory may advantageously be applied for modelling of irregular waves by superposition of many linear waves with different amplitudes and frequencies. However, since the linear Airy wave theory defines particle kinematics from the seabed to the still sea level, the Wheeler-stretching method (Wheeler 1970) may be applied in order to consider the kinematics at the free surface to be identical to those calculated at the still sea level. The random ocean waves are taken into account by a wave spectrum enabling realisations of the amplitude and phase of the particular frequency component of the wave. The most commonly used wind-generated sea spectra from an engineering point of view are the one-dimensional Pierson-Moskowitz (Pierson and Moskowitz 1964) and JONSWAP (Joint European North Sea Wave Project) (Hasselmann *et al.* 1973) spectra. The energy content and frequency range of both spectra are governed by prescribed values of the significant wave height and the zero up-crossing wave period. A third parameter — a peak enhancement factor — is, however, needed for the JONSWAP spectrum that controls the shape of the spectrum. It should be noted that for extreme waves in deep water, Stokes finite amplitude wave theory may advantageously be applied instead of the linear Airy wave theory, just like IEC 61400-3 (2009) recommends the Stream function wave theory for shallow waters and steep waves.

Given the particle kinematics, the wave load per unit length can be determined by the Morison equation consisting of an inertia and a drag term. According to the formula, the inertia force is linear proportional to the water particle acceleration and quadratic proportional to the structural diameter, whereas the drag force is quadric proportional to the water particle velocity and linear proportional to the diameter. The drag term becomes small when the diameter of the structure is large compared to the wave length. Hence, for offshore wind turbine foundations like the gravity base foundation or the monopile foundation with diameters above 5 m, the drag term becomes negligible. Nevertheless, Morison's equation assumes that the structure is hydrodynamically transparent, *i.e.* the structure does not alter the wave kinematics which may be a problem for multi-piled foundation in particular due to shadow effects. A gravity base foundation or a monopile with a large diameter do not fulfil this requirement and hence, a corrected inertia term

must be used, for instance by the McCamy-Fuchs solution (MacCamy and Fuchs 1954).

Contrary to the wave loads, the loading from sea currents generated by wind and tides is rather small. According to IEC 61400-3 (2009), the phenomenon may be taken into account by considering the sea current as a horizontally uniform flow field of constant velocity that only varies as a function of depth. Based on a simple empirical power law for the determination of the tidal current velocity and a linear distribution of the wind-generated current velocity, the total water particle velocities are determined by adding the current velocities to the wave-induced water particle velocity. Note that even though the fatigue loading based on sea current in most cases is of lower significance, it should be included for extreme load calculations.

Parametric Harmonic Loads

As indicated in the previous sections, an offshore wind turbine operates in a hostile environment. The varying dynamic loads in combination with a cost-effective, lightweight and flexible structure imply that induced vibration and resonance problems are crucial to consider in the design phase. Amplification of the response must be avoided in order to reduce the fatigue damage accumulation during the lifetime of the wind turbine structure. Consequently, sufficient system stiffness is required to ensure that the natural frequency related to the lowest eigenmode of the wind turbine does not coalesce with excitations from the operation frequency of a three-bladed turbine and waves. Fig. 1–13a illustrates the realistic spectra representing aerodynamic and hydrodynamic excitation for the North Sea and the excitation ranges 1P and 3P associated with the mass imbalances in the blades and shadowing effect from the wind each time a blade passes the tower, respectively. The forcing frequency 1P is the frequency of the rotor revolution, and the 3P frequency is the frequency of blades passing the tower on a three-bladed turbine. The mass imbalance can be due to differences in the blade weight during manufacturing and installation or cracking in a blade where moisture finds its way. Three possible designs can be chosen for a wind turbine: a very stiff structure with the natural frequency f_1 above 3P ("stiff-stiff"), the natural frequency f_1 in the range between 1P and 3P ("soft-stiff") or a very soft structure with the natural frequency f_1 below 1P ("soft-soft"). A "soft-stiff" wind turbine structure is often chosen in current practice because a huge amount of steel is required for a "stiff-stiff" structure.

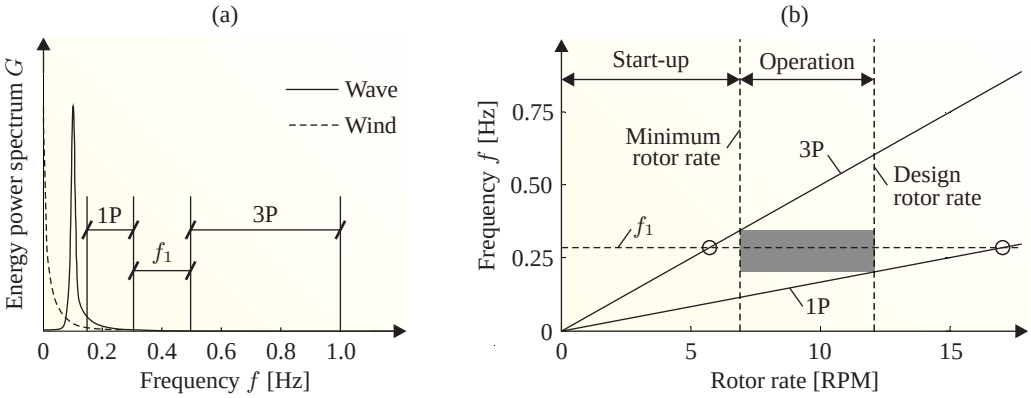

Figure 1–13 Excitation range for a modern offshore three-bladed wind turbine structure: (a) environmental and structural excitations, (b) sparse Campbell diagram for a "soft-stiff" design.

As the trend is to create larger turbines, rotor blades become longer, generator masses greater and hub heights higher. Thus, the rotation frequency and the first natural frequency will decrease. It may then seem impossible to design wind turbine structures as "soft-soft" structures since the risk of the hydrodynamic frequency range falls into 1P is relatively high. Nevertheless, notice that floating concepts are designed as "soft-soft" structures. The first eigenfrequency is, however, very low meaning the dynamic amplifications from waves and blades are insignificant.

In order to identify potential sources of resonance and the safe region for the "soft-stiff" design, a Campbell diagram is useful to illustrate the relation between resonance frequency and excitations, see Fig. 1–13b. As indicated, the intersection of the natural frequency f_1 and excitations takes place outside the operational range meaning no significant resonance is expected. It should be noted that during a start-up sequence, resonance will occur for very limited time.

Gyroscopic Loads

In general, a wheel that spins around its spin axis and tilted about a second axis will try to rotate about the third axis due to gyroscopic effects. Evidently, under the right circumstances a wind turbine is exposed to gyroscopic forces. In principle, two motions of the wind turbine will cause gyroscopic forces. In the case where the rotating rotor is yawed into the wind by a rotation θ_z around the z-axis, a bending moment M_y will arise, see Fig. 1–14a. The magnitude of the gyroscopic moment depends on how fast the yaw motion is. In practice, however, an active yaw control system ensures a slow yawing rate which makes the gyroscopic moment insignificant. In addition, gyroscopic effects may occur when the rotating rotor tilts upwards and downwards caused by a rotation θ_y around the y-axis. As a consequence, a moment M_z is introduced around the tower axis, see Fig. 1–14b.

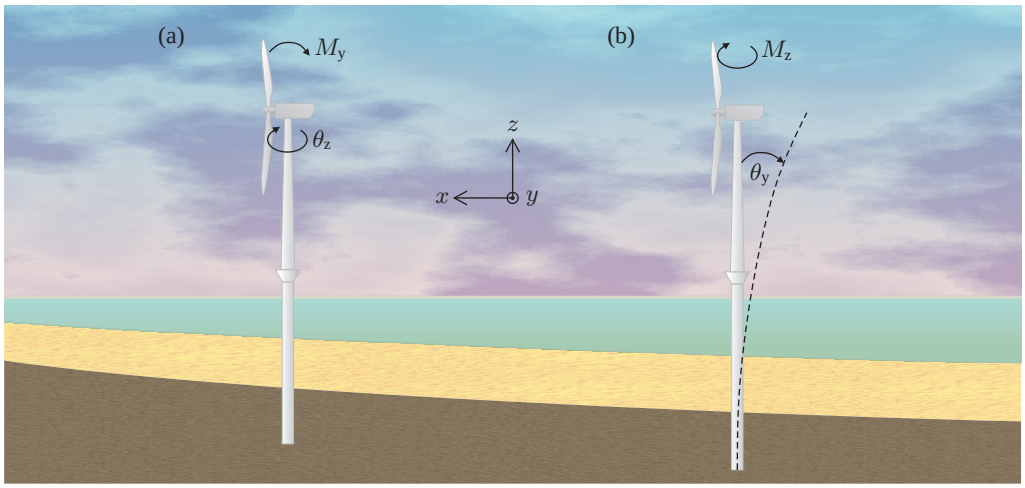

Figure 1–14 Gyroscopic effects for wind turbine structures: (a) the rotating rotor is yawed into the wind by a rotation θ_z. Hence, the yaw torque M_z causes an additional bending moment M_y around the y-axis, (b) the rotating rotor tilts upwards and downwards due to a cyclic rotation θ_y. The introduced bending moment M_y causes an additional torsional moment M_z around the z-axis.

1.3.2 Model Reduction

The design of an offshore wind turbine structure requires the analysis of three limit states in accordance with the codes of practice (GL 2005b; IEC 61400-3 2009; DNV 2011). Firstly, the strength and stability of the turbine, foundation and subsoil must be high enough to avoid collapse in the ultimate limit state (ULS). Secondly, the structural stiffness of the turbine as well as the stiffness of the combined soil–foundation system should ensure that the displacements and rotations of the structure are below a threshold value in the serviceability limit state (SLS). Finally, welded details in the steel structure must be analysed regarding failure in the fatigue limit state (FLS) where S-N curves (or Wöler curves) and rainflow-counting are used to determine the fatigue damage. A large number of load cases is needed for these limit states, especially for FLS conditions which means that the computational effort has to be limited. The balancing point of simplicity and accuracy depends to a great extent on the load case representation as well as on the modelling technique of the wind turbine and the soil–foundation interaction. A proper reduction strategy of the load cases and a computational model with few degrees of freedom (DOFs), without significant loss of accuracy, are therefore a must.

Lumping of Load Cases

Contrary to onshore, the set of wind conditions needs to be extended with hydrodynamic conditions for offshore wind turbines, *i.e.* attention must be drawn to the correlation between wind and wave conditions. The joint probability relies on site measurement or hindcast data of the long-term sea parameters at the specific site. As an example, Fig. 1–15 shows the distribution of the longitudinal mean wind and wave direction for an offshore site in the North Sea showing prevailing winds from south-west, whereas the south-western and northern directions govern the waves, *i.e.* wind-wave misalignment is present for this site. For a set of 10-minute mean wind speed intervals representing 20 years of design life, typically 0–2 m/s, 2–4 m/s, . . ., 22–24 m/s for FLS

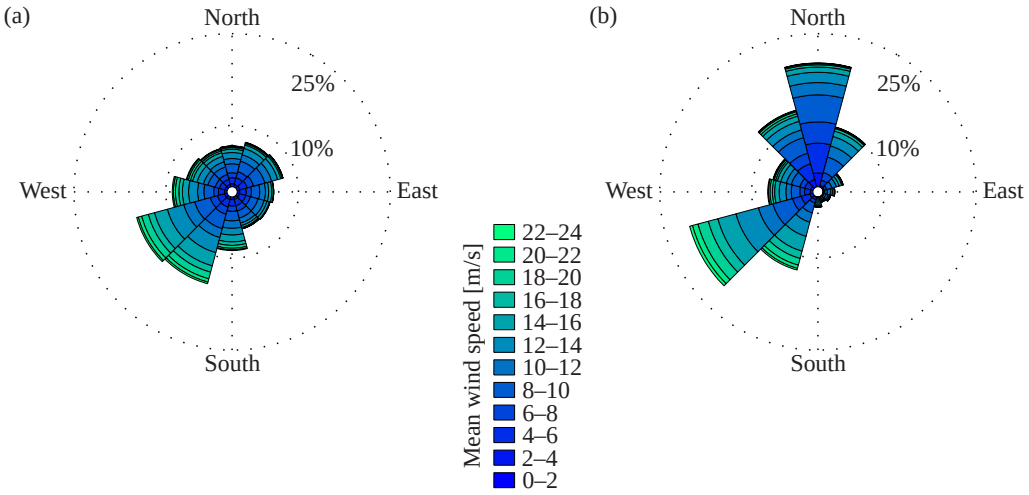

Figure 1–15 Distribution of mean wind speed and wave direction at an offshore wind turbine site in the North Sea: (a) wind rose, (b) wave rose.

analysis, and Weibull fits to the wind and wave distributions for each of the 12 sectors, combinations of longitudinal mean wind speeds, significant wave heights and zero up-crossing wave periods can be derived for each individual wind and wave direction. In other words, for a given longitudinal mean wind speed component as well as a given wind and wind direction, the significant wave height is determined by equalling the probability of wind and wave exceedence, cf. Fig. 1–16. Based on the significant wave height, the zero up-crossing wave period is typically found from a linear relationship between the two sea state parameters. Note that it is assumed that the mean value and standard deviation of the fitted Weibull distributions of the mean wind speed and significant wave height do not change with time. Long random realisations per load case are needed of, for instance, one hour. Consequently, different random seeds must be used for the generation of the wind and wave field. Finally, it should be mentioned that the fact that the wind comes from different directions is not used for onshore wind turbines in most cases. Instead, all wind is assumed to come from the same direction.

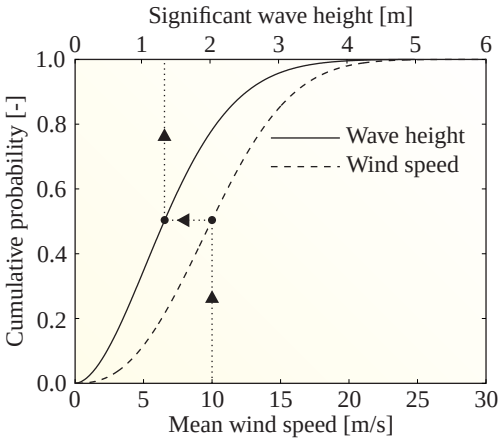

Figure 1–16 Correlation procedure of wind and waves.

Simulation Approaches

Evidently, it becomes too expensive from a computational point of view to simulate the ULS or FLS load cases using fully integrated finite element models of the wind turbine and substructure. As already mentioned, existing wind turbine simulation codes have been developed in the past capable of accounting for the nacelle that revolves about the tower, the rotor that rotates about its axis and the blade pitch that depends on the incoming flow field and aerodynamics of the rotor blades. The aeroelastic models of the wind turbine are characterised by a limited number of DOFs which means that the computational time is reasonably limited. For offshore applications, the foundation and subsoil should consequently only add few additional DOFs to the global system; a complicated task since the soil–structure interaction involves energy dissipation through wave propagation and material damping. As indicated in Fig. 1–17a, stress waves induced by the vibrations of the foundation will travel in the subsoil. Depending on the soil layer depth and the material of the underlying soil layer, part of the wave energy will be reflected back towards the ground, whereas the other part will continue travelling downward. Hence, the radiation effects reduce the structural vibration amplitudes caused by, for instance, a transient load from a breaking wave or wind gust. Depending on the magnitude of the cyclic loads acting on the wind turbine structure and thereby the cyclic soil shear stress τ, the soil may exhibits material hysteresis as indicated in Fig. 1–17b due to its nonlinear behaviour. The shape of the hysteresis loop is governed by the tangent shear modulus G_{tan} that varies during one cycle of loading. Its average value may advantageously be approximated with the secant shear modulus G_{sec}, and hence, G_{sec} determines the inclination of the loop. The area of the hysteresis loop is a measure of energy dissipation during one cycle. It then becomes clear that a high soil stiffness will lead to low soil damping since a low shear strain amplitude γ will be present reducing the area of the hysteresis

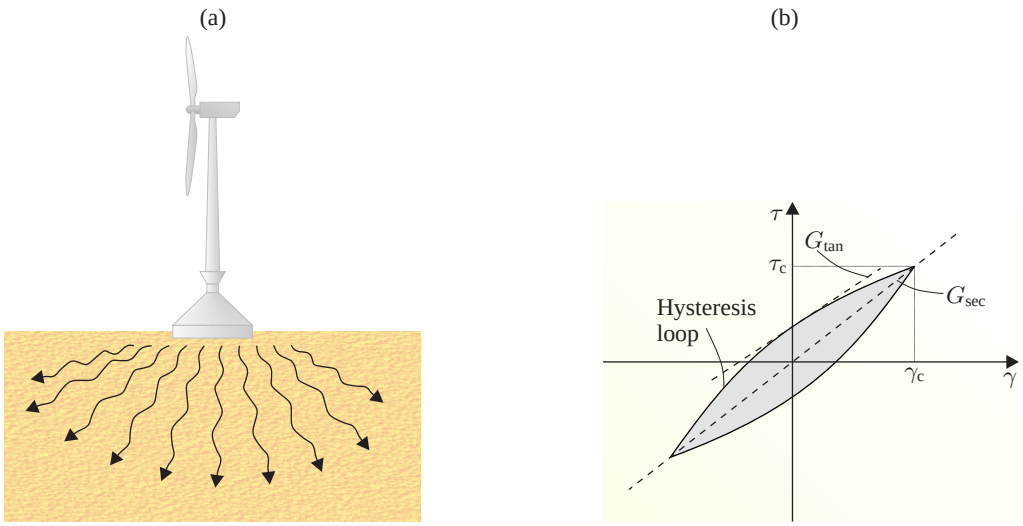

Figure 1–17 Mechanical behaviour of soil: (a) wave propagation emitted from the vibrations on the soil–foundation interface, (b) hysteresis material behaviour characterised by the tangent and secant shear modulus G_{tan} and G_{sec}, respectively.

loop. Evidently, the opposite holds for a low soil stiffness.

From a wind turbine simulation point of view, the challenge is to find a sensible way of characterising the important aspects of the soil–structure interaction with relative simple models. The requirement of simplicity and accuracy has in the past led to many different approaches, some more sophisticated than others. The ideal approach of a fully integrated model including the interrelation effects between the wind turbine and subsoil by static or advanced cyclic nonlinear springs and viscous dashpots applied along the foundation may fail when it comes to computational speed for time-domain simulations. On the other hand, the concept of an apparent fixity length of the tower calibrated to the first natural frequency of the combined tower–foundation system with the soil damping applied as modal damping may seem too simple. A straightforward approach is therefore to use classical spatial reduction methods to reduce the global mass, damping and stiffness matrices of a rigorous foundation model or to fit a parallel coupling of discrete masses, springs and dashpots to a viscoelastic ground response. With relative few DOFs and a high accuracy of the actual nonlinear soil behaviour, the reduced system matrices of the foundation and subsoil can be implemented into an aeroelastic wind turbine code.

1.4 Motivation for Research

As discussed in the previous sections, modern offshore wind turbines are highly dynamically loaded structures characterised by complex interrelation effects between the wind field, wind turbine, foundation and subsoil. The costs are kept as low as possible by reducing the overall weight which leads to slender and flexible structures sensitive to the dynamic amplification of the response from wave- and wind-induced loads. This in turn necessitates a reliable estimate of the basic dynamic properties of the entire wind turbine structure in order to decrease the fatigue damage accumulation. In this regard, the wave propagation in the subsoil emitted from the vi-

brations on the soil–foundation interface and the hysteresis soil behaviour are crucial to consider since the complicated wave pattern with reflection and refraction of waves and irreversible soil deformations lead to radiation and material damping, respectively.

The aim of the present thesis is to evaluate to what extent the soil–structure interaction affects the dynamic structural response of offshore wind turbines that highly depends on the modal frequencies and damping ratios. With this in mind, an accurate mathematical model is needed based on physical and fundamental laws. Instead of using a black box model without regard to physical knowledge of the dynamic behaviour of wind turbines, a grey box model is advantageously developed based on so-called "rotor-stop" tests and operational modal identification of offshore wind turbines.

The analysis requires that the mathematical model reflects the reality to a high degree. However, even though a rapid increase in the computation power has been observed over the last decades — and still is observed — advanced finite element models of the wind turbine and substructure combined with the Navier-Stokes equations for the determination of the flow around the blades and tower may not seem feasible, not least because the design of the turbine and foundation requires the computation and analysis of thousands of load cases. Consequently, to improve the numerical efficiency, a fully coupled aero-hydro-elastic model is utilised. Here, it should be noted that since focus is drawn on the soil–structure interaction, special attention is given on modelling techniques of accounting for the mechanical behaviour of soil. The characterisation of aeroelasticity and wave loading, well-covered in the literature, are therefore based on existing aeroelastic wind turbine codes.

1.4.1 Overview of the Thesis

Following the introduction, the structure of the thesis is given below.

- **Chapter 2** presents a review of some of the methods proposed in the literature for the analysis of soil–structure interaction as well as system identification methods, substructure models and simulation strategies for time-domain analysis of offshore wind turbines. The review is categorised into different topics within experimental and numerical work highlighting the most relevant techniques that during the years have been developed.

- **Chapter 3** describes the scope of the thesis. A short summary of the literature review is given which forms the basis for a clear definition of the methods used in thesis.

- **Chapter 4** contains a summary of the included international conference and journal papers.

- **Chapter 5** concludes the thesis with a summary and discussion of the methods and analyses presented in the thesis. The main results achieved in the project are pointed out and directions for future work are given.

- **Appendix A** describes how to obtain dynamic impedance functions of a linear elastic monopile placed in a linear, viscoelastic soil layer overlaying a rigid bedrock.

- **Appendix B** gives a short introduction to the fundamental theory of linear structural dynamics and stationary random processes. In addition, the theory of the Frequency Domain Decomposition method applicable for operational modal analysis is touched upon.

- **Appendix C** contains the enclosed journal paper: “Cross-wind modal properties of offshore wind turbines identified by full scale testing”.
- **Appendix D** contains the enclosed conference paper: “Damping estimation of a prototype bucket foundation for offshore wind turbines identified by full scale testing”.
- **Appendix E** contains the enclosed journal paper: “Assessment of dynamic substructuring of a wind turbine foundation applicable for aeroelastic simulations”.
- **Appendix F** contains the enclosed journal paper: “Computationally efficient modelling of dynamic soil–structure interaction of offshore wind turbines on gravity footings”.
- **Appendix G** contains the enclosed journal paper: “Effects of soil–structure interaction on real time dynamic response of offshore wind turbines on monopiles”.
- **Appendix H** contains the enclosed journal paper: “Dynamic response sensitivity of an offshore wind turbine: A fully coupled time-domain approach for varying subsoil conditions”.
- **Appendix I** contains the enclosed journal paper: “A probabilistic analysis of the dynamic response of monopile foundations: Soil variability and its consequences”.

CHAPTER 2
State of the Art

Offshore wind energy is a fast-growing interdisciplinary field that involves different methodologies and theories within civil engineering and science. The dynamic response is made up of a complex interaction of components and subsystems. The nacelle revolves about the tower, the rotor rotates about its axis and the blade pitch depends on the incoming flow field and the aerodynamics of the rotor blades, just like the soil–foundation interaction leads to energy dissipation through wave radiation and material damping. This chapter provides an overview of current knowledge and substantive findings of the dynamic response of offshore wind turbines. The review is categorised into different classes, covering different system identification methods, substructure models and simulation strategies for time-domain analysis of offshore wind turbines as well as analytical, numerical and experimental solution techniques for dynamic soil–structure interaction.

2.1 Overview of State-of-the-Art

The analysis of dynamic soil–structure interaction is a young discipline, many of its most important developments within the analytical and numerical framework having occurred in the past 30 to 40 years. The analysis requires a sound understanding of soil as an engineering material, and the derivation of the mathematical model often calls for experimental analysis to support calibrating, updating and validating the dynamic model. The aim of this chapter is to provide an overview of some of the methods which have been proposed in the literature for the analysis of soil–structure interaction and their availability for wind turbine applications. The chapter reviews the work related to the analysis of the highly dynamic and tightly coupled wind turbine system, *i.e.* experimental methods of evaluating the dynamic modal properties as well as numerical approaches of including the highly fluctuating and irregular loads for prediction of the dynamic wind turbine response. Supported by Fig. 2–1, the chapter covers the following aspects:

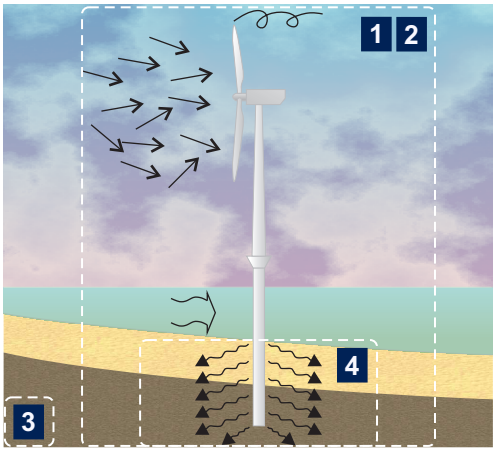

Figure 2–1 Investigated topics in the state-of-the-art.

1 **Experimental modal analysis:** Full-scale testing of offshore wind turbines is reviewed where traditional and operational modal analysis are in focus. The tests may be used for

evaluations of eigenfrequencies and damping ratios of offshore wind turbines that implicitly explain the dynamic effects of the soil–structure interaction.

2 **Time-domain analysis:** A review of state-of-the-art wind turbine simulation codes is presented. In addition, assessment of load simulation approaches for offshore wind turbines is considered with special focus on the coupling between the foundation and wind turbine dynamics.

3 **Soil as an engineering material:** Before a review of current methods for analysing soil–structure interaction is presented, an introductory remark regarding soil behaviour is given. It is clarified why a viscoelastic model often is used for wave propagation problems.

4 **Interrelation effects between foundation and subsoil:** A review of the most important analytical, numerical and experimental methods for the analysis of dynamic soil–structure interaction is given. The aim is to find a reliable and time-efficient approach of including the soil–structure interaction into wind turbine simulation codes based on the knowledge from item 1 and item 2.

2.2 Offshore Wind Turbine Response

Wind turbines are complex engineering systems. Their response is governed by highly fluctuating and irregular loads which means that the design of the tower and foundation, in particular, is a nontrivial task. This section aims to present an overview of current technologies of modal testing of wind turbine structures that can be used for the determination of resonance frequencies, damping ratios and mode shapes of the dynamic system. A further description of state-of-the-art wind turbine simulation codes is given, as well as a literature review of different aero-hydro-elastic simulation approaches for wind turbine applications is presented.

2.2.1 Full-Scale Modal Testing

Vibration measurements of civil engineering structures have been practised for many years. The design and construction of more and more complex and ambitious civil engineering structures require accurate identification of the local and global dynamic properties of the structure and subsoil. Often, experimental full-scale modal analysis is applied to obtain a qualified estimate of inherent structural properties in terms of natural frequencies, damping ratios and mode shapes of the entire structural system, whereas small-scale testing advantageously can be used for detailed dynamic analysis of substructures and soil properties. The methods contribute to the validation and improvement of the computational models.

Traditional Experimental Modal Analysis

The determination of structural modal parameters can be determined by forced vibrations. The most used approach is to excite the structure artificially in one single point and measure the response in different points together with the forcing excitation. Using Fourier transformation of the time signals, a set of frequency response functions at several points along the structure is estimated from the measured response divided by the measured excitation. The ratio between

the individual entries in the frequency response function for a frequency equal to the resonance frequency represents the corresponding mode shape.

Traditional experimental modal testing has widely been used for bridge structures. Among others, Askegaard and Mossing (1988), Agardh (1991), Wood *et al.* (1992), Aktan *et al.* (1992), Green and Cebon (1994) and Pate (1997) used impact excitation methods to excite full-scale bridges. The aim was to provide white noise excitation, *i.e.* the spectral density function of the impulse loading is constant over all frequencies, in order to obtain an output spectrum that contained full information of the structure. In addition, Shepherd and Charleson (1971), Kuribayashi and Iwasaki (1973), Ohlsson (1986), Cantieni and Pietrzko (1993), Deger *et al.* (1993), Deger *et al.* (1994), Miloslav *et al.* (1994) and Caetano *et al.* (2000) used electrodynamic shakers with sinusoidal load excitation to evaluate the modal properties of bridges, just like Duron (1995a, 1995b), Cantieni (2001) and Nuss *et al.* (2003) applied forced shaker excitation on dam structures.

The application of traditional experimental modal testing for onshore wind turbines has been reported by Carne *et al.* (1988), Molenaar (2003), Hansen *et al.* (2006) and Osgood *et al.* (2010). However, for offshore applications, the forced vibration tests become highly expensive due to special equipment and relatively long test duration involving a separate test for each mode. In addition, the main problem with forced vibration tests on large civil engineering structures is that the most significant modes of vibration in a low range of frequencies are difficult to excite. Consequently, "rotor-stop" tests or free vibration tests may be preferred for offshore wind turbines in which the natural frequency and damping ratio of the lowest eigenmode can be identified from the free structural vibration response after the application of an impulse.

Free Vibration Analysis

Using an impulse test, Mangalhães *et al.* (2010) analysed the free vibration response of a cable-stayed bridge, a suspended roof of a stadium and a footbridge after the application of an impulse. For these analyses, it was needed to apply several band-pass filters to isolate the contribution of a single mode before fitting an exponential function to the relative maxima of the vibration decay in order to estimate the structural damping ratio. Nevertheless, for "rotor-stop" tests of wind turbines in which the structure is effectively left to freely vibrate after the generator shuts

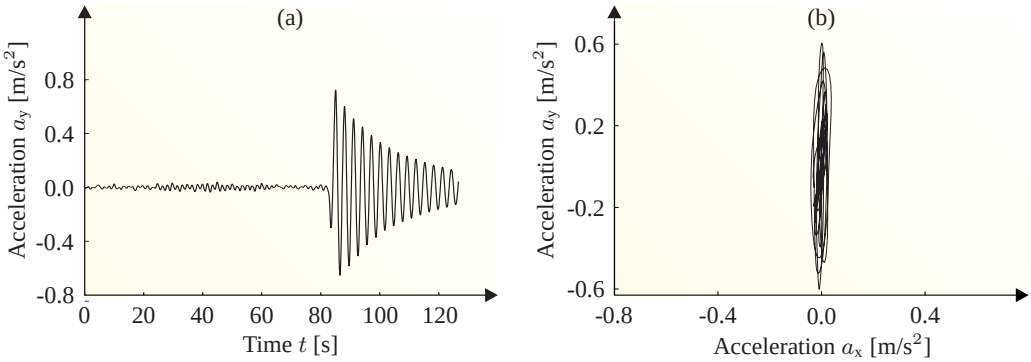

Figure 2–2 Raw output signal during a "rotor-stop" test of an offshore wind turbine installed on a monopile: (a) fore-aft tower acceleration a_y vs. time t, (b) fore-aft tower acceleration a_y vs. side-side acceleration a_x.

down and the blades pitch out of the wind, it turns out that the free decay often only contains modal vibrations from one single mode, even though the wind turbine has closely spaced natural frequencies, see Fig. 2–2.

The approach has been used by Tarp-Johansen *et al.* (2009), who investigated two offshore wind turbines installed on monopiles at Horns Reef I and Burbo wind farms. Due to low level of damping in the cross-wind direction compared to the fore-aft direction that increases the fatigue loads notably, the authors studied free vibration tests to verify the cross-wind modal damping related to the lowest eigenmode of the structures. Damping values in terms of the logarithmic decrement of 0.12 and 0.06 were observed for the Horns Reef I and Burbo wind farms, respectively. A tower damper was active during the measurements. In addition, the authors postulated that up to 0.05 soil damping could be expected during normal turbine operation. A similar study was carried out by Versteijlen *et al.* (2011) that analysed twelve "rotor-stop" tests on an offshore wind turbine at Burbo wind farm. The research showed a logarithmic decrement up to approximately 0.21, *i.e.* around 3 times higher damping than Tarp-Johansen *et al.* (2009) estimated for the same wind turbine site. Further, based on strain gauges at the tower top and tower bottom, it could be observed that a local blade mode, in addition to the first tower mode, was present in the power spectrum of the measured signal at the tower top. Fitting of an analytical expression to the two dominant peaks in the frequency domain, Versteijlen *et al.* (2011) claimed that the difference between the damping values related to the two modes was caused by the soil damping since only the first tower mode mobilised soil reactions. A logarithmic decrement of the soil damping contribution of around 0.09 was obtained by the authors. However, the approach and results may be questionable since the installed tower damper performance obviously will contribute with different damping values to the two identified vibration modes. Recently, Shirzadeh *et al.* (2013) performed "rotor-stop" test of an offshore wind turbine with a monopile substructure at the Belwind wind farm. With the exclusion of the mass damper, the authors estimated damping in terms of the logarithmic decrement related to the first tower mode of approximately 0.06 which is in agreement with the recommendation given by the design regulation GL (2005a) and in close correspondence with the findings of Tarp-Johansen *et al.* (2009).

Operational Modal Analysis

As an alternative to traditional experimental modal analysis and free vibration tests, operational modal analysis might be used. The method allows determination of the inherent structural properties by measuring only the response of the structure without using an artificial excitation which means that the technique can provide a complete modal model under operating conditions, *i.e.* within true boundary conditions and actual force and vibration level. For wind turbine applications, the method is useful since the presence of rotational loads and considerable aeroelastic effects influence the mode shapes, *i.e.* whereas no coupling between the fore-aft and side-side tower modes is present during a "rotor-stop" test, the modes may couple during normal wind turbine operations and change the

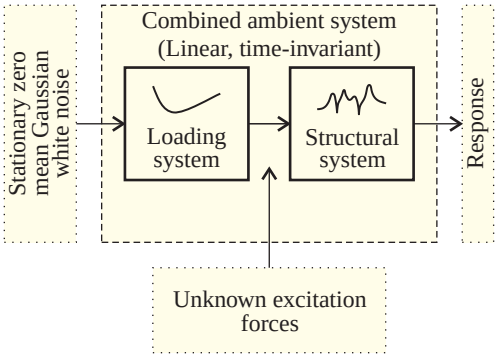

Figure 2–3 Combined ambient model.

modal damping significantly. Fig. 2–3 shows the stochastic framework of operational modal analysis. It is assumed that the excitation forces that drive a virtual linear and time-invariant system, consisting of a loading system (excitation filter) and the structural system, are a Gaussian white noise process meaning that all modes are excited equally. In reality, however, the excitation forces at some frequencies always contain more energy than others. As a consequence, the unknown excitation forces being modelled in the stochastic framework are a result of a linear filter that shapes the white noise spectrum into the correct shape having an energy distribution like the true unknown excitation forces. This also means that modes belonging to the real structural system (lightly damped modes) and modes that belong to the virtual loading system (highly damped modes) are identified.

Different methods of identifying the structural modal parameters exist in operational modal analysis. Frequency Domain Decomposition (FDD) and Stochastic Subspace Identification (SSI) techniques are widely used. Whereas the FDD technique works in the frequency domain that implies leakage introduced by Fourier transformation (a result of the assumption of periodicity) and thereby a slight overestimation of the damping, the SSI algorithm works in the time domain where a parametric model is fitted directly to the raw time signals. More information of the two operational modal techniques can be found in the included *Paper 2* and Appendix B or publications by Brincker *et al.* (2000), Zang *et al.* (2001) and Brincker *et al.* (2001) for the FDD technique as well as Andersen (1997) and Andersen and Brincker (2006) for the SSI approach.

Although the identification of natural frequencies and mode shapes provided by current operational modal techniques shows a low level of dispersion, a high variation can be encountered in damping estimations. The scatter can be caused by changes in the operating conditions as well as uncertainties related to the mathematical algorithms used and the limited length of the measurements. Nevertheless, the literature on ambient vibration testing of bridge structures is extensive. Among others, Biggs and Suer (1956), Vincent (1958), Vincent *et al.* (1979), Van Nunen and Persoon (1982), Wilson (1986), Swannell and Miller (1987), Agarwal and Billing (1990), Proulx *et al.* (1992), Gates and Smith (1982), Farrar *et al.* (1994), Felber and Cantieni (1996), Ventura *et al.* (1996), Brownjohn (1997), Asmussen *et al.* (1998), Brincker *et al.* (2000) and Cantieni *et al.* (2008) reported ambient vibration tests for bridges where traffic, wind and wave loading were used to excite the structures. An experimental dynamic study of the Vasco da Gama Bridge in Lisbon with a total length of 12 km was studied by Peeters *et al.* (2002). The study was based on an ambient and a free vibration test in 1998 described by Cunha *et al.* (2001). The intention was to assess the aerodynamic and seismic behaviour of the bridge. The ambient test revealed which modes of the bridge that could be excited by natural wind excitation. The aim of the free vibration test was to verify the ambient test results. Using the SSI method, the modal parameters obtained from the ambient data were compared with those from the free vibration data. Overall, comparable results were obtained. A small deviation was found between the damping ratios. According to Peeters *et al.* (2002), this deviation was caused by that the damping ratio varied with the magnitude of vibrations and that an aerodynamic component was presented in the ambient vibration test due to the relatively high wind speed during the test. Also, Cunha *et al.* (2004) analysed the ambient data of the Vasco da Gama Bridge with the purpose of testing the efficiency and accuracy of the FDD and SSI methods using ARTEMIS EXTRACTOR (SVS 2004). The applications of the two methods led to very close estimates of the modal frequencies and mode shapes. Ambient vibration measurements of large buildings have been described among others by Cheryl and Ventura (1998), Lord and Ventura (2002), Turek *et al.* (2006) and Kuroiwa and Lemura (2007). Based on the study made by Cheryl and Ventura (1998), the response data

of the Heritage Court Building structure was analysed by Brincker and Andersen (2000) using two different techniques: the FDD technique and the SSI technique. Eleven modes were well estimated from the two techniques where three of them were closely spaced modes around 1.1–1.4 Hz. Overall, comparable modal parameters were obtained from the two methods. This proves the capability of the methods to identify a number of closely spaced modes.

In case of a parked wind turbine, the assumptions within operational modal identification are valid, also the ones regarding modal analysis (linear system, stationary and time-invariant). Liingaard (2006) and Shirzadeh *et al.* (2013) used operational modal identification for a parked offshore wind turbine to evaluate the structural natural frequencies and damping ratios, respectively. In addition, Osgood *et al.* (2010) compared the modal properties of a parked wind turbine excited by a shaker using traditional experimental modal testing with ambient vibration test in conjunction with the SSI technique. The aim of the study was to verify operational modal identification for parked wind turbines. The two ways of evaluating the natural frequencies agreed very well which clearly shows the advantage of operational modal identification.

In general, wind turbines have very specific characteristics and challenging operational conditions which makes special demands on operational modal identification. According to Tcherniak *et al.* (2010), two numbers of inherent problems reveal when using operational modal identification on operational wind turbines:

1. The assumption of structure time invariance is violated. The nacelle rotates about the tower, the rotor rotates around its axis and the pitch of the blades may change. The assumption of constant dynamic mass, damping and stiffness properties of the wind turbine during the structural analysis is therefore not generally satisfied.

2. In the operational modal identification theory, it is assumed that the excitation forces must have broadband frequency spectra, they must be distributed over the entire structure such that all modes of the system can be excited with sufficient levels of energy and they must be uncorrelated. Forces due to wind turbulence fulfil these requirements. However, the effect of rotor rotation changes the nature of aerodynamic forces. The shape of the input spectra transforms from being flat to a curve with distinct peaks at the rotation frequency and its harmonics. Moreover, the excitation forces now become correlated around the rotation frequency and its harmonics.

As indicated, application of operational modal analysis to operational wind turbines is not a straightforward task. As the input forces are not measured in operational modal identification, it is important to identify and separate the harmonic components (deterministic signals) from the structural modes and eliminate the influence of the harmonic components in the modal estimation process. According to Jacobsen *et al.* (2007), the harmonic components cannot be removed by simple filtering as this would significantly change the poles of the structural modes and thereby their natural frequency and modal damping. An elegant way of identifying and removing harmonic components is by Kurtosis techniques. Basically, the idea is that the probability density function (PDF) for structural modes excited by stochastic excitation from wind and waves differ significantly from the PDF for deterministic excitation such as harmonic components. Therefore, testing of the shape of the PDF of the measured response is a way of determining whether sinusoidal excitation forces are present using Kurtosis techniques. The identified harmonics are removed by performing a linear interpolation across the harmonic components in the single-degree-of-freedom (SDOF) function (Gade *et al.* 2009).

Jacobsen *et al.* (2007) demonstrated the harmonic detection approach on measurements from an aluminium plate structure excited by a combination of a single sinusoidal signal and a broadband stochastic signal. By comparing the modal parameters obtained with pure stochastic excitation of the same structure, the approach showed good agreement, even in the case of having a harmonic component located at the peak of a structural mode. Also, Andersen *et al.* (2008) and Gade (2009) applied the harmonic detection approach with success on measurements from a gravity dam structure and a gearbox, respectively.

Hansen *et al.* (2006) studied estimations of natural frequencies and damping ratios of an onshore wind turbine for different mean wind speeds. The SSI algorithm was compared with an excitation method where turbine vibrations were obtained by blade pitch and generator torque variations. For the excitation method, the decaying response after the end of excitation gave an estimate of the damping. However, the conclusion of the excitation method was that the excited turbine vibrations were not pure modal vibrations and hence, the estimated modal properties were not the actual modal properties of the wind turbine. For the operational modal identification analysis, Hansen *et al.* (2006) scanned three months of measurements to find 1–3 hours long periods of low standard deviations for wind and rotor speeds in order to improve the assumption of a time-invariant system. For that reason, several 10-minute measurements series were collected. With the SSI approach, the natural frequency of the first two tower bending modes was almost constant with the mean wind speed (Campbell diagram), whereas the side-side damping related to the tower mode decreased with 60% from rated wind speed at around 8 m/s to 18 m/s.

Bir (2008) and Tcherniak *et al.* (2010) presented the application of operational modal identification using SSI of computational simulated responses of a wind turbine structure. The authors discussed the time variation of the system due to the rotating rotor which causes time-dependent eigenvalues and eigenmodes when measurements are taken on the rotating frame. In order to avoid the time-dependent modal parameters and thereby a time-dependent equation of motion, the authors made use of a Coleman transformation. Basically, the technique converted the motion of each individual blade described in the rotating blade frame into the ground-fixed frame. Recently, Ozbek and Rixen (2011, 2013) applied the operational modal technique, Natural Excitation Technique (NExT) (Carne and James 2010), to estimate the modal properties of a parked and operational 2.5 MW wind turbine. The authors concluded that a suitable selection of low-noise-ratio data series, a sufficient data length and a check of the changes at excitation levels were needed in order to obtain realistic modal parameters.

2.2.2 Time-Domain Analysis of Offshore Wind Turbines

Offshore wind turbines have very specific characteristics and challenging operating conditions. They are designed and optimised to provide optimal power production for changing wind speeds and directions. In addition, the rotor is subjected to aeroelastic effects that together with wave slamming from breaking waves in shallow water result in nonlinear, time-dependent loads acting on the foundation. The wind turbine, prone to dynamic effects and excitation from wind and waves, experiences a large number of load cycles during its service life. Consequently, fatigue assessment is mandatory and is typically evaluated by a rainflow-counting approach (Matsuishi and Endo 1968) in conjunction with the Palmgren-Miner linear damage rule (Palmgren 1968; Miner 1945) with a material S-N curve. The analysis of the loads on the turbine, forming the basis of the post-processing, is commonly based on numerical models and consists of simulating several thousands of 10-minute load cases that represent the possible loads experienced by

the wind turbine during the service life. The loads highly depend on the interrelation effects between the wind field, wind turbine and support structure. As an example, the relative wind velocity experienced by the blades changes when the wind turbine turns into the wind resulting in an increase of the aerodynamic forces in the fore-aft direction. Consequently, additional damping occurs that influences the horizontal displacement of the tower and foundation and thereby changes the soil stiffness and damping contribution, *i.e.* the system is tightly coupled and separate optimisation of the subsystems does not apply.

Aerolelastic Wind Turbine Simulation Tools

During the years, a number of design codes has been developed to analyse the dynamic behaviour of wind turbines or to carry out the design calculations. Originally, most of the codes have been developed for onshore wind turbines, but have during the years been extended to deal with offshore problems with different degree of detail. A thorough comparison of the different available aeroelastic codes was reported by Musial *et al.* (2009) and Jonkman and Musial (2010) based on the Offshore Code Comparison Collaboration project (OC3) under the International Energy Agency (IEA) Wind Task 23 and the Offshore Code Comparison Collaboration Continuation (OC4) project formed under the IEA Wind Task 30, respectively. The projects focused on fully aero-hydro-elastic simulations of offshore wind turbines founded on different foundation types. No soil–structure interaction was taken into account in the comparison. Below, a short presentation of three of the most commonly used wind turbine simulation codes are given.

- **FLEX5** is developed at the Department of Fluid Mechanics, Technical University of Denmark by Øye (1994, 1999). The equations of motion are based on a linear modal condensation technique where coupling effects between the tower deformation and rotor system are included. The number of degrees of freedom (DOFs) is limited to 28 which ensures fast evaluation of the nonlinear wind turbine response. Since the source code of FLEX5 is freely accessible, it is possible to adapt and improve the code for individual needs. The tool has further been extended to account for monopile foundations. The module is based on a super-element formulation with the top node of the element linked to the tower bottom forming the boundary to the support structure. The construction of the super-element is based on two shape functions derived as the static deformation of the super-element from a unit deformation and a unit rotation of the top node. The soil–structure boundary is simulated by constraints applied at a given depth below mudline. Wave kinematics is generated externally by the included WAVEKIN tool.

- **FAST** is, in a similar manner as FLEX5, a modal based program developed by the National Renewable Energy Laboratory (NREL) (Jonkman and Buhl 2007) and is free to download. The accuracy of the modal representation depends on the choice of mode shapes and the applied damping for each mode which are input into FAST. Normally, the flexible elements are represented by their first two eigenmodes. Since a coupling between FAST and the multi-body code ADAMS (Professional Services Group 1998) can be done, it is possible to model arbitrary foundation and floating structures. In addition, FAST accounts for simple hydrodynamic loading.

- **HAWC2** is a nonlinear multi-body code meaning that the structural system is modelled as a full finite element (FE) model of both the blades and tower. The time-domain code, developed at the Department of Wind Energy, Technical University of Denmark (DTU), Risø

(Larsen and Hansen 2007; Larsen *et al.* 2013), uses a linear Timoshenko beam model for the structural modelling of the wind turbine. Although the beam model assumes small rotations, it is possible to account for the nonlinear effects in HAWC2 by dividing the structure into several substructures with their own coordinate system restricted in their movement relative to each other through constraints. Foundation modelling capabilities include bottom-mounted multipods as well as floating type concepts. The aeroelastic code offers the inclusion of soil–pile interaction using p–y and t–z curves as proposed by the design regulations (API 2000; DNV 2011), just like a huge range of wave theories including irregular sea states is available. System damping including soil damping is incorporated via frequency-dependent Rayleigh damping for each body.

Note that computational fluid dynamics (CFD) are a supplement to the above-mentioned time-domain wind turbine simulation codes for calculation of aerodynamics due to the development of computer technology. The method is especially useful for detailed investigation of phenomena, *e.g.* wind shear, tower shadow, and large blade deflection as well as lift and drag forces along with the angle of attack. Among others, Hansen *et al.* (1997), Sørensen and Hansen (1998), Duque *et al.* (1999) as well as Sørensen and Michelsen (2001) used CFD on wind turbines and confirmed its ability by comparing the simulated results with wind tunnel test data performed by Fingersh *et al.* (2001) and Simms *et al.* (2001).

Integrated Load Analysis of Offshore Wind Turbines

During the last years, different methodologies of simulating the dynamic response of offshore wind turbines subjected to combined wind and wave loads in an integrated and/or superimposed manner have been proposed. Since commercial offshore software packages like ROSAP (Rambøll 2009) and ANSYS ASAS(NL) (ANSYS 2008) are suitable for time-domain analysis of offshore structures excited with pure wave loads, the most straightforward way of analysing the offshore wind turbine response is by a superposition approach. Based on operational loads as well as wind load time series at the tower top or bottom generated from an onshore wind turbine with approximately same natural frequencies as the offshore wind turbine structure, the offshore design code superimposes the wave and wind loads, meaning local member forces of the tower and the complex foundation can be determined. Although a fast evaluation of the structural response is achieved by the superposition method, it is obvious that it does not account for the interaction between the wind turbine and foundation, and implies that the aerodynamic damping only is considered for the wind load calculation. As an example, Haselbach *et al.* (2013) compared fully coupled aero-hydro-elastic simulations of an offshore wind turbine installed on a jacket foundation with uncoupled wind/wave load simulations in ABAQUS (Dassault Systèmes Simulia Corp 2012) and showed that aeroelastic and hydrodynamic coupling could account for at least 25% of difference in loading on the jacket compared to the uncoupled simulations. Approximately constant aerodynamic damping values may advantageously be used in the offshore design code as described by Kühn (2001) in order to minimise this difference.

A modification of the superimposed method, a so-called semi-integrated approach, allows a better description of the wave loads, even though interrelation effects between the wind turbine and foundation still is neglected. The idea of the method described by Seidel *et al.* (2004) is to generate an equivalent monopile for the aeroelastic load simulations that has approximately same mass, damping, stiffness and hydrodynamic characteristics as the “real” complex sub-

structure and thereby able to produce representative kinematics at the tower/foundation interface in which equivalent wave loads are included, cf. Fig. 2–4. Hence, the response at the interface is a result of combined wind/wave loading where aerodynamic effects are included. A retrieval run for calculating the member forces of the detailed foundation is performed in the offshore design package (foundation, tower and nacelle mass are modelled) by applying foundation top displacement and rotation time series together with wave loading on the foundation, simultaneously. As pointed out by Seidel *et al.* (2004), reliable results using this method imply that the damping level in the aeroelastic code and the offshore design package is identical and that the stiffness of the substitute model is modelled very carefully. The authors proposed a methodology for deriving the equivalent stiffness of the monopile based on the displacement shapes for unit displacement and unit rotation of a monopile—a method that straightforwardly can be used for the modal based aeroelastic code FLEX5 which uses a 2×2 generalised stiffness matrix of the monopile. However, using the approach means that the considered "real" complex foundation should have mode shapes similar to those of the monopile. Whereas the diagonal elements of the generalised stiffness matrix are fitted reasonably well for many foundation types, the off-diagonal elements are often difficult to match.

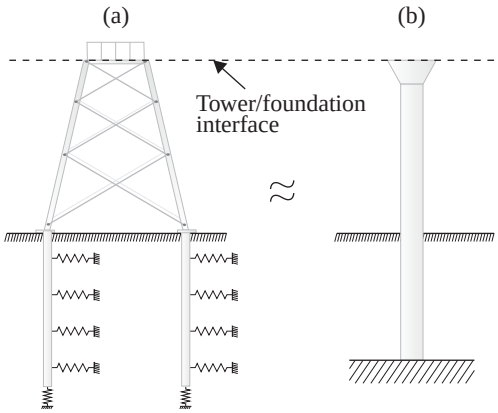

Figure 2–4 Semi-integrated approach: (a) "real" foundation, (b) monopile with equivalent dynamic properties as the "real" complex foundation.

As a consequence of the limitations of the semi-integrated method, Seidel *et al.* (2005) presented the sequential approach. Instead of using an equivalent monopile model, a system reduction scheme is applied to the "real" complex foundation structure in order to have an accurate representation of the structure with few DOFs. Following the procedure as indicated in Fig. 2–5a, reduced structural mass, damping and stiffness matrices as well as a reduced wave load time vector generated in the offshore design package are implemented into the aeroelastic code where the actual dynamic analysis is carried out. The approach is similar to the semi-integrated approach with the only difference that the wave loading is computed in the offshore design package. A final analysis is afterwards performed in the offshore design package (foundation, tower and nacelle mass are modelled) to recover the member forces in the detailed foundation model by applying the foundation top node displacement time series obtained from the aeroelastic code together with the wave loading.

Seidel *et al.* (2005) used a Guyan reduction approach (Guyan 1965) and showed that the sequential approach provided reliable results in terms of damage equivalent fatigue loads compared to a fully integrated analysis in FLEX5 for an offshore wind turbine installed on a monopile fixed at seabed. Although the stiffness properties of the complete foundation system are reflected exactly by the Guyan reduction, this is not the case for the reduced mass matrix. As a consequence, the internal dynamics of the substructure is not represented correctly which, contrary to a monopile foundation, has significant impact on the structural response of multipods like a jacket or tripod. In order to fully describe the mass matrix, the Craig-Bampton method (Bampton and Craig 1968) may be used in which the dynamic response of the internal DOFs are included by adding fixed interface modes. The approach was applied by Hald and Høgedal (2005), who

decomposed an FE model of a foundation with arbitrary geometry using a Craig-Bampton reduction scheme and applied it into the aeroelastic code FLEX5 as a super-element with six interface DOFs and a number of internal DOFs. Van der Valk and Voormeeren (2012) used the sequential approach to compare the static Guyan reduction method with different other component mode synthesis methods (de Klerk *et al.* 2008) for a jacket foundation with fixed boundary conditions at seabed and concluded that the internal dynamics of the support structure was needed in order to obtain reliable results. For the same foundation type, Voormeeren *et al.* (2013) more recently applied a sophisticated super-element approach based on the Craig-Bampton reduction scheme in conjunction with a so-called modal truncation argumentation method that should be able to describe the response of the component to hydrodynamic excitation in a more appropriate manner than traditional reduction methods.

As an alternative to the sequential approach, Kaufer *et al.* (2009) applied a fully coupled approach. The concept is to retain the full foundation structure in the offshore design package and include the system matrices from the aeroelastic code in the solution process in each time

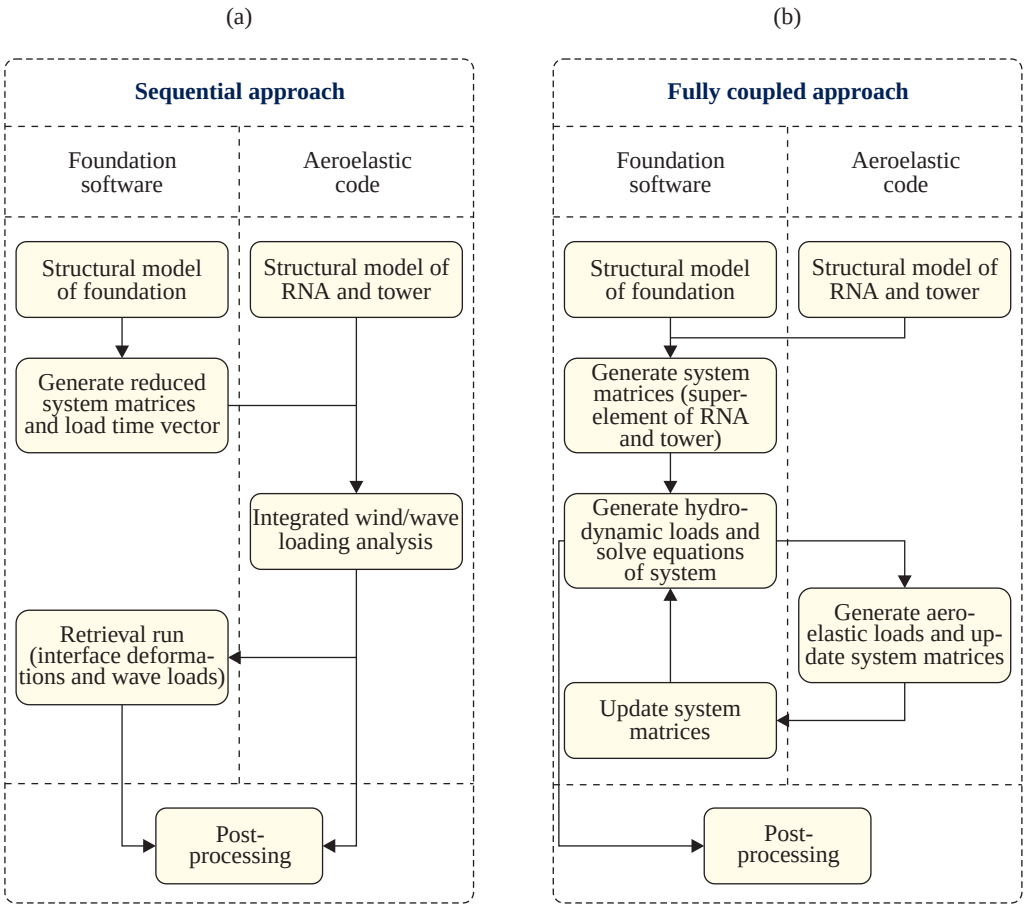

Figure 2–5 Schematic overview of simulation strategies for offshore wind turbines: (a) sequential approach, (b) fully coupled approach.

step. Fig. 2–5b shows a schematic overview of the fully coupled procedure where the wind turbine structure modelled in the aeroelastic code is treated as a super-element and implemented into the offshore design package where the time simulation can start. For each time step, the time-dependent system matrices of the tower and rotor system modelled in the aeroelastic code as well as the aerodynamic force vector based on the displacement, velocities and accelerations at the tower/foundation interface from the previous time step are transferred into the offshore design package where hydrodynamic loads are added. Subsequently, the global system matrices are updated and time integration is carried out to find a new solution. Seidel and Ostermann (2009) and Böker (2009) compared the fully coupled approach with the sequential approach and concluded that the two approaches were in good agreement in terms of the frequency response of a jacket support structure fixed at the seabed for low frequencies, whereas the sequential approach in most cases over-predicted the local response at higher frequencies.

2.3 Soil–Structure Interaction

Soil as an engineering material shows a complex mechanical behaviour. The material consists of a collection of granular particles with different shapes and voids in between them. Any loading permanently alters the soil fabric and the volume of voids which causes the soil to either compress (settle) or expand (dilate), just like local hysteretic energy dissipation takes place due to inter-granular sliding of grains and, in the case of saturated soil, viscous effects. In addition, a vibrating soil–structure interface exposed to cyclic loads may eventually emit stress waves propagating in the soil towards infinity, and reflections and refractions of waves occur in layered soil. The magnitude of the damping related to the radiation phenomenon depends on the soil properties including the depth of layers and the excitation frequency.

The kinematics and mechanical behaviour of the material is typically approximated by continuum mechanics and differential calculus by which the notion of strains and stresses is introduced. Evidently, the soil material is modelled as a continuous mass rather than as discrete particles. However, on length scales, much greater than that of inter-particle distances, such models are highly accurate, and fundamental physical laws can advantageously be applied for the derivation of differential equations describing the material behaviour. In addition, local inhomogeneities in terms of the variations of the soil density and strength are of little importance to wave propagation since the wave lengths in the ground are usually much larger than the particle size—even for high frequencies and soft soil deposits. The assumption of a continuous material is therefore reasonable, and only the inhomogeneities such as layers of different soil deposits are important.

Often, the finite element method (FEM) (Bathe 1996) is applied to solve the partial differential equations with appropriate boundary conditions—especially for complex, nonlinear continuum mechanical problems with sophisticated structural geometries where several thousands DOFs may be introduced. The computational expense is, however, large and it becomes difficult from an economical point of view to use the approach for parametric studies or time-domain simulations with a long time length. To overcome this, linearity of the soil behaviour may be assumed which offers the applicability of several semi-analytical solutions for soil–structure interaction problems. In this regard, a viscoelastic soil material seems reasonable for operational conditions of offshore wind turbines since very large strains only take place in the top of the soil layer close to the foundation. Farther away, the strains are smaller, and a model including

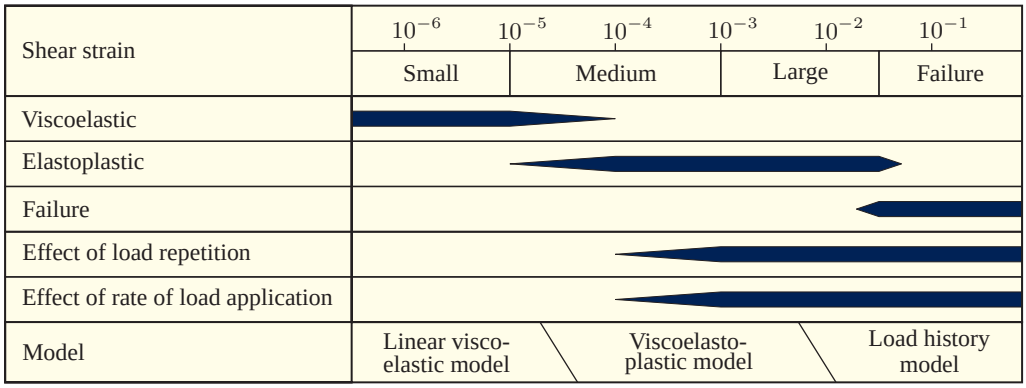

Figure 2–6 Indication of whether load repetition and rate of load application are important at different levels of soil shear strain and which kind of model that describes the soil material with sufficient accuracy. After Krätzig and Niemann (1996).

an appropriate choice of the soil shear modulus and material damping, *e.g.* in terms of a loss factor, may be sufficiently accurate, see Fig. 2–6. The same conclusion is typically drawn for the analysis of ground vibrations caused by earthquakes, trains or road traffic where the strain levels typically below about 0.001% are not large enough to induce significant nonlinear stress-strain behaviour in the soil (Bogaez 1983; Kramer 1996; Vostroukhov and Metrikine 2003).

As pointed out in the previous section, aeroelastic codes have been developed during the years ensuring a reliable and accurate estimate of the wind turbine response for a number of DOFs well-below one hundred. With the rapid increase in the computation power, a doubling of the DOFs in the aeroelastic model may be acceptable for the inclusion of the soil–structure interaction but not more so. In the following, a review of the most important analytical, numerical and experimental investigations of soil–structure interaction are given. The aim is to strengthen the knowledge on how the soil–structure interaction can be incorporated into existing aeroelastic codes by adding only few DOFs to the model.

2.3.1 Analytical and Semi-Analytical Methods

Several analytical solutions for calculating the dynamic soil–structure interaction effects, *i.e.* energy dissipation by radiation of stress waves and hysteretic actions in the supporting medium, are well established in the literature. It may not be surprising that the application of the methods lead to some loss of accuracy, and detailed information about, for instance, liquefaction of the soil is not accounted for. However, in many cases, the analytical solutions permit a good engineering approximation of the soil–structure interaction effects.

Elastic-Continuum-Type Formulations

For the elastic-continuum-type formulation approach or the impedance approach, the foundation of the structure is assumed to be rigid. The subsoil is regarded as a half-space of a linear solid which may be elastic or viscoelastic. The force-displacement relationship for each DOF (impedance function or dynamic stiffness) is frequency-dependent and complex-valued where the real part represents stiffness and the imaginary part represents damping. Since Reissner

(1936) published his work on the response of a vertically loaded cylindrical disk on an elastic half-space and revealed the existence of radiation damping, tremendous effort has been made to determine these functions for various types of foundations. Luco and Westmann (1971) applied prescribed conditions under a rigid massless surface foundation and zero traction at the remaining free surface of a homogeneous elastic half-space in order to solve the system as a mixed boundary-value problem for studying the torsional vibrations. Veletsos and Wei (1971) used a classical method for analysing coupled horizontal and rocking vibrations of a massless rigid circular foundation supported at the surface of a homogeneous linearly elastic half-space. Based on a harmonically varying horizontal force and an overturning moment, the corresponding impedance functions were derived, and stiffness and damping coefficients for an equivalent spring-dashpot system (Kelvin-Voigt model for each DOF) representing the soil–foundation system were presented. The latter were already investigated by Lysmer (1965) and Hsieh (1967) some years earlier, who discovered that the dynamic behaviour of a vertically loaded foundation could be represented by an SDOF system with frequency-dependent spring and dashpot coefficients. In addition, Lysmer (1965) also derived frequency-independent coefficients to approximate the vertical response in the low and medium frequency range. The approximation was extended by Richart and Whitman (1967), who showed that all modes of vibration could be studied by means of a lumped-parameter model consisting of few masses, springs and dashpots with frequency-independent coefficients; a model that will be discussed later in this chapter.

The described work by Luco and Westmann (1971) and Veletsos and Wei (1971) as well as research performed by Lysmer and Richart, Jr. (1966), Hall, Jr. (1967) and Shah (1968) all assumed a massless circular foundation resting on a non-dissipative elastic half-space, *i.e.* the only form of energy dissipation considered was the radiation damping. As a consequence, Veletsos and Verbic (1973) investigated the impedance functions for vertical, horizontal and rocking vibrations and their sensitivity to material damping. Both a massless circular foundation and a foundation with mass were investigated, and the dissipation of energy through material damping were modelled with respectively a linear viscous and hysteretic model. For the same type of foundation placed on an elastic isotropic homogeneous half-space, Weissmann (1973) considered torsional vibrations where the hysteretic damping of the soil was accounted for in terms of a loss coefficient. Later, Luco (1974) presented analytical solutions for a circular surface foundation on a layered stratum, *i.e.* without rigid bedrock as the last layer. An important contribution to the study of foundation vibration was presented by Wong and Luco (1985) and Luco and Mita (1987), who derived tables of horizontal, coupling, rocking, vertical and torsional impedance functions for a rigid massless square foundation and a circular foundation resting on a layered viscoelastic and a homogeneous viscoelastic half-space, respectively.

At about the same time as Weissmann (1973) published his work, Novak and Sachs (1973) obtained approximate analytical solutions for torsional and coupled vibrations involving translation, rocking and torsion (in case of the centre of gravity of the footing does not lie on the vertical geometric axis of the footing) of a cylindrical embedded footing. By applying a correction for the effect of embedment to already known solutions of foundations resting on an elastic half-space, Novak and Sachs (1973) concluded that embedment produced a drastic decrease in resonant amplitudes and a marked increase in resonant frequencies of the torsional vibrations. In addition, it could be stated that layering appeared much less important when embedment was taken into account. The latter was analysed under the assumption that the soil could be represented approximately by a set of infinitesimally thin independent horizontal layers that extended to infinity, *i.e.* a so-called dynamic Winkler model. The model will be explained in more detail later in this

chapter. With some modifications of the work performed by Novak and Sachs (1973), Avilés and Péres-Rocha (1996) presented a simplified calculation procedure for torsional impedance functions of circular foundations embedded in a soil layer with rigid base and showed, in addition, that the damping coefficient of the torsional impedance function was insensitive to the type of soil material damping (hysteretic or viscous damping). This was contrary to the stiffness coefficient where the differences among hysteretic and viscous damping increased with increasing frequency.

Work performed by Tajimi (1969), Penzien (1970) and Novak (1973) as well as Novak and Sachs (1973) formed the basis of the well-known theoretical expressions for vertical and horizontal pile vibrations given by Nogami and Novak (1976, 1977) and Novak and Nogami (1977). The key to the findings of the interaction between the vertical linear pile of circular cross section and the soil was the description of the resistance of the soil to the motion of the pile. Assuming a viscoelastic layer overlying rigid bedrock yielded that the resistance of the soil could be written as a sum of contributions from individual modes from which the response of the pile to external excitation could be predicted and the impedance functions of the pile cap established. A more detailed explanation of the method is given in Appendix A. Among others, Zania (2014) recently used the derived impedance functions for horizontal pile vibrations from Nogami and Novak (1977) and Novak and Nogami (1977) to present a rigorous semi-analytical solution of the eigenfrequency and damping ratio of an offshore wind turbine placed on a monopile that accounted for the cross coupling stiffness and damping terms of the soil–pile system.

Novak and Howell (1976) developed a theoretical and fairly simple approach to the torsional vibrations of a vertical, elastic, end bearing pile embedded in a linear viscoelastic soil accounting for dissipation of energy through radiation of elastic waves as well as material damping. Even though the proposed method did not account for slippage between pile and soil as well as the variation of shear modulus of soil with depth, the approximate linear theory still provided a good basis for the understanding of the soil-pile interaction in torsion.

The Layer-Transfer-Matrix Method

As an alternative to the rigorous elastic-continuum solutions, a semi-analytical approach may be used in which a triple Fourier transform is carried out over the horizontal spatial coordinates

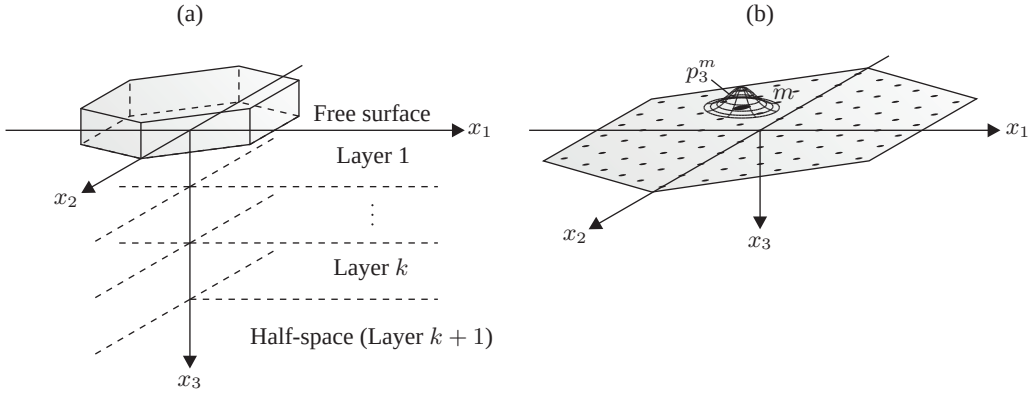

Figure 2–7 Layer-transfer-matrix model for wave propagation problems: (a) a rigid surface foundation over a layered half-space, (b) discretisation of the soil–foundation interface with a "bell-shaped" load at point m.

and time. Based on transfer matrices for a layered half-space, originally proposed by Thomson (1950) and Haskell (1953), it is possible to describe the relationship between displacements and traction at two neighbouring interfaces in the frequency-wavenumber domain where an analytical expression for the Green's function can be found. Here, it should be noted that it is assumed that the material within each individual layer is linear viscoelastic, homogeneous and isotropic. Once the solution has been established in the wavenumber domain, a transformation back into Cartesian space is readily achieved by inverse Fourier transformation. The approach has widely been used for ground response of homogeneous and layered half-spaces, see for instance work performed by Jones and Petyt (1991, 1992, 1993), Auersch (1994), Jones *et al.* (1997, 1998, 1998) and Sheng *et al.* (1999a, 1999b).

For soil–structure interaction problems, a coupling between the layer-transfer-matrix method and a numerical scheme for the structure may be used. Guan and Moore (1997) investigated the dynamic response of a reservoir-dam and its interaction with the underlying soil using a layer-transfer-matrix model for the ground and a finite element model for the dam. More recently, Andersen and Clausen (2008) investigated rigid surface foundations with arbitrary shapes on homogeneous and layered half-spaces. Modelling the contact stresses between the foundation and subsoil by a number of distributed loads around a point on the soil–foundation interface, cf. Fig. 2–7, the authors concluded that the soil stratification strongly affected the dynamic impedance functions for horizontal and rocking motions in the frequency range close to the first resonance frequency of an offshore wind turbine. The obtained impedance functions were in good agreement with a coupled boundary element/finite element (BE/FE) model and proved the main advantage of the time-efficient approach.

Simplified Ground Models

Many attempts have been made to simplify soil–structure interaction analysis by representing the continuous soil with frequency-independent models. The well-known Winkler or elastic subgrade reaction model, originally formulated by Winkler (1867), has successfully been employed during the years due to its versatility and efficiency. The stiffness characteristics of the soil–foundation system are modelled by replacing the supporting soil by a set of independent (non)linear elastic springs resting on a rigid base, *i.e.* displacements are counteracted by forces in the opposite direction. The spring stiffness is governed by the so-called p–y curves, where p and y are the resulting force per unit length in the horizontal direction and the corresponding displacement, respectively. As an example, Fig. 2–8 shows the Winkler approach for offshore wind turbine applications. Reasonable information on the low-frequency response may be obtained by the model. However, since the dissipation effects in the soil are neglected, the response amplitudes near resonance cannot be determined in a reasonable manner. Consequently, a Winkler-

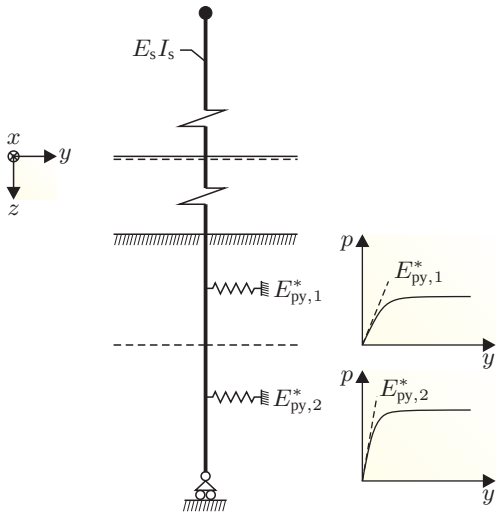

Figure 2–8 A Winkler foundation model for wind turbine applications.

Voigt model may advantageously be applied where a set of independent viscous dampers are placed in parallel with the independent elastic springs (Kelvin models along the foundation) (Kenny 1954; Achenbach and Sun 1965; Sun 2001; Sun 2002).

Following the concept, Novak (1974) analytically approximated the restraining action of the soil around a pile by a series of mutually uncoupled springs and dashpots arranged in parallel. The properties of the elements were determined by assuming that the soil could be represented by a set of infinitesimally thin independent horizontal layers of infinite extent in the horizontal plane. Evidently, it was assumed that waves in the soil only could propagate in the horizontal plane. The assumption, used first by Baranov (1967), has further been applied by Novak and Beredugo (1972), Novak (1977) and Novak and Howell (1978) as well as Novak *et al.* (1978). Novak and El-Sharnouby (1983) extended the solution presented by Novak (1974) to the case of soil properties varying with depth. To improve the realistic dynamic pile behaviour at frequencies below the fundamental frequency of the soil, Nogami and Lam (1987) introduced a coupling mechanism between two adjacent thin layers. Based on the improved approach, Nogami and Leung (1990), Nogami *et al.* (1992) and Nogami (1996) investigated the dynamic response of both piles and surface foundations. Recently, Hirai (2012) presented analytical solutions by a Winkler model approach for the analysis of single piles and pile groups subjected to vertical and lateral loads in nonhomogeneous soils. However, with the increased computational power during the years, the application of the dynamic Winkler and Winkler-Voigt models have widely been used in connection with the FEM. Section 2.3.2 provides a discussion and overview of these computational models.

Assuming that the principle of superposition is valid for soil–structure interaction, a substructure approach may serve as an alternative to the dynamic Winkler-Voigt model in which the discrete superstructure and the unbounded continuous soil are separately modelled. The approach consists of two distinct parts: 1) a determination of the impedance functions of the foundation and subsoil and 2) a formulation of the governing equations for the whole system by assembling the foundation impedance functions with the property matrices of the superstructure. However, since the complex-valued impedance functions are frequency-dependent, they cannot be used directly for time-domain analysis. Consequently, simple physical models like cone or lumped-parameter models with frequency-independent coefficients (Wolf 1994) are needed to represent the frequency-dependent stiffness of the soil–foundation system. Early works, however, usually employed representative dashpots and springs with constant values to approximate the soil system (Perelman *et al.* 1968; Parmelee *et al.* 1969; Jennings and Bielak 1973). In addition, Adhikari and Bhattacharya (2010) used a Euler-Bernoulli beam-column with elastic end supports to model a wind turbine structure. Based on static small-scale tests used to determine the translational and rotational spring coefficients, an analytical expression was derived for the first natural frequency of the wind turbine.

As indicated in Fig. 2–9a, the impedance of a rigid surface foundation with radius r_0 on an undamped homogeneous elastic half-space may be approximated by modelling the half-space as a truncated rod with its area varying as a cone. The aspect ratio z_0/r_0 is calculated by equating the static stiffness coefficient of the cone to the corresponding value of the half-space for each DOF. The main advantage of the cone model is that the complex wave pattern in the half-space with body and surface waves is replaced by a simple wave propagation governed by the shear wave velocity c_S of the conical rod. This means that the impedance functions obtained by the cone model can rigorously be represented by a discrete-element model as shown in Fig. 2–9b for the rocking DOF. The approach has been practised for both surface and embedded foundations

by Veletsos and Nair (1974), Meek and Wolf (1992a, 1992b, 1993, 1994) and Wolf and Meek (1993) as well as Jaya and Prasad (2002) and Wolf and Preisig (2003) for layered soil.

For more complicated soil–structure interaction problems, the cone model, based on rod theory (plane sections remain plane) with the corresponding one-dimensional wave propagation, may fail. Instead, a family of consistent lumped-parameter models can be applied as indicated in Fig. 2–9c. The model is chosen by arranging a few sets of connected springs, dashpots and masses with unknown frequency-independent real coefficients which are determined by minimizing the total square errors between the dynamic impedance functions of the lumped-parameter model and the exact value (for simple problems as shown in Fig. 2–9 by a closed-form solution and for more complex problems by a rigorous procedure such as the FEM, the boundary element method (BEM) or on-site measurement results). The discrete physical model leads to mass, damping and stiffness matrices of finite dimensions which makes it straightforward to couple the soil–foundation problem to the superstructure. Applications in the frequency domain as well as in the time domain are possible and hence, the model is attractive for wind turbine problems involving linear response in the ground and nonlinear behaviour of the wind turbine structure which may typically be the situation for serviceability and fatigue limit state conditions.

Several improved lumped-parameter models have been reported by Wolf and Somaini (1986), Nogami and Konagai (1986), Francisco *et al.* (1990) and Jean *et al.* (1990). All references made use of curve-fitting techniques to achieve an optimum fit between the impedance function for each DOF of the lumped-parameter model and the rigorous solution in order to determine the coefficients of the masses, dashpots and springs—in general, a complicated task since, depending on the choice of the lumped-parameter model, some of the coefficients may turn out to be complex numbers complicating the implementation of the lumped-parameter model into standard software. A straightforward choice of the lumped-parameter model that provided real coefficients was not possible to make based on the mentioned references. As a consequence, Wolf (1991a, 1991b) derived a systematic procedure of the calibration of a lumped parameter model that would ensure real coefficients. The idea was to decompose each impedance coefficient (the impedance function for each DOF normalised with the corresponding static stiffness) into a singular part equal to its asymptotic value in the high-frequency limit and a regular part. Whereas the singular part was represented by a linear function with the imaginary frequency-parameter $\mathrm{i}a_0$ leading to a discrete-element model with a spring in parallel to a dashpot, the regular part was approximated by a ratio of two polynomials (the degree of the denominator was one more than that of the

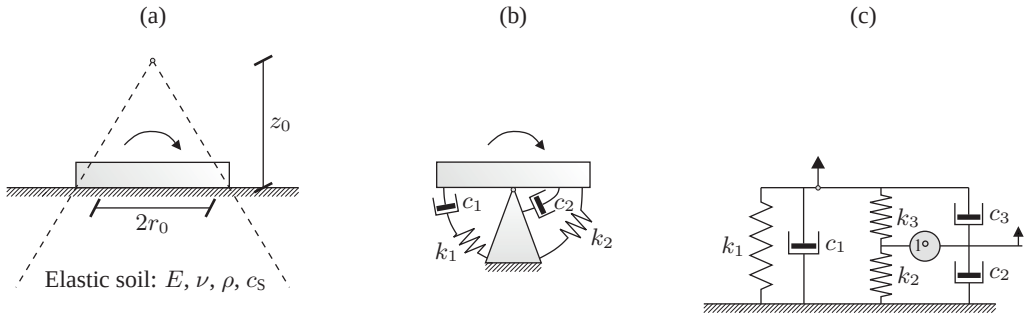

Figure 2–9 Physical models: (a) one-sided cone model for the rotational DOF, (b) discrete-element model representing the rotational cone's dynamic stiffness, (c) consistent lumped-parameter model for a translational DOF.

nominator polynomial). Using a partial-fraction expansion on the ratio of the two polynomials, the regular part of the complex valued impedance function could be expressed as the sum of few first-order and second-order partial fractions, each associated with a certain type of a fundamental discrete model. Hence, together with the discrete-element model for the singular term, a family of discrete-element models could be arranged in parallel to build the lumped-parameter model. Wolf (1997) specified in tables coefficients of the spring-dashpot-mass model for rigid surface and embedded foundations placed on and embedded in homogeneous and layered half-spaces.

Following the overall concept proposed by Wolf (1991a, 1991b), Andersen (2007, 2008) constructed consistent lumped-parameter models for a rigid surface foundation placed on homogeneous and layered grounds and concluded that the models in a reasonable manner were able to describe the geometrical damping related to free vibrations. In addition, the same author with colleagues, Andersen *et al.* (2009), formulated a consistent lumped-parameter model for a bucket foundation validated in both the frequency and time domain. Instead of using the lumped-parameter models suggested by Wolf (1991a, 1991b), Wu and Chen (2001) developed simple discrete-element models representing the horizontal, vertical, rocking and torsional vibrations of rigid foundations. Based on values of impedance functions of surface circular foundations by Veletsos and Wei (1971) as well as by Veletsos and Tang (1987) and embedded square foundations by Mita and Luco (1989), it was demonstrated that the investigated lumped-parameter models were effectively able to represent the soil–foundation system.

Instead of constructing a lumped-parameter model based on the rigorous impedance functions of a foundation, Wu and Lee (2002) made use of the flexibility formulation to express the displacement-force relationship in the frequency domain. They represented the dynamic flexibility function of the foundation with a ratio of two polynomials and used a partial-fraction expansion to design two discrete-element models corresponding to the partial fractions. A connection of the basic units in series led to lumped-parameter models that excellently were able to duplicate the rigorous dynamic impedance functions of circular and square foundations resting on an elastic half-space. Based on the work by Wu and Lee (2002), other nested types of systematic lumped-parameter models for unbounded soil were derived by Wu and Lee (2004) as well as by Chen and Shi (2013). For the last-mentioned, the parameters for the model were determined efficiently without lengthy optimisation analysis.

Saitoh (2011, 2012) proposed a gyro-mass lumped-parameter model consisting of springs, dashpots and gyro-mass elements. The last-mentioned generated a reaction force proportional to the relative acceleration of the nodes in which it was placed. Instead of using a discrete mass element, the benefit of using the gyro-mass element was that a more accurate representation of the complex-valued impedance functions could be obtained with few numbers of elements. More recently, Wang *et al.* (2013) presented a more sophisticated lumped-parameter model based on the complex Chebyshev polynomials. It is well-known that wiggling of the approximation outside the fitted range of frequencies for high orders of the rational filter may be a problem for the approach suggested by Wolf (1991a, 1991b). The proposed method from Wang *et al.* (2013) reduces the unexpected wiggling.

2.3.2 Numerical Methods

As an alternative to the analytical and semi-analytical approaches for the determination of the dynamic impedance functions of the soil–foundation system, numerical solutions like the FEM or the FEM coupled with the BEM can be used. The solutions allow complex foundation geome-

tries to be modelled using sophisticated material laws, just like soil–foundation separation, gap formation and other interface nonlinearities can be included in the analysis. However, it must be highlighted that such an approach is time-consuming and inadequate for parametric studies. To overcome this for embedded foundations, a Winkler type approach in an FE sense may be used.

The Finite Element Method

In case of static loading of a foundation resting on/in a soil stratum, the structure and subsoil may advantageously be discretised into a number of elements surrounded by an artificial boundary at a sufficient distance from the structure. For dynamic loading, however, the motion of the foundation emits waves propagating in all directions towards infinity. Reflections occur at the free surface of the soil and refractions arise at the interfaces between the soil layers. Hence, the artificial boundary from the static case using either Dirichlet boundary conditions (*e.g.* a fixed boundary representing a soil layer over bedrock) or Neumann boundary conditions (*e.g.* a free surface with no traction applied) is not desirable for dynamic wave propagation problems since the fictitious boundary reflects waves originating from the vibrating structure back into the discretised soil region (according to the radiation condition, no incoming waves propagating from infinity towards the structure exist). Instead so-called transmitting boundary conditions (TBCs), originally proposed by Lysmer and Kuhlemeyer (1969), should be implemented for simulating outward radiation of energy. In general, the boundary conditions can be local or global in time and space. The global TBCs provide high accuracy, but computationally this is a very expensive solution. Consequently, the local TBCs are the most efficient ones from a computational point of view. Different ways of formulating absorbing boundary conditions for FEM computations of infinite domains have been presented in the literature, see for instance Bamberger *et al.* (1988), Kim *et al.* (1996), Krenk *et al.* (1999), Semblat and Broist (2000), Kellezi (2000) and Krenk and Kirkegaard (2001). Alternatively, semi-infinite elements can be applied, see for instance Dassault Systèmes Simulia Corp (2012).

For soil–structure interaction problems, Wu and Finn (1997a) proposed a three-dimensional FE approach for the analysis of the dynamic response of a pile foundation embedded in an elastic medium. A simplified three-dimensional wave equation and dashpots connected to the pile shaft for taking the loss of energy due to radiation damping into account was used to describe the dynamic response of the soil–foundation system. The approach showed good agreement with full-scale low-amplitude field vibration tests as well as existing elastic solutions from Kaynia and Kausel (1982) and Novak *et al.* (1990) in terms of stiffness and damping components of the dynamic impedance functions. The same authors extended the method to the analysis of nonlinear soil response (Wu and Finn 1997b). In addition, Halabian and El Naggar (2002) used a consistent infinitesimal finite element cell method (Wolf and Song 1996) and coupled it with the FEM to analyse the vibrating behaviour of TV-towers.

Yegian and Wright (1973), Randolph (1981), Trochanis *et al.* (1991) and Achmus *et al.* (2009) used the FEM for analysing the dynamic response of pile-supported structures. The latter focussed on a monopile foundation under cyclic loading where results of drained cyclic triaxial tests on cohesionless soil were implemented into the FE program ABAQUS using a “degradation stiffness model” in conjunction with a Mohr-Coulomb failure criterion. In a similar way, Maheshwari *et al.* (2004, 2005) used a three-dimensional nonlinear FE model in conjunction with an advanced plasticity model to evaluate to what extent material nonlinearity of soil caused by strong excitation influenced the dynamic pile vibrations. Pile and soil were discretised into finite

elements, and Kelvin elements were attached along the mesh boundaries in order to model the far field conditions for allowing wave propagation. Based on a perfectly bounded connection between soil and pile, it was found that the nonlinearity of soil had significant effects on the pile response for lower and moderate frequencies of excitations.

The discretisation of soil and foundation using the FEM often comes at the cost of great computation times. A three-dimensional soil–pile interaction problem may therefore be advantageously solved by discretisation of the soil continuum into horizontal thin layers where each layer is represented by an uncoupled plane strain problem. The approach, classified as a beam on (non)linear Winkler foundation (BNWF) model, may be used in conjunction with two-dimensional FE codes. The versatile and economical approach has in the past widely been used for pile foundations that undergo large deformations, either by static loading or by moderate and strong dynamic seismic loading. The latter is obtained by adding a dashpot in parallel to the nonlinear spring element in order to account for radiation damping effect, see for instance the work presented by Matlock *et al.* (1978). Nogami *et al.* (1992), Badoni and Makris (1996) as well as El Naggar and Novak (1995, 1996) studied the lateral response of single piles to transient horizontal dynamic loading. Based on inner and far field models accounting for the soil nonlinearity and wave propagation away from the pile, reasonable agreement between the developed model and field tests was obtained.

The BNWF model has further been used by Wang *et al.* (1998) and Boulanger *et al.* (1999) where the nonlinear p–y curves consisted of elastic (p–y^{e}), plastic (p–y^{p}) and gap (p–y^{g}) components in a series together with a linear radiation dashpot in parallel with the elastic (p–y^{e}) component, see Fig. 2–10. Boulanger *et al.* (1999) used the model to analyse experimental centrifuge tests carried out by Wilson *et al.* (1997) for seismic loading on piles. The computed response was in good agreement with the measured one. The dashpot arrangement is termed "hysteretic/viscous damping" series because the hysteretic damping from the (p–y^{p}) and gap (p–y^{g}) components are in series with the viscous damping on the elastic (p–y^{e}) component. The model was also used by Memarpour *et al.* (2012), who investigated the cyclic soil–pile behaviour via ABAQUS without taking the radiation dashpot into account.

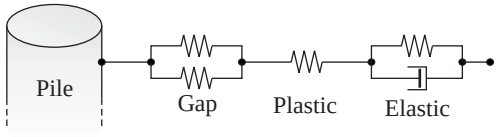

Figure 2–10 Characteristics of p–y curve components used by Wang *et al.* (1998) and Boulanger *et al.* (1999).

El Naggar *et al.* (2005) considered the elastic and plastic components in one specific nonlinear spring (p–y) in parallel with a dashpot representing linear radiation damping. However, it has been noticed that such an arrangement can lead to unrealistically large damping forces due to forces bypassing the hysteretic system (Wang *et al.* 1998). Instead of using a linear viscous dashpot for modelling the radiation damping, Badoni and Makris (1996), El Naggar and Bentley (2000) as well as Allotey and El Naggar (2008) applied a stiffness proportional nonlinear damper in parallel to the nonlinear spring where the damping constant at each time was related to the current stiffness. More recently, Kampitsis *et al.* (2013) considered the soil nonlinearity by means of hybrid spring configurations consisting of a nonlinear p–y spring connected in series to a Kelvin-Voigt element (spring-damper system). The BNWF model was adopted based on the BEM. Whereas the nonlinear spring captured the plastic soil behaviour in the near-field, the Kelvin-Voigt element represented the far-field viscoelastic characteristic of the soil. A case study was carried out on a pile-column-deck system, and the results of the proposed model were compared with a rigorous fully three-dimensional continuum FE scheme using ABAQUS. Reasonable

agreement was obtained, *i.e.* the proposed model obtained accurate results with a minimum computational time required.

Finally, it should be noted that the BNWF model in many cases has been used for probabilistic analysis of dynamic pile response and its sensitivity to the inherent random variations of soil properties. Among others, Ruiz (1984), Folse (1989), Tandjiria *et al.* (2000) and Low *et al.* (2001) as well as Carswell *et al.* (2013) used random nonlinear p–y curves for analysing the lateral response of piles. Andersen *et al.* (2012) used the BNWF model with the purpose of identifying the variation of the first natural frequency of a wind turbine due to random variation of the soil properties, whereas Fenton and Griffiths (2007) used bilinear soil springs to prove the dependency between soil variability and ultimate load statistics of a pile.

Coupled Boundary and Finite Element Method

As earlier mentioned, the FEM has problems for wave propagation in the soil due to the unbounded property of soils. Even though many solutions with absorbing boundary conditions exist for the FEM, they only represent numerical approximations to the problem, and the BEM becomes an attractive alternative. The basic idea of this method is to formulate the equation of motion of the unbounded domain in the form of an integral equation instead of a differential equation. Green's function (may include the influence of a free surface at a given location or take into account that the medium is stratified) is used as a weight function, and integration is then carried out over the boundary of a domain in order to find the response at each point to the applied traction and forced boundary displacements. A coupling between the BEM and the FEM may be used in order to model complex structures and correct dissipation effects in the soil, *i.e.* the advantages of both methods are combined and some of the disadvantages are eliminated, see Fig. 2–11.

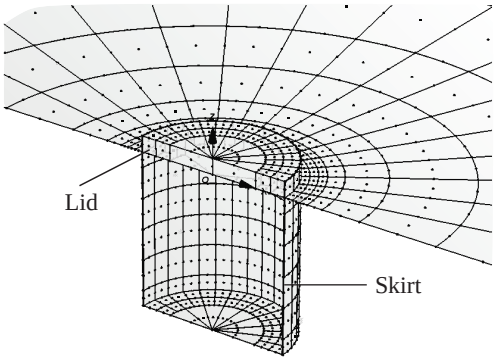

Figure 2–11 Coupled BE/FE model of a bucket foundation embedded in a homogeneous viscoelastic half-space employed by Liingaard *et al.* (2007) and Andersen *et al.* (2008).

The BEM has been applied to determine the response of rigid foundations subjected to either static or dynamic loads. Mita and Luco (1989) presented tables of impedance functions for a rigid embedded square foundation in a homogeneous elastic half-space for vertical, torsional, horizontal, rocking and coupling terms. Qian *et al.* (1998) and Karabalis and Mohammadi (1998) as well as Rizos (2000) and Pyl *et al.* (2003) used the BEM based on the Green's function for homogeneous and layered viscoelastic half-spaces to investigate the impedance functions of rigid massless circular surface and embedded foundations. Likewise, Ahmad and Rupani (1999) made an extensive parametric study on the horizontal impedance function of a rigid square foundation resting on or embedded in an elastic soil layer overlying an elastic half-space. The conclusion was that the horizontal impedance was strongly affected by the ratio of shear wave velocities, the thickness of the top layer, the depth of embedment and the degree of contact between the footing-sidewall and the soil.

Among others, the FEM–BEM in the time domain has been employed by von Estorff (1991)

for the analysis of linear interaction between elastic blocks and underlying soil. von Estorff and Firuziaan (2000) carried out a similar study for nonlinear soil–structure interaction. Furthermore, Kim *et al.* (2000, 2001) and Spyrakos and Xu (2004) employed a frequency-domain BEM–FEM model to analyse the dynamic response of a surface foundation and a strip-foundation on a layered ground, respectively. Yazdchi *et al.* (1999) studied the response of dam–foundation interaction for seismic loads including the effects of pre-seismic loads such as water pressure and self weight of the dam. A similar structure was investigated by Touhei and Ohmachi (1994) and Wegner and Zhang (2001), who evaluated the natural modes of vibration of a dam–foundation system.

For different geometries of circular foundations embedded in a non-homogeneous half-space, Doherty and Deeks (2003) used a frequency-domain FE/BE approach to obtain semi-analytical stiffness coefficients for the footings subjected to vertical, horizontal, rocking and torsional loads. Tham *et al.* (1994) investigated the transient dynamic response of single piles in a layered half-space under time-dependent torque in which the pile was modelled by the FEM and the stratum by a time-domain BEM. The ratio between the shear modulus of pile and soil had a significant impact on the dynamic torsional response of the pile, whereas the pile slenderness ratio between the pile length and pile radius had a rather weak influence for values greater than 30. For a much lower slenderness ratio, Liingaard *et al.* (2007) and Andersen *et al.* (2008) evaluated the impedance functions of a bucket foundation for offshore wind turbines using the dynamic three-dimensional coupled FE/BE program BEAST (Andersen and Jones 2001), see Fig. 2–11. With a lid diameter of 10 m, a skirt thickness of 50 mm and material properties corresponding to construction steel, a sensitivity study was carried out for different skirt lengths and values of the viscoelastic soil properties of a homogeneous half-space. The skirt length highly influenced the torsional, rocking and coupled sliding-rocking impedances. In addition, it turned out that Poisson's ratio of the soil changed the magnitude and phase angle of the horizontal, rocking and coupled sliding-rocking impedances, whereas the torsional impedance function was independent of Poisson's ratio due to the fact that the torsional motion of the foundation only produced shear waves.

2.3.3 Experimental Methods

Often, small-scale experimental work is used to develop and validate theoretical models. Once the theoretical approaches are at an appropriate level of complexity capable of replicate the physical reality, they can be fine tuned to particular site-specific problems using scaling laws. The literature is rather extensive on the subject of static and dynamic soil–structure interaction problems using experimental methodologies. A number of researchers have computed experimental impedance functions directly from the response data obtained from vibration tests on small-scale foundations, *e.g.* Lin (1982), Lin and Jennings (1984) and Crouse *et al.* (1984). Using similar approaches, Novak (1970, 1985), Beredugo and Novak (1972), Novak and Howell (1978) and Verbic (1985) performed field tests and compared the response measurements with predictions from theoretical methods. Especially, Stokoe and Erden (1985) conducted controlled vibration test of surface foundation in a soil bin. Based on these measurement data, Dobry *et al.* (1986) validated simple theoretical models and determined successfully approximated natural frequencies and damping ratios.

Regarding dynamic Winkler models, various laboratory and centrifuge cyclic and seismic soil–structure interaction experiments have been conducted by, among others, Yan (1990), Gohl

(1991), Dou and Byrne (1996) and Meymand (1998). Overall, the tests showed that the pile response due to horizontal loading was governed by many interaction factors that a dynamic Winkler model, dependent on the problem in question, should account for, *e.g.* cyclic soil degradation/hardening, soil and structural yielding, gap development as well as material and geometrical damping. The cyclic behaviour of rigid piles subjected to lateral loading has been investigated by Leblanc *et al.* (2010, 2010), Sørensen *et al.* (2012) and Sørensen and Ibsen (2012) using small-scale tests at normal stress level. Romo and Ovando-Shelley (1999) proposed an experimental procedure for building dynamic p–y curves. Based on cyclic triaxial and resonant column tests used to derive stiffness-strain and damping-strain functions, p–y curve formulations for clay were established that in a simple manner took the hyperbolic functions as well as radiation damping into account. In addition, the behaviour of model piles subjected to cyclic axial loading has been thoroughly investigated during the years by the oil and gas industry as well as the offshore wind industry; the latter as a consequence of the application of piled multipod substructures for offshore wind turbines that undergo large tensile loading, see for instance the experimental cyclic work performed by Al-Douri and Poulos (1993), Le Kouby *et al.* (2004) and Tsuha *et al.* (2012).

Several formulations of p–y curves exist for sand and clay. Originally, the formulations were developed as a consequence of the oil and gas industry's expansion of offshore platforms where the soil–pile interaction became crucial to analyse. Design regulations such as API (2000) and DNV (2011) have adopted the p–y curve formulation for sand proposed by Murchison and O'Neil (1984) based on field tests presented by Cox *et al.* (1974). For soft and stiff clay, the p–y curve formulations recommended by the design regulations are based on cyclic field and laboratory tests of laterally loaded piles performed by Matlock (1970), Reese and Welch (1975) and Dunnavant and O'Neill (1989). Overall, the p–y curve formulations are based on a number

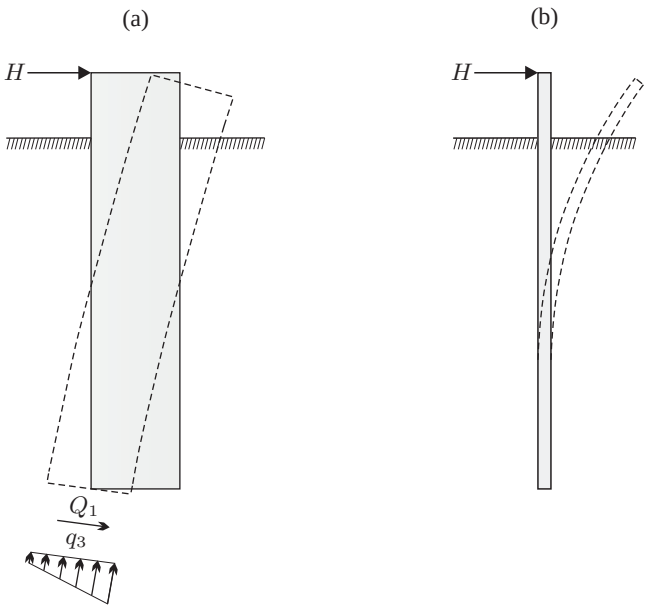

Figure 2–12 Rigid and flexible pile behaviour: (a) rigid plugged pile where forces and stresses act on the pile toe, (b) flexible pile.

of tests on fully instrumented flexible piles with significantly smaller slenderness ratio compared to offshore wind turbine monopile foundations. Several assumptions of the derivations of the formulations can be questioned. The most important ones are listed below:

- The soil is not treated as a continuum but as a series of discrete, uncoupled resistances. As a consequence, there is no rigorous description of three-dimensional failure and deformation mechanisms in the soil surrounding the pile.
- The p–y curve formulations were originally developed and verified for flexible piles with diameters up to 2 m. However, for offshore wind turbines, monopiles with diameters of 4–6 m exist. Hence, a pile which behaves rigidly will have a negative deflection at the pile toe. This deflection causes shearing stresses at the pile toe which increases the total lateral resistance. In addition, rotations at the pile toe will provide a moment on the pile caused by vertical stresses acting on the pile toe, see Fig. 2–12. These effects are neglected in the p–y curve formulations, and an extra horizontal spring and a rotational spring at the pile toe are therefore required for rigid piles.
- The p–y curve formulations are based on full-scale tests on piles installed in rather homogeneous soil. However, piles are often installed in a stratum.
- The initial stiffness of the p–y curves is independent of the pile diameter. Sørensen *et al.* (2010) provided an expression for the initial stiffness of sand that depended on the depth below soil surface, the pile diameter and Young's modulus of elasticity of the soil. Validated against laboratory tests, it was found that the initial stiffness of the p–y curves depended strongly on the pile diameter.

A direct application of the derived p–y curves from the above-mentioned experimental tests was performed by Damgaard *et al.* (2014). A thorough data processing of 510 free vibration

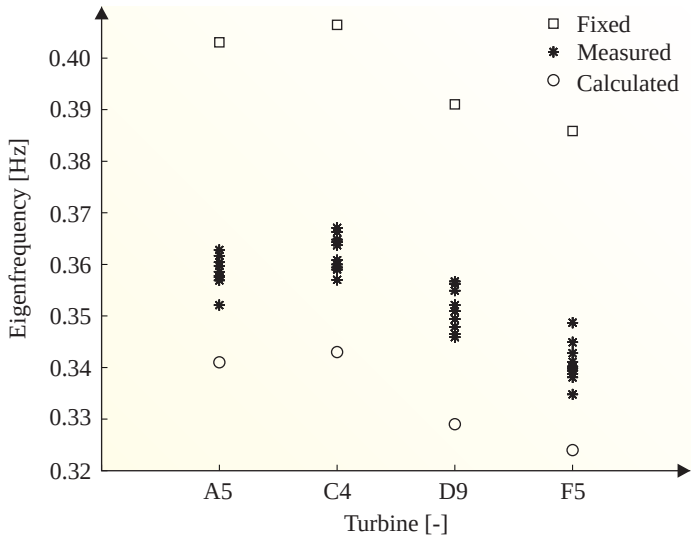

Figure 2–13 Comparison of measured and calculated undamped eigenfrequencies of offshore wind turbines founded on monopiles based on the work performed by Damgaard *et al.* (2014). The computational eigenfrequencies are based on a Winkler type approach. Calculated eigenfrequencies for fixed boundary conditions at the seabed are included.

tests on 54 offshore wind turbine structures installed on monopiles in water depths up to 30 m were performed to estimate the first eigenfrequencies of the structures and compare them with the Winkler type approach. Based on a piezocone penetration test for each wind turbine location, the authors found that the experimental eigenfrequencies systematically were higher than the corresponding calculated values, *i.e.* the minimum, mean and maximum values of the measured undamped eigenfrequencies for each turbine were 2–13% higher. Fig. 2–13 shows the results from Damgaard *et al.* (2014) for four wind turbines.

Recently, Bhattacharya and Adhikari (2011) and Lombardi *et al.* (2013) investigated the frequency response of a scaled wind turbine installed on a monopile foundation for a series of 1-g laboratory tests with different soil conditions. A simple computational model of the dynamic system with uncoupled springs at the seabed was established, and the eigenfrequency related to the lowest eigenmode was evaluated and successfully compared with the measured results. For a similar test set-up, Bhattacharya *et al.* (2013) demonstrated that the natural frequency of a wind turbine installed on monopile or tripod shifted with cycles of loading due to stiffening or softening of the foundation system.

CHAPTER 3
Scope of the Thesis

As pointed out in the previous chapter, several semi-analytical, numerical and experimental methods have been proposed in the literature for the analysis of soil–structure interaction as well as transient response of offshore wind turbines. To the best of the author's belief, however, the coupling between the wind turbine response and the subsoil has, to a great extent, been neglected or miscalculated—primarily in lack of field investigations and application of soil models that are inappropriate for offshore wind turbine foundations. This chapter explains the overall aim and specific objectives of the current PhD thesis based on the literature review from Chapter 2. The main focus of the research project as well as its novelty and contribution to the offshore wind industry are highlighted.

3.1 Main Findings of State-of-the-Art

In general, the conventional design of offshore wind turbines and their support structure requires the involvement of two parties: the foundation designer and the wind turbine manufacturer that in a close cooperation should ensure that the designed structures are in accordance with the limit states defined by the design regulations. The design procedure is sketched in Fig. 3–1. Based on the interpretation of site specific geotechnical in situ tests as well as aerodynamic and hydrodynamic field tests, the wind turbine manufacturer creates an initial design of the wind turbine tower and delivers the initial wind turbine loads to the foundation designer that comes up with an initial foundation design. Subsequently, an iterative process is started where the coupled dynamic response of the wind turbine structure for several thousands load cases is analysed by a sequential approach using system reduction or a fully coupled approach. For each iteration, the section forces of the tower and foundation are checked and the geometry is updated until a satisfactory design is found. In order to keep computation times acceptable for the retrieval run, three-dimensional Bernoulli-Euler or Timoshenko beam theories are commonly used to model piled foundations. Advanced wave load calculation tools apply these theories, and as such sophisticated three-dimensional continuum finite element models of the foundation and secondary steel including hydrodynamic effects fail from a computational time-efficient point of view.

Prior to the iterative design process, as indicated in Fig. 3–1, it must be ensured that the numerical approach of modelling the wind turbine and foundation captures the dynamic effects in a reasonable manner, *i.e.* system stiffness and damping as well as external and operational loads should reflect the reality as close as possible. Therefore, a verification of the modelling approach and, if necessary, model updating are needed by comparing the modal properties and dynamic loads of already existing offshore wind turbines with the applied computational modelling procedure. In this regard, free vibration tests and operational modal identification may be applied

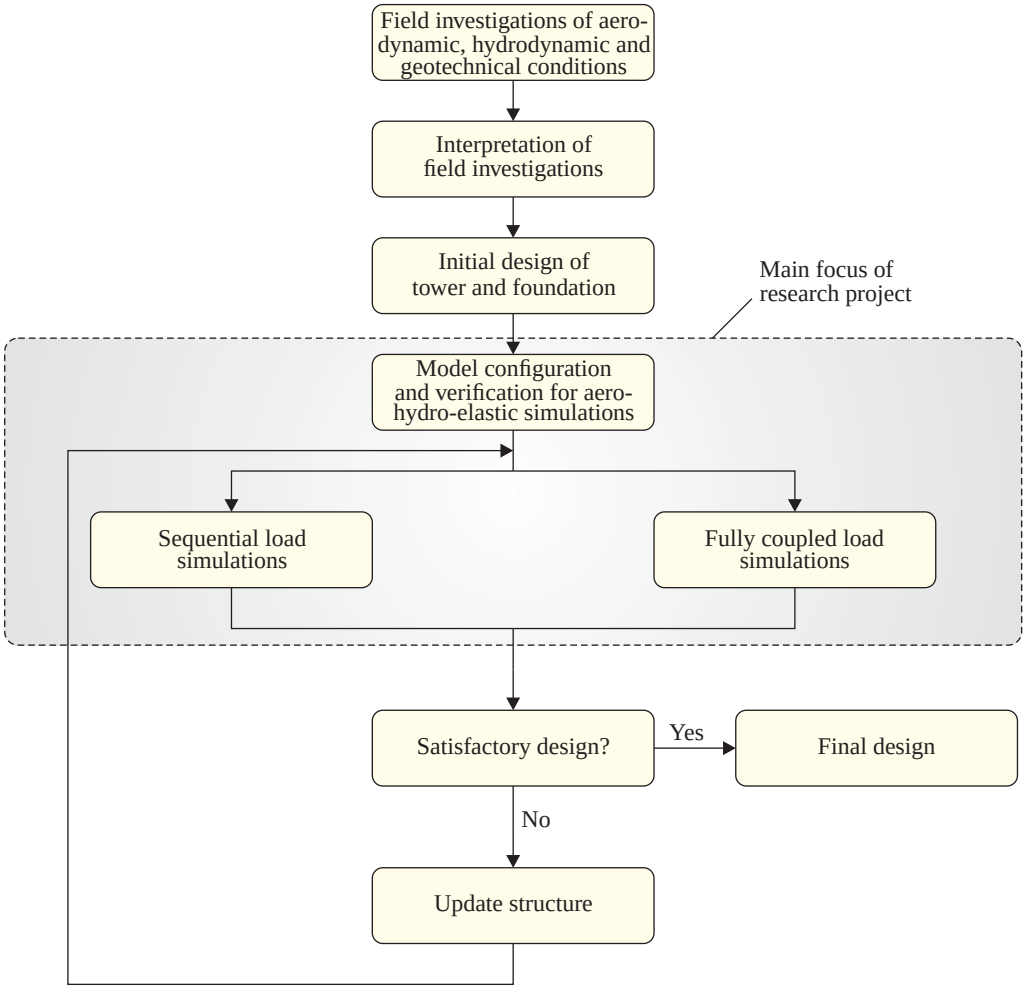

Figure 3–1 Conventional design of offshore wind turbines. The shaded area indicates the main focus of the current research project.

advantageously for the determination of inherent modal parameters related to the offshore wind turbine structure for stand-still and operational conditions, although the latter violates the general requirement of a time-invariant structure during testing. The model verification is highly important for offshore wind turbine sites characterised with a high degree of misalignment between wind and wave directions since the cross-wind fatigue in this situation typically is increased notably compared to the along-wind fatigue. Eigenfrequencies close to wave excitation and low system damping in the cross-wind direction cause this tendency and hence, the soil–foundation interaction becomes crucial to consider since it modifies the system stiffness and dissipates energy through wave propagation and material damping.

The usual method for including the soil–structure interaction for offshore wind turbines is the Winkler type approach with p–y and t–z curves recommended and described by the design regu-

lations where the energy dissipation effects typically are incorporated via modal-based Rayleigh damping. However, several limitations and drawbacks of using the method for offshore foundations exist; the most important ones are that the p–y curves are calibrated for long slender piles which is in contrast to large monopiles defined by a small length-to-diameter ratio, that the p–y and t–z curves do not account for dynamic stiffness due to inertia forces and that the approach does not provide a well-defined representation of dissipation effects in the soil. Even though the method can be modified using a Winkler-Voigt approach with a set of independent viscous dampers placed in parallel with the independent springs, it requires knowledge of hysteretic and radiation damping in the soil prior to the simulation that complicates the calibration of the viscous dashpots, not least because a strong disagreement of the level of soil damping for offshore wind turbine problems can be found in the literature.

On the other hand, dynamic frequency-dependent impedance functions of the soil–foundation system, where the imaginary part represents the combination of hysteretic and radiation damping, can be determined by semi-analytical, viscoelastic-continuum-type formulations as well as rigorous boundary element or finite element models with transmitting boundary conditions. But such models are, in general, difficult to incorporate directly for time-domain analyses of offshore wind turbines. To overcome this problem, a consistent lumped-parameter model may be useful, capable of reproducing the dynamic impedance functions of the soil–foundation system based on fitting procedures. However, only few attempts of using the approach are present in the literature for simplified wind turbine structures that neglect aeroelastic effects, and the calibration and implementation of a lumped-parameter model into aeroelastic wind turbine codes have so far not been employed.

3.2 Aim and Objectives

During the years, the number of installed offshore wind turbines has increased exponentially due to inevitably growing energy demands. The design of more efficient and higher capacity wind turbines with larger rotor diameters and hub heights results in a complicated dynamic interaction between different parts of the turbine and the surrounding environment. Understanding these dynamic interrelation effects and response characteristics are essential for optimising the energy produced and ensuring safe as well as reliable operation.

The aim of the present PhD project is to improve the knowledge of the dynamic behaviour of offshore wind turbines and their interaction with the subsoil and thereby allowing a reliable structural design of the wind turbine and foundation. It is believed that (a) modal parameters of offshore wind turbines change during the structural design life, mainly driven by the soil–structure interaction that consequently influences the dynamic wind turbine response, (b) the magnitude of modal damping related to the lowest eigenmode for standstill and normal operating offshore wind turbines differ significantly since the contribution of aerodynamic damping and soil damping is different for the two situations and, finally, (c) the loads of offshore wind turbines are estimated incorrectly if the soil–structure interaction is neglected. An improved solution can be ensured advantageously by couple consistent lumped-parameter models with aeroelastic wind turbine codes. With the hypotheses in mind, the specific objectives of the study have been categorised as follows:

- Evaluate to what extent inherent natural frequencies and damping ratios of offshore wind turbines are time-dependent and influenced by the soil–structure interaction based on “rotor-

stop" tests, simple numerical quasi-static approaches including the Winkler type formulation and aeroelastic wind turbine simulations.

- Provide valid damping estimations of offshore wind turbines and evaluate the expected amount of soil damping for standstill and operating wind turbines based on "rotor-stop" tests and operational modal analysis using frequency- and time-domain identification techniques.
- Develop a widely applicable approach for including the dynamic interrelation effect between foundation and subsoil into aeroelastic wind turbine codes that advantageously accounts for dissipation effects in the soil based on a substructure methodology.
- Identify to what extent the soil–structure interaction influences the fatigue loading of offshore wind turbines based on deterministic and stochastic soil properties using a fully coupled aero-hydro-elastic approach.

From a structural design point of view, the main focus of the present research project is indicated in Fig. 3–1. To the author's knowledge, few field tests of the dynamic behaviour of offshore wind turbines are available and consequently, the present study contributes with experimental test results that can be used by the foundation designer and wind turbine manufacturer as well as the academic researcher for model calibration and benchmarking. In addition, the development of a novel and computationally efficient time-domain approach, useful for sequential or fully coupled aero-hydro-elastic simulations, may seem attractive for the offshore wind industry, just like the PhD thesis in general quantifies and highlights the importance of including soil–structure interaction for dynamic offshore wind turbine problems. In conclusion, the following aspects of the present theory and analyses may be regarded as novel:

1. a detailed full-scale experimental study of time-varying dynamic properties in terms of eigenfrequencies and damping ratios of offshore wind turbines for several wind parks,
2. an estimation of soil damping for standstill and normal operating wind turbine conditions based on full-scale testing and numerical approaches,
3. the implementation of a consistent lumped-parameter model into aeroelastic wind turbine simulation codes accounting for the dynamic soil–structure interaction for gravity and monopile supported structures,
4. a detailed parameter study of the soil–structure interaction and its influence on the modal properties and fatigue loads of offshore wind turbines based on a deterministic approach,
5. the application of a Monte Carlo method that accounts for the uncertainty of soil properties facilitating the derivation of the probability densities of the modal properties and the fatigue loading of offshore wind turbines.

CHAPTER 4
Summary of Included Papers

The current research project is based on seven scientific peer-reviewed papers, including six journal papers and one conference paper that can be found in the enclosed appendices. The papers comply with the listed objectives of the PhD project covering experimental and numerical investigations of the dynamic response of offshore wind turbines and their interaction with the soil. In the following chapter, the major outcome of the articles is given including background, rationale and methodology.

4.1 Overview of Publications

As already stated in the preface, the PhD thesis has been divided into two research parts and reported in seven scientific papers, cf. Fig. 4–1. Part I focusses on the cross-wind modal properties of offshore wind turbines based on full-scale testing and numerical methods. “Rotor-stop” tests and operational modal analysis on offshore wind turbines are used to evaluate natural frequencies and damping ratios of the structures and identify their time-dependency supported by simple

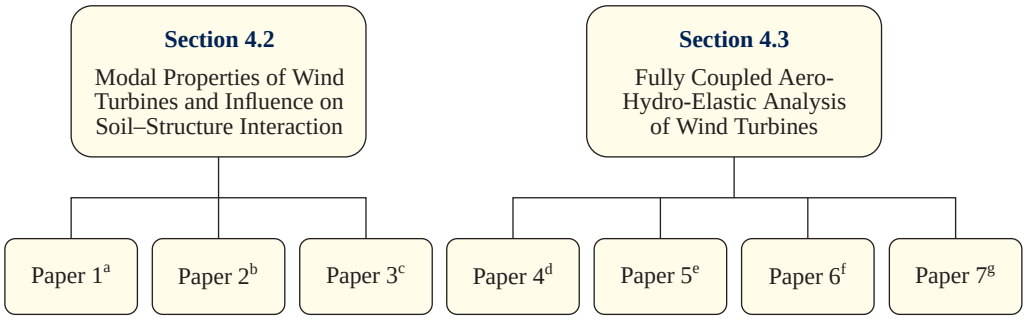

a) *Cross-wind modal properties of offshore wind turbines identified by full scale testing*
b) *Damping estimation of a prototype bucket foundation for offshore wind turbines identified by full scale testing*
c) *Assessment of dynamic substructuring of a wind turbine foundation applicable for aeroelastic simulations*
d) *Computationally efficient modelling of dynamic soil–structure interaction of offshore wind turbines on gravity footings*
e) *Effects of soil–structure interaction on real time dynamic response of offshore wind turbines on monopiles*
f) *Dynamic response sensitivity of an offshore wind turbine: A fully coupled time-domain approach for varying subsoil conditions*
g) *A probabilistic analysis of the dynamic response of monopile foundations: Soil variability and its consequences*

Figure 4–1 Overview of research topics and scientific papers.

numerical approaches. Conservative estimates of the soil damping contribution for standstill and normal operational conditions are stated, just like modal updating is conducted. Part II presents a computationally efficient modelling approach of including the dynamic soil–structure interaction into wind turbine simulations codes. The approach is used to evaluate to what extent the soil–structure interaction influences the vibration characteristics of offshore wind turbines.

4.2 Modal Properties of Wind Turbines and Influence of Soil–Structure Interaction

Recently, offshore wind turbine towers and blades have increased significantly in height and length, respectively, with only a small increase in weight. Therefore, the dynamic response of the wind turbine structure occurs in a frequency range close to the excitation frequencies related to environmental and structural harmonic loads. In this context, sufficient geometrical and material damping in the structure and soil are required to counteract large amplitudes of vibration. Especially for wind parks characterised by a large degree of wind-wave misalignment, a proper estimate of the eigenfrequency and inherent damping is needed due to low aerodynamic forces in the rotor plane. Aeroelastic wind turbine simulations should reflect these modal properties in a reasonable manner in order to obtain reliable and safe designs.

The purpose of Part I is to investigate cross-wind modal properties of offshore wind turbines and identify to what extent they are influenced by the subsoil—an issue that so far not has been investigated in sufficient detail. A total of three scientific papers has been published for this part in which the dynamic modal properties of wind turbines installed on monopiles, buckets and gravity base foundations are investigated. The latter is compared with aeroelastic simulations using a simple foundation model. The most important findings of each paper are given below.

4.2.1 Paper 1

Published in *Journal of Wind Engineering and Industrial Aerodynamics*, Volume 116, August 2013, Pages 94–108, DOI: 10.1016/j.jweia.2013.03.003.

Paper 1: “Cross-wind modal properties of offshore wind turbines identified by full scale testing” presents a thorough investigation of more than 1500 “rotor-stop” tests performed on Vestas V90-3.0 MW offshore wind turbines installed on monopile foundations. During each test, an oil damper placed in the top of the tower is active. A total of four wind parks are analysed, all characterised by mean water depths in the interval 6–20 m with respect to the lowest astronomical tide (LAT) and soil profiles consisting of cohesionless soil in the top layers followed by cohesive soils. Based on two accelerometers placed in the nacelle, the eigenfrequency and modal damping of each wind turbine are experimentally estimated from the acceleration decay when the turbine generator shuts down and the blades pitch out of the wind. The experimental results are compared with a Winkler-Voigt model where the soil–structure interaction is taken into account by Kelvin-Voigt elements along the monopile. The paper further analyses side-side acceleration signals for operating wind turbines in order to determine the cross-wind modal damping for normal operating conditions by fitting theoretical energy spectra to the measured response spectra.

Main Results

The following main findings from *Paper 1* can be stated:

- Even though wind turbines are characterised by closely spaced modes occurring at nearly identical frequencies, "rotor-stop" tests can be efficiently applied for the determination of inherent modal properties of wind turbine structures. Based on more than 1500 tests for four wind parks, reliable and similar quantiles of the modal damping related to the lowest eigenmode are observed for each wind park. A 5% quantile in the range 0.09–0.11 logarithmic decrement is found for each wind park which corresponds very well with the findings for each considered turbine.
- Eliminating the tower damper performance tends to reduce the large variation of the modal parameters. However, distinctly time-dependent eigenfrequencies and modal damping ratios are still obtained—even for ideal fits, cf. Fig. 4–2. Based on a selected wind turbine, a Winkler-Voigt model concludes that the observed time-dependent modal properties might be caused by sediment transportation at seabed. Scour development and backfilling change the eigenfrequency with 8%, and the modal soil damping varies in the range 0.05–0.08 logarithmic decrement according to Fig. 4–3.
- Spectral analysis on cross-wind accelerations during normal wind turbine operations shows

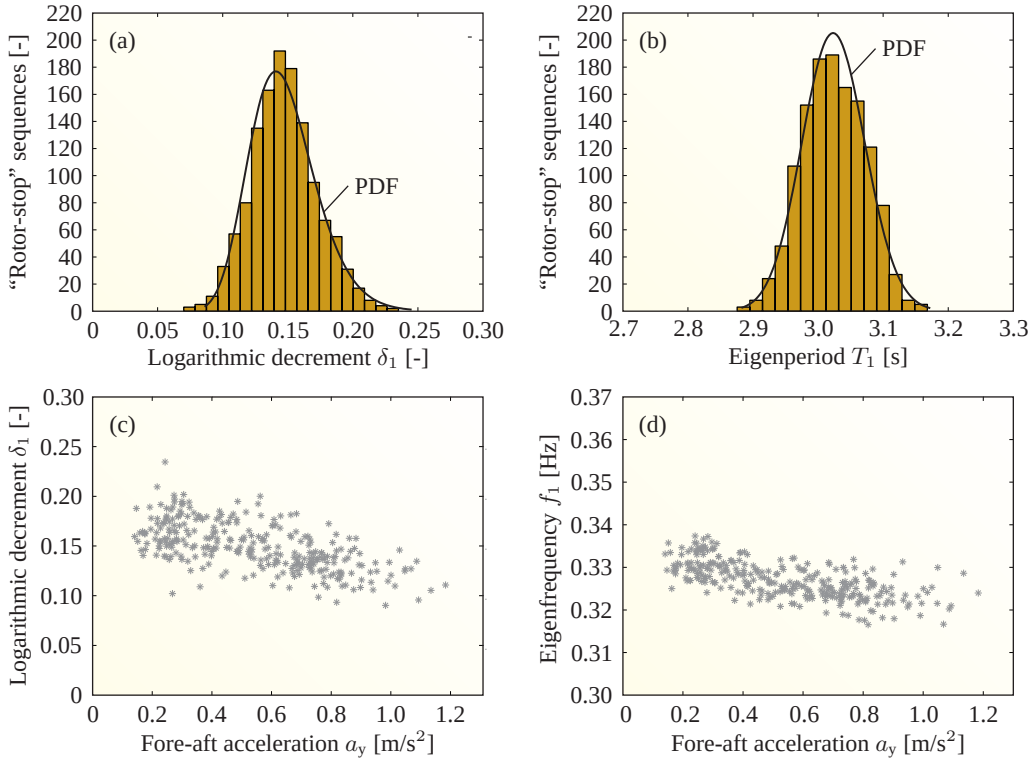

Figure 4–2 *Paper 1* — "Rotor-stop" tests for a wind park with a total of 30 offshore wind turbines: (a) and (b) damping and eigenperiod histograms, (c) and (d) damping δ_1 and eigenfrequency f_1 vs. acceleration level a_y.

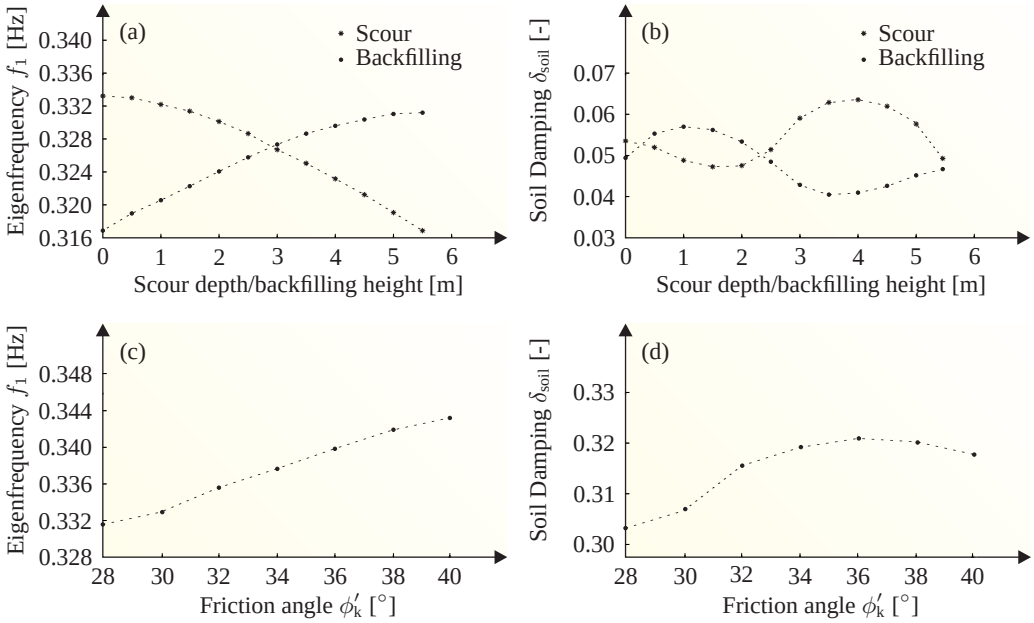

Figure 4–3 *Paper 1* — Scour and backfilling analysis based on a Winkler-Voigt foundation model: (a) and (b) eigenfrequency f_1 and soil damping δ_{soil} vs. scour depth/backfilling height, (c) and (d) eigenfrequency f_1 and soil damping δ_{soil} vs. friction angle ϕ'_k of backfill material.

a mean value of the modal damping in the range of 0.16–0.18 logarithmic decrement which corresponds very well to the mean damping values from the "rotor-stop" tests. The agreement is believed to be caused by the fact that higher aerodynamic damping and lower soil damping contributions are present during normal wind turbine operations.

4.2.2 Paper 2

Published in *5th International Operational Modal Analysis Conference*, May 2013, Guimarães, Portugal, Pages 1–11.

Paper 2: "Damping estimation of a prototype bucket foundation for offshore wind turbines identified by full scale testing" deals with ambient vibration and "rotor-stop" tests performed on a Vestas V90-3.0 MW offshore wind turbine installed on a prototype bucket foundation. The diameter of the bucket is 12 m and the skirt length is 6 m. The wind turbine structure is located in a water basin with 4 m water depth, and the soil profile consists primarily of cohesionless soils. Based on a monitoring system consisting of 15 accelerometers placed along the foundation and tower, the cross-wind damping related to the lowest eigenmode for standstill and operational conditions is evaluated. The latter is determined by three different approaches in order to obtain valid cross-wind modal damping values: the Enhanced Frequency Domain Decomposition (EFDD) technique and the Stochastic Subspace Identification (SSI) technique with an Unweighted Principal Component (UPC) and a Weighted Principal Component (PC) algorithm. A total of 100 ambient vibration tests are investigated, each with a time duration of two

hours including low standard deviations for wind speeds and rotor rates in order to improve the assumption of a time-invariant system and reduce leakage introduced by Fourier transformation.

Main Results

The following main findings from *Paper 2* can be stated:

- Frequency- and time-domain operational modal identification techniques provide useful damping results—especially for the SSI algorithms where excellent agreement between modelled and measured auto-spectra is observed.
- Independent of the operational modal identification technique, the cross-wind modal damping during wind turbine operations reaches an extreme value of approximately 0.05 logarithmic decrement at rated wind speed. For higher wind speeds, the damping slightly decreases as indicated in Fig. 4–4. The phenomenon may be caused by coupling effects between the closely spaced fore-aft and side-side mode shapes that occur a nearly identical frequencies which lead to transferring of vibrational energy from the highest to the lowest damped mode. Since the blade pitch angle increases drastically for wind speeds higher than rated wind speed, the damping related to the fore-aft mode as well as the side-side mode is reduced.
- Assuming that the hydrodynamic and aeroelastic damping have negligible impact on the measured damping during "rotor-stop" tests performed on the wind turbine installed in 4 m water depth, the soil damping is found to be in the range of 0.004–0.04 logarithmic decrement

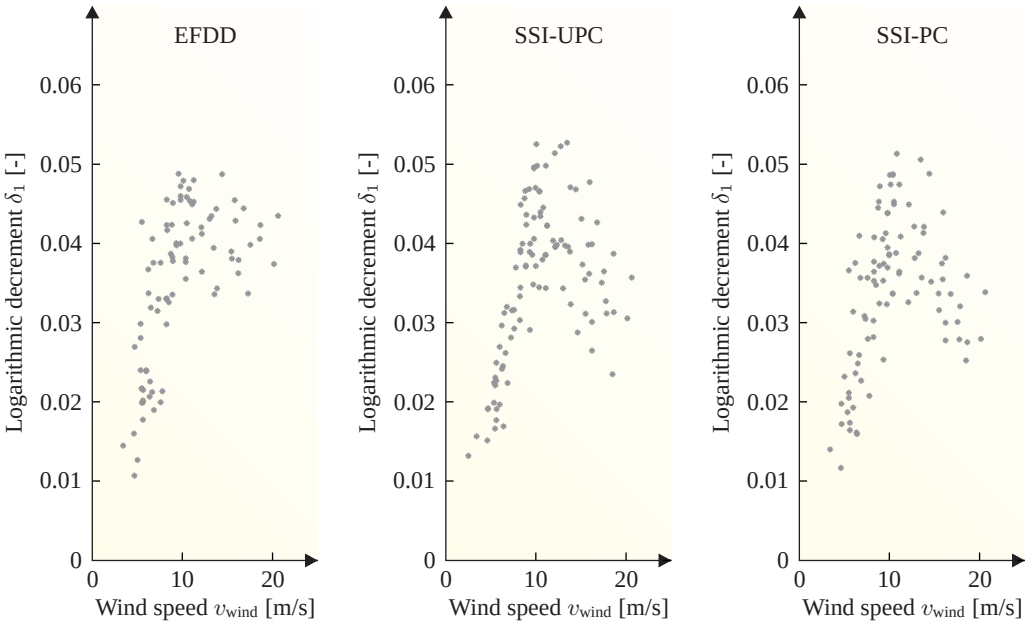

Figure 4–4 *Paper 2* — Cross-wind modal damping δ_1 vs. mean wind speed v_{wind} for ambient vibration tests performed on an offshore wind turbine installed on a bucket foundation. The Enhanced Frequency Domain Decomposition (EFDD) technique and the Stochastic Subspace Identification technique (SSI) with Unweighted Principal Component (UPC) and Weighted Principal Component (PC) algorithms are used to identify the modal damping.

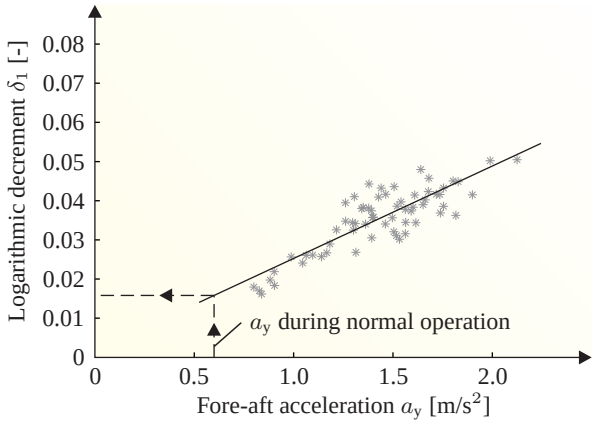

Figure 4–5 *Paper 2* — Cross-wind modal damping δ_1 vs, fore-aft acceleration a_y based on "rotor-stop" tests performed on an offshore wind turbine installed on a bucket foundation. Expected maximum soil damping during normal wind turbine operations is indicated by the dashed line.

proportional to the acceleration range 0.8–2.1 m/s^2. The acceleration range during normal operation is much lower, about 0.02–0.6 m/s^2. With this in mind, Fig. 4–5 shows the damping estimations of the 67 "rotor-stop" tests that mainly is driven by steel hysteretic damping and soil damping. The expected maximum acceleration level during normal wind turbine operations is indicated in Fig. 4–5 and hence, a rough estimate of the expected soil damping during power production is found to 0.01 logarithmic decrement for the considered bucket foundation.

4.2.3 Paper 3

Published in *Wind Energy*, May 2014, Early view, DOI: 10.1002/we.1763.

Paper 3: "Assessment of dynamic substructuring of a wind turbine foundation applicable for aeroelastic simulations" considers full-scale testing performed on a Vestas V112-3.3 MW onshore wind turbine installed on an octahedral surface foundation. The aim of the article is to verify to what extent a simple substructure approach for including the dynamic soil–structure interaction into aeroelastic simulations is able to reproduce the measured dissipation effects. Geotechnical field tests at the site show that the soil profile consists of cohesionless soils from the surface down to a great depth, and a standard lumped-parameter model calibrated to a rigorous model based on transfer matrices for a homogeneous half-space may therefore seem sufficient to represent the soil–structure interaction, not least because the lowest eigenmode only is of interest in this paper. The standard lumped-parameter model is implemented into the aeroelastic tool FLEX5 where simulated "rotor-stop" tests and ambient vibration tests are compared with measurements. Analysing the free vibration decays and using a Stochastic Subspace Identification technique with an Unweighted Principal Component algorithm makes it possible to evaluate the measured and simulated cross-wind modal damping for situations with the inclusion and exclusion of an oil damper placed in the top of the tower.

Main Results

The main findings from *Paper 3* are as follow:

- A standard lumped-parameter model based on a rigorous approach using transfer matrices for a homogeneous, linear viscoelastic half-space verified against a three-dimensional coupled boundary element/finite element approach, is able to predict the dynamic impedance functions of a surface foundation in the frequency range 0–3 Hz since no resonance in the soil layer takes place. It is found that the static stiffness matrix derived by the lumped-parameter model is in reasonable agreement with the one obtained by a Guyan reduction scheme.

- Using different loss factors of the soil, it is concluded that FLEX5 "rotor-stop" tests with the implementation of a lumped-parameter model calibrated with a loss factor of 0.01 for the soil produce cross-wind modal damping values that correspond well with full-scale test results, cf. Fig. 4–6. Same agreement is obtained for the ambient vibration tests indicated in Fig. 4–7 that show higher cross-wind damping than the "rotor-stop" tests. This is mainly due to higher aerodynamic damping during normal wind turbine operations as well as the fact that vibrational effects of an onshore wind turbine installed on a surface foundation, in general, lead to low geometrical and material soil damping. Even for "rotor-stop" tests that may introduce high acceleration levels in the turbine, deformations in the subsoil are small.

- The inclusion of an oil damper in the top of the Vestas V112-3.3 MW wind turbine tower provides considerable additional cross-wind modal damping for both standstill and normal wind turbine operations. In addition, using the theory of a damped two degree-of-freedom system, FLEX5 simulations with the implemented lumped-parameter model show reliable

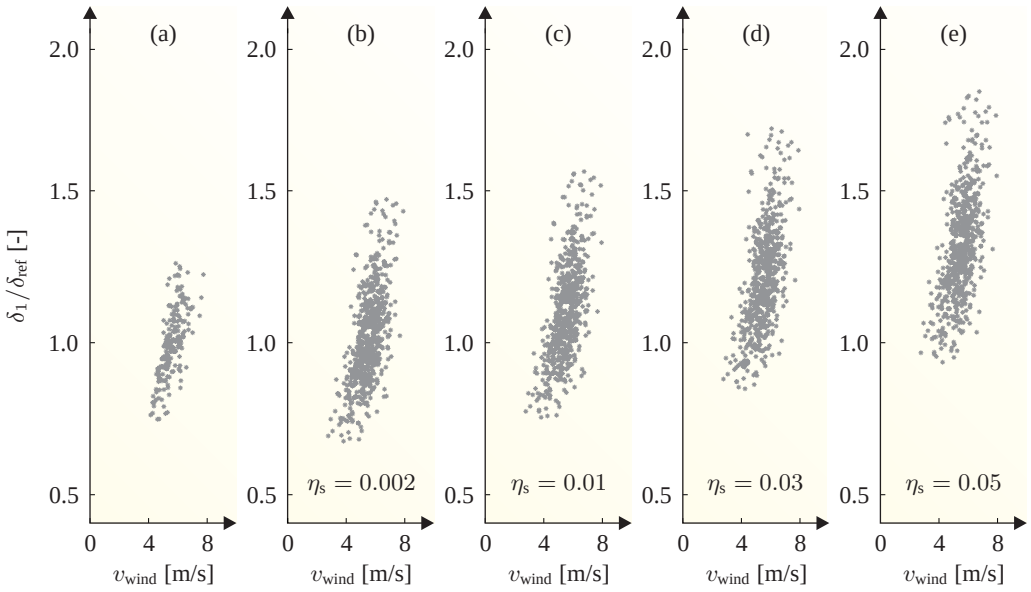

Figure 4–6 *Paper 3* — Normalised cross-wind modal damping $\delta_1/\delta_{\text{ref}}$ vs. mean wind speed v_{wind} based on experimental and simulated "rotor-stop" tests using FLEX5 coupled with a standard lumped-parameter model: (a) full-scale test results, (b)–(e) simulated results with different loss factor η_s of the soil.

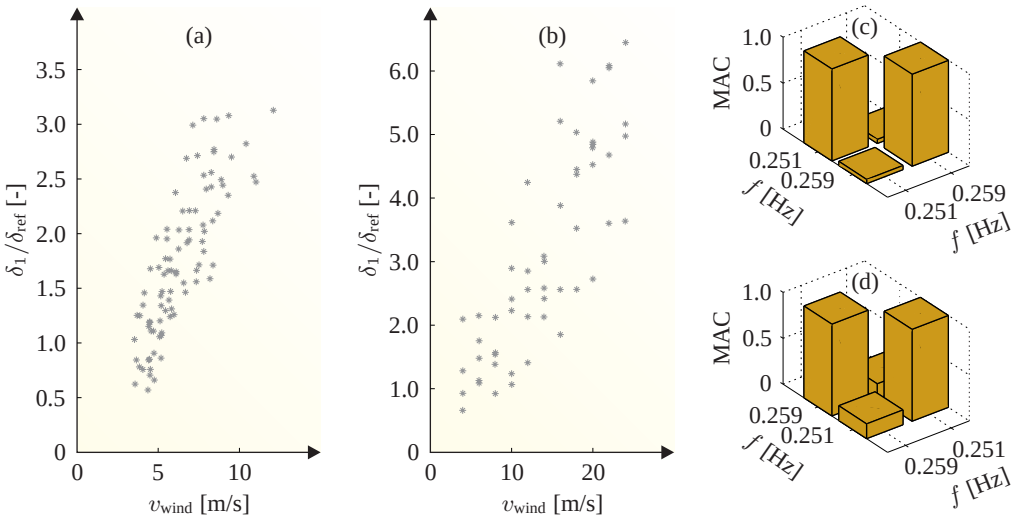

Figure 4–7 *Paper 3* — Normalised cross-wind modal damping $\delta_1/\delta_{\text{ref}}$ evaluated by operational modal analysis: (a) and (b) $\delta_1/\delta_{\text{ref}}$ vs. mean wind speed v_{wind} based on experimental and simulated data, respectively, (c) and (d) modal assurance criterion (MAC) values of the fore-aft and side-side modes based on experimental and simulated data, respectively, indicating geometrically orthogonal mode shapes.

damping results compared to measured "rotor-stop" tests with the oil damper activated, cf. Fig. 4–8.

4.3 Fully Coupled Aero-Hydro-Elastic Analysis of Wind Turbines

Offshore wind turbines are highly dynamically loaded structures that provide significant interrelation effects between the turbine and the support structure. In this regard, the impedance of the foundation must be described accurately without increasing the number of degrees of freedom in the computational model significantly since the design of wind turbines requires the computation and analysis of thousands of load cases. Hence, fully integrated models that account for the coupling effects between wind field, wind turbine, foundation and subsoil may not seem feasible. Instead, different kinds of reduction strategies can be applied for improving the numerical efficiency of the time-domain simulations and for ensuring that the foundation only adds a few additional degrees of freedom to the wind turbine model. Whereas static condensation methods or classical spatial reduction methods follow the principle of reducing the global mass, stiffness and damping matrices from a rigorous finite element model, the dynamic impedance of the foundation from a rigorous frequency-domain analysis can be formulated into a so-called consistent lumped-parameter model consisting of a few springs, dashpots and point masses which are easily implemented into aeroelastic codes for time-domain simulations of offshore wind turbines. The advantage of the formulation is that dissipation effects in the soil through wave radiation and material damping (due to the aggregation only) are accounted for by specifying a few number of viscoelastic soil properties. Although it is recognised that the shear stiffness and damping must

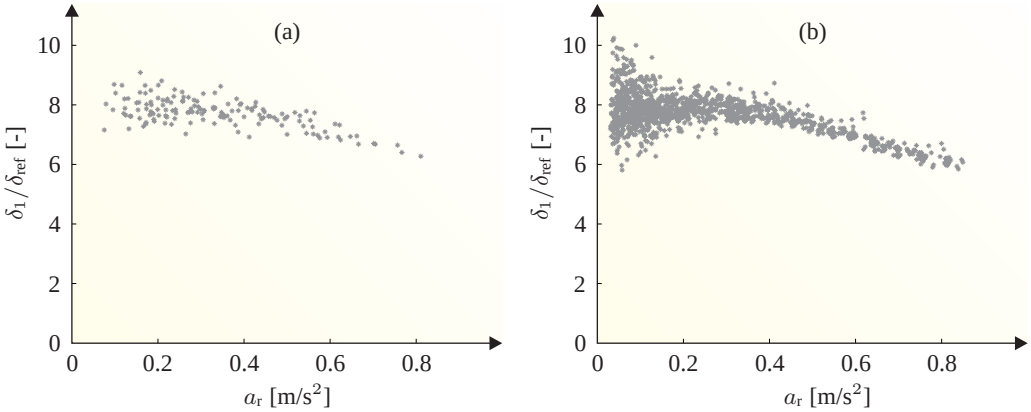

Figure 4–8 *Paper 3* — Normalised cross-wind modal damping $\delta_1/\delta_{\text{ref}}$ vs. resultant acceleration level a_{r} based on experimental and simulated "rotor-stop" tests with an oil damper installed in the wind turbine: (a) and (b) measured and simulated $\delta_1/\delta_{\text{ref}}$ vs. a_{r} based on experimental and simulated data, respectively.

be taken to decrease and increase with increasing shear strain, respectively, it may seem reasonable to select equivalent linear elastic properties, taking into account the expected magnitude of shear strain during normal wind turbine operations.

Part II deals with the formulation and quality of a consistent lumped-parameter model of offshore wind turbine foundations useful for sequential or fully coupled time-domain simulations. The goal is to develop a model that is able to capture the dissipation effects in the soil in a fast and reliable manner. This also means that special focus is put on the rigorous model that underlies the substructuring since a fast evaluation of the impedance functions of the soil–foundation system is required. Based on the developed model, it is investigated to what extent the soil–structure interaction and the soil variability influence the modal parameters and fatigue loading of offshore wind turbines. A total of four papers are included in Part II. All these papers consider the consistent lumped-parameter model. This also means that the description of the model and its applicability may be repeated in the four papers. Nevertheless, the included papers cover different aspects of Part II and contribute significantly to the thesis.

4.3.1 Paper 4

Published in *Renewable Energy*, Volume 68, August 2014, Pages 289–303, DOI: 10.1016/j.renene.2014.02.008.

Paper 4: "Computationally efficient modelling of dynamic soil–structure interaction of offshore wind turbines on gravity footings" deals with the calibration of a consistent lumped-parameter model of a rigid hexagonal surface foundation installed on homogeneous and layered half-spaces. The impedance of the foundation is determined in the frequency domain by the layer-transfer-matrix method that relies on an analytical solution for the wave propagation over depth, *i.e.* in a similar manner as described in *Paper 3* for a homogeneous half-space. For different soil stratifications, the quality of the consistent lumped-parameter model is evaluated in the frequency- and time-domain, the latter by application of a pulse load where emphasis is put on the geometrical damping related to the free vibrations of the foundation. Subsequently, the derived mass, damp-

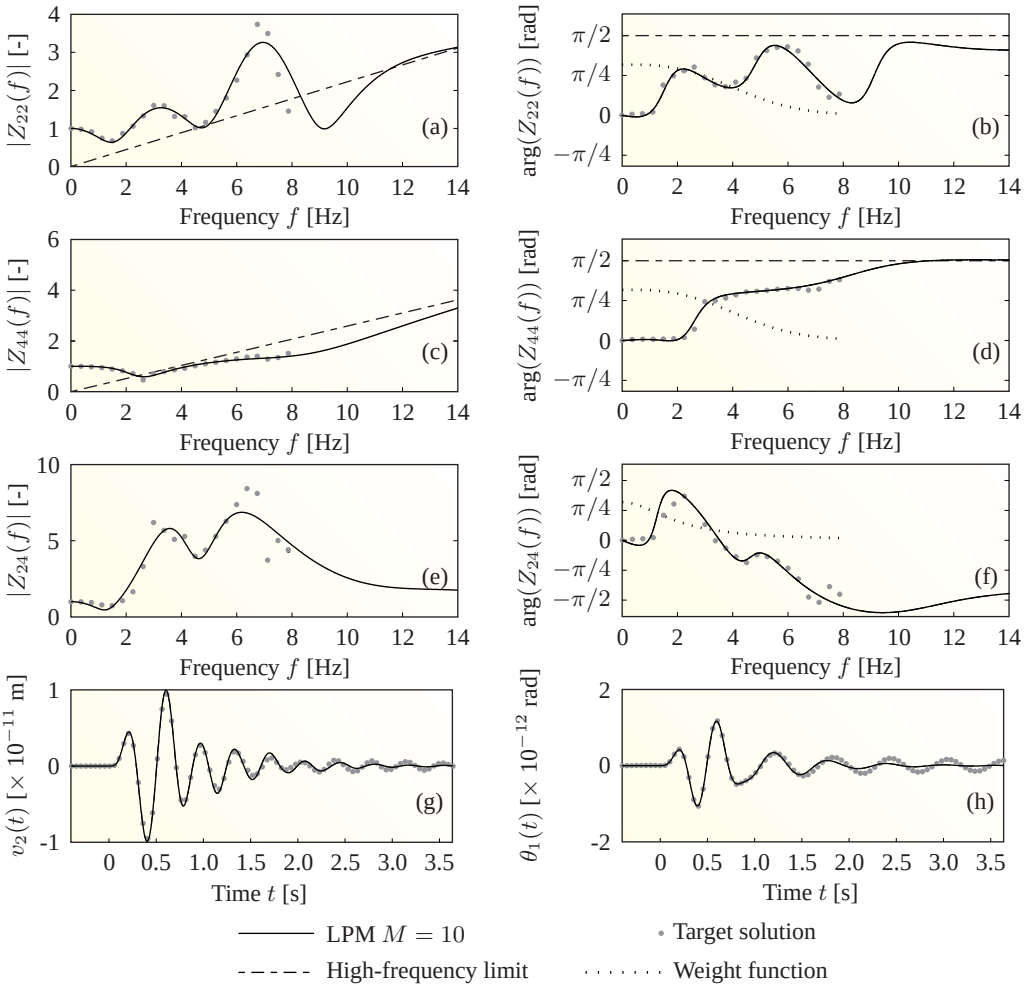

Figure 4–9 *Paper 4* — Vibration characteristics of a surface foundation on a layered half-space evaluated by a consistent lumped-parameter model and its target solution: (a)–(f) normalised dynamic horizontal and rocking as well as coupled sliding-rocking impedance functions $Z_{ij}(f)$, (g) and (h) transient response for sliding $v_2(t)$ and rocking $\theta_1(t)$ motions after the application of a pulse load.

ing and stiffness submatrices are implemented into the aeroelastic nonlinear multi-body code HAWC2 based on a Lagrange multiplier method in order to perform fully coupled aero-hydro-elastic simulations of a 5.0 MW offshore wind turbine. The aim of the study is to demonstrate the applicability of the consistent lumped-parameter models for transient analysis of wind turbines. For the different soil and loading conditions as well as foundation geometries, the structural vibration response is compared with a reference model with no soil–structure interaction taken into account.

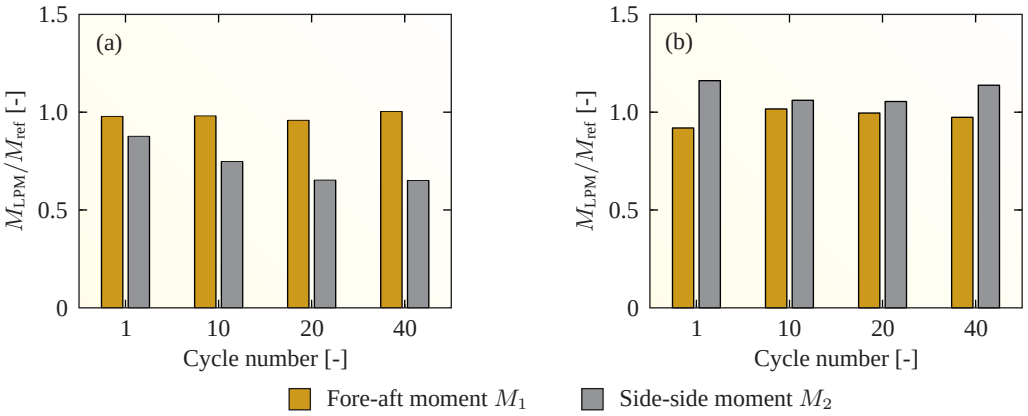

Figure 4–10 *Paper 4* — Identified load cycles of the fore-aft and side-side moments at seabed for 10-minute simulations: (a) wind-wave alignment and turbulent wind speed of 12 m/s, (b) 90° wind-wave misalignment and turbulent wind speed of 8 m/s.

Main Results

The most important conclusions from *Paper 4* are stated below:

- Successful fully coupled aero-hydro-elastic simulations of a 5.0 MW wind turbine installed on a surface foundation have been performed in the aeroelastic code HAWC2 based on constraint equations that describe how the degrees of freedom from the foundation module are related to the degrees of freedom from the wind turbine code. However, this requires a stable solution of the consistent lumped-parameter model, *i.e.* it must be ensured that the real part of the poles in the rational filter are negative and that the lumped-parameter model does not wiggle outside the frequency range covered by the rigorous solutions, just like the Newmark parameters β and γ need to be very close to 0.25 and 0.5, respectively.

- For a layered half-space, strong constructive and destructive interferences between waves going upwards and downwards may take place. This in turn calls for a consistent lumped-parameter model with up to five internal degrees of freedom, see Fig. 4–9.

- Fully-coupled aero-hydro-elastic simulations show that even for a surface foundation with a huge self-weight, the soil–structure interaction cannot be neglected for normal wind turbine operations. The side-side vibrations are sensitive to the soil–structure interaction. Both the magnitude and phase of the loading amplitudes are significantly changed compared to a reference model with fixed boundary conditions at seabed, in spite of almost similar eigenfrequencies and damping ratios related to the lowest eigenmode between the coupled model and the reference model, see Fig. 4–10.

4.3.2 Paper 5

Published in *Engineering Structures*, Volume 75, September 2014, Pages 388–401, DOI: 10.1016/j.engstruct.2014.06.006.

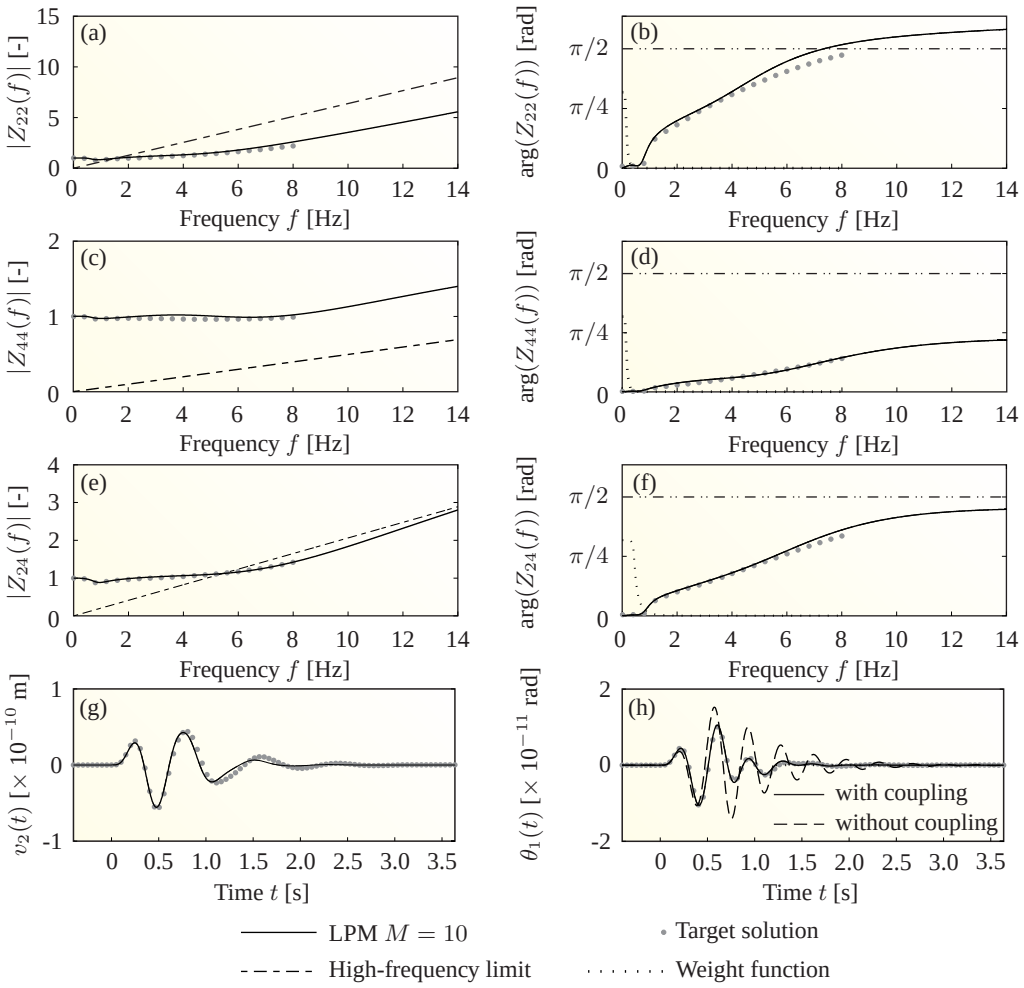

Figure 4–11 *Paper 5* — Vibration characteristics of a monopile foundation embedded in a homogeneous half-space evaluated by a consistent lumped-parameter model and its target solution: (a)–(f) normalised dynamic horizontal and rocking as well as coupled sliding-rocking impedance functions $Z_{ij}(f)$, (g) and (h) transient response for sliding $v_2(t)$ and rocking $\theta_1(t)$ motions after the application of a pulse load.

Contrary to *Paper 4* that deals with gravity base foundations, *Paper 5*: "Effects of soil–structure interaction on real time dynamic response of offshore wind turbines on monopiles" proposes an efficient method for including soil–pile interaction into wind turbine simulation codes. The general algorithm for the calibration of a consistent lumped-parameter model based on a weighted least-squares technique from *Paper 4* is applied with slight modifications, but the rigorous solution that underlies the substructuring is now based on semi-analytical solutions for piles vibrating in homogeneous, viscoelastic half-spaces, cf. Appendix A. Compared to a three-dimensional coupled boundary element/finite element model, the semi-analytical methods provide a fast and reliable evaluation of the dynamic impedance matrices of large-diameter monopiles. The foundation is implemented into the aeroelastic multi-body code HAWC2 where the response of a 5.0

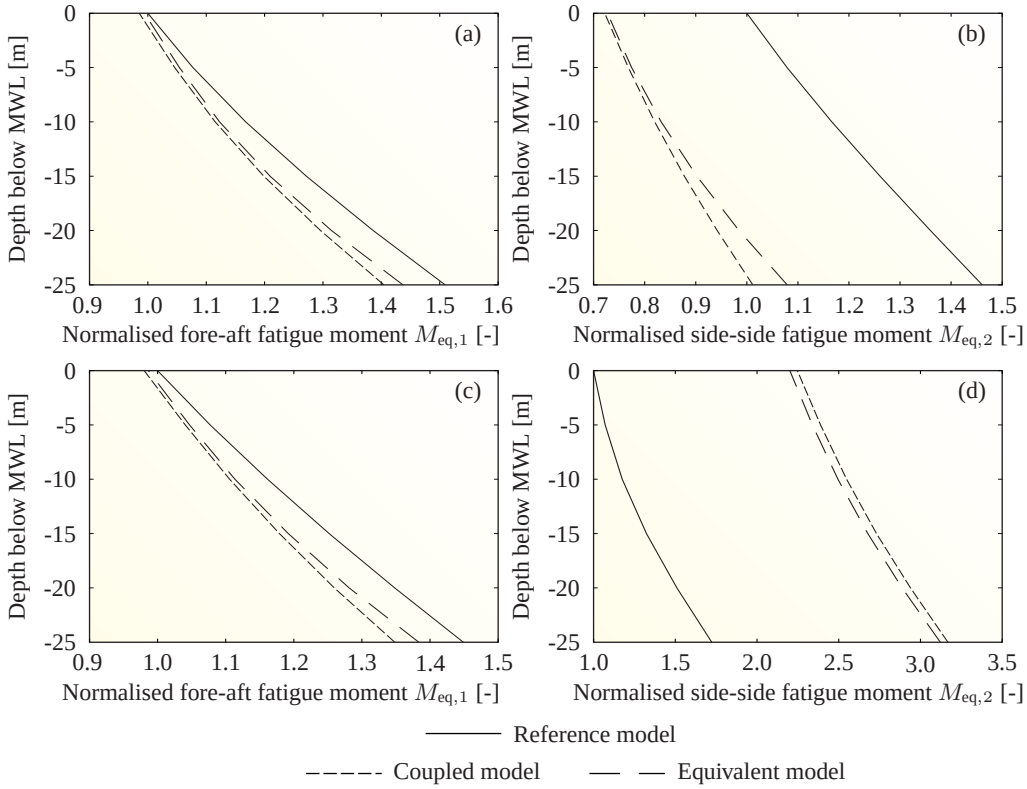

Figure 4–12 *Paper 5* — Fore-aft and side-side fatigue damage 1 Hz equivalent fatigue moment $M_{\mathrm{eq},1}$ and $M_{\mathrm{eq},2}$ evaluated from MWL to seabed level along the monopile structure: (a) and (b) wind-wave alignment and turbulent wind speed of 8 m/s, (c) and (d) 90° wind-wave misalignment and turbulent wind speed of 8 m/s.

MW wind turbine is evaluated and compared against two different foundation models: an apparent fixity length of the tower calibrated to the modal parameters related to the lowest eigenmode of the coupled model and a reference model with fixed support at the seabed with no inclusion of soil–structure interaction.

Main Results

The most relevant conclusions from *Paper 5* are listed below:

- Semi-analytical elastic-continuum formulations provide reliable dynamic impedance functions for offshore monopiles where the lower part is placed in a relatively stiff soil layer that prevents pile deflections during normal wind turbine operations. This is supported by a three-dimensional coupled boundary element/finite element approach. The magnitude and phase angle of the complex-valued impedance functions are captured in a reasonable manner by the consistent lumped-parameter model according to Fig. 4–11. Here, it should be noted that whereas coupling between horizontal sliding and rocking can be disregard for a gravity base foundation, this is not the case for a monopile.

- The dynamic response of the investigated offshore wind turbine is sensitive to the soil–structure interaction—especially for the side-side vibrations due to low aerodynamic damping in this direction, see Fig. 4–12.
- Compared to the coupled aeroelastic model, an equivalent foundation model with a fixity depth calibrated to the modal properties of the coupled model provide reliable vibration results of the wind turbine structure, although the modal properties related to the second tower modes in the two models differ significantly from each other. However, keep in mind that physical insight of the structural eigenfrequency and soil damping is needed for the application of the equivalent foundation approach.

4.3.3 Paper 6

Submitted to *Ocean Engineering*, In review.

Paper 6: "Dynamic response sensitivity of an offshore wind turbine: A fully coupled time-domain approach for varying subsoil conditions" is one out of two papers investigating the soil variability and its consequences for the dynamic properties and vibrations of offshore wind turbines installed on large-diameter monopiles with eigenfrequencies well below 0.30 Hz. The

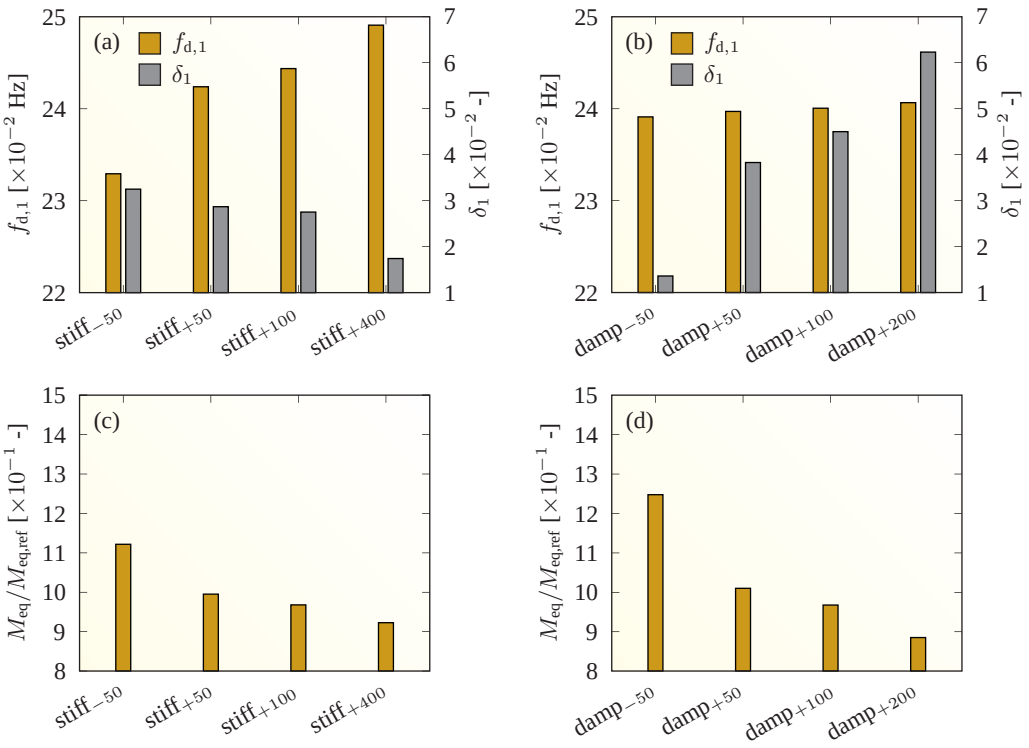

Figure 4–13 *Paper 6* — Modal parameters and accumulated fatigue damage equivalent moment for all wind directions for different soil stiffness and soil damping values: (a) and (b) damped eigenfrequency $f_{d,1}$ and damping δ_1 related to the lowest eigenmode, (c) and (d) accumulated fatigue moment M_{eq} normalised with a reference model $M_{eq,ref}$.

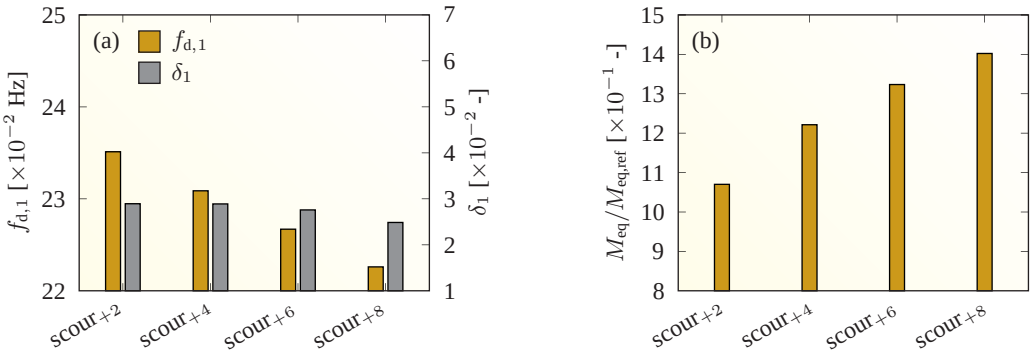

Figure 4–14 *Paper 6* — Modal parameters and accumulated fatigue damage equivalent moment for all wind directions for different mudline positions: (a) damped eigenfrequency $f_{d,1}$ and damping δ_1 related to the lowest eigenmode, (b) accumulated fatigue moment M_{eq} normalised with a reference model $M_{eq,ref}$ with no scour hole development.

rationale is that offshore wind turbines are typically designed for deterministic soil properties. However, it is a fact that these properties are random in nature following a probability distribution due to physical (*aleatoric*), measurement, model and statistical (*epistemic*) uncertainties. For parked wind turbine conditions, the aim of *Paper 6* is to document to what extent changes of the soil properties and boundary conditions at the seabed affect the fatigue loads as well as the structural eigenfrequencies and damping ratios of an offshore wind turbine. Based on wind-wave scatter diagrams from the North Sea, load cases for parked conditions are established that represent around 14% of the wind turbine design life. Fully coupled aero-hydro-elastic simulations of a 5.0 MW offshore wind turbine are performed for the sensitivity study using a consistent lumped-parameter model in conjunction with the aeroelastic code HAWC2.

Main Results

The most important findings from *Paper 6* are listed below:

- Changes of the soil stiffness and soil damping in terms of Young's modulus and loss factor of the soil of a homogeneous, viscoelastic soil layer strongly affect the modal properties related to the lowest eigenmode of the investigated offshore wind turbine structure. Evidently, this also influences the fatigue damage equivalent moment at seabed that increases up to approximately 20% for a 50% reduction of the soil stiffness and damping properties compared to a reference model, see Fig. 4–13.
- Lowering the mudline position reflecting the seabed erosion due to current actions has a high impact on the modal properties and the fatigue damage equivalent moment compared to a reference model with no scour hole development. According to Fig. 4–14, a fully developed scour hole of 8 m increases the moment with around 40% at the position that corresponds to the seabed level of the reference model.

4.3.4 Paper 7

Submitted to *Probabilistic Engineering Mechanics*, In review.

Paper 7: "A probabilistic analysis of the dynamic response of monopile foundations: Soil variability and its consequences" aims to assess the uncertainties of the inherent modal properties and fatigue loads of a fully operational 5.0 MW offshore wind turbine installed on a monopile caused by stochastic soil characteristics. The probabilistic analysis relies on a Monte Carlo approach in which each realisation of the correlated lognormal random soil properties underlies the calibration of a consistent lumped-parameter model implemented into the aeroelastic tool HAWC2. In turn, this enables fully coupled aero-hydro-elastic simulations of the offshore wind turbine structure facilitating the derivation of the probability densities of the modal properties and fatigue damage equivalent loads. The latter is based on load cases representing the operational life of the wind turbine where the nonlinear soil response is accounted for in a simplified and cost-effective manner assuming that the soil stiffness and soil damping are functions of the longitudinal mean wind speed component during each load case. The rationale behind this assumption is that the overall deformation level in the ground increases with an increase of the load which again increases with the mean wind speed.

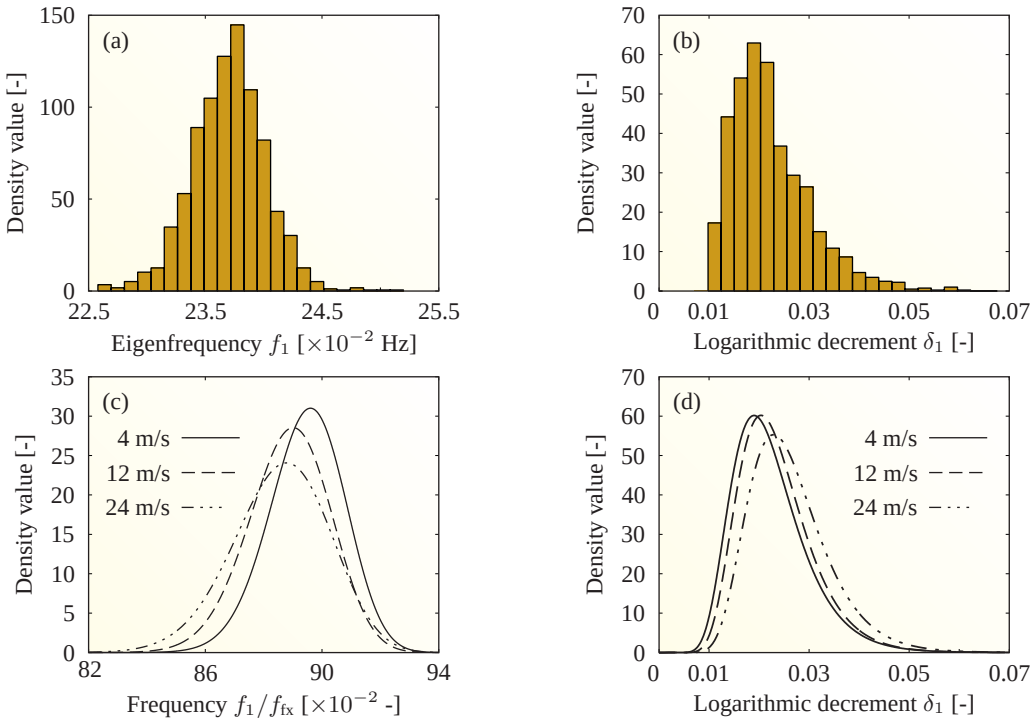

Figure 4–15 *Paper 7* — Probability densities of the modal properties related to the lowest eigenmode: (a) and (b) histogram of the undamped eigenfrequency f_1 and modal damping δ_1 for a longitudinal mean wind speed component of 4 m/s, (c) and (d) fitted beta and lognormal distributions of the normalised frequency f_1/f_{fx} and modal damping δ_1 for different longitudinal mean wind speed components. The frequency f_{fx} corresponds to the eigenfrequency of a wind turbine fixed at the seabed.

Main Results

Based on the applied Monte Carlo method, the main findings from *Paper 7* are stated below:

- The soil variability causes lognormally distributed modal damping related to the lowest eigenmode of the considered wind turbine with a mean value of approximately 0.02 logarithmic decrement and a coefficient of variation of 30%, cf. Fig. 4–15.
- A negative skew distribution of the first eigenfrequency is obtained with a mean value of approximately 0.24 Hz and a coefficient of variation of 2%, see Fig. 4–15. A plausible explanation of the skewness is that an upper limit of the eigenfrequency is present equal to the eigenfrequency of the wind turbine structure with no inclusion of soil–pile interaction. Normalising the distribution of the eigenfrequency with the fixed eigenfrequency value, a quantile-quantile plot shows that a beta distribution in a reasonable manner represents the normalised frequencies.
- The observed variations of the modal properties of the wind turbine cause distinctly varying fatigue loads in the side-side direction. The accumulated side-side fatigue damage equivalent moment for all wind directions below mean water level has a coefficient of variation of approximately 8%, see Fig. 4–16. It is found that a Gumbel (minimum) distribution describes the high quantiles of the negative skew discrete distribution of the side-side fatigue moment

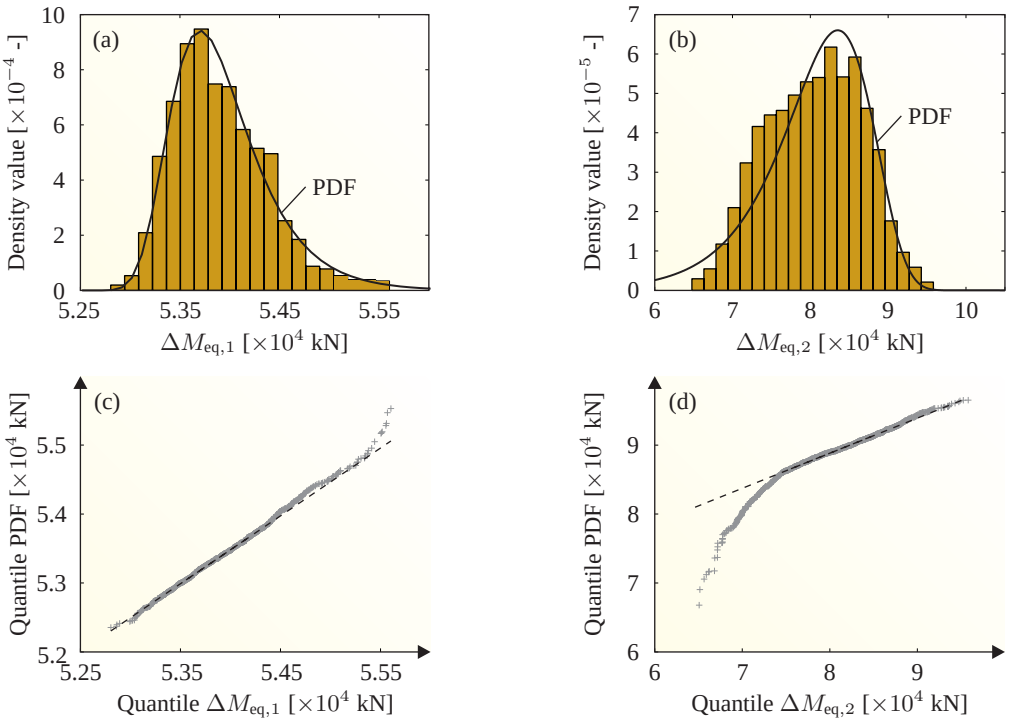

Figure 4–16 *Paper 7* — Probability densities of the accumulated fore-aft and side-side fatigue damage equivalent moment for all wind directions $M_{\mathrm{eq},1}$ and $M_{\mathrm{eq},2}$, respectively, 15 m below mean water level: (a) and (b) histograms and fitted Gumbel (minimum and maximum) distributions, (c) and (d) Q-Q plot of moments vs. theoretical quantiles.

reasonably well. This is in contrast to the fore-aft fatigue damage equivalent moment that is described accurately by a Gumbel (maximum) distribution.

CHAPTER 5
Conclusions and Future Directions

The dynamic response of wind turbines and their interaction with the subsoil have been studied. In the work carried out the main emphasis has been attached to full-scale modal testing and numerical analyses of onshore and offshore wind turbines where the aim is to improve the physical knowledge of the complex dynamically loaded structures. This chapter gives an overall discussion and conclusion of the topics treated in the thesis and addresses recommendations for future work.

5.1 Overall Conclusions

Current focus of designing cost-optimised and powerful offshore wind turbines has put several engineering challenges in front of the wind turbine and foundation designer. The immense, flexible and complex loaded structures with aerodynamic forces acting on the rotating blades and tower are characterised by low eigenfrequencies which means that the dynamic response of the wind turbine structures occurs in a frequency range close to excitation frequencies related to environmental and structural harmonic loads. A further complication is that the structural modal damping in the direction orthogonal to the mean wind direction is low and consequently, wind turbines are sensitive to dynamic amplifications, and the dynamic response becomes highly dependent on the impedance of the foundation. Therefore, proper characterisation of the modal properties based on extensive experimental testing is needed to refine and validate the computer simulations in order to obtain reliable and safe designs of the wind turbine structures demanded for cost-efficient power production where resonance problems are avoided.

The design of modern offshore wind turbines heavily depends on the numerical model used for the simulation of the structural system under different loading conditions. Approximations are necessary as it is computationally intractable to model the interrelation effects between wind/wave field, wind turbine, foundation and subsoil in one closed software and solve the entire system of equations. Whereas advanced time-efficient wind turbine simulation codes have been developed in the past to take the interaction of various environmental conditions as well as the tower and control system into account, the soil–structure interaction has to a great extent been neglected or poorly represented, typically by static springs and dissipation effects applied as modal damping related to the lowest structural eigenmode. In conclusion, this calls for further analysis of the following two areas investigated in the current PhD thesis:

1. Experimental characterisation of modal properties of offshore wind turbines including their dependency on soil–structure interaction.

2 Efficient modelling of soil–structure interaction useful for wind turbine simulation codes.

Based on so-called “rotor-stop” tests or free vibration tests of onshore and offshore wind turbines, thorough investigations of inherent structural modal properties have been carried out in the thesis. The contribution of soil damping to the overall system damping during the tests has been evaluated, and state-of-the-art soil–structure interaction models have been applied to strengthen possible reasons for time-varying dynamic properties of the wind turbines. The test procedure, however, does not provide the true boundary conditions and actual force and vibration level for operational wind turbines. Therefore, experimental operational modal analysis based on frequency- and time-domain solutions has been applied in the thesis where significant aerodynamic damping is expected to be present. The combination of the two experimental modal approaches leads to qualified estimations of expected soil damping during normal wind turbine operation and verification of computational models.

The inclusion of interaction between the offshore wind turbine, its foundation and the surrounding or underlying soil is a complicated task for aeroelastic simulations. The requirement of time-efficient modelling with proper description of the dissipation effects and effortless implementation into aeroelastic codes or offshore design packages for sequential or coupled analysis is not straightforward to follow. Simplified approaches are inevitably providing approximate solutions—but, by reducing the number of parameters to the few most significant ones, they may still produce sufficient accuracy for practical purposes. With this in mind, the calibration and application of consistent lumped-parameter models for fully-coupled aero-hydro-elastic simulations of offshore wind turbines, accounting for material hysteresis and radiation effects in the soil, have been demonstrated in the thesis. For symmetric gravity base foundations and large-diameter monopiles embedded in homogeneous and viscoelastic layered half-spaces, the importance of including the soil–structure interaction has been addressed, taking into account the inherent stochastic soil properties and their effect on the modal properties and fatigue loading of offshore wind turbines.

The main conclusions of the project may be summarised in the following points:

- “Rotor-stop” tests indicate time-varying eigenfrequencies and damping ratios of offshore wind turbines installed on monopile foundations. Isolating the oscillation oil damper performance, moveable seabed conditions may lead to the observed time dependency. In this regard, a beam on a Winkler foundation model concludes that the scour development and backfilling change the first eigenfrequency with 8%, and the corresponding modal soil damping varies in the range 0.05-0.08 logarithmic decrement.

- Experimental and numerical analyses show that the modal soil damping is low for normal wind turbine operations compared to “rotor-stop” tests since plastic soil deformation is small or inexistent. As an example, an offshore wind turbine installed on a bucket foundation only exhibits approximately 0.01 logarithmic decrement during normal wind turbine operation, whereas approximately 0.04 logarithmic decrement is observed during “rotor-stop” tests introducing high acceleration levels in the turbine. Nevertheless, whereas these observations hold for a bucket foundation and a monopile, this is not the case for a gravity base foundations. For this type of substructure, the geometrical damping in the soil as well as the hysteretic dissipation effects are insignificant during“rotor-stop” tests and normal wind turbine operations.

- Coupling effects between the lowest fore-aft and side-side damped wind turbine modes provide significant aerodynamic damping in the cross-wind direction. Experimental testing indicate proportional cross-wind modal damping up to rated wind speed. For higher wind speeds, stagnation or decreasing modal damping is observed. Fully coupled wind turbine simulations do not seem to cover this tendency where proportional damping is present for the entire operational mean wind speed range.

- A family of consistent lumped-parameter models, established by an optimum fit between the dynamic impedances of the lumped-parameter model and a rigorous solution, turns out to capture the dynamic soil–structure interaction efficiently for aeroelastic simulations of offshore wind turbines. Contrary to a gravity base foundation, it is highly important that the lumped-parameter model accounts for the coupling between horizontal sliding and rocking motion for a monopile, just like it is recommended, in general, to consider a high weight in the low-frequency range in the least-squares fitting algorithm—especially if the rigorous solution makes use of a hysteretic damping model.

- For wind turbines installed on gravity base foundations resting on a homogeneous half-space, a standard lumped-parameter model is able to fit the complex-valued impedance function of the soil–foundation system. However, in case of a monopile or a gravity base foundation placed on a layered half-space, a consistent lumped-parameter model must be applied to capture the wave propagation effects in the soil.

- The dynamic cross-wind response of offshore wind turbines installed on gravity base foundations and monopiles is highly sensitive to the soil–structure interaction and must be considered in the design phase. This is especially true for large-diameter monopiles where a 50% reduction of the soil stiffness and soil damping as well as the development of an 8 m scour hole tend to increase the accumulated fatigue damage equivalent moment for all wind directions by up to approximately 40%.

- Physical, measurement, model and statistical uncertainties of soil properties strongly affect the modal parameters and fatigue loads of offshore wind turbines installed on monopiles. The relatively low eigenfrequencies of the structural system mean that a coefficient of variation of 2% for the first eigenfrequency and 30% for the corresponding modal damping cause a coefficient of variation of approximately 8% for the accumulated side-side fatigue damage equivalent moment below mean water level.

This PhD thesis has proposed a computationally time-efficient approach accounting for the soil–structure interaction in aero-hydro-elastic design codes utilised in the wind turbine industry. The study has shown the importance of including the interrelation effects between the foundation and the subsoil that change the structural mode shapes as well as the system stiffness and damping as a result of the frequency-dependent dynamic stiffness of the soil–foundation system. The soil stiffness and soil damping are strongly negatively correlated and depend on the shear strain level in the soil. As a consequence, it is not possible for the foundation designer to achieve optimum soil stiffness and soil damping, *i.e.* either a rigid foundation can be designed introducing insignificant soil deformations and evidently increase the soil stiffness and decrease the soil damping or a flexible foundation can be applied providing the opposite situation. Nevertheless, from a fatigue point of view, this thesis clearly indicates that high system stiffness is needed to ensure that the first eigenfrequency is well above the wave frequency range. The affected system damping can then be advantageously magnified by active or passive dampers.

5.2 Recommendations for Further Research

Below, a number of subjects and ideas are listed suitable for further investigations.

- Although challenging, experimental investigation of the impedances of offshore wind turbine foundation is needed. This in turn will justify the derived semi-analytical impedance functions applied in this thesis or lead to modifications of the approaches.
- The soil damping level for offshore wind turbines highly depends on the magnitude of the excitation forces. Testing of wind turbines installed on different types of offshore foundations in a controlled environment based on traditional and operational modal identification analysis for different equivalent magnitudes of the excitation forces representing the reality as well as different soil conditions, could be useful. Evidently, this would lead to excitation forces vs. soil damping diagrams.
- For a monopile foundation, the current thesis has only applied impedance functions for a homogeneous half-space. This may seem reasonable for wind turbine sites where the soil profile is dominated by soil layers with approximately same physical properties, but the approach may fail in other situations. Therefore, a computationally inexpensive approach of deriving impedance functions for piles embedded in a layered half-space is recommended for further research.
- In the present research, viscoelastic soil properties underlie the calibration of the consistent lumped-parameter models. All of the soil parameters are, however, typically not available from a standard soil investigation campaign since low-strain field and laboratory tests are required. To strengthen the proposed method of including soil–structure interaction for offshore wind turbines via a consistent lumped-parameter model based on viscoelastic soil properties, it is recommended to establish a comprehensive data base with viscoelastic soil properties for different soil types.
- Preliminary research according to Damgaard *et al*. (2014) has shown that even at the frequency related to the first mode of an offshore wind turbine on a monopile, drained response is not obtained in sandy soil around the foundation. The pore pressure leads to additional system stiffness. Instead of treating the soil as a viscoelastic material (single-phase system), the soil may advantageously be modelled as a poreelastic medium (two-phase system) for the determination of the dynamic impedance functions of the soil–foundation system.

References

Achenbach, J. D. and Sun, C. (1965). Dynamic response of beam on viscoelastic subgrade. *Journal of Engineering Mechanics* **91**(5), 61–76.

Achmus, M., Yu-Shu, K., and Abdel-Rahman, K. (2009). Behavior of monopile foundations under cyclic lateral load. *Computers and Geotechnique* **36**(5), 725–735.

Adhikari, S. and Bhattacharya, S. (2010). Vibrations of wind-turbines considering soil–structure interaction. *Wind and Structures* **14**(2), 85–112.

Agardh, L. (1991). Modal analysis of two concrete bridges in Sweden. In *Structural Engineering International*, Volume 1, Sweden, pp. 35–39.

Agarwal, A. C. and Billing, J. R. (1990). Dynamic testing of the St. Vincent Street Bridge. In *Proceedings of the Annual Conference, Canadian Society for Civil Engineering*, Volume 4, pp. 163–181.

Ahmad, S. and Rupani, A. K. (1999). Horizontal impedance of square foundation in layered soil. *Soil Dynamics and Earthquake Engineering* **18**(1), 59–69.

Aktan, A. E., Zwick, J., Miller, R. A., and Sharooz, B. M. (1992). Nondestructive and destructive testing of a decommissioned RC slab highway bridge and associated analytical studies. *Transportation Research Record*.

Al-Douri, R. H. and Poulos, H. G. (1993). Predicted and observed cyclic performance of piles in calcareous sand. *Journal of Geotechnical Engineering* **121**(1), 1–15.

Allotey, N. and El Naggar, M. H. (2008). Generalized dynamic Winkler model for nonlinear soil–structure interaction analysis. *Canadian Geotechnical Journal* **45**(4), 560–573.

Andersen, L. V. (2007). Do lumped-parameter models provide the correct geometrical damping. DCE Technical Memorandum No. 5, Aalborg University.

Andersen, L. V. (2008). Assessment of lumped-parameter models for rigid footings. *Computers and Structures* **88**, 1333–1347.

Andersen, L. V. and Clausen, J. (2008). Impedance of surface footings on layered ground. *Computers and Structures* **86**, 72–87.

Andersen, L. V., Ibsen, L. B., and Liingaard, M. A. (2008). Impedance of bucket foundations: Torsional, horizontal and rocking motion. In Papadrakakis, M. and Topping, B. H. V. (Eds.), *Proceedings of the Sixth International Conference on Engineering Computational Technology*, Athens, Greece.

Andersen, L. V., Ibsen, L. B., and Liingaard, M. A. (2009). Lumped-parameter model of a bucket foundation. Technical Report, MBD Offshore Power A/S and Aalborg University.

Andersen, L. V. and Jones, C. J. C. (2001). BEASTS—A computer program for boundary element analysis of soil and three-dimensional structures. ISVR Technical Memorandum 868, Institute of Sound and Vibration Research, University of Southampton.

Andersen, L. V., Vahdatirad, M. J., Sichani, M. T., and Sørensen, J. D. (2012). Natural frequencies of wind turbines on monopile foundations in clayey soils—a probabilistic approach. *Computers and Geotechnics* **43**, 1–11.

Andersen, P. (1997). *Identification of civil engineering structures using vector ARMA models*. PhD Thesis, Department of Building Technology and Structural Engineering, Aalborg University.

Andersen, P. and Brincker, R. (2006). Understanding stochastic subspace identification. In *Proceedings of the 24th International Modal Analysis Conference (IMAC)*, St. Louis, Missouri.

Andersen, P., Brincker, R., Ventura, C., and Cantieni, R. (2008). Mode estimation of civil structures subject to ambient and harmonic excitation. In *Proceedings of the 26th International Modal Analysis Conference (IMAC)*, Orlando, Florida.

ANSYS (2008). ASAS™ (Non-linear) User manual. Technical Report, ANSYS INC.

API (2000). Recommended practice for planning, designing and constructing fixed offshore platforms, RP2a-WSD. American Petroleum Institute, Dallas, Texas, USA.

Askegaard, V. and Mossing, P. (1988). Long term observation of RC-bridge using changes in natural frequencies. In *Nordic Concrete Research*, Number 7, Oslo, Norway, pp. 20–27.

Asmussen, J. C., Brincker, R., and Rytter, A. (1998). Ambient modal testing of the Vestvej Bridge using random decrement. In *Proceedings of the 16th International Modal Analysis Conference (IMAC)*, Santa Barbara, California, pp. 922–928.

Auersch, L. (1994). Wave propagation in layered soils: Theoretical solution in wavenumber domain and experimental results of hammer and railway traffic excitation. *Journal of Sound and Vibration* **173**(2), 233–264.

Avilés, J. and Péres-Rocha, L. E. (1996). A simplified procedure for torsional impedance functions of embedded foundations in a soil layer. *Computers and Geotechnics* **19**(2), 97–115.

Badoni, D. and Makris, N. (1996). Nonlinear response of single piles under lateral inertial and seismic loads. *Soil Dynamics and Earthquake Engineering* **15**(1), 29–43.

Bakmar, C. L. (2009). Recent experience and challenges ahead. In *Hamburg Offshore Wind*, Hamburg, pp. 1–37.

Bamberger, A., Chalindars, B., Joly, P., Roberts, J. E., and Teron, J. L. (1988). Radiation boundary conditions for elastic wave propagation. *SIAM Journal of Scientific Statisitics and Computation* **9**(6), 1016–1049.

Bampton, M. C. C. and Craig, R. R. (1968). Coupling of substructures for dynamic analyses. *AIAA Journal* **6**(7), 1313–1319.

Baranov, V. A. (1967). On the calculation of excited vibrations of an embedded foundation. In *Voprosy Dinamiki i Prochnosti*, Polytechnic Institute, Riga, pp. 195–209.

Bathe, K-J. (1996). *Finite element procedures*. United States of America: Prentice-Hall.

Bendat, J. S. and Piersol, A. G. (2000). *Random data: Analysis and measurement procedures* (3 ed.). New York: John Wiley & Sons, Inc.

Beredugo, Y. O. and Novak, M. (1972). Coupled horizontal and rocking vibration of embedded footings. *Canadian Geotechnical Journal* **9**(4), 477–497.

Bhattacharya, S. and Adhikari, S. (2011). Experimental validation of soil–structure interaction of offshore wind turbines. *Soil Dynamics and Earthquake Engineering* **31**(5–6), 805–816.

Bhattacharya, S., Nikitas, N., Garnsey, J., Alexander, N. A., Cox, J., Lombardi, D., Wood, D. M., and Nash, D. F. T. (2013). Observed dynamic soil–structure interaction in scale testing of offshore wind turbine foundations. *Soil Dynamics and Earthquake Engineering* **54**, 47–60.

Biggs, J. M. and Suer, H. S. (1956). Vibration measurements on simple-span bridges. Highway Research Board Bulletin 1–15, Washington D.C.

Bir, G. (2008). Multiblade coordinate transformation and its application to wind turbine analysis. In *Proceedings of ASME Wind Energy Symposium*, Reno, Nevada.

Bogaez, R. (1983). On dynamics and stability of continuous systems subjected to a distributed moving load. *Ingenieur-Archiv* **53**, 243–255.

Böker, C. (2009). *Load Simulation and Local Dynamics of Support Structures for Offshore Wind Turbines*. PhD Thesis, Institute for Steel Construction, Leibniz University of Hannover, Germany.

Bossanyi, E. A. (2003). GH Bladed version 3.6 user manual. In *Garrad Hassan and Partners Limited, Document No. 282/BR/010*, Bristol, England.

Boulanger, R. W., Curras, C. J., Kutter, B. L., Wilson, D. W., and Abghari, A. (1999). Seismic soil–pile–structure interaction experiments and analysis. *Journal of Geotechnical and Geoenvironmental Engineering* **125**(9), 750–759.

Brincker, R. and Andersen, P. (2000). Ambient response analysis of the Heritage Court Building structure. In *Proceedings of the 18th International Modal Analysis Conference (IMAC)*, San Antonio, Texas, pp. 1081–1087.

Brincker, R., Andersen, P., and Frandsen, J. B. (2000). Ambient response analysis of the Great Belt Bridge. In *Proceedings of the 18th International Modal Analysis Conference (IMAC)*, San Antonio, Texas, pp. 26–32.

Brincker, R., Andersen, P., and Zang, L. (2000). Modal identification from an ambient response using frequency domain decomposition. In *Proceedings of the 18th International Modal Analysis Conference (IMAC)*, pp. 625–630.

Brincker, R., Ventura, C. E., and Andersen, P. (2001). Damping estimation by frequency domain decomposition. In *Proceedings of the 19th International Modal Analysis Conference (IMAC)*, Kissimmee, Florida, pp. 698–703.

Brownjohn, J. M. W. (1997). Vibration characteristics of a suspension footbridge. *Journal of Sound and Vibration* **202**(1), 29–46.

Burton, T., Sharpe, D., Jenkins, N., and Bossanyi, E. (2001). *Wind energy handbook*. Wiley.

Burton, T., Sharpe, D., Jenkins, N., and Bossanyi, E. (2011). *Wind energy handbook* (2 ed.). Chichester: John Wiley & Sons.

Byrne, B. W. (2000). *Investigations of suction caissons in dense sand*. PhD thesis, University of Oxford, England.

Byrne, B. W. and Houlsby, G. T. (2003). Foundations for offshore wind turbines. *Philosophical Transactions of the Royal Society of London* **361**, 2909–2930.

Caetano, E., Cunha, A., and Taylor, C. A. (2000). Investigation of dynamic cable-deck interaction in a physical model of a cable-stayed bridge part I: Modal analysis. *International Journal Earthquake Engineering and Structural Dynamics* **29**(4), 481–498.

Cantieni, R. (2001). Assessing a dam's structural properties using forced vibration testing. In *Proceedings of IABSE International Conference on Safety, Risk and Reliability - Trends in Engineering*, Malta, pp. 1001–1005.

Cantieni, R., Brehm, M., Zabel, T., V. Rauert, and Hoffmeister, B. (2008). Ambient testing and model updating of a bridge for high-speed trains. In *Proceedings of the 26th International Modal Analysis Conference (IMAC-XXVI)*, Orlando, Florida.

Cantieni, R. and Pietrzko, S. (1993). Modal testing of a wooden footbridge using random excitation. In *Proceedings of the 11th International Modal Analysis Conference*, Volume 2, pp. 1230–1236.

Carne, T. G. and James, G. H. (2010). The inception of OMA in the development of modal testing technology for wind turbines. *Mechanical Systems and Signal Processing* **24**(5), 1213–1226.

Carne, T. G., Lauffer, J. P., and Gomez, A. J. (1988). Modal testing of a very flexible 110 m wind turbine structure. In *Proceedings of 6th International Modal Analysis Conference*, Kissimmee, Florida.

Carswell, W., Arwade, S. R., Myers, A. T., and Hajjar, J. F. (2013). Reliability analysis of monopile offshore wind turbine support structures. In *11th International Conference on Structural Safety & Reliability*, Columbia University, New York, pp. 1–8.

Chen, S-S. and Shi, J-Y. (2013). A simplified model for coupled horizontal and rocking vibrations of embedded foundations. *Soil Dynamics and Earthquake Engineering* **48**, 209–219.

Cheryl, D. and Ventura, C. E. (1998). Ambient vibration measurements of Heritage Court Tower. Earthquake Engineering Research, University of British Columbia.

Cook, R. D., Malkus, D. S., Plesha, M. E., and Witt, R. J. (2002). *Concept and applications of finite element analysis* (4 ed.). New York: John Wiley & Sons.

Cox, W. R., Reese, L. C., and Grubbs, B. R. (1974). Field testing of laterally loaded piles in sand. In *Proceedings of the Sixth Annual Offshore Technology Conference*, Houston, Texas.

Crouse, C. B., Liang, G. C., and Martin, G. R. (1984). Experimental study of soil–structure interaction at an accelerograph station. *Bulletin of the Seismological Society of America* **75**(6), 1783–1826.

Cunha, A., Caetano, E., Brincker, R., and Andersen, P. (2004). Identification from the natural response of the Vasco da Gama Bridge. In *Proceedings of the 22nd International Modal Analysis Conference IMAC*, Detroit, Michigan.

Cunha, A., Caetano, E., and Delgado, R. (2001). Dynamic tests on large cable-stayed bridge: An efficient approach. *Journal of Bridge Engineering* **6**, 54–62.

Damgaard, M., Andersen, L. V., and Ibsen, L. B. (2014). The importance of including dynamic soil–structure interaction into wind turbine simulation codes. In Group, Taylor & Francis (Ed.), *8th European Conference on Numerical Methods in Geotechnical Engineering*, Delft, The Netherlands, pp. 1111–1116.

Damgaard, M., Bayat, M., Andersen, L. V., and Ibsen, L. B. (2014). Assessment of the dynamic behaviour of saturated soil subjected to cyclic loading from offshore monopile wind turbine foundations. *Computers and Geotechnics* **61**, 116–126.

Damkilde, L. (1998). Introduktion til dynamik. Technical Report, Aalborg University.

Dassault Systèmes Simulia Corp (2012). ABAQUS 6.12 analysis user's manual. Technical Report, Dassault Systèmes Simulia Corp.

de Klerk, D., Rixen, D. J., and Voormeeren, N., S (2008). General framework for dynamic substructuring: History, review, and classification of techniques. *AIAA Journal* **46**(5), 1169–1181.

Deger, Y., Cantieni, R., and Pietrzko, S. (1994). Modal analysis of an arch bridge: Experiment, finite element analysis and link. In *Proceedings of the 12th International Modal Analysis Conference*, Volume 1, pp. 425–432.

Deger, Y., Cantieni, S. J., Pietrzko, S., Rücker, W., and Rohrmann, R. (1993). Modal analysis of a highway bridge: Experiment, finite element analysis and link. In *Proceedings of the 13th International Modal Analysis Conference*, Volume 2, pp. 1141–1149.

Den Hartog, J. P. (1984). *Mechanical vibrations*. New York: Dover Publications Inc.

DNV (2011). Design of offshore wind turbine structures. DNV-OS-J101. Det Norske Veritas Classification A/S, Høvik, Norway.

Dobry, R., Gazetas, G., and Stokoe, K. H. (1986). Dynamic response of arbitrarily shaped foundations: Experimental verification. *Journal of Geotechnical Division, ASCE* **112**(2), 136–154.

Doe Ringo (2014). Foundations. `http://www.dongenergy.com/hornsrev2/en/about_horns_rev_2/about_the_project/pages/foundations.aspx`. Accessed: 2014.

Doherty, J. P. and Deeks, A. J. (2003). Elastic response of circular footings embedded in a non-homogeneous half-space. *Géotechnique* **53**(8), 703–714.

Dou, H. and Byrne, P. M. (1996). Dynamic response of single piles and soil–pile interaction. *Canadian Geotechnical Journal* **33**(1), 80–96.

Dunnavant, T. W. and O'Neill, M. W. (1989). Experimental p–y model for submerged stiff clay. *Journal of the Geotechnical Engineering Division, ASCE* **115**(1), 95–114.

Duque, E., van Dam, C. P., and Hughes, S. C. (1999). Navier-stokes simulations of the NREL combined experiment phase II rotor. In *Proceedings of the 37th Aerospace Sciences Meeting and Exhibition*, Reno, USA,.

Duron, Z. H. (1995a). Seven mile vibration testing results from the first series of test performed February 20-07. Research Report Prepared for B.C Hydro and Power Authority, Canada.

Duron, Z. H. (1995b). Seven mile vibration testing results from the second series of test performed august 14-20. Research Report Prepared for B.C Hydro and Power Authority, Canada.

El Naggar, M. and Novak, M. (1995). Nonlinear lateral interaction in pile dynamics. *Soil Dynamics and Earthquake Engineering* **14**(2), 141–157.

El Naggar, M. and Novak, M. (1996). Nonlinear analysis for dynamic lateral pile response. *Soil Dynamics and Earthquake Engineering* **15**(4), 233–244.

El Naggar, M. H. and Bentley, K. J. (2000). Dynamic analysis for laterally loaded piles and dynamic p–y curves. *Canadian Geotechnical Journal* **37**(6), 1166–1183.

El Naggar, M. H., Shayanfar, M. A., Kimiaei, M., and Aghakouchak, A. A. (2005). Simplified BNWF model for nonlinear seismic response analysis of offshore piles with nonlinear input ground motion analysis. *Canadian Geotechnical Journal* **42**(2), 365–380.

Engels, W., Obdam, T., and Savenije, F. (2009). Current developments in wind - 2009: Going to great lengths to improve wind energy. Technical Report ECN-E-09-96, Energy Research Centre of the Netherlands.

European Union Committee (2008). The EU's target for renewable energy: 20% by 2020. Technical Report, European Commissions.

EWEA (1999). Wind energy — the facts. Technical Report, European Wind Energy Association.

EWEA (2013). The European offshore wind industry - key trends and statistics 2013. Technical Report, European Wind Energy Association.

Ewins, D. J. (2000). *Modal testing: Theory, practice and application* (2 ed.). England: Research Studies Press LDT.

Farrar, C. R., Baker, W. E., Bell, T. M., Cone, K. M., Darling, T. W., Duffey, T. A., Eklund, A., and Migliori, A. (1994). Dynamic characterization and damage detection in the I-40 Bridge over the Rio Grande. Technical Report 153, United States.

Felber, A. J. and Cantieni, R. (1996). Introduction of a new ambient vibration system - Description of the system and Seven Bridge tests. Technical Report, Duebendorf.

Fenton, G. and Griffiths, D. V. (2007). Reliability-based optimization of laterally loaded piles. In *Probabilistic Applications in Geotechnical Engineering, GSP No. 170, proceedings of Geo-Denver 2007 symposium.*, Denver, CO: American Society of Civil Engineers.

Fingersh, L. J., Simms, D., Hand, M., Jager, D., Cotrell, J., Robinson, M., Schreck, S., and Larwwood, S. (2001). Wind tunnel testing of NREL's unsteady aerodynamics experiment. In *Proceedings of the 39th Aerospace Sciences Meeting and Exhibition*, New York, USA,.

Folse, M. D. (1989). Reliability analysis for laterally loaded piling. *Structural Engineering* **115**(5), 1011–1020.

Francisco, C. P., de Barros, F. C. P., and Enrique, J. E. (1990). Discrete models for vertical vibrations of surface and embedded foundations. *Earthquake Engineering and Structural Dynamics* **19**(2), 289–303.

Gade, S., Schlombs, R., Hundeck, C., and Fenselau, C. (2009). Operational modal analysis on a wind turbine gearbox. In *IMAC-XXVII: Conference & Exposition on Structural Dynamics*.

Gates, J. H. and Smith, M. J. (1982). Verification of dynamic modeling methods by prototype excitation. Technical Report 192, California.

Geniusstrande (2014). Alpha Ventus Tripods vor der Verladung. `http://www.geniusstrand.de/03-04-2009/tripod-suedwestkai-wilhelmshaven`. Accessed: 2014.

GL (2005a). Overall damping for piled offshore support structures. Note on Engineering Details, Germanischer Lloyd Wind Energie GmbH.

GL (2005b). Rules and guidelines iv industrial services. Technical Standard, Germanischer Lloyd Wind Energie GmbH.

Gohl, W. B. (1991). *Response of pile foundation to simulated earthquake loading: Experimental and analytical results*. PhD Thesis, University of British Columbia, Vancouver, B.C.

Green, M. F. and Cebon, D. (1994). Dynamic response of highway bridges to heavy vehicle loads: Theory and experimental validation. *Journal of Sound and Vibration* **170**(1), 51–78.

Guan, F. and Moore, D. (1997). New techniques for modelling reservoir–dam and foundation–dam interaction. *Soil Dynamics and Earthquake Engineering* **16**(4), 285–293.

Guyan, R. J. (1965). Reduction of stiffness and mass matrices. *AIAA Journal* **3**(2), 380–380.

Halabian, M. and El Naggar, M. H. (2002). Effect of non-linear soil–structure interaction on seismic response of tall slender structures. *Soil Dynamics and Earthquake Engineering* **22**(8), 639–658.

Hald, T. and Høgedal, M. (2005). Implementation of a finite element foundation module in FLEX5 using Craig-Bampton substructuring. In *European Offshore Wind Conference & Exhibition 2005, EWEA*, Copenhagen, Denmark.

Hall, Jr., J. R. (1967). Coupled rocking and sliding oscillations of rigid circular footings. In *Proceedings International Symposium on Wave Propagation and Dynamic Properties of Earth Materials*, University of New Mexico Press, Albuquerque, pp. 139–148.

Hansen, M. H., Thomsen, K., Fuglsang, P., and Knudsen, T. (2006). Two methods for estimating aeroelastic damping of operational wind turbine modes from experiments. *Wind Energy* **9**(1–2), 179–191.

Hansen, M. O. L., Sørensen, J. N., Michelsen, J. A., and Sørensen, N. N. (1997). A global Navier-Stokes rotor prediction model. In *Proceedings of the 35th Aerospace Sciences Meeting and Exhibition*, Reno, USA,.

Haselbach, P., Natarajan, A., Jiwinangun, R. G., and Branner, K. (2013). Comparison of coupled and uncoupled load simulations on a jacket support structure. In *10th Deep Sea Offshore Wind R&D Conference, DeepWind'2013*, Trondheim, Norway, pp. 244–252.

Haskell, N. (1953). The dispersion of surface waves on multilayered medium. *Bulletin of the Seismological Society of America* **73**, 17–43.

Hasselmann, K., Barnett, T. P., Bouws, E., Carlson, H., Cartwright, D. E., Enke, K., Ewing, J. A., Gienapp, H., Hasselmann, D. E., Kruseman, P., Meerburg, A., Müller, P., Olbers, D. J., Richter, K., Sell, W., and Walden, H. (1973). Measurements of wind-wave growth and swell decay during the Joint North Sea Wave Project (JONSWAP). Technical report, Deutches Hydrographisches Institut.

Hirai, H. (2012). A Winkler model approach for vertically and laterally loaded piles in nonhomogeneous soil. *International Journal for Numerical and Analytical Methods in Geomechanics* **36**(17), 1869–1897.

Houlsby, G. T., Kelly, R. B., Huxtable, J., and Byrne, B. W. (2005). Field trials of suction caissons in clay for offshore wind turbine foundations. *Géotechnique* **55**(4), 287–296.

Hsieh, T. K. (1967). Foundation vibrations. In *Proceedings – Institution of Civil Engineers*, Volume 22, London, pp. 211–225.

Ibsen, L. B., Schakenda, B., and Nielsen, S. A. (2003). Development of the bucket foundation for offshore wind turbines: A novel principle. In *Proceedings of the US Wind Energy Conference*, Boston, pp. 1–12.

IEC 61400-3 (2009). Wind turbines - part 3: Design requirements for offshore wind turbines. Technical Standard, European Committee for Electrotechnical Standardization.

Jacobsen, N. J., Andersen, P., and Brincker, R. (2007). Eliminating the influence of harmonic components in operational modal analysis. In *Proceedings of the 28th International Modal Analysis Conference IMAC XXVIII*, Orlando, Florida.

Jaya, K. P. and Prasad, A. (2002). Embedded foundation in a layered soil under dynamic excitations. *Soil Dynamics and Earthquake Engineering* **22**(6), 485–498.

Jean, W. Y., Lin, T. W., and Penzien, J. (1990). System parameters of soil foundations for time domain dynamic analysis. *Earthquake Engineering and Structural Dynamics* **19**(4), 541–553.

Jennings, P. C. and Bielak, J. (1973). Dynamics of building soil interaction. *Bulletin of the Seismological Society of America* **63**(1), 9–48.

Jones, D. V., Laghrouche, O., Le Houedec, D., and Petyt, M. (1997). Ground vibration in the vicinity of a rectangular load acting on a viscoelastic layer over a rigid foundation. *Journal of Sound and Vibration* **202**(2), 307–319.

Jones, D. V., Le Houedec, D., Peplow, A. T., and Petyt, M. (1998). Ground vibration in the vicinity of a moving harmonic rectangular load on a half-space. *European Journal of Mechanics, A/Solids* **17**(1), 153–166.

Jones, D. V., Le Houedec, D., and Petyt, M. (1998). Ground vibrations due to a rectangular harmonic load. *Journal of Sound and Vibration* **212**(1), 61–74.

Jones, D. V. and Petyt, M. (1991). Ground vibration in the vicinity of a strip load: A two-dimensional half-space model. *Journal of Sound and Vibration* **147**(1), 155–166.

Jones, D. V. and Petyt, M. (1992). Ground vibration in the vicinity of a strip load: An elastic layer on a rigid foundation. *Journal of Sound and Vibration* **152**(3), 501–515.

Jones, D. V. and Petyt, M. (1993). Ground vibration in the vicinity of a rectangular load on a half-space. *Journal of Sound and Vibration* **166**(1), 141–159.

Jonkman, J. and Buhl, M. (2005). FAST user's guide. In *Technical Report NREL/EL-500-38230*, National Renewable Energy Laboratory, Colorado, United States of America.

Jonkman, J. and Buhl, M. (2007). FAST User's guide. NREL/EL-500-38230, National Renewable Energy Laboratory.

Jonkman, J. and Musial, W. (2010). Offshore code comparison collaboration (OC3) for IEA Task 23 Offshore wind technology and deployment. NREL/TP-500-48191, International Energy Agency.

Kaimal, J. C., Wyngaard, J. C., Izumi, Y., and Coté, O. R. (1964). Spectral characteristics of surface-layer turbulence. *Quarterly Journal of the Royal Meteorological Society* **98**(417), 563–589.

Kampitsis, A. E., Sapountzakis, E. J., Giannakos, S. K., and Gerolymos, N. A. (2013). Seismic soil–pile–structure kinematic and inertial interaction—A new beam approach. *Soil Dynamics and Earthquake Engineering* **55**, 211–224.

Karabalis, D. L. and Mohammadi, M. (1998). 3-D dynamic foundation–soil–foundation interaction on layered soil. *Soil Dynamics and Earthquake Engineering* **17**(3), 139–152.

Kaufer, D., Cosack, N., Böker, C., Seidel, M., and Kühn, M. (2009). Integrated analysis of the dynamics of offshore wind turbines with arbitrary support structures. In *European Offshore Wind Conference & Exhibition 2009, Stockholm*, Stockholm, Sweden.

Kaynia, A. M. and Kausel, E. (1982). Dynamic stiffnesses and seismic response of pile groups. Report R 8203, Department of Civil Engineering, Massachusetts Institute of Technology, Cambridge.

Kellezi, L. (2000). Local transmitting boundaries for transient elastic analysis. *Soil Dynamics and Earthquake Engineering* **19**(7), 533–547.

Kenny, J. T. (1954). Steady-state vibrations of beams on elastic foundation for moving load. *Journal of Applied Mechanics* **21**(4), 359–364.

Kim, J, Varadan, V. V., and K., Varadan V. (1996). Finite element modelling of scattering problems involving infinite domains using drilling degrees of freedom. *Computer Methods in Applied Mechanics and Engineering* **134**(1–2), 57–70.

Kim, M. K., Lim, Y. M., and Cho, W. Y. (2001). Three dimensional dynamic response of surface foundation on layered half-space. *Engineering Structures* **23**(11), 1427–1436.

Kim, M. K., Lim, Y. M., and Rheel, J. W. (2000). Dynamic analysis of layered half planes by coupled finite and boundary elements. *Engineering Structures* **22**(6), 670–680.

Kramer, S. L. (1996). *Geotechnical Earthquake Engineering*. Belgium: Prentice-Hall Upper Saddle River.

Krätzig, W. B and Niemann, H. J. (1996). *Dynamics of civil engineering structures*. Rotterdam: A. A. Balkema.

Krenk, S., Kellezi, L., Nielsen, S. R. K., and Kirkegaard, P. H. (1999). Finite elements and transmitting boundary conditions for moving loads. In *Proceedings of the 4th European Conference on Structural Dynamics, Eurodyn '99*, Praha, pp. 447–452.

Krenk, S. and Kirkegaard, P. H. (2001). Local tensor radiation conditions for elastic waves. *Journal of Sound and Vibration* **247**(5), 875–896.

Kühn, M. (2001). *Dynamics and design optimisation of offshore wind energy conversion systems*. PhD thesis, DUWIND Delft University Wind Energy Research Institute, The Netherlands.

Kuribayashi, E. and Iwasaki, T. (1973). Dynamic properties of highway bridges. In *Proceedings of the 5th World Conference on Earthquake Engineering*, pp. 938–941.

Kuroiwa, T. and Lemura, H. (2007). Comparison of modal identification of output-only systems with simultaneous and non simultaneous monitoring. In *Proceedings of World Forum on Smart Materials and Smart Structures Technology (SMSSTâĂŹ07)*, Chongqing & Nanjing, China.

Larsen, J. W. (2005). *Nonlinear dynamics of wind turbine wings*. PhD thesis, Aalborg University, Denmark.

Larsen, T. J. and Hansen, A. (2007). How to HAWC2, the user's manual. In *Technical Report Risø-R-1597(en)*, Risø National Laboratory, Technical University of Denmark, pp. 1–101.

Larsen, T. J., Madsen, H. A., Larsen, G. C., and Hansen, K. S. (2013). Validation of the dynamic wake meander model for loads and power production in the Egmond aan Zee wind farm. *Wind Energy* **16**(4), 605–624.

Le Kouby, A., Canou, J., and Dupla, J. C. (2004). Behaviour of model piles subjected to cyclic axial loading. In Group, Taylor & Francis (Ed.), *Cyclic Behaviour of Soils and Liquefaction Phenomena*, London.

Leblanc, C., Byrne, B. W., and Houlsby, G. T. (2010). Response of stiff piles to random two-way lateral loading. *Géotechnique* **960**(9), 715–721.

Leblanc, C., Houlsby, G. T., and Byrne, B. W. (2010). Response of stiff piles in sand to long-term cyclic lateral loading. *Géotechnique* **60**(2), 79–90.

Lesny, K. (2010). *Foundations for offshore wind turbines*. VGE Verlag GmbH.

Liingaard, M. (2006). *Dynamic behaviour of suction caissons*. PhD thesis, Aalborg University, Denmark.

Liingaard, M. A., Andersen, L. V., and Ibsen, L. B. (2007). Impedance of flexible suction caissons. *Earthquake Engineering and Structural Dynamics* **36**(22), 2249–2271.

Lin, A. N. (1982). Experimental observations of the effect of foundation embedment on structural response. Report EERL 82-01, Earthquake Engineering Research Laboratory.

Lin, A. N. and Jennings, P. C. (1984). Effect of embedment on foundation soil impedances. *Journal of Engineering Mechanics, ASCE* **110**(7), 1060–1075.

Liu, Z. and Frigaard, P. (2001). Generation and analysis of random waves. Technical Report, Aalborg University.

Lombardi, D., Bhattacharya, S., and Wood, D. M. (2013). Dynamic soil–structure interaction of monopile supported wind turbines in cohesive soil. *Soil Dynamics and Earthquake Engineering* **49**, 165–180.

Lord, J-F. and Ventura, C. E. (2002). Measured and calculated modal characteristics of a 48-story tuned mass system building in Vancouver. In *International Modal Analysis Conference-XX: A Conference on Structural Dynamics Society for Experimental Mechanics*, Volume 2, Los Angeles, USA, pp. 1210–1215.

Low, B. K., Teh, C. I., and Tang, W. H. (2001). Stochastic nonlinear p–y analysis of laterally loaded piles. In *Proceeding of the Eight International Conference on Structural Safety and reliability (ICOSSAR)*, Newport Beach, California, pp. 17–22.

Luco, J. E. and Mita, A. (1987). Response of a circular foundation on a uniform half-space to elastic waves. *Earthquake Engineering and Structural Dynamics* **15**(1), 105–118.

Luco, J. E. and Westmann, R. A. (1971). Dynamic response of circular footings. *Journal of Engineering Mechanics, ASCE* **97**(5), 1381–1395.

Lucu, J. E. (1974). Impedance functions for a rigid foundation on a layered medium. *Nuclear Engineering and Design* **31**(2), 204–217.

Lysmer, J. (1965). *Vertical motions of rigid footings*. PhD Thesis, University of Michigan, Ann Arbor.

Lysmer, J. and Kuhlemeyer, R. L. (1969). Finite dynamic model for infinite media. *Journal of the Engineering Mechanics Division, ASCE* **95**(4), 859–878.

Lysmer, J. and Richart, Jr., F. E. (1966). Dynamic response of footings to vertical loading. *Journal of Soil Mechanics, ASCE* **92**(1), 65–91.

MacCamy, R. C. and Fuchs, R. A. (1954). Wave forces on piles: A diffraction theory. Technical Memorandum 69, U.S. Army Corps of Engineering, Beach Erosion Board.

Madsen, S., Andersen, L. V., and Ibsen, L. B. (2013). Numerical buckling analysis of large suction caissons for wind turbines on deep water. *Engineering Structures* **6**, 443–452.

Maheshwari, B. K., Truman, K. Z., El Naggar, M. H., and Gould, P. L. (2004). Three-dimensional nonlinear analysis for seismic soil–pile–structure interaction. *Soil Dynamics and Earthquake Engineering* **24**(4), 343–356.

Maheshwari, B. K., Truman, K. Z., El Naggar, M. H., and Gould, P. L. (2005). Three-dimensional nonlinear seismic analysis of single piles using finite element model: Effects of plasticity of soil. *International Journal of Geomechanics, ASCE* **5**(1), 35–44.

Mangalhães, P., Cunha, A., Caetano, E., and Brincker, R. (2010). Damping estimation using free decays and ambient vibration tests. *Mechanical Systems and Signal Processing* **24**(5), 1274–1290.

Mann, J. (1994). The spatial structure of neutral atmospheric surface layer turbulence. *Journal of Fluid Mechanics* **273**, 141–168.

Matlock, H. (1970). Correlation for design of laterally loaded piles in soft clays. In *2nd Offshore Technology Conference*, Houston, Texas, pp. 577–594.

Matlock, H., Foo, S. H., and Bryant, L. L. (1978). Simulation of lateral pile behavior. In *Proceedings of Earthquake Engineering and Soil Dynamics, ASCE*, New York, pp. 600–619.

Matsuishi, M. and Endo, T. (1968). Fatigue of metals subjected to varying stress. In *Japan Society of Mechanical Engineers: Fukuoka, Japan*, pp. 37–40.

Meek, J. W. and Wolf, J. P. (1992a). Cone models for homogeneous soil. *Journal of Geotechnical Engineering* **118**(5), 667–685.

Meek, J. W. and Wolf, J. P. (1992b). Cone models for soil layer on rigid rock. II. *Journal of Geotechnical Engineering* **118**(5), 686–703.

Meek, J. W. and Wolf, J. P. (1993). Cone models for nearly incompressible soil. *Earthquake Engineering and Structural Dynamics* **22**(5), 649–663.

Meek, J. W. and Wolf, J. P. (1994). Cone models for embedded foundation. *Journal of Geotechnical Engineering* **120**(1), 60–80.

Memarpour, M. M., M., Kimiaei, M., Shayanfar, and Khanzadi, M. (2012). Cyclic lateral response of pile foundations in offshore platforms. *Computers and Geotechnics* **42**, 180–192.

Meymand, P. J. (1998). *Shaking table scale model tests of nonlinear soil–pile–superstructure interaction in soft clay*. PhD Thesis, University of California, Berkeley.

Miloslav, B., Vladimir, B., and Michal, P. (1994). Dynamic behaviour of footbridge by analysis and test. In *Proceedings of the 13th International Modal Analysis Conference*, Volume 1, pp. 687–693.

Miner, M. A. (1945). Cumulative damage in fatigue. *Journal of Applied Mechanics, ASME* **12**(3), 159–164.

Mita, A. and Luco, J. E. (1989). Impedance functions and input motions for embedded square foundations. *Journal of Geotechnical Engineering, ASCE* **115**(4), 491–503.

Molenaar, D. P. (2003). Experimental modal analysis of a 750 kW wind turbine for structural modal validation. In *41st Aerospace Sciences Meeting and Exhibit*, Reno, Nevada.

Murchison, J. M. and O'Neill, M. W. (1984). Evaluation of p–y relationships in cohesionless soils. In *Analysis and Design of Pile Foundations. Proceedings of the Symposium in Conjunction with the ASCE National Convention*, pp. 174–191.

Musial, W., Jonkman, J., Vorpahl, F., and Quesnel, L. (2009). Annex 30 Task Proposal comparison of dynamic computer codes and models offshore code comparison collaboration continuation (OC4) project. Technical Report, International Energy Agency.

National Research Council (1991). Assessment of research needs for wind turbine rotor materials technology. Technical Report, Energy Engineering Board-Commission on Engineering and Technical Systems, Washington, D. C.

Nielsen, S. R. K. (2004). *Linear vibration theory* (1 ed.). Denmark: Aalborg Tekniske Universitetesforlag.

Nogami, T. (1996). Simplified subgrade model for three-dimensional soil–foundation interaction analysis. *Soil Dynamics and Earthquake Engineering* **15**(7), 419–429.

Nogami, T. and Konagai, K. (1986). Time domain axial response of dynamically loaded single piles. *Journal of Engineering Mechanics, ASCE* **112**(11), 1241–1249.

Nogami, T. and Lam, Y. (1987). A two parameter layer model for analysis of slab on elastic foundation. *Journal of the Engineering Mechanics Division, ASCE* **113**(9), 1279–1291.

Nogami, T. and Leung, M. B. (1990). Simplified mechanical subgrade model for dynamic response analysis of shallow foundations. *Earthquake Engineering and Structural Dynamics* **19**(7), 1041–1055.

Nogami, T. and Novak, M. (1976). Soil–pile interaction in vertical vibrations. *International Journal of Earthquake Engineering and Structural Dynamics* **4**(3), 277–293.

Nogami, T. and Novak, M. (1977). Resistance of soil to a horizontally vibrating pile. *Earthquake Engineering and Structural Dynamics* **5**(3), 249–261.

Nogami, T., Otani, J., Konagai, K., and Chen, H-L. (1992). Nonlinear soil–pile interaction model for dynamic lateral motion. *Journal of Geotechnical Engineering, ASCE* **118**(1), 89–106.

Nogami, T., Zhu, J. X., and Itoh, T. (1992). First and second order dynamic subgrade models for dynamic soil–pile interaction analysis. In *Geotechnical Special Technical Publication on Piles under Dynamic Loads*, Polytechnic Institute, Riga, pp. 187–206.

Novak, M. (1970). Prediction of footing vibrations. *Journal of Soil Mechanics and Foundation Engineering Division, ASCE* **96**(3), 837–861.

Novak, M. (1973). Vibrations of embedded footings and structures. In *ASCE National Structural Engineering Meeting*, San Francisco.

Novak, M. (1974). Dynamic stiffness and damping of piles. *Canadian Geotechnical Journal* **11**(4), 574–598.

Novak, M. (1977). Vertical vibrations of floating piles. *Journal of the Engineering Mechanics Division, ASCE* **103**(1), 153–168.

Novak, M. (1985). Experiments with shallow and deep foundations. In ASCE, (Ed.), *Proceedings of Vibration Problems in Geotechnical Engineering*, New York, pp. 1–26.

Novak, M. and Beredugo, Y. O. (1972). Vertical vibration of embedded footings. *Journal of the Soil Mechanics and Foundation Division, ASCE* **98**(12), 1291–1310.

Novak, M. and El-Sharnouby, B. (1983). Stiffness constants of single piles. *Journal of the Geotechnical Engineering Division, ASCE* **109**(7), 961–974.

Novak, M. and Howell, J. F. (1976). Torsional vibrations of pile foundations. *Journal of the Geotechnical Engineering Division, ASCE* **103**(4), 271–285.

Novak, M. and Howell, J. F. (1978). Dynamic response of pile foundations in torsion. *Journal of the Geotechnical Engineering Division, ASCE* **104**(5), 535–552.

Novak, M. and Nogami, T. (1977). Soil–pile interaction in horizontal vibration. *Earthquake Engineering and Structural Dynamics* **5**(3), 263–281.

Novak, M., Nogami, T., and Aboul-Ella, F. (1978). Dynamic soil reactions for plane strain case. *Journal of the Engineering Mechanics Division, ASCE* **104**(4), 953–959.

Novak, M. and Sachs, K. (1973). Torsional and coupled vibrations of embedded footings. *Earthquake Engineering and Structural Dynamics* **2**(1), 11–33.

Novak, M., Sheta, M., El-Hifnawy, L., El-Marsafawi, H., and Ramadan, O. (1990). DYNA3: A computer program for calculation of foundation response to dynamic loads. Technical Report, Geotechnical Research Centre, the University of Western Ontario, London.

Nuss, L. K., Chopra, A. K., and Hall, J. F. (2003). Comparison of vibration generator tests to analyses including dam–foundation–reservoir interaction for morrow point dam. In *The Commission Internationale Des Grande Barrages, 20th Congress of Large Dams*.

Ohlsson, S. (1986). Modal testing of the Tjorn Bridge. In *Proceedings of the 4th International Modal Analysis Conference*, Florida, pp. 599–605.

Osgood, R., Bir, G., and Mutha, H. (2010). Full-scale modal wind turbine tests: Comparing shaker excitation with wind excitation. In *Proceedings of the 28th International Modal Analysis Conference IMAC XXVIII*, Jacksonville, Florida, pp. 113–124.

Øye, S. (1994). FLEX4 user manual. Technical Report, Department of Fluid Mechanics, Technical University of Denmark.

Øye, S. (1996). FLEX4 – Simulation of wind turbine dynamics. In *State of the Art of Aeroelastic Codes for Wind Turbine Calculations*, Lyngby, Denmark, pp. 71–76.

Øye, S. (1999). FLEX5 user manual. Technical Report, Department of Fluid Mechanics, Technical University of Denmark.

Ozbek, M. and Rixen, D. J. (2011). Optical measurements and operational modal analysis on a large wind turbine: Lessons learned. In *Conference Proceedings of the Society for Experimental Mechanics Series*, pp. 257–276.

Ozbek, M. and Rixen, D. J. (2013). Operational modal analysis of a 2.5 MW wind turbine using optical measurement techniques and strain gauges. *Wind Energy* **16**(3), 367–381.

Palmgren, A. G. (1968). Die Lebensdauer von Kugellagern (Life length of roller bearings). *Zeitschrift des Vereines Deutscher Ingenieure (VDI Zeitschrift)* **68**(14), 339–341.

Parmelee, R. A., Perelman, D. S., and Lee, S. L. (1969). Seismic response of multiple-story structures on flexible foundations. *Bulletin of the Seismological Society of America* **59**(3), 1061–1070.

Pate, J. W. (1997). Dynamic testing of a highway bridge. In *Proceedings of the 15th International Modal Analysis Conference*, pp. 2028–2037.

Peeters, B., De Roeck, G., Caetano, E., and Cunha, A. (2002). Dynamic study of the Vasco da Gama Bridge. In *Proceedings of the International Conference on Noise and Vibration Engineering ISMA*, Volume 2, pp. 545–554.

Peire, K., Nonneman, H., and Bosschem, E. (2008a). Gravity base foundations for the Thornton Bank offshore wind farm. In *CEDA Dredging Days*, Antwerp, pp. 1–96.

Peire, K., Nonneman, H., and Bosschem, E. (2008b). Ormonde offshore wind farm. In *Found Ocean*, UK, pp. 1–8.

Penzien, J. (1970). Soil–pile foundation interaction. *Earthquake Engineering and Structural Dynamics* **3**, 349–381.

Perelman, D. S., Parmelee, R. A., and Lee, S. L. (1968). Seismic response of single-story interaction systems. *Journal of Structural Division, ASCE* **94**(11), 2597–2608.

Pierson, W. J. and Moskowitz, J. L. (1964). A proposed spectral form fully developed wind seas on similarity theory of S.A. Kitaigorodskii. *Journal of Geophysical Research* **69**(24), 5181–5190.

Professional Services Group (1998). ADAMS/WT 2.0 user's guide. Technical Report, Mechanical Dynamics.

Proulx, J., Herbert, D., and Paultre, P. (1992). Evaluation of the dynamic properties of a steel arch bridge. In *Proceedings of the 10th International Modal Analysis Conference*, Volume 2, San Diego, pp. 1025–1031.

Pyl, L., Clouteau, D., and Degrande, G. (2003). The soil impedance of embedded structures in the higher frequency range, computed with the boundary element method. In *16th ASCE Engineering Mechanics Conference*, University of Washington, Seattle.

Qian, J., Tham, L. G., and Cheung, Y. K. (1998). Dynamic analysis of rigid surface footings by boundary element method. *Journal of Sound and Vibration* **214**(4), 747–759.

Rambøll (2009). Rambøll offshore structural analysis programme package, version 4.3. Technical Report, Rambøll Oil & Gas.

Randolph, M. F. (1981). The response of flexible piles to lateral loading. *Géotechnique* **31**(2), 247–259.

Reese, L. C. and Welch, R. C. (1975). Lateral loading of deep foundation in stiff clay. *Journal of the Geotechnical Engineering Division, ASCE* **101**(7), 633–649.

Reissner, E. (1936). Stationare, axialsymmetrische durch eine schuttelnde Masse erregte. Schwingungen eines homogenen elastichen Halbraumes. *Ingenieur-Archives* **7**(6), 381–396.

Richart, F. E. and Whitman, R. V. (1967). Comparison of footing vibration tests with theory. *Journal of Soil Mechanics, ASCE* **93**(6), 143–168.

Rizos, D. C. (2000). A rigid surface boundary element for soil–structure interaction analysis in the direct time domain. *Computational Mechanics* **26**(6), 582–591.

Romo, M. P. and Ovando-Shelley, E. (1999). p–y Curves for piles under seismic lateral loads. *Geotechnical and Geological Engineering* **16**(4), 251–272.

Ruiz, S. E. (1984). Reliability index for offshore piles subjected to bending. *Structural Safety* **2**(2), 83–90.

Saitoh, M. (2011). Lumped parameter models representing impedance functions at the interface of a rod on a viscoelastic medium. *Journal of Sound and Vibrations* **330**(9), 2062–2072.

Saitoh, M. (2012). Lumped parameter models representing impedance functions at the end of a finite beam on a viscoelastic medium. *Computers and Structures* **92–93**, 317–327.

Sarpkaya, T. and Isaacson, M. (1981). *Mechanics of wave forces on offshore structures*. Van Nostrand Reinhold Company.

Scharff, R. and Siems, M. (2013a). Monopile foundations for offshore wind turbines — solutions for greater water depths. *Steel Construction* **6**(1), 47–53.

Scharff, R. and Siems, M. (2013b). Pushing the limits — mega monopile foundations for offshore wind turbines. *Steel Construction* **6**(3), 178–185.

Seidel, M. and Ostermann, F. (2009). Validation of offshore load simulations using measurement data from the DOWNWInD project. In *European Offshore Wind Conference & Exhibition 2009, Stockholm*, Stockholm, Sweden.

Seidel, M., von Mutius, M., Rix, P., and Steudel, D. (2005). Integrated analysis of wind and wave loading for complex support structures of offshore wind turbines. In *Copenhagen Offshore Wind 2005*, Copenhagen, Denmark.

Seidel, M., von Mutius, M., and Steudel, D. (2004). Design and load calculations for offshore foundations of 5 MW turbine. In *German Wind Energy Conference*, Wilhelmshaven, Germany.

Semblat, J. F. and Broist, J. J. (2000). Efficiency of higher order finite elements for the analysis of seismic wave propagation. *Journal of Sound and Vibration* **231**(2), 460–467.

Shah, P. M. (1968). *On the dynamic response of foundation systems*. PhD Thesis, Rice University, Houston, Texas.

Sheng, X., Jones, C. J. C., and Petyt, M. (1999a). Ground vibration generated by a harmonic load acting on a railway track. *Journal of Sound and Vibration* **225**(1), 3–28.

Sheng, X., Jones, C. J. C., and Petyt, M. (1999b). Ground vibration generated by a load moving along a railway track. *Journal of Sound and Vibration* **228**(1), 129–156.

Shepherd, R. and Charleson, A. W. (1971). Experimental determination of the dynamic properties of a bridge substructure. *Bulletin of the Seismological Society of America* **61**(6), 1529–1548.

Shirzadeh, R., Devriendt, C., Bidakhvidi, M. A., and Guillaume, P. (2013). Experimental and computational damping estimation of an offshore wind turbine on monopile foundation. *Journal of Wind Engineering and Industrial Aerodynamics* **120**, 96–106.

Simms, D., Hand, M., Schreck, S., and Fingersh, L. J. (2001). NREL unsteady aerodynamics experiment in the NASA-Ames wind tunnel: A comparison of predictions to measurements. Technical Report NREL/TP-500-29494, National Renewable Energy Laboratory, Colorado, USA.

Smith, S.W. (1997). *The scientist and engineer's guide to digital signal processing* (1 ed.). USA: California Technical Publishing.

Sørensen, N. N. and Hansen, M. O. L. (1998). Rotor performance predictions using a navier-stokes method. In *Proceedings of the 36th Aerospace Sciences Meeting and Exhibition*, Reno, USA,.

Sørensen, N. N. and Michelsen, J. (2001). Aerodynamic predictions for the unsteady aerodynamics experiment phase-II rotor at the National Renewable Energy Laboratory. In of Mechanical Engineers, American Society (Ed.), *Proceedings of the 2000 ASME Wind Energy Symposium*, New York, USA,.

Sørensen, S. P. H., Foglia, A., and Ibsen, L. B. (2012). Testing of laterally loaded rigid piles with applied overburden pressure. In Forening, Dansk Geoteknisk (Ed.), *Proceedings of the 16th Nordic Geotechnical Meeting*, Copenhagen, Denmark.

Sørensen, S. P. H. and Ibsen, L. B. (2012). Experimental comparison of non-slender piles under static loading and under cyclic loading in sand. In of Offshore & Polar Engineers, International Society (Ed.), *Proceedings of the Twenty-second (2012) International Offshore and Polar Engineering Conference*, Number 22, Rhodos, Greece, pp. 732–738.

Sørensen, S. P. H., Ibsen, L. B., and Augustesen, A. H. (2010). Effects of diameter on initial stiffness of p–y curves for large-diameter piles in sand. In *Numerical Methods in Geotechnical Engineering, NUMGE*, Trondheim, Norway, pp. 907–912.

Spera, D. A. (1994). *Wind turbine technology: Fundamental concepts of wind turbine engineering* (2 ed.). New York: ASME PRESS.

Spyrakos, C. C. and Xu, C. (2004). Dynamic analysis of flexible massive strip-foundations embedded in layered soils by hybrid BEM–FEM. *Computers and Structures* **82**(29–30), 2541–2550.

Stokoe, K. H. and Erden, S. M. (1985). Influence of base shape on dynamic response of surface foundations. Geotechnical Engineering Report GP 85-1, Civil Engineering Department, University of Texas at Austin, Texas.

Sun, L. (2001). A closed-form solution of Bernoulli-Euler beam on viscoelastic foundation under harmonic line loads. *Journal of Sound and Vibrations* **242**(4), 619–627.

Sun, L. (2002). A closed-form solution of beam on viscoelastic subgrade subjected to moving loads. *Computers and Structures* **80**(1), 1–8.

SVS (2004). ARTEMIS software. Technical report, Structural Vibration Solutions (SVS), Novi Science Park, Niels Jernes Vej 10, DK 9220 Aalborg East, Denmark.

Swannell, P. and Miller, C. W. (1987). Theoretical and experimental studies of a bridge vehicle system. In *Proceedings of the Institute of Civil Engineers, Part 2*, Volume 83, pp. 613–615.

Tajimi, E. (1969). Dynamic analysis of a structure embedded in an elastic stratum. In *Proceedings of the Fourth World Conference on Earthquake Engineering*, Santiago, Chile.

Tandjiria, V., Teh, C. I., and Low, B. K. (2000). Reliability analysis of laterally loaded piles using response surface methods. *Structural Safety* **22**(4), 335–355.

Tarp-Johansen, N. J., Andersen, L. V., Christensen, E. D., Mørch, C., Kallesøe, B., and Frandsen, S. (2009). Comparing sources of damping of cross-wind motion. In *The European Offshore Wind Conference & Exhibition*, Stockholm, Sweden.

Tcherniak, D., Chauhan, S., Rosseth, M., Font, I., Basurko, J., and Salgado, O. (2010). Output-only modal analysis on operating wind turbines: Application to simulated data. In *European Wind Energy Conference*, Warsaw, Poland.

Tcherniak, T., Chauhan, S., and Hansen, M. H. (2010). Applicability limits of operational modal analysis to operational wind turbines. In *Proceedings of the 28th International Modal Analysis Conference IMAC XXVIII*, Volume 1, Jacksonville, Florida, pp. 317–327.

Tham, L. G., Cheung, Y. K., and Lei, Z. X. (1994). Torsional dynamic analysis of single piles by time-domain BEM. *Journal of Sound and Vibration* **174**(4), 505–519.

Thomson, W. (1950). Transmission of elastic waves through a stratified solid medium. *Journal of Applied Physics* **21**, 89–93.

Touhei, T. and Ohmachi, T. (1994). Modal analysis of a dam–foundation system based on an FE–BE method in the time domain. *Earthquake Engineering and Structural Dynamics* **23**(1), 1–15.

Trochanis, A. M., Bielak, J., and Christiano, P. (1991). Three-dimensional nonlinear study of piles. *Journal of Geotechnical Engineering, ASCE* **117**(3), 429–447.

Tsai, H. C. and Lin, G. C. (1994). Explicit formulae for optimum absorber parameters for force-excited and viscously damped systems. *Journals of Sound and Vibration* **176**(5), 585–596.

Tsuha, C. H. C., Foray, P. Y., Jardine, R. J., Yang, Z. X., Silva, M., and Rimoy, S. (2012). Behaviour of displacement piles in sand under cyclic axial loading. *Soils and Foundations* **52**(3), 393–410.

Turek, M., Thibert, C., K. Ventura, and Kuan, S. (2006). Ambient vibration testing of three unreinforced brick masonry buildings in Vancouver, Canada. In *Proceedings of the 24th International Modal Analysis Conference (IMAC)*, St. Louis, Missouri.

van der Valk, P. L. C. and Voormeeren, S. N. (2012). An overview of modeling approaches for complex offshore wind turbine support structures. In *Proceedings of ISMA2012-USD2012*, Leuven, Belgium.

Van Nunen, J. W. G. and Persoon, A. J. (1982). Investigation of the vibrational behavior of a cable-stayed bridge under wind loads. *Engineering Structures* **4**(2), 99–105.

Veletsos, A. S. and Nair, D. V. V. (1974). Torsional vibration of viscoelastic foundations. *Journal of Geotechnical Engineering* **100**(3), 225–246.

Veletsos, A. S. and Tang, Y. (1987). Vertical vibration of ring foundations. *Earthquake Engineering and Structural Dynamics* **15**(1), 1–21.

Veletsos, A. S. and Verbic, B. (1973). Vibration of viscoelastic foundations. *Earthquake Engineering and Structural Dynamics* **2**(1), 87–102.

Veletsos, S. and Wei, Y. (1971). Lateral and rocking vibration of footings. *Journal of Soil Mechanics and Foundation Engineering Division, ASCE* **97**(9), 1227–1248.

Ventura, C. E., Felber, A. J., and Stiemer, S. F. (1996). Determination of the dynamic characteristics of the Colquiz River Bridge by full-scale testing. *Canadian Journal of Civil Engineering* **23**, 536–548.

Verbic, B. (1985). Experimental and analytical analysis of soil–structure interaction; part one: Block foundations. Research report, Institute for Materials and Structures.

Versteijlen, W. G., Metrikine, A. V., Hoving, J. S., Smid, E., and de Vries, W. E. (2011). Estimation of the vibration decrement of an offshore wind turbine support structure caused by its interaction with soil. In *Proceedings of the EWEA Offshore 2011 Conference*, Amsterdam, Holland.

Vestas Wind Systems A/S (2011). Vestas V90-1.8/2.0 MW. Technical Report, Vestas Wind Systems A/S.

Vincent, G. S. (1958). Golden Gate Bridge vibration study. *Journal of the Structural Division, ASCE* **84**.

Vincent, P. G., Hooley, R., Morgenstern, B. D., Rainer, J. H., and van Selst, A. M. (1979). Suspension bridge vibrations: Computed and measured. *Journal of the Structural Division ASCE* **105**(5), 859–874.

von Estorff, O. (1991). Dynamic response of elastic blocks by time domain BEM and FEM. *Computers and Structures* **38**(3), 289–300.

von Estorff, O. and Firuziaan, M. (2000). Coupled BEM/FEM approach for nonlinear soil/structure interaction. *Engineering Analysis with Boundary Elements* **24**(10), 715–725.

Voormeeren, S. N., van der Valk, P. L. C., Nortier, B. P., Molenaar, D-P., and Rixen, D. J. (2013). Accurate and efficient modeling of complex offshore wind turbine support structures using augmented superelements. *Wind Energy* **17**(7), 1035–1054.

Vostroukhov, A. V. and Metrikine, A. V. (2003). Periodically supported beam on a visco-elastic layer as a model for dynamic analysis of a high-speed railway track. *International Journal of Solids and Structures* **40**(21), 5723–5752.

Wang, H., Liu, W., Zhou, D., Wang, S., and Du, D. (2013). A lumped-parameter model of foundations based on complex Chebyshev polynomial fraction. *Soil Dynamics and Earthquake Engineering* **50**, 192–203.

Wang, S., Kutter, B. L., Chacko, M. J., Wilson, D. W., Boulanger, R. W., and Abghari, A. (1998). Nonlinear seismic soil–pile–structure interaction. *Earthquake Spectra* **14**(2), 377–396.

Wegner, J. L. and Zhang, X. (2001). Free-vibration analysis of a three-dimensional soil–structure system. *Earthquake Engineering and Structural Dynamics* **30**(1), 43–57.

Weissmann, G. F. (1973). Torsional vibrations of circular foundations. *Journal of Soil Mechanics, ASCE* **97**(9), 1293–1316.

Wheeler, J. D. (1970). Method for calculating forces produced by irregular waves. *Journal of Petroleum Technology* **22**(3), 359–367.

Wilson, D., Boulanger, R., and Kutter, B. L. (1997). Soil–pile superstructure interaction at soft or liquefiable soil sites—centrifuge data report for Csp4. Report No. UCD/CGMDR-97/06, Center for Geotechnical Modelling, Department of Civil and Environmental Engineering, University of California.

Wilson, J. C (1986). Analysis of the observed seismic response of a highway bridge. *Earthquake Engineering and Structural Dynamics* **14**(3), 339–354.

Winkler, E. (1867). *Die Lehre von Elasticzitat und Festigkeit (On Elasticity and Fixity)*. Prague.

Wolf, J. P (1991a). Consistent lumped-parameter models for unbounded soil: Frequency-independent stiffness, damping and mass matrices. *Earthquake Engineering and Structural Dynamics* **20**(1), 33–41.

Wolf, J. P (1991b). Consistent lumped-parameter models for unbounded soil: Physical representation. *Earthquake Engineering and Structural Dynamics* **20**(1), 11–32.

Wolf, J. P. (1994). *Foundation Vibration Analysis Using Simple Physical Models*. Englewood Cliffs, NJ: Prentice-Hall.

Wolf, J. P. (1997). Spring-dashpot-mass models for foundation vibrations. *Earthquake Engineering and Structural Dynamics* **26**(9), 931–949.

Wolf, J. P. and Meek, J. W. (1993). Cone models for soil layer on a flexible rock half-space. *Earthquake Engineering and Structural Dynamics* **22**(3), 185–193.

Wolf, J. P. and Preisig, M. (2003). Dynamic stiffness of foundation embedded in layered halfspace based on wave propagation in cones. *Earthquake Engineering and Structural Dynamics* **32**(7), 1075–1098.

Wolf, J. P. and Somaini, D. R. (1986). Approximate dynamic model of embedded foundation in time domain. *Earthquake Engineering and Structural Dynamics* **14**(5), 683–703.

Wolf, J. P. and Song, C. (1996). *Finite-Element Modeling of Unbounded Media* (1 ed.). Chichester: John Wiley & Sons Ltd.

Wong, H. and Luco, J. (1985). Tables of impedance functions for square foundations on layered media. *Soil Dynamics and Earthquake Engineering* **4**(2), 64–81.

Wood, M. G., Friswell, M. I., and T., Penny J. E. (1992). Exciting large structures using a bolt gun. In *Proceedings of the 10th International Modal Analysis Conference*, pp. 233–238.

Wu, G. and Finn, W. D. L. (1997a). Dynamic elastic analysis of pile foundations using finite element method in the frequency domain. *Canadian Geotechnical Journal* **34**(1), 34–43.

Wu, G. and Finn, W. D. L. (1997b). Dynamic nonlinear analysis of pile foundations using finite element method in the time domain. *Canadian Geotechnical Journal* **34**(1), 44–52.

Wu, W-H. and Chen, C-Y. (2001). Simple lumped-parameter models of foundation using mass-spring-dashpot oscillators. *Journal of the Chinese Institute of Engineers* **24**(6), 681–697.

Wu, W-H. and Lee, W-H. (2002). Systematic lumped-parameter models for foundations based on polynomial-fraction approximation. *Earthquake Engineering and Structural Dynamics* **31**(7), 1383–1412.

Wu, W-H. and Lee, W-H. (2004). Nested lumped-parameter models for foundation vibrations. *Earthquake Engineering & Structural Dynamics* **33**(9), 1051–1058.

Yan, L. (1990). *Hydraulic gradient similitude method for geotechnical modelling tests with emphasis on laterally loaded piles*. PhD Thesis, University of British Columbia, Vancouver, B.C.

Yazdchi, M., Khalili, N., and Valliappan, S. (1999). Dynamic soil–structure interaction analysis via coupled finite-element–boundary-element method. *Soil Dynamics and Earthquake Engineering* **18**(7), 499–517.

Yegian, M. K. and Wright, S. G. (1973). Lateral soil resistance-displacement relationships for deep pile foundations in soft clays. In *Proceedings of the 5th Annual Offshore Technology Conference*, Texas.

Zang, R., L. Brincker and Andersen, P. (2001). Modal indicators for operational modal identification. In *Proceedings of the 19th International Modal Analysis Conference (IMAC)*, Kissimmee, Florida, pp. 746–752.

Zania, V. (2014). Natural vibration frequency and damping of slender structures founded on monopiles. *Soil dynamics and Earthquake Engineering* **59**, 8–20.

APPENDIX A
Dynamic Impedance Functions for Piles in Horizontal and Vertical Vibrations

The dynamic response of foundations in a homogeneous or layered half-space can be calculated rigorously based on three-dimensional elastodynamics using the boundary element method, the finite element method with transmitting boundaries or the thin-layer method. The procedures, which require a formidable theoretical background, often include thousands of degrees of freedom in order to provide an accurate prediction of the wave propagation away from the foundation, and may therefore not fit the size and economics of an optimisation project. As a consequence, numerous studies in the past few decades have developed several simple semi-analytical expressions for the force-displacement relationship of the soil–foundation system in the frequency domain. For wind turbine applications, the expressions are attractive since only the response at the soil–foundation interface is important with regard to the dynamic structural behaviour. In this chapter, a short introduction to the pioneering studies by Novak and colleagues of horizontal and vertical pile vibrations are given. Expressions of the complex-valued impedance functions are presented which are essential for the derivation of simple physical models that exploit the advantages of easy incorporation with conventional dynamic codes.

A.1 Soil–Pile Interaction in Horizontal Vibration

In the early pioneering studies by Nogami and Novak (1977) and Novak and Nogami (1977), rigorous semi-analytical solutions were derived and presented of the interaction between a linear viscoelastic soil layer overlying rigid bedrock (fixed at the bottom) with hysteretic material damping and a vertical, uniform and linearly elastic pile vibrating horizontally. Even though no displacements occur at the bottom of the soil layer and the pile is clamped or pinned at the tip, these assumptions may seem reasonable for many offshore wind turbine locations where the lower part of the monopile is placed in a relatively stiff soil layer that prevents pile deflections during normal turbine operation, see Fig. A–1a and b. In addition, it must be highlighted that the semi-analytical solutions of the dynamic impedance functions are limited to soil profiles with constant stiffness along the depth, nonlinear soil behaviour is disregarded, and the separation and sliding along the soil–pile interface is not accounted for.

The theoretical foundation of the abovementioned studies is based on a description of the relationship between the horizontal displacement of the soil layer at the pile $V_2(x_3)$ and the soil

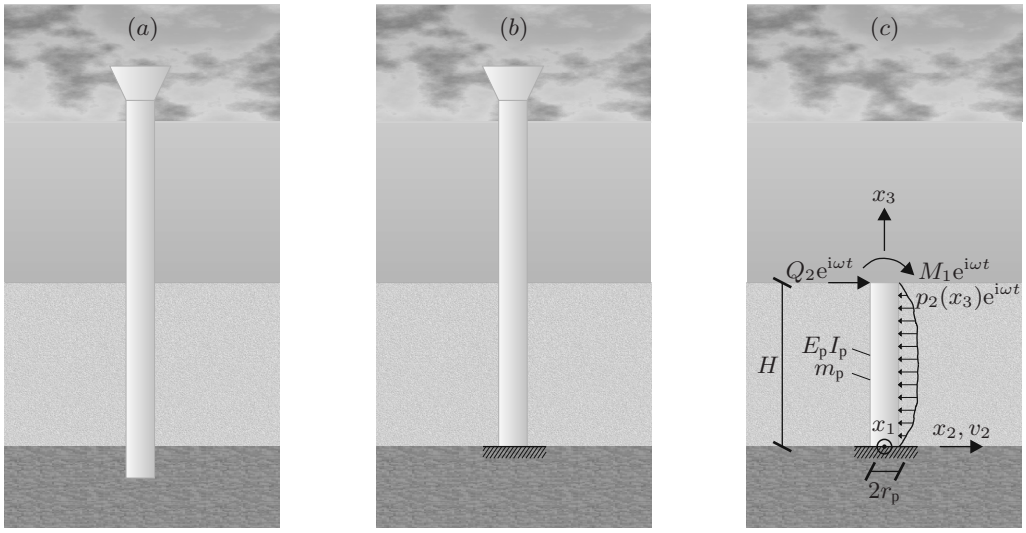

Figure A–1 Main assumptions in the derivation of the dynamic impedance functions for horizontal pile vibrations: (a) tip of monopile installed in a rigid soil layer that prevents pile displacements, (b) equivalent model with fixed boundary conditions at the top of the rigid soil layer, (c) external forces and soil resistance to horizontal pile vibrations.

resistance $p_2(x_3)$. Neglecting the vertical soil displacements $V_3(x_2)$, Nogami and Novak (1977) suggested the expression of the soil resistance $p_2(x_3)$ as a sum of contributions from individual wave modes, in case of the motion of the soil at the pile surface is equal to the harmonic motion of the pile, *i.e.*

$$p_2(x_3) = \alpha_\mathrm{h} V_2(x_3) = \sum_{n=1}^{\infty} \alpha_{\mathrm{h},n} V_{2,n} \sin h_n x_3, \tag{A–1}$$

where $\alpha_{\mathrm{h},n}$ is the horizontal resistance factor in the nth mode given by

$$\alpha_{\mathrm{h},n} = \pi r_\mathrm{p} \mu \left[(1 + \mathrm{i}\zeta_\mathrm{s}) h_n^2 - \left(\frac{\omega}{\upsilon_\mathrm{S}} \right)^2 \right] T_n. \tag{A–2}$$

$V_{2,n}$ is the modal amplitude independent of the depth x_3, r_p is the pile radius and μ is the shear modulus of the soil. Further, ζ_s is the hysteretic damping ratio associated with shear strains and assumed hereafter equal to the corresponding damping ratio of the volumetric strains ζ_v (for their definition, the reader is referred to Nogami and Novak (1977)), $h_n = \pi(2n-1)/2H$, H is the depth of the soil layer, ω is the angular excitation frequency, υ_S is the shear wave velocity and T_n is given by

$$T_n = \frac{4K_1(q_n r_\mathrm{p})K_1(s_n r_\mathrm{p}) + s_n r_\mathrm{p} K_1(q_n r_\mathrm{p})K_0(s_n r_\mathrm{p}) + q_n r_\mathrm{p} K_0(q_n r_\mathrm{p})K_1(s_n r_\mathrm{p})}{q_n K_0(q_n r_\mathrm{p})K_1(s_n r_\mathrm{p}) + s_n K_1(q_n r_\mathrm{p})K_0(s_n r_\mathrm{p}) + q_n s_n r_\mathrm{p} K_0(q_n r_\mathrm{p})K_0(s_n r_\mathrm{p})}, \tag{A–3}$$

where K_m, $m = 0, 1$ is the modified Bessel function of second kind and order m. The variables q_n and s_n take the form

$$q_n = \sqrt{\frac{(1 + \mathrm{i}\zeta_\mathrm{s}) h_n^2 - (\omega/\upsilon_\mathrm{S})^2}{\eta^2 + \mathrm{i}\left[(\eta^2 - 2)\zeta_\mathrm{s} + 2\zeta_\mathrm{s}\right]}}, \qquad s_n = \sqrt{\frac{(1 + \mathrm{i}\zeta_\mathrm{s}) h_n^2 - (\omega/\upsilon_\mathrm{S})^2}{1 + \mathrm{i}\zeta_\mathrm{s}}}, \tag{A–4}$$

where $\eta = v_\mathrm{p}/v_\mathrm{S}$ is the ratio between the P- and S-wave velocities in the soil. It is noteworthy that even though the harmonic wave propagation equations of the soil layer are formulated considering the vertical displacements associated with horizontal pile vibration as negligible, the approximation is considered rational when the pile deforms in bending without substantial shear deformations.

With the soil resistance $p_2(x_3)$ defined in Eq. (A–1), the dynamic response of a pile subjected to harmonic excitation at the pile cap can be determined according to Fig. A–1c. The governing equation of horizontal pile vibrations reads

$$E_\mathrm{p}I_\mathrm{p}\frac{\partial^4}{\partial x_3^4}\left(v_2\mathrm{e}^{\mathrm{i}\omega t}\right) + m_\mathrm{p}\frac{\partial^2}{\partial t^2}\left(v_2\mathrm{e}^{\mathrm{i}\omega t}\right) = -p_2(x_3)\mathrm{e}^{\mathrm{i}\omega t} \Rightarrow$$
$$E_\mathrm{p}I_\mathrm{p}\frac{\partial^4 v_2}{\partial x_3^4} - m_\mathrm{p}\omega^2 v_2 = -\sum_{n=1}^{\infty}\pi r_\mathrm{p}\mu\left[(1+\mathrm{i}\zeta_\mathrm{s})h_n^2 - \left(\frac{\omega}{v_\mathrm{S}}\right)^2\right]T_n V_{2,n}\sin h_n x_3, \tag{A–5}$$

where $E_\mathrm{p}I_\mathrm{p}$ is the the bending stiffness of the pile, m_p is mass per unit length of the pile and $v_2 = v_2(x_3)$ is the complex amplitude of the pile motion. The solution to Eq. (A–5) is a summation of the complete solution of the homogeneous equation $v_{2,\mathrm{I}}$ and the particular solution of the non-homogeneous equation $v_{2,\mathrm{II}}$, *i.e.*

$$v_2(x_3) = v_{2,\mathrm{I}} + v_{2,\mathrm{II}} = \Bigg[A\sin\sqrt[4]{m_\mathrm{p}\omega^2/E_\mathrm{p}I_\mathrm{p}}x_3 + B\cos\sqrt[4]{m_\mathrm{p}\omega^2/E_\mathrm{p}I_\mathrm{p}}x_3$$
$$+ C\sinh\sqrt[4]{m_\mathrm{p}\omega^2/E_\mathrm{p}I_\mathrm{p}}x_3 + D\cosh\sqrt[4]{m_\mathrm{p}\omega^2/E_\mathrm{p}I_\mathrm{p}}x_3\Bigg]$$
$$+\left[-\sum_{n=1}^{\infty}\frac{\alpha_{\mathrm{h},n}V_{2,n}}{E_\mathrm{p}I_\mathrm{p}h_n^4 - m_\mathrm{p}\omega^2}\sin h_n x_3\right]. \tag{A–6}$$

Since the motion of the soil $V_2(x_3)$ at (r_p, x_3) is assumed equal to the motion of the pile $v_2(x_3)$, Eq. (A–6) equals $V_2(x_3)$. Further, expanding the trigonometric functions into a Fourier sine series of argument $h_n x_3$, Eq. (A–6) can be written in the form

$$v_2(x_3) = A\sin\sqrt[4]{m_\mathrm{p}\omega^2/E_\mathrm{p}I_\mathrm{p}}x_3 + B\cos\sqrt[4]{m_\mathrm{p}\omega^2/E_\mathrm{p}I_\mathrm{p}}x_3 + C\sinh\sqrt[4]{m_\mathrm{p}\omega^2/E_\mathrm{p}I_\mathrm{p}}x_3$$
$$+ D\cosh\sqrt[4]{m_\mathrm{p}\omega^2/E_\mathrm{p}I_\mathrm{p}}x_3 - \sum_{n=1}^{\infty}\frac{\alpha_{\mathrm{h},n}\left(AF_{1,n} + BF_{2,n} + CF_{3,n} + DF_{4,n}\right)}{E_\mathrm{p}I_\mathrm{p}h_n^4 - m_\mathrm{p}\omega^2 + \alpha_{\mathrm{h},n}}\sinh_n x_3, \tag{A–7a}$$

where

$$F_{1,n} = \frac{2}{H}\int_0^H \sin\sqrt[4]{m_\mathrm{p}\omega^2/E_\mathrm{p}I_\mathrm{p}}x_3\sin h_n x_3\mathrm{d}x_3, \tag{A–7b}$$

$$F_{2,n} = \frac{2}{H}\int_0^H \cos\sqrt[4]{m_\mathrm{p}\omega^2/E_\mathrm{p}I_\mathrm{p}}x_3\sin h_n x_3\mathrm{d}x_3, \tag{A–7c}$$

$$F_{3,n} = \frac{2}{H}\int_0^H \sinh\sqrt[4]{m_\mathrm{p}\omega^2/E_\mathrm{p}I_\mathrm{p}}x_3\sin h_n x_3\mathrm{d}x_3, \tag{A–7d}$$

$$F_{4,n} = \frac{2}{H}\int_0^H \cosh\sqrt[4]{m_\mathrm{p}\omega^2/E_\mathrm{p}I_\mathrm{p}}x_3 \sin h_n x_3 \mathrm{d}x_3. \tag{A–7e}$$

Introducing the non-dimensional parameters

$$\tilde{\lambda} = H\sqrt[4]{\frac{m_\mathrm{p}\omega^2}{E_\mathrm{p}I_\mathrm{p}}}, \tag{A–8a}$$

$$\tilde{x}_3 = \frac{x_3}{H}, \tag{A–8b}$$

$$\tilde{r}_\mathrm{p} = \frac{r_\mathrm{p}}{H}, \tag{A–8c}$$

$$\tilde{h}_n = Hh_n = \frac{\pi(2n-1)}{2}, \tag{A–8d}$$

$$Y = \frac{\pi\mu H^4}{E_\mathrm{p}I_\mathrm{p}}, \tag{A–8e}$$

$$\tilde{\alpha}_{\mathrm{h},n} = \frac{\alpha_{\mathrm{h},n}}{\pi\mu}, \tag{A–8f}$$

Eq. (A–7) may advantageously be written in its final form

$$\begin{aligned} v_2(x_3) = &\left(\sin\tilde{\lambda}\tilde{x}_3 - Y\sum_{n=1}^{\infty} f_{1,n}\sin\tilde{h}_n\tilde{x}_3\right)A \\ &+\left(\cos\tilde{\lambda}\tilde{x}_3 - Y\sum_{n=1}^{\infty} f_{2,n}\sin\tilde{h}_n\tilde{x}_3\right)B + \left(\sinh\tilde{\lambda}\tilde{x}_3 - Y\sum_{n=1}^{\infty} f_{3,n}\sin\tilde{h}_n\tilde{x}_3\right)C \\ &+\left(\cosh\tilde{\lambda}\tilde{x}_3 - Y\sum_{n=1}^{\infty} f_{4,n}\sin\tilde{h}_n\tilde{x}_3\right)D, \end{aligned} \tag{A–9}$$

where

$$\begin{bmatrix} f_{1,n} \\ f_{2,n} \\ f_{3,n} \\ f_{4,n} \end{bmatrix} = \frac{\tilde{\alpha}_{\mathrm{h},n}}{\tilde{h}_n^4 - \tilde{\lambda}_n^4 + Y\tilde{\alpha}_{\mathrm{h},n}} \begin{bmatrix} F_{1,n} \\ F_{2,n} \\ F_{3,n} \\ F_{4,n} \end{bmatrix}. \tag{A–10}$$

According to the classical beam theory (Cook *et al.* 2002), the rotation $\Theta_1(x_3)$, the moment $M_1(x_3)$ and the internal horizontal force $Q_2(x_3)$ are easily found from the horizontal pile

displacement $v_2(x_3)$ given by Eq. (A–9), *i.e.*

$$\Theta_1(x_3) = \frac{\mathrm{d}v_2(x_3)}{\mathrm{d}x_3} = \left(\tilde{\lambda}\cos\tilde{\lambda}\tilde{x}_3 - Y\sum_{n=1}^{\infty}\tilde{h}_n f_{1,n}\cos\tilde{h}_n\tilde{x}_3\right)\frac{A}{H}$$
$$+\left(-\tilde{\lambda}\sin\tilde{\lambda}\tilde{x}_3 - Y\sum_{n=1}^{\infty}\tilde{h}_n f_{2,n}\cos\tilde{h}_n\tilde{x}_3\right)\frac{B}{H}$$
$$+\left(\tilde{\lambda}\cosh\tilde{\lambda}\tilde{x}_3 - Y\sum_{n=1}^{\infty}\tilde{h}_n f_{3,n}\cos\tilde{h}_n\tilde{x}_3\right)\frac{C}{H}$$
$$+\left(\tilde{\lambda}\sinh\tilde{\lambda}\tilde{x}_3 - Y\sum_{n=1}^{\infty}\tilde{h}_n f_{4,n}\cos\tilde{h}_n\tilde{x}_3\right)\frac{D}{H}, \tag{A–11a}$$

$$M_1(x_3) = E_\mathrm{p}I_\mathrm{p}\frac{\mathrm{d}^2v_2(x_3)}{\mathrm{d}x_3^2} = \left(-\tilde{\lambda}^2\sin\tilde{\lambda}\tilde{x}_3 + Y\sum_{n=1}^{\infty}\tilde{h}_n^2 f_{1,n}\sin\tilde{h}_n\tilde{x}_3\right)\frac{E_\mathrm{p}I_\mathrm{p}}{H^2}A$$
$$+\left(-\tilde{\lambda}^2\cos\tilde{\lambda}\tilde{x}_3 + Y\sum_{n=1}^{\infty}\tilde{h}_n^2 f_{2,n}\sin\tilde{h}_n\tilde{x}_3\right)\frac{E_\mathrm{p}I_\mathrm{p}}{H^2}B$$
$$+\left(\tilde{\lambda}^2\sinh\tilde{\lambda}\tilde{x}_3 + Y\sum_{n=1}^{\infty}\tilde{h}_n^2 f_{3,n}\sin\tilde{h}_n\tilde{x}_3\right)\frac{E_\mathrm{p}I_\mathrm{p}}{H^2}C$$
$$+\left(\tilde{\lambda}^2\cosh\tilde{\lambda}\tilde{x}_3 + Y\sum_{n=1}^{\infty}\tilde{h}_n^2 f_{4,n}\sin\tilde{h}_n\tilde{x}_3\right)\frac{E_\mathrm{p}I_\mathrm{p}}{H^2}D, \tag{A–11b}$$

$$Q_2(x_3) = E_\mathrm{p}I_\mathrm{p}\frac{\mathrm{d}^3v_2(x_3)}{\mathrm{d}x_3^3} = \left(-\tilde{\lambda}^3\cos\tilde{\lambda}\tilde{x}_3 + Y\sum_{n=1}^{\infty}\tilde{h}_n^3 f_{1,n}\cos\tilde{h}_n\tilde{x}_3\right)\frac{E_\mathrm{p}I_\mathrm{p}}{H^3}A$$
$$+\left(\tilde{\lambda}^3\sin\tilde{\lambda}\tilde{x}_3 + Y\sum_{n=1}^{\infty}\tilde{h}_n^3 f_{2,n}\cos\tilde{h}_n\tilde{x}_3\right)\frac{E_\mathrm{p}I_\mathrm{p}}{H^3}B$$
$$+\left(\tilde{\lambda}^3\cosh\tilde{\lambda}\tilde{x}_3 + Y\sum_{n=1}^{\infty}\tilde{h}_n^3 f_{3,n}\cos\tilde{h}_n\tilde{x}_3\right)\frac{E_\mathrm{p}I_\mathrm{p}}{H^3}C$$
$$+\left(\tilde{\lambda}^3\sinh\tilde{\lambda}\tilde{x}_3 + Y\sum_{n=1}^{\infty}\tilde{h}_n^3 f_{4,n}\cos\tilde{h}_n\tilde{x}_3\right)\frac{E_\mathrm{p}I_\mathrm{p}}{H^3}D. \tag{A–11c}$$

Thereafter, by applying the appropriate boundary conditions at the pile tip fixed to the ground,

$$v_2(x_3 = 0) = 0, \qquad \Theta_1(x_3 = 0) = 0, \tag{A–12}$$

the dynamic impedance function $\tilde{S}_{22}$ for horizontal sliding, $\tilde{S}_{44}$ for rocking motion and $\tilde{S}_{24}$ for coupling between horizontal sliding in the x_2-direction and rocking in the x_1-direction for the

frequency of interest can be obtained from Eq. (A–11) by a unit horizontal translation or rotation of the pile cap, *i.e.*

$$\tilde{S}_{22} = Q_2(x_3 = H) \quad \text{for} \quad v_2(x_3 = H) = 1, \;\; \Theta_1(x_3 = H) = 0, \tag{A–13a}$$

$$\tilde{S}_{42} = -M_1(x_3 = H) \quad \text{for} \quad v_2(x_3 = H) = 1, \;\; \Theta_1(x_3 = H) = 0, \tag{A–13b}$$

$$\tilde{S}_{44} = M_1(x_3 = H) \quad \text{for} \quad \Theta_1(x_3 = H) = 1, \;\; v_2(x_3 = H) = 0, \tag{A–13c}$$

$$\tilde{S}_{24} = -Q_2(x_3 = H) \quad \text{for} \quad \Theta_1(x_3 = H) = 1, \;\; v_2(x_3 = H) = 0. \tag{A–13d}$$

Note that $\tilde{S}_{11} = \tilde{S}_{22}$, $\tilde{S}_{55} = \tilde{S}_{44}$ and $\tilde{S}_{15} = -\tilde{S}_{24}$.

A.2 Soil–Pile Interaction in Vertical Vibration

Based on a vertical, elastic, end bearing monopile embedded in a linearly viscoelastic soil layer with hysteretic material damping overlying rigid bedrock, the vertical pile vibrations is found according to Nogami and Novak (1976) in a similar way as described for the horizontal pile vibrations. Firstly, the soil response to the dynamic load is established and secondly, the dynamic pile response is calculated assuming a full compliance of the pile with the surrounding soil where the soil resistance is applied on the pile as a dynamic pressure. Some of the variables introduced for the vertical pile vibrations are identical to the ones presented for the horizontal pile vibrations. Evidently, these will not be repeated in this section.

As indicated in Fig. A–2, the soil around a vertical deformed pile will tend to resist the deformations. Assuming that no sliding between soil and pile occurs, the vertical displacement of the soil $v_3(x_3)$ at the circumference of the pile and the resistance force $p_3(x_3)$ take the form

$$v_3(r_\mathrm{p}, x_3) = \sum_{n=1}^{\infty} A_n K_0(\tilde{q}_n \tilde{r}_\mathrm{p}) \sin \tilde{h}_n \tilde{x}_3, \tag{A–14}$$

$$p_3(x_3) = -2\pi \tilde{r}_\mathrm{p} \mu (1 + \mathrm{i}\zeta_\mathrm{s}) \sum_{n=1}^{\infty} A_n \tilde{q}_n K_1(\tilde{q}_n \tilde{r}_\mathrm{p}) \sin \tilde{h}_n \tilde{x}_3, \tag{A–15}$$

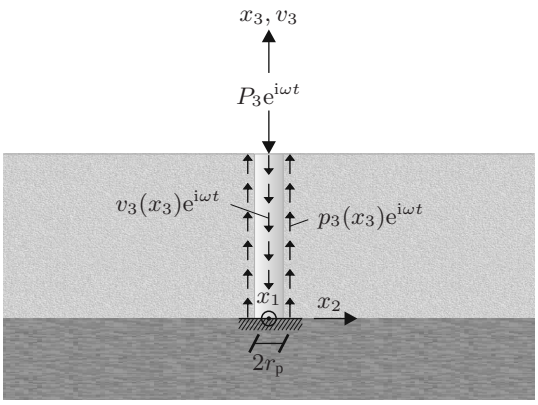

Figure A–2 Resistance of a viscoelastic soil layer to vertical deformation of a pile.

where A_n is a constant for the nth wave mode. The dimensionless parameter $\tilde{q}_n$ is given by

$$\tilde{q}_n = \sqrt{\frac{\left[\eta^2 + \mathrm{i}\left(\zeta_\mathrm{s}(\eta^2 - 2) + 2\zeta_\mathrm{s}\right)\right]\tilde{h}_n^2 - \left(\frac{H}{v_\mathrm{S}}\right)^2}{1 + \mathrm{i}\zeta_\mathrm{s}}}. \tag{A–16}$$

The resistance force $p_3(x_3)$ and the vertical deformation at the circumferences of the pile v_3 are related through the resistance factor α, *i.e.*

$$p_3 = -\alpha v_3 \Rightarrow \alpha_n = 2\pi\mu\tilde{\alpha}_n, \tag{A–17a}$$

where the dimensionless resistance factor $\tilde{\alpha}_n$ for the nth wave mode is defined as

$$\tilde{\alpha}_n = \tilde{r}_\mathrm{p}(1 + \mathrm{i}\zeta_\mathrm{s})\tilde{q}_n \frac{K_1(\tilde{q}_n\tilde{r}_\mathrm{p})}{K_0(\tilde{q}_n\tilde{r}_\mathrm{p})}. \tag{A–17b}$$

According to Fig. A–2, the end bearing pile is forced to vibrate vertically due to a concentrated harmonic force $P_3(x_3)\mathrm{e}^{\mathrm{i}\omega t}$ acting at the pile cap. The strong formulation in terms of vertical displacements then reads

$$m_\mathrm{p}\frac{\partial^2}{\partial t^2}\left(v_3\mathrm{e}^{\mathrm{i}\omega t}\right) - E_\mathrm{p}A_\mathrm{p}\frac{\partial^2}{\partial x_3^2}\left(v_3\mathrm{e}^{\mathrm{i}\omega t}\right) = P_3(x_3)\mathrm{e}^{\mathrm{i}\omega t} + p_3(x_3)\mathrm{e}^{\mathrm{i}\omega t}, \tag{A–18}$$

where E_p and A_p are the Young's modulus and section area of the pile, respectively. The amplitude of the steady-state solution of Eq. (A–18) is sought in the form

$$v_3(x_3) = \sum_{n=1}^{\infty} C_n \sin h_n x_3, \tag{A–19}$$

where the amplitude C_n can be determined from the boundary conditions. As a rough interface between the pile and the surrounding soil is assumed, the vertical soil displacement equals the pile displacement. Hence, using Eqs. (A–17) and (A–19), the soil resistance $p_{3,n}(x_3)$ for the nth mode can be written as

$$p_{3,n}(x_3) = -2\pi\mu\tilde{\alpha}_n v_{3,n}(x_3), \tag{A–20}$$

and thereby

$$p_3(x_3) = -2\pi\mu\sum_{n=1}^{\infty} C_n\tilde{\alpha}_n \sin h_n x_3. \tag{A–21}$$

The amplitude of the vertical excitation force P_3 acting at the pile cap may advantageously be expanded in a Fourier series, *i.e.*

$$P_3(x_3) = \frac{2P_3}{H}\sum_{n=1}^{\infty}(-1)^{n-1}\sin h_n x_3, \tag{A–22}$$

which together with Eqs. (A–19) and (A–20) can be inserted into Eq. (A–18),

$$E_{\mathrm{p}}A_{\mathrm{p}}\sum_{n=1}^{\infty}C_n\left(h_n^2-\lambda^2\right)\sin h_n x_3=\frac{2P_3}{H}\sum_{n=1}^{\infty}(-1)^{n-1}\sin h_n x_3$$
$$-2\pi\mu\sum_{n=1}^{\infty}C_n\tilde{\alpha}_n\sin h_n x_3, \tag{A–23a}$$

where

$$\lambda=\sqrt{\frac{m_{\mathrm{p}}}{E_{\mathrm{p}}A_{\mathrm{p}}}\omega^2}. \tag{A–23b}$$

Now, solving Eq. (A–23) for the amplitude C_n for the nth wave mode

$$C_n=\frac{2P_3}{H}\frac{(-1)^{n-1}}{E_{\mathrm{p}}A_{\mathrm{p}}\left(h_n^2-\lambda^2\right)+2\pi\mu\tilde{\alpha}_n} \tag{A–24}$$

and introducing the non-dimensional parameters

$$\tilde{\lambda}=\sqrt{\frac{m_{\mathrm{p}}H^2}{E_{\mathrm{p}}A_{\mathrm{p}}}\omega^2}, \tag{A–25a}$$

$$\gamma=2\pi\frac{\mu H^2}{E_{\mathrm{p}}A_{\mathrm{p}}}, \tag{A–25b}$$

the amplitude of the pile motion according to Eq. (A–19) reads

$$v_3(x_3)=\frac{P_3 r_{\mathrm{p}}}{E_{\mathrm{p}}A_{\mathrm{p}}}\tilde{v}_3, \tag{A–26a}$$

where

$$\tilde{v}_3=\frac{2}{\tilde{r}_{\mathrm{p}}}\sum_{n=1}^{\infty}\frac{(-1)^{n-1}}{\tilde{h}_n^2-\tilde{\lambda}^2+\gamma\tilde{\alpha}_n}\sin\tilde{h}_n\tilde{x}_3. \tag{A–26b}$$

Hence, the dynamic impedance function for vertical vibrations follows directly from Eq. (A–26)

$$\tilde{S}_{33}=\frac{E_{\mathrm{p}}A_{\mathrm{p}}}{r_{\mathrm{p}}}\tilde{s}_{33}, \tag{A–27a}$$

where

$$\tilde{s}_{33}=\tilde{r}_{\mathrm{p}}\Bigg/\left(2\sum_{n=1}^{\infty}\frac{(-1)^{n-1}}{\tilde{h}_n^2-\tilde{\lambda}^2+\gamma\tilde{\alpha}_n}\right). \tag{A–27b}$$

APPENDIX B
Continuous-Time Structural Systems

The dynamic behaviour of civil engineering structures are characterised in terms of their modal properties. In most cases, however, the exact determination of the mass, damping and stiffness properties are difficult to obtain. Therefore, it is common to assume that the structure can be determined by one or more linear ordinary differential equations. A correct estimate of the structural properties based on pure physics and fundamental laws is often difficult for large civil engineering structures. In these cases, it can be justified to conduct modal testing in order to support calibrating, updating and validating computational models used in the design stage. This appendix contains an introduction to the fundamental theory of linear structural dynamics and stationary random processes. The derivation and description of the theory forms the theoretical basis of operational modal identification methods. In addition, general digital data analysis required prior to the main estimation of the structural modal parameters is shortly explained.

B.1 Basic Theory of Linear Structural Dynamics

A real structure is a continuous system with distributed mass. Consequently, a numerical model should in principle have infinite numbers of degrees of freedom (DOFs). However, often only a limited number of dynamic modes are of interest which justifies the construction of a reduced model capable of describing the behaviour of the dynamic modes of interest. In spite of the fact that practical structures cannot be modelled as a single-degree-of-freedom (SDOF) system, the theory is important, as a complex multi-degree-of-freedom (MDOF) system often can be represented as a linear superposition of a number of SDOF characteristics. It should be noted that linearity of the dynamic systems is assumed which is often not the case for real systems. For example, a loading-strain relationship for concrete will actually start deviating from a linear relationship long before material failure. However, the response characteristic may be assumed linear for many physical systems, at least over some limited range of inputs without involving great errors. The section is based on Damkilde (1998), Bendat and Piersol (2000), Ewins (2000) and Nielsen (2004).

B.1.1 Single-Degree-of-Freedom-System Theory

Fig. B–1 shows an SDOF system. The system consists of a point mass m, a massless linear elastic spring with the spring constant k and a viscous damper characterised by the constant

c that transforms kinetic energy to heat. The spring is assumed free of damping, so all energy dissipation in the system takes place in the viscous damper. An external force $f(t)$ is applied to the point mass m. $f(t)$ is considered positive in the same direction as the degree of freedom $x(t)$ which is selected as the displacement from the static state of equilibrium, *i.e.* the gravity force can be ignored. Cutting the mass free from the spring and the damping element provides that the internal and external dynamic forces are applied as external loads on the mass. The damping and spring force f_d and kx are considered positive in the opposite direction of the external force $f(t)$. Using Newton's 2nd law of motion, the equation of motion for forced vibration of a linear viscous damped SDOF system is given by

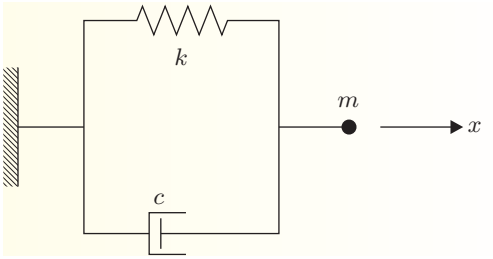

Figure B–1 Dynamic system with one degree of freedom.

$$-kx - c\dot{x} + f(t) = m\ddot{x}. \tag{B–1}$$

Eigenvibrations of Undamped SDOF Systems

For eigenvibrations of an undamped system, no external loading is applied, *i.e.* $f(t) = 0$ and no viscous damping exists. According to Eq. (B–1), the governing equation of motion then becomes

$$-kx = m\ddot{x}. \tag{B–2}$$

Rewriting of Eq. (B–2 provides

$$\ddot{x} + \omega_0^2 x = 0. \tag{B–3}$$

The circular eigenfrequency ω_0 included in Eq. (B–3) is given by

$$\omega_0 = \sqrt{\frac{k}{m}}. \tag{B–4}$$

The solution of Eq. (B–3) then reads

$$x(t) = A\cos(\omega_0 t - \phi), \tag{B–5}$$

where A is the amplitude and ϕ is the phase angle. Eq. (B–5) describes a harmonic motion with the circular eigenfrequency ω_0 determined by Eq. (B–4). The eigenvibration period becomes

$$T_0 = \frac{2\pi}{\omega_0} = 2\pi\sqrt{\frac{m}{k}}. \tag{B–6}$$

The natural frequency f_0 is then

$$f_0 = \frac{1}{T_0} = \frac{1}{2\pi}\omega_0 = \frac{1}{2\pi}\sqrt{\frac{k}{m}}. \tag{B–7}$$

Civil engineering structures like large cable-stayed bridges, high-rise buildings and wind turbines often have an eigenfrequency f_0 related to the lowest eigenmode between 0.1 Hz to 2.0 Hz.

Eigenvibrations of Viscously Damped SDOF Systems

In case of a damped dynamic system, the viscous damping term is included in the equation of motion with $f(t) = 0$, *i.e.*

$$m\ddot{x} + c\dot{x} + kx = 0. \tag{B–8}$$

The damping term is characterised by the so-called damping ratio ζ given by

$$\zeta = \frac{c}{c_0}, \tag{B–9a}$$

where c_0 defines the critical damping expressed by

$$c_0 = 2\sqrt{km}. \tag{B–9b}$$

Most civil engineering structures have a damping ratio from 0.01 to 0.05. Using Eqs. (B–4) and (B–9), the equation of motion for a viscously damped system can be rewritten,

$$\ddot{x} + 2\omega_0\zeta\dot{x} + {\omega_0}^2 x = 0. \tag{B–10}$$

The differential equation specified in Eq. (B–10) can be solved by standard methods, and for $\zeta < 1$, the equation of motion reads

$$x(t) = A\mathrm{e}^{-\alpha t}\left(\frac{\alpha}{\omega_\mathrm{d}}\sin\omega_\mathrm{d}t + \cos\omega_\mathrm{d}t\right) = A\mathrm{e}^{-\alpha t}\sqrt{\frac{1}{1-\zeta^2}}\cos(\omega_\mathrm{d}t - \phi), \tag{B–11}$$

where A is the amplitude to time $t = 0$ determined by initial conditions. The frequency ω_d in Eq. (B–11) is identified as the damped angular eigenfrequency, defined by

$$\omega_\mathrm{d} = \omega_0\sqrt{1-\zeta^2}. \tag{B–12}$$

The variable α in Eq. (B–11) represents the damping of the system,

$$\alpha = \omega_0\zeta. \tag{B–13}$$

The delay of the response $x(t)$ due to the damping is represented by the phase angle ϕ in Eq. (B–11) given by

$$\tan\phi = \frac{\zeta}{\sqrt{1-\zeta^2}}. \tag{B–14}$$

The response $x(t)$ in Eq. (B–11) is non-periodic due to the factor $\mathrm{e}^{-\alpha t}$ which specifies the decrease of the vibration amplitude with the time. Contrary to an undamped system, the eigenvibrations of a viscously damped system is characterised by dispersion of energy. The damped eigenvibration period T_d reads

$$T_\mathrm{d} = \frac{2\pi}{\omega_0\sqrt{1-\zeta^2}}. \tag{B–15}$$

At the time t, the motion $x(t)$ is given by Eq. (B–11). At the time $t+nT_\mathrm{d}$ after n damped periods, the motion can be found using the definitions in Eqs. (B–11), (B–12) and (B–15),

$$x(t+nT_\mathrm{d}) = A\mathrm{e}^{-\zeta\omega_0(t+nT_\mathrm{d})}\sqrt{\frac{1}{1-\zeta^2}}\cos\left(\omega_\mathrm{d}t+\omega_\mathrm{d}nT_\mathrm{d}-\phi\right) = \mathrm{e}^{-\zeta\omega_0 nT_\mathrm{d}}x(t) \Rightarrow$$

$$\frac{x(t+nT_\mathrm{d})}{x(t)} = \mathrm{e}^{-\zeta\omega_0 nT_\mathrm{d}} = \mathrm{e}^{-2\pi n\frac{\zeta}{\sqrt{1-\zeta^2}}}. \tag{B–16}$$

It means that the motion $x(t)$ will decrease with the factor $\mathrm{e}^{-2\pi n\frac{\zeta}{\sqrt{1-\zeta^2}}}$ during the time interval nT_d. Fig. B–2 shows the free vibration characteristic of a damped SDOF system. In order to find the damping ratio ζ, the logarithmic decrement δ is presented using Eq. (B–16),

$$\delta = \ln\left(\frac{x(t)}{x(t+T_\mathrm{d})}\right) = 2\pi\frac{\zeta}{\sqrt{1-\zeta^2}}. \tag{B–17}$$

According to Fig. B–2, the logarithmic decrement δ can be found by observing two upcrossings in the response A_0 and A_n placed with the time interval nT_d,

$$\delta = \frac{1}{n}\ln\left(\frac{A_0}{A_n}\right). \tag{B–18}$$

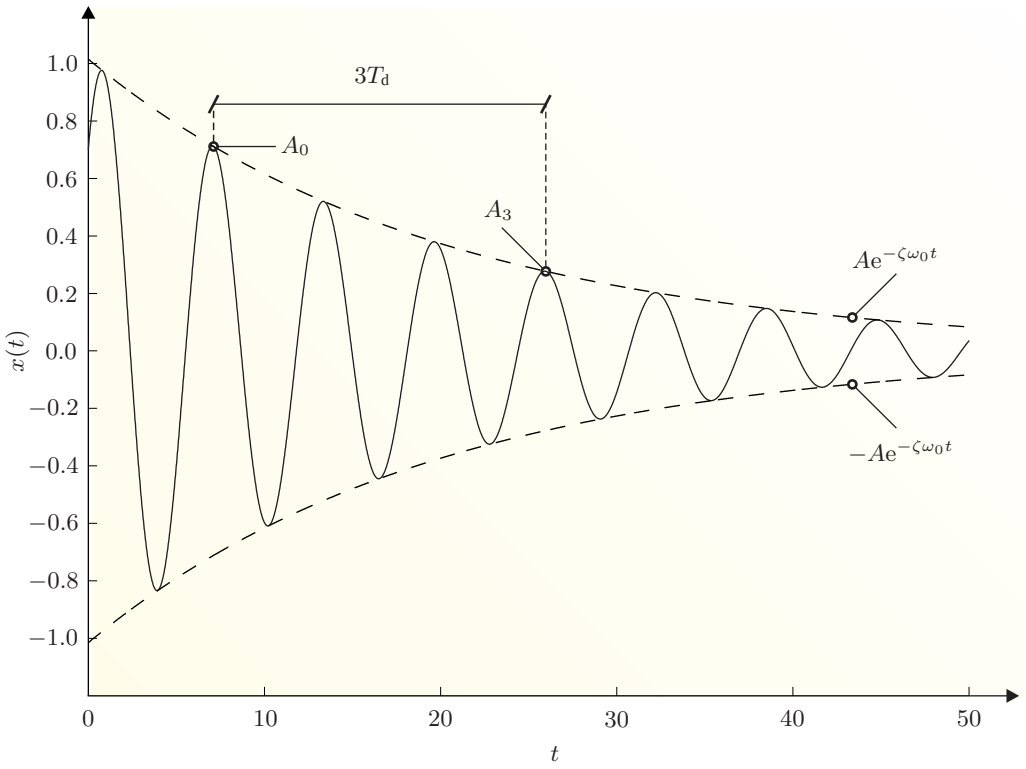

Figure B–2 Response of a damped system with $\zeta < 1$.

Forced Harmonic Vibrations for SDOF Systems

The equation of motion for forced harmonic vibrations is given by Eq. (B–1). An external force $f(t)$ of the following form is assumed:

$$f(t) = f_0 \cos \omega t, \tag{B–19}$$

where ω is the load frequency. Using Eqs. (B–4) and (B–9), the equation of motion for forced harmonic vibration reads

$$\ddot{x} + 2\omega_0 \zeta \dot{x} + \omega_0^2 x = \frac{f_0}{k} \omega_0^2 \cos \omega t. \tag{B–20}$$

The solution to the inhomogeneous differential equation given by Eq. (B–20) is searched for on the form

$$x(t) = C_1 \sin \omega t + C_2 \cos \omega t. \tag{B–21}$$

Inserting Eq. (B–21) into Eq. (B–20) provides

$$(\omega_0^2 - \omega^2)(C_1 \sin \omega t + C_2 \cos \omega t) + 2\zeta\omega_0(C_1 \cos \omega t - C_2 \sin \omega t) = \frac{f_0}{k} \omega_0^2 \cos \omega t. \tag{B–22}$$

By matching terms with $\sin \omega t$ and $\cos \omega t$, the two arbitrary constants C_1 and C_2 are determined

$$C_1 = \frac{f_0}{k} 2\zeta \frac{\omega}{\omega_0} f_1, \tag{B–23a}$$

$$C_2 = \frac{f_0}{k} \left(1 - \left(\frac{\omega}{\omega_0} \right)^2 \right) f_1, \tag{B–23b}$$

where the dynamic amplification factor f_1 is given by

$$f_1 = \sqrt{\frac{1}{\left(1 - \left(\frac{\omega}{\omega_0} \right)^2 \right)^2 + \left(2\zeta \frac{\omega}{\omega_0} \right)^2}}. \tag{B–24}$$

Inserting Eq. (B–24) into Eq. (B–21) provides

$$x(t) = \frac{f_0}{k} f_1 \cos(\omega t - \phi). \tag{B–25}$$

The phase delay of the motion ϕ in Eq. (B–25) can be written in the following way:

$$\tan \phi = \frac{2\zeta \frac{\omega}{\omega_0}}{1 - \left(\frac{\omega}{\omega_0} \right)^2} = \frac{2\zeta\omega_0\omega}{\omega_0^2 - \omega^2}. \tag{B–26}$$

The phase delay ϕ indicates that the maximum motion is observed ϕ later than the maximum loading.

Another way of deriving Eqs. (B–25) and (B–26) is by formulating the excitation $f(t)$ in complex notation. Eq. (B–19) then reads

$$f(t) = |F|\cos(\omega t - \alpha) = \text{Re}\left(F\text{e}^{\text{i}\omega t}\right), \tag{B–27a}$$

where i is the imaginary unit and

$$F = |F|\text{e}^{-\text{i}\alpha}. \tag{B–27b}$$

In this case, the equation of motion for forced vibration is given by

$$\ddot{x} + 2\zeta\omega_0\dot{x} + \omega_0^2 x = \text{Re}\left(\frac{F}{m}\text{e}^{\text{i}\omega t}\right). \tag{B–28}$$

A solution to Eq. (B–28) is searched for on the form

$$x(t) = |X|\cos(\omega t - \phi) = \text{Re}\left(X\text{e}^{\text{i}\omega t}\right) = \text{Re}\left(X\text{e}^{\text{i}\omega t}\right), \tag{B–29a}$$

where

$$X = |X|\text{e}^{-\text{i}\phi}. \tag{B–29b}$$

Inserting Eq. (B–29) into Eq. (B–28) provides

$$\text{Re}\left([m(\omega_0^2 - \omega^2 + 2\text{i}\zeta\omega_0\omega)X - F]\text{e}^{\text{i}\omega t}\right) = 0. \tag{B–30}$$

Eq. (B–29) is a possible motion if and only if Eq. (B–30) is fulfilled at all times. This is only possible if the term within the sharp-edged brackets is equal to zero. This leads to

$$X = H(\omega)F, \tag{B–31}$$

where $H(\omega)$ is characterised as the frequency response function

$$H(\omega) = \frac{1}{m(\omega_0^2 - \omega^2 + 2\text{i}\zeta\omega_0\omega)}. \tag{B–32}$$

It should be noted that $H(\omega)$ is the complex amplitude of $x(t)$ for $F = 1$. The denominator N in Eq. (B–32) becomes

$$N = m(\omega_0^2 - \omega^2 + 2\text{i}\zeta\omega_0\omega) = \left(m\sqrt{(\omega_0^2 - \omega_0)^2 + 4\zeta^2\omega_0^2\omega^2}\right)\text{e}^{\text{i}\phi}, \tag{B–33}$$

where ϕ is given by Eq. (B–26). Eq. (B–33) is illustrated graphically in Fig. B–3. Hence, Eq. (B–31) can be written in the following way:

$$X = \frac{|F|}{m\sqrt{\left(\omega_0^2 - \omega^2\right)^2 + 4\zeta^2\omega_0^2\omega^2}}\text{e}^{-\text{i}\phi_1}, \tag{B–34}$$

where $\phi_1 = \phi + \alpha$. Taken the absolute value of Eq. (B–34) gives

$$|X| = \frac{|F|}{m\omega_0^2\sqrt{\left(1 - \left(\frac{\omega}{\omega_0}\right)^2\right)^2 + 4\zeta^2\left(\frac{\omega}{\omega_0}\right)^2}} = X_{\text{s}}f_1, \tag{B–35}$$

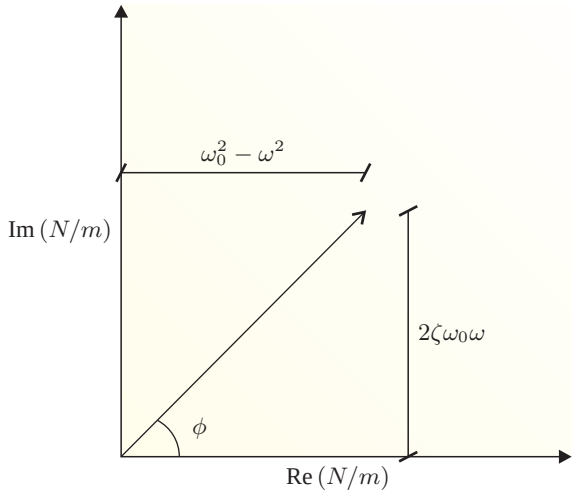

Figure B–3 Graphic illustration of Eq. (B–33).

where $X_s = |F|/k$ denotes the amplitude of the motion for a harmonic external load with the amplitude $|F|$ and an infinitely small circular eigenfrequency ω, *i.e.* the inertia and the damping force are ignored. Inserting Eq. (B–35) into Eq. (B–29) provides exactly the same result as stated in Eq. (B–25). As mentioned earlier f_1 is the dynamic amplification factor which describes the relative increase of the amplitude $|X|$ when the inertia and the damping force have significant influence of the motion. Harmonic excitations with $\omega = \omega_0$ lead to resonance in which case the dynamic amplification factor and the phase angle become $f_1 = 1/2\zeta$ and $\phi = 90°$, respectively. Fig. B–4a shows the dynamic amplification factor f_1 as a function of the frequency ratio $\frac{\omega}{\omega_0}$ for different damping ratios ζ. Similarly, the phase angle ϕ is shown in Fig. B–4b.

B.1.2 Multi-Degree-of-Freedom-System Theory

Dynamic systems that require n degrees of freedom specified by n coordinates to describe their motion are called MDOF systems. In general, the force equilibrium of an MDOF system can be established where the inertia forces $\mathbf{M}\ddot{\mathbf{x}}$ are balanced by a set of linear elastic restoring forces $\mathbf{Kx}$, viscous damping forces $\mathbf{C}\dot{\mathbf{x}}$ and the external force $\mathbf{f}(t)$, *i.e.*

$$\mathbf{M}\ddot{\mathbf{x}} + \mathbf{C}\dot{\mathbf{x}} + \mathbf{kx} = \mathbf{f}(t), \tag{B–36}$$

where $\mathbf{M}$, $\mathbf{C}$ and $\mathbf{K}$ are the mass, damping and stiffness matrices, respectively, and have the dimensions $n \times n$. $\mathbf{x}(t)$ and $\mathbf{f}(t)$ are the $n \times 1$ generalized displacement and force vectors, respectively. The mass matrix $\mathbf{M}$, stiffness matrix $\mathbf{K}$ and damping matrix $\mathbf{C}$ fulfil the following positive definite and symmetric properties for any given vector $\mathbf{a} \neq 0$:

$$\left\{ \begin{array}{lll} \mathbf{a}^\top\mathbf{Ka} > 0 & , & \mathbf{K} = \mathbf{K}^\top \\ \mathbf{a}^\top\mathbf{Ma} > 0 & , & \mathbf{M} = \mathbf{M}^\top \\ \mathbf{a}^\top\mathbf{Ca} > 0 & & \end{array} \right\}. \tag{B–37}$$

In general, any non-zero velocity of the structural system should be related with energy dissipation. Hence, it is often a usual assumption that the damping matrix $\mathbf{C}$ is symmetric due to

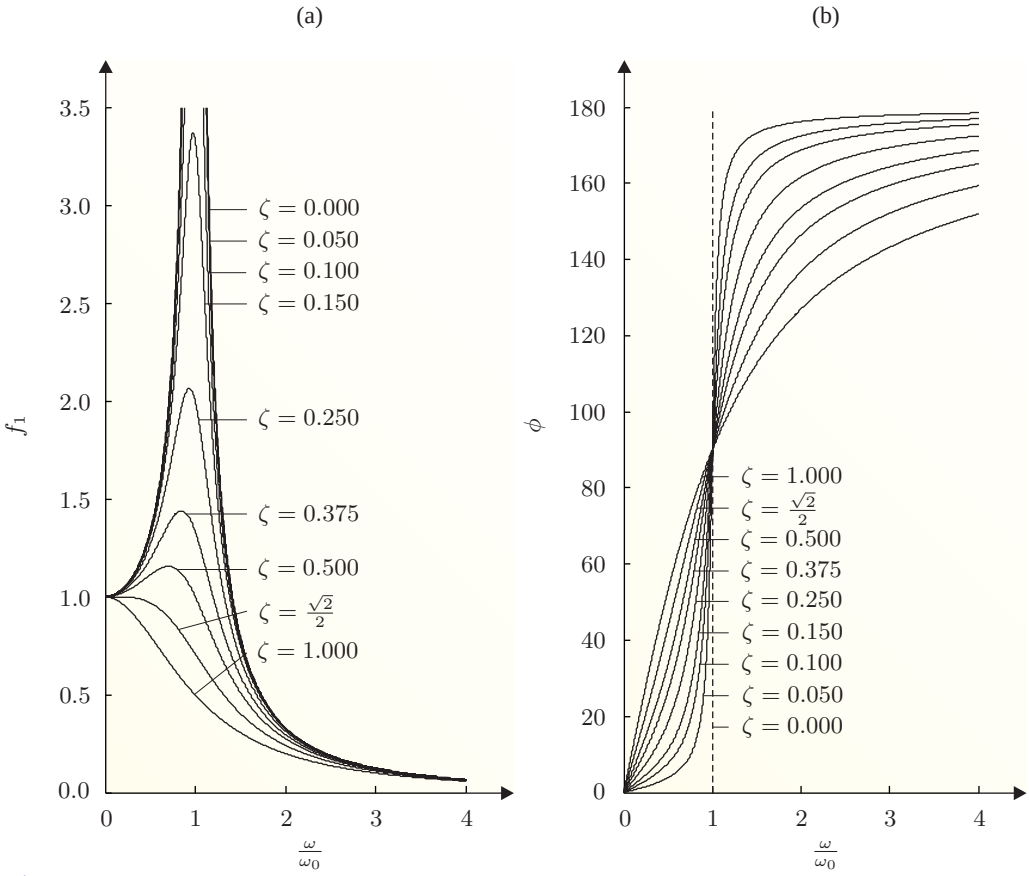

Figure B–4 Dynamic response vs. frequency ratio $\frac{\omega}{\omega_0}$ and damping ratio ζ: (a) dynamic amplification factor f_1, (b) phase angle ϕ.

the fact that energy dissipation is confirmed only to the symmetric part of the matrix. However, notice that the damping matrix $\mathbf{C}$ does not necessarily need to fulfil any symmetric properties in the linear vibration theory.

In case of vibrations due to an arbitrary excitation, the solution to Eq. (B–36) can be described by an impulse response function $\mathbf{h}(\tau)$, also called the weighting function. The function is defined as the output of the system at any time to a unit impulse input applied a time τ before and takes the form of a matrix for an MDOF system. For zero initial conditions, *i.e.* the displacement vector $\mathbf{x}(0)$ and the velocity vector $\dot{\mathbf{x}}(0)$ equal to zero, the solution to Eq. (B–36) can be written in terms of the convolution integral,

$$\left\{ \begin{array}{l} \mathbf{x}(t) = \displaystyle\int_0^\infty \mathbf{h}(\tau)\mathbf{f}(t-\tau)d\tau \\ \mathbf{x}(0) = 0\,,\ \dot{\mathbf{x}}(0) = 0 \end{array} \right\}. \tag{B–38}$$

Eq. (B–38) specifies that the response $\mathbf{x}(t)$ is given by a weighted linear sum over the entire history of the input $\mathbf{f}(t)$. The function fully describes the dynamic behaviour of the structural

system in the time domain. Letting $\mathbf{F}(\omega)$ be the Fourier transform of the input $\mathbf{f}(t)$ and letting $\mathbf{X}(\mathrm{i}\omega)$ be the Fourier transform of the output $\mathbf{x}(t)$, it follows from Eq. (B–38) that

$$\mathbf{X}(\mathrm{i}\omega) = \mathbf{H}(\mathrm{i}\omega)\mathbf{F} = \int_0^\infty \mathbf{h}(\tau)\mathrm{e}^{-\mathrm{i}\omega\tau}d\tau\mathbf{F} = \left(-\omega^2\mathbf{M} + \mathrm{i}\omega\mathbf{C} + \mathbf{K}\right)^{-1}\mathbf{F}. \tag{B–39}$$

The last term in Eq. (B–39) can easily be proofed. Assuming an MDOF dynamic system being exposed to an external harmonic varying force $\mathbf{f}(t)$ given by

$$\mathbf{f}(t) = \mathrm{Re}\left(\mathbf{F}\mathrm{e}^{\mathrm{i}\omega t}\right), \tag{B–40}$$

Eq. (B–36) can be written as

$$\mathbf{M}\ddot{\mathbf{x}} + \mathbf{C}\dot{\mathbf{x}} + \mathbf{k}\mathbf{x} = \mathrm{Re}\left(\mathbf{F}\mathrm{e}^{\mathrm{i}\omega t}\right). \tag{B–41}$$

Similarly to Eq. (B–29) for an SDOF system, the stationary solution to Eq. (B–41) is searched for on the form

$$\mathbf{X}(t) = \mathrm{Re}\left(\mathbf{X}\mathrm{e}^{\mathrm{i}\omega t}\right), \tag{B–42}$$

where $\mathbf{X}$ is a complex amplitude. Inserting Eq. (B–42) into Eq. (B–41) provides

$$\mathrm{Re}\left(\left[(-\omega^2\mathbf{M} + \mathrm{i}\omega\mathbf{C} + \mathbf{K})\mathbf{X} - \mathbf{F}\right]\mathrm{e}^{\mathrm{i}\omega t}\right) = \mathbf{0}. \tag{B–43}$$

As mentioned in relation to Eq. (B–30), Eq. (B–42) is a possible motion if and only if Eq. (B–43) is fulfilled at all times. Hence, the term inside the sharp-edged brackets must be equal to zero. This leads to Eq. (B–39). Overall, this means that by use of the frequency response function $\mathbf{H}(\omega)$ and Fourier transform of the input and the output, the convolution integral in Eq. (B–38) reduces to simple algebraic expression in Eq. (B–39).

Eigenvibrations of Undamped MDOF Systems

Assuming that the structural system is given a unit impulse and then left on its own, the differential equation for undamped vibrations of an MDOF system follows from Eq. (B–36) for $\mathbf{C} = \mathbf{0}$ and $\mathbf{f}(t) = \mathbf{0}$,

$$\mathbf{M}\ddot{\mathbf{x}} + \mathbf{k}\mathbf{x} = \mathbf{0}. \tag{B–44}$$

The solution to Eq. (B–44) is sought on the form

$$\mathbf{x}(t) = \mathrm{Re}\left(\mathbf{\Phi}\mathrm{e}^{\mathrm{i}\omega t}\right). \tag{B–45}$$

The vector $\mathbf{\Phi}$ in Eq. (B–45) is an unknown complex amplitude vector. Inserting Eq. (B–45) into Eq. (B–44) provides, when same arguments are used as in Eq. (B–30),

$$\mathrm{Re}\left(\left[-\omega^2\mathbf{M} + \mathbf{K}\right]\mathbf{\Phi}\mathrm{e}^{\mathrm{i}\omega t}\right) = \mathbf{0} \Rightarrow$$

$$\left(\mathbf{K} - \omega^2\mathbf{M}\right)\mathbf{\Phi} = \mathbf{0}. \tag{B–46}$$

Eq. (B–46) represents a homogeneous system of n linear equations for the determination of the circular eigenfrequency ω and the unknown amplitude $\mathbf{\Phi}$. The necessary condition for non-trivial solutions $\mathbf{\Phi} \neq \mathbf{0}$ is

$$\det\left(\mathbf{K} - \omega^2\mathbf{M}\right) = 0. \tag{B–47}$$

Eq. (B–47) is denoted the frequency condition. For each of the roots $\omega_1^2, \omega_2^2, \ldots, \omega_n^2$, which forms the eigenvalues of Eq. (B–47), a non-trivial solution $\mathbf{\Phi}^{(1)}, \mathbf{\Phi}^{(2)}, \ldots, \mathbf{\Phi}^{(n)}$ exists to Eq. (B–47). These solutions are denoted the undamped eigenmodes. Given the circular eigenfrequencies $\omega_j = \sqrt{\omega_j^2}$ and the mode shapes $\mathbf{\Phi}^{(j)}$, Eq. (B–45) can be written in the following way:

$$\mathbf{x}(t) = \mathrm{Re}\left(\mathbf{\Phi}^{(j)}\mathrm{e}^{\mathrm{i}\omega_j t}\right) = \mathbf{\Phi}^{(j)}\mathrm{Re}\left(\mathrm{e}^{\mathrm{i}\omega_j t}\right) = \mathbf{\Phi}^{(j)}\cos\omega_j t. \tag{B–48}$$

However, it can be shown that $\mathbf{x}(t) = \mathbf{\Phi}^{(j)}\sin\omega_j t$ also is a solution to Eq. (B–44). $2n$ linear independent solutions to the homogeneous differential equation formulated in Eq. (B–44) then exist,

$$\left.\begin{array}{l}\mathbf{x}(t) = \mathbf{\Phi}^{(j)}\cos\omega_j t \\ \mathbf{x}(t) = \mathbf{\Phi}^{(j)}\sin\omega_j t\end{array}\right\} j = 1, \ldots, n. \tag{B–49}$$

Thus, any solution to Eq. (B–44) can be written as a linear combination of the fundamental solutions in Eq. (B–49),

$$\mathbf{x}(t) = a_1\mathbf{\Phi}^{(1)}\cos\omega_1 t + \cdots + a_n\mathbf{\Phi}^{(n)}\cos\omega_n t + b_1\mathbf{\Phi}^{(1)}\sin\omega_1 t + \cdots + b_n\mathbf{\Phi}^{(n)}\sin\omega_n t. \tag{B–50}$$

The task is now to determine the coefficients a_1, a_2,…, a_n and b_1, b_2,…, b_n, so the initial conditions $\mathbf{x}_0$ and $\dot{\mathbf{x}}_0$ are fulfilled

$$\mathbf{x}(0) = \mathbf{x}_0 = a_1\mathbf{\Phi}^{(1)} + a_2\mathbf{\Phi}^{(2)} + \cdots + a_n\mathbf{\Phi}^{(n)} \Rightarrow$$

$$\mathbf{x}_0 = \mathbf{P}\mathbf{a} \Rightarrow \mathbf{a} = \begin{bmatrix} a_1 \\ a_2 \\ \vdots \\ a_n \end{bmatrix} = \mathbf{P}^{-1}\mathbf{x}_0, \tag{B–51}$$

where $\mathbf{P} = \left[\mathbf{\Phi}^{(1)}, \ldots, \mathbf{\Phi}^{(n)}\right]$ is denoted the modal matrix.

$$\dot{\mathbf{x}}(0) = \dot{\mathbf{x}}_0 = b_1\omega_1\mathbf{\Phi}^{(1)} + b_2\omega_2\mathbf{\Phi}^{(2)} + \cdots + b_n\omega_n\mathbf{\Phi}^{(n)} \Rightarrow$$

$$\dot{\mathbf{x}}_0 = \mathbf{P}\mathbf{b}\omega \Rightarrow \mathbf{b}\omega = \begin{bmatrix} b_1\omega_1 \\ b_2\omega_2 \\ \vdots \\ b_n\omega_n \end{bmatrix} = \mathbf{P}^{-1}\dot{\mathbf{x}}_0. \tag{B–52}$$

Eigenvibrations of Damped MDOF Systems

Just like the eigenvibrations for an undamped MDOF system, it is assumed that the damped structural system is given a unit impulse and then left on its own. Since the vibrations now are viscously damped, it is necessary to consider a complex eigenvalue problem to determine the modal parameters. Combining the identity $\mathbf{M}\ddot{\mathbf{x}} - \mathbf{M}\ddot{\mathbf{x}} = \mathbf{0}$ with Eq. (B–36) produce the following system of differential equations:

$$\begin{bmatrix} \mathbf{C} & \mathbf{M} \\ \mathbf{M} & \mathbf{0} \end{bmatrix} \begin{bmatrix} \dot{\mathbf{x}} \\ \ddot{\mathbf{x}} \end{bmatrix} + \begin{bmatrix} \mathbf{K} & \mathbf{0} \\ \mathbf{0} & -\mathbf{M} \end{bmatrix} \begin{bmatrix} \mathbf{x} \\ \dot{\mathbf{x}} \end{bmatrix} = \begin{bmatrix} \mathbf{f}(t) \\ \mathbf{0} \end{bmatrix}, \tag{B–53}$$

which may be written in the so-called state vector formulation

$$\left\{ \begin{array}{ll} \mathbf{A}\dot{\mathbf{z}}(t) + \mathbf{B}\mathbf{z}(t) = \mathbf{F}(t) & , \quad t > 0 \\ \mathbf{z}(0) = \mathbf{z}_0 & \end{array} \right\}, \tag{B–54a}$$

where

$$\mathbf{z}(t) = \begin{bmatrix} \mathbf{x}(t) \\ \dot{\mathbf{x}}(t) \end{bmatrix} \quad , \quad \mathbf{z}_0 = \begin{bmatrix} \mathbf{x}_0 \\ \dot{\mathbf{x}}_0 \end{bmatrix}, \tag{B–54b}$$

$$\mathbf{F}(t) = \begin{bmatrix} \mathbf{f}(t) \\ \mathbf{0} \end{bmatrix}, \tag{B–54c}$$

$$\mathbf{A} = \begin{bmatrix} \mathbf{C} & \mathbf{M} \\ \mathbf{M} & \mathbf{0} \end{bmatrix} \quad , \quad \mathbf{B} = \begin{bmatrix} \mathbf{K} & \mathbf{0} \\ \mathbf{0} & -\mathbf{M} \end{bmatrix}. \tag{B–54d}$$

The state vector formulation reduces the second-order differential equation system in Eq. (B–36) to a first-order differential equation system. Eq. (B–54b) is denoted the state vector. The eigenvibrations of the system in Eq. (B–54a) are then given by

$$\mathbf{A}\dot{\mathbf{z}}(t) + \mathbf{B}\mathbf{z}(t) = \mathbf{0}, \tag{B–55}$$

and the solution is search for on the form

$$\mathbf{z}(t) = \mathbf{\Psi}\mathrm{e}^{\lambda t}, \tag{B–56}$$

where $\mathbf{\Psi}$ is a complex vector of dimension $2n \times 1$ and λ is a complex constant for $j = 1$ to $j = 2n$. Insertion Eq. (B–56) into Eq. (B–55) shows that Eq. (B–56) is a solution if and only if $\mathbf{\Psi}$ is a solution to the following first-order eigenvalue problem:

$$(\lambda\mathbf{A} + \mathbf{B})\mathbf{\Psi} = \mathbf{0}. \tag{B–57}$$

As mentioned earlier, a necessary condition for non-trivial solutions to the homogeneous system of equations $\mathbf{\Psi} \neq \mathbf{0}$ is that

$$\det(\lambda\mathbf{A} + \mathbf{B}) = 0. \tag{B–58}$$

The polynomial in Eq. (B–58) has the order $2n$. A total of $2n$ roots λ_j are present in the polynomial which are the eigenvalues of Eq. (B–57). For each eigenvalue, a non-trivial solution $\mathbf{\Psi}^{(j)}$ to Eq. (B–57) exists. The eigenvalues λ_j and the corresponding eigenvectors $\mathbf{\Psi}^{(j)}$ can either be

real or complex. For lightly damped structures, all eigenvalues are complex. In this case, only n eigenvalues and eigenvectors need to be considered due to complex conjugated eigen-pairs. Similarly, if the eigenvalues are real, the system is overcritically damped. In the following, only lightly damped structures are considered. The complex conjugated eigenvalue-pairs for $j = 1$ to $j = n$ are then given by

$$\left.\begin{bmatrix}\lambda_j \\ \lambda_j^*\end{bmatrix}\right\} = -\zeta_j\omega_j \pm \mathrm{i}\omega_j\sqrt{1-\zeta_j^2}. \tag{B–59}$$

If the eigenvalues are written as $\lambda_j = -\mu_j + \mathrm{i}\nu_j$, it follows that

$$\mu_j = \zeta_j\omega_j, \tag{B–60a}$$

$$\nu_j = \omega_j\sqrt{1-\zeta_j^2}. \tag{B–60b}$$

The first n components of the eigenvector $\boldsymbol{\Psi}^{(j)}$ is now assembled in the n-dimensional sub-vector $\boldsymbol{\Phi}^{(j)}$. Thus, based on Eqs. (B–54) and (B–56), it follows that

$$\mathbf{x}(t) = \boldsymbol{\Phi}^{(j)}\mathrm{e}^{\lambda_j t}, \tag{B–61}$$

$$\dot{\mathbf{x}}(t) = \lambda_j\boldsymbol{\Phi}^{(j)}\mathrm{e}^{\lambda_j t}. \tag{B–62}$$

It means that the eigenvectors $\boldsymbol{\Psi}^{(j)}$ must be characterised as

$$\boldsymbol{\Psi}^{(j)} = \begin{bmatrix}\boldsymbol{\Phi}^{(j)} \\ \lambda_j\boldsymbol{\Phi}^{(j)}\end{bmatrix}. \tag{B–63}$$

Consequently, only the first n components of the eigenvectors $\boldsymbol{\Psi}^{(j)}$ need to be determined. Insertion of Eqs. (B–54d) and (B–63) into Eq. (B–57) yields

$$(\lambda_j^2\mathbf{M} + \lambda_j\mathbf{C} + \mathbf{K})\boldsymbol{\Phi}^{(j)} = \mathbf{0}, \tag{B–64}$$

with the characteristic equation given by

$$\det(\mathbf{M}\lambda_j^2 + \mathbf{C}\lambda_j + \mathbf{K}) = 0. \tag{B–65}$$

Eq. (B–64) is a nonlinear eigenvalue problem of order n. The roots λ_j to the characteristic equations, Eqs. (B–58) and (B–65), are identical. In addition, the eigenvectors $\boldsymbol{\Phi}^{(j)}$ to Eq. (B–64) represent the half of the eigenvectors $\boldsymbol{\Psi}^{(j)}$. The eigenvectors $\boldsymbol{\Phi}^{(j)}$ of dimension n are called damped eigenmodes. For structural systems with few DOFs, the nonlinear eigenvalue problem can be used. However, for increasing number of DOFs, the linear eigenvalue problem is recommended despite the double size of the eigenvectors.

With the definition of solving an eigenvalue problem for MDOF systems, the impulse response function $\mathbf{h}(\tau)$ in Eq. (B–38) can be expressed in terms of the modal decomposed system as

$$\mathbf{h}(\tau) = \sum_{j=1}^{2n}\frac{\boldsymbol{\Phi}^{(j)}\boldsymbol{\Phi}^{(j)\top}}{m_j}\mathrm{e}^{\lambda_j\tau} = \sum_{j=1}^{2n}\mathbf{R}_j\mathrm{e}^{\lambda_j\tau}, \tag{B–66}$$

where m_j is the jth damped modal mass and $\mathbf{R}_j$ is the residue matrix that corresponds to the jth eigenvalue λ_j. Similarly, the frequency response function $\mathbf{H}(\mathrm{i}\omega)$ in Eq. (B–39) then reads

$$\mathbf{H}(\mathrm{i}\omega) = \sum_{j=1}^{2n}\frac{\mathbf{R}_j}{\mathrm{i}\omega - \lambda_j}. \tag{B–67}$$

Modal Decomposition

Due to the fact that the undamped eigenmodes $\mathbf{\Phi}^{(j)}$ are linearly independent, they may be used as a basis in the n-dimensional vector space. Hence, the displacement vector $\mathbf{x}(t)$ in Eq. (B–36) can be written as

$$\mathbf{x}(t) = \sum_{j=1}^{n} \mathbf{\Phi}^{(j)} q_j(t) = \mathbf{\Phi}\mathbf{q}(t) \quad , \quad \mathbf{q}(t) = \begin{bmatrix} q_1(t) \\ q_2(t) \\ \vdots \\ q_n(t) \end{bmatrix}, \tag{B–68}$$

where the coordinates $q_1(t), \ldots, q_n(t)$ are termed the undamped modal coordinates. In other words, the undamped eigenmodes $\mathbf{\Phi}^{(1)}, \ldots, \mathbf{\Phi}^{(n)}$ constitute the transformation matrix from the modal coordinate system to the Cartesian coordinate system. In general, two undamped eigenmodes $\mathbf{\Phi}^{(i)}$ and $\mathbf{\Phi}^{(j)}$ with different eigenvalues λ_i and λ_j fulfil the orthogonality conditions

$$\mathbf{\Phi}^{(i)\top}\mathbf{M}\mathbf{\Phi}^{(j)} = \begin{cases} 0, & i \neq j \\ M_i, & i = j \end{cases}, \tag{B–69a}$$

$$\mathbf{\Phi}^{(i)\top}\mathbf{K}\mathbf{\Phi}^{(j)} = \begin{cases} 0, & i \neq j \\ \omega_i^2 M_i, & i = j \end{cases}. \tag{B–69b}$$

The parameter M_i is denoted the undamped modal mass. Assuming that the undamped eigenmodes $\mathbf{\Phi}^{(j)}$ also are orthogonal weighted with the damping matrix $\mathbf{C}$, the decoupling condition is

$$\mathbf{\Phi}^{(i)\top}\mathbf{C}\mathbf{\Phi}^{(j)} = \begin{cases} 0, & i \neq j \\ 2\zeta_i\omega_i M_i, & i = j \end{cases}. \tag{B–69c}$$

The orthogonality properties may be expressed in the following matrix equation:

$$\mathbf{\Phi}^{\top}\mathbf{M}\mathbf{\Phi} = \begin{bmatrix} M_1 & 0 & \cdots & 0 \\ 0 & M_2 & \cdots & 0 \\ \vdots & \vdots & \ddots & \vdots \\ 0 & 0 & \cdots & M_n \end{bmatrix} = \mathbf{m}, \tag{B–70a}$$

$$\mathbf{\Phi}^{\top}\mathbf{K}\mathbf{\Phi} = \begin{bmatrix} \omega_1^2 M_1 & 0 & \cdots & 0 \\ 0 & \omega_2^2 M_2 & \cdots & 0 \\ \vdots & \vdots & \ddots & \vdots \\ 0 & 0 & \cdots & \omega_n^2 M_n \end{bmatrix} = \mathbf{k}, \tag{B–70b}$$

$$\mathbf{\Phi}^{\top}\mathbf{C}\mathbf{\Phi} = \begin{bmatrix} 2\zeta_1\omega_1 M_1 & 0 & \cdots & 0 \\ 0 & 2\zeta_2\omega_2 M_2 & \cdots & 0 \\ \vdots & \vdots & \ddots & \vdots \\ 0 & 0 & \cdots & 2\zeta_n\omega_n M_n \end{bmatrix} = \mathbf{c}, \tag{B–70c}$$

where $\mathbf{m}$, $\mathbf{k}$ and $\mathbf{c}$ are the modal mass, stiffness and damping diagonal matrices, respectively. Insertion of Eq. (B–70) into Eq. (B–36) followed by a pre-multiplication with $\mathbf{\Phi}^{\top}$, gives the

matrix differential equation for the modal coordinates

$$\ddot{q}_i + 2\omega_i \left(\zeta_i \dot{q}_i + \sum_{j=1}^{n} \sqrt{\frac{\omega_j M_j}{\omega_i M_i}} \zeta_{ij} \dot{q}_j \right) + \omega_i^2 q_i = \frac{1}{M_i} F_i(t) =$$

$$\mathbf{m}\ddot{\mathbf{q}}(t) + \mathbf{c}\dot{\mathbf{q}}(t) + \mathbf{k}\mathbf{q}(t) = \mathbf{F}(t) \quad , \quad i,j = 1,\ldots,n \quad , \quad j \neq i, \quad t > 0, \tag{B–71a}$$

where

$$\zeta_i = \frac{\boldsymbol{\Phi}^{(i)\top} \mathbf{C} \boldsymbol{\Phi}^{(i)}}{2\omega_i M_i} \quad , \quad i = 1,\ldots,n, \tag{B–71b}$$

$$\zeta_{ij} = \frac{\boldsymbol{\Phi}^{(i)\top} \mathbf{C} \boldsymbol{\Phi}^{(j)}}{2\sqrt{\omega_i \omega_j M_i M_j}} \quad , \quad i,j = 1,\ldots,n, \quad j \neq i, \tag{B–71c}$$

$$\mathbf{F}(t) = \boldsymbol{\Phi}^{\top} \mathbf{f}(t) = \begin{bmatrix} F_1(t) \\ F_2(t) \\ \vdots \\ F_n(t) \end{bmatrix}. \tag{B–71d}$$

Notice that Eq. (B–71b) is general and even valid in the special case of not fulfilling the orthogonality property according to Eq. (B–70c). The initial conditions to Eq. (B–71a) reads

$$\mathbf{q}(t_0) = \boldsymbol{\Phi}^{-1} \mathbf{x}_0 \quad , \quad \dot{\mathbf{q}}(t_0) = \boldsymbol{\Phi}^{-1} \dot{\mathbf{x}}_0. \tag{B–72}$$

Since $\mathbf{m}$, $\mathbf{k}$ and $\mathbf{c}$ are diagonal matrices, the differential equations in Eq. (B–71a) decouple completely. Hence, the differential equation for the kth modal coordinate reads

$$\ddot{q}_k(t) + 2\zeta_k \omega_k \dot{q}_k(t) + \omega_k^2 q_k(t) = \frac{1}{M_k} F_k(t). \tag{B–73}$$

From Eq. (B–73), it is seen that the decoupling condition reduces the integration of a linear n DOF system to the integration of n SDOF systems. In other words, Eq. (B–73) is identical to the equation of motion of an SDOF system from Eqs. (B–1), (B–4), and (B–9) with M_k, ω_k, ζ_k and $F_k(t)$ replacing the mass m, the circular eigenfrequency ω_0, the damping ratio ζ and the external loading $f(t)$. The neglection of the coupling between the modal differential equations via modal velocities, cf. Eq. (B–71a), is often acceptable if the circular eigenfrequencies are well separated and the system is lightly damped. In this regard, the following conditions should be fulfilled:

$$\omega_i(1 + a\zeta_i) < \omega_{i+1}(1 - a\zeta_{i+1}) \quad , \quad i = 1,\ldots,n-1, \tag{B–74}$$

where $a \approx 2 - 3$.

Just like Eq. (B–68) is a solution to Eq. (B–36), the following expression is a solution to Eq. (B–55):

$$\mathbf{z}(t) = \sum_{j=1}^{n} \boldsymbol{\Psi}^{(j)} q_j(t) + \boldsymbol{\Psi}^{(j)*} q_j^*(t) = \sum_{j=1}^{2n} \mathrm{Re}\left(\boldsymbol{\Psi}^{(j)} q_j(t) \right), \tag{B–75}$$

where the coordinates $q_1(t), \ldots, q_n(t)$ represent the damped modal coordinates. Similar to the matrices $\mathbf{M}$ and $\mathbf{K}$, $\mathbf{A}$ and $\mathbf{B}$ in Eq. (B–54a) are symmetric. Hence, the following orthogonality properties exist

$$\boldsymbol{\Psi}^{(i)\top}\mathbf{A}\boldsymbol{\Psi}^{(j)} = \begin{cases} 0, & i \neq j \\ m_j, & i = j \end{cases}, \tag{B–76a}$$

$$\boldsymbol{\Psi}^{(i)\top}\mathbf{B}\boldsymbol{\Psi}^{(j)} = \begin{cases} 0, & i \neq j \\ -\lambda_j m_j, & i = j \end{cases}, \tag{B–76b}$$

where m_j is denoted the damped modal mass. The damped modal mass m_j may alternatively be written in the following way using Eqs. (B–54d) and (B–63):

$$m_j = \boldsymbol{\Phi}^{(j)\top}\mathbf{C}\boldsymbol{\Phi}^{(j)} + 2\lambda_j \boldsymbol{\Phi}^{(j)\top}\mathbf{M}\boldsymbol{\Phi}^{(j)}. \tag{B–77}$$

With the orthogonality properties defined, Eq. (B–75) is inserted into Eq. (B–54a) followed by pre-multiplication with $\boldsymbol{\Psi}^{(i)}$. The initial value equation is pre-multiplied with $\boldsymbol{\Psi}^{(i)\top}\mathbf{A}$, *i.e.*

$$\left\{ \begin{array}{ll} \dot{q}_i - \lambda_i q_i = \frac{1}{m_i}\boldsymbol{\Psi}^{(i)\top}\mathbf{F}(t) & , \quad t > 0 \\ q_i(0) = \frac{1}{m_i}\boldsymbol{\Psi}^{(i)\top}\mathbf{A}\mathbf{z}_0 & \end{array} \right\}. \tag{B–78}$$

The solution to Eq. (B–78) is

$$q_i(t) = \mathrm{e}^{\lambda_i t}\left(\int_0^t \mathrm{e}^{-\lambda_i \tau}\frac{1}{m_i}\boldsymbol{\Psi}^{(i)\top}\mathbf{F}(\tau)\mathrm{d}\tau + q_i(0)\right) \quad , \quad t > 0. \tag{B–79}$$

From Eqs. (B–54c) and (B–63) it follows that

$$\boldsymbol{\Psi}^{(i)\top}\mathbf{F}(\tau) = \boldsymbol{\Phi}^{(i)\top}\mathbf{f}(\tau). \tag{B–80}$$

The initial values $q_i(0)$ from Eq. (B–78) can be written in the following way using Eqs. (B–54b) and (B–63):

$$q_i(0) = \frac{1}{m_i}\begin{bmatrix}\boldsymbol{\Phi}^{(i)} \\ \lambda_i\boldsymbol{\Phi}^{(i)}\end{bmatrix}^\top \begin{bmatrix}\mathbf{C} & \mathbf{M} \\ \mathbf{M} & \mathbf{0}\end{bmatrix}\begin{bmatrix}\mathbf{x}_0 \\ \dot{\mathbf{x}}_0\end{bmatrix} =$$

$$\frac{1}{m_i}\boldsymbol{\Phi}^{(i)\top}\left((\mathbf{C} + \lambda_i\mathbf{M})\mathbf{x}_0 + \mathbf{M}\dot{\mathbf{x}}_0\right) \quad , \quad i = 1, \ldots, n. \tag{B–81}$$

The displacements $\mathbf{x}(t)$ are then obtained using Eqs. (B–54b), (B–63) and (B–75):

$$\mathbf{x}(t) = 2\sum_{j=1}^{n}\mathrm{Re}\left(\boldsymbol{\Phi}^{(j)}q_j(t)\right). \tag{B–82}$$

B.1.3 2DOF System Equivalence of a Wind Turbine Structure with Viscous Tuned Mass Damper

Passive dynamic dampers are often installed in offshore wind turbines in order to attenuate any undesirable vibrations. In general, the natural frequency of the passive damper is tuned to a frequency near the natural frequency of the primary system. Hence, near resonance the vibrations

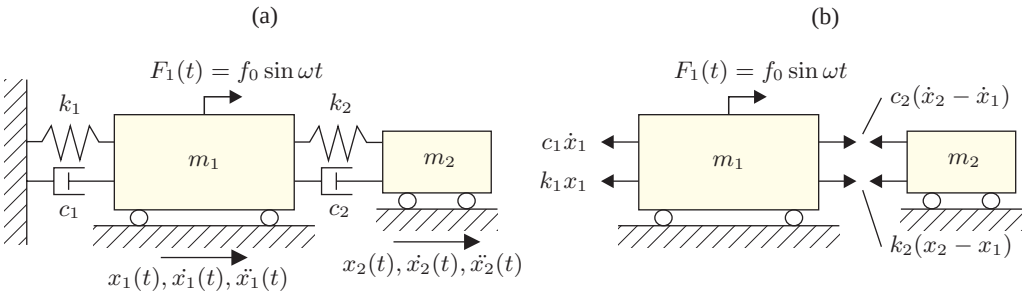

Figure B–5 Equivalent dynamic system with two degrees of freedom representing the offshore wind turbine with an oil damper installed: (a) linear viscous damped system, (b) free body diagram.

of the primary system cause the passive damper to vibrate which dissipate the energy. Many different types of passive dynamic dampers exist, one of them is the so-called oil damper applicable for wind turbines. A steel cylinder is hanging up on chains just beneath the nacelle where a pendulum is partly immersed in high viscous oil.

In order to model the total system behaviour of the wind turbine structure with an oil damper installed, a 2DOF viscously damped system can be used, see Fig. B–5a. The system consists of the generalised mass m_1, the spring stiffness k_1 and the inherent damping c_1 of the wind turbine structure. x_1 is the displacement of the primary system. Similar, m_2, k_2, c_2 and x_2 are the mass, stiffness, damping and displacement of the oil damper. The basic equation of motion for a 2DOF system subjected to a harmonic load can be determined by cutting the masses free from the springs and damping elements. The springs forces and damping forces in the dynamically deformed state are applied as external forces on the masses with the sign shown in Fig. B–5b,

$$\begin{bmatrix} m_1 & 0 \\ 0 & m_2 \end{bmatrix} \begin{bmatrix} \ddot{x}_1 \\ \ddot{x}_2 \end{bmatrix} + \begin{bmatrix} c_1 + c_2 & -c_2 \\ -c_2 & c_2 \end{bmatrix} \begin{bmatrix} \dot{x}_1 \\ \dot{x}_2 \end{bmatrix} + \begin{bmatrix} k_1 + k_2 & -k_2 \\ -k_2 & k_2 \end{bmatrix} \begin{bmatrix} x_1 \\ x_2 \end{bmatrix} = \begin{bmatrix} F_1 \\ 0 \end{bmatrix}. \tag{B–83}$$

Dynamic Response for Undamped and Damped Primary Structures

Referring to Fig. B–5a, the undamped natural frequency of the wind turbine structure ω_1 and the oil damper ω_2 can be defined by Eq. (B–4),

$$\omega_1 = \sqrt{\frac{k_1}{m_1}}, \tag{B–84a}$$

$$\omega_2 = \sqrt{\frac{k_2}{m_2}}, \tag{B–84b}$$

with the associated damping ratios given by Eq. (B–9)

$$\zeta_1 = \frac{c_1}{2\omega_1 m_1}, \tag{B–85a}$$

$$\zeta_2 = \frac{c_2}{2\omega_2 m_2}. \tag{B–85b}$$

In the following, $c_1 = 0$ is considered, *i.e.* an undamped primary structure. Due to the fact that a solution for the forced vibrations from Eq. (B–83) with $c_1 = 0$ is sought, x_1 and x_2 are harmonic

motions of the frequency ω. All the parts in Eq. (B–83)—acceleration, velocity, displacement and force—can then be represented by vectors. Thus, the vectors can be written as complex numbers. The displacements x_1 and x_2 are written on the form

$$x = a\mathrm{e}^{\mathrm{i}\omega t} = a\cos\omega t + \mathrm{i}a\sin\omega t. \tag{B–86}$$

Hence,

$$\dot{x} = \frac{\mathrm{d}}{\mathrm{d}t}a\mathrm{e}^{\mathrm{i}\omega t} = \mathrm{i}\omega a\mathrm{e}^{\mathrm{i}\omega t} = \mathrm{i}\omega x, \tag{B–87}$$

and

$$\ddot{x} = \frac{\mathrm{d}^2}{\mathrm{d}t^2}a\mathrm{e}^{\mathrm{i}\omega t} = \mathrm{i}^2\omega^2 a\mathrm{e}^{\mathrm{i}\omega t} = -\omega^2 x. \tag{B–88}$$

Based on Eqs. (B–87) and (B–88), Eq. (B–83) can be written as

$$\left\{ \begin{array}{l} \left(-m_1\omega^2 + k_1 + k_2 + \mathrm{i}\omega c_2\right) x_1 - \left(k_2 + \mathrm{i}\omega c_2\right) x_2 = F_1 \\ \left(-m_2\omega^2 + k_2 + \mathrm{i}\omega c_2\right) x_2 - \left(k_2 + \mathrm{i}\omega c_2\right) x_1 = 0 \end{array} \right\}. \tag{B–89}$$

Two equations with two unknowns are present in Eq. (B–89). Due to the fact that the motion of the primary structure x_1 is of most interest, x_2 can be expressed in terms of x_1. Hence,

$$\frac{x_1}{F_1} = \frac{\left(k_2 - m_2\omega^2\right) + \mathrm{i}\omega c_2}{\left(-m_1\omega^2 + k_1\right)\left(-m_2\omega^2 + k_2\right) - m_2\omega^2 k_2 + \mathrm{i}\omega c_2\left(-m_1\omega^2 + k_1 - m_2\omega^2\right)}. \tag{B–90}$$

Eq. (B–90) can be reduced on the form

$$\frac{x_1}{F_1} = \frac{a + \mathrm{i}b}{c + \mathrm{i}d} = \frac{(a + \mathrm{i}b)(c - \mathrm{i}d)}{(c + \mathrm{i}d)(c - \mathrm{i}d)} = \frac{(ac + bd) + \mathrm{i}(bc - ad)}{(c^2 + d^2)}, \tag{B–91}$$

where a, b, c and d are real numbers. The absolute value of x_1/F_1 then reads

$$\frac{x_1}{F_1} = \sqrt{\left(\frac{ac + bd}{c^2 + d^2}\right)^2 + \left(\frac{bc - ad}{c^2 + d^2}\right)^2} = \sqrt{\frac{a^2 + b^2}{c^2 + d^2}}. \tag{B–92}$$

Introducing the tuning frequency ν, the input frequency θ and mass ratio μ in the form

$$\nu = \frac{\omega_2}{\omega_1}, \tag{B–93}$$

$$\theta = \frac{\omega}{\omega_1}, \tag{B–94}$$

$$\mu = \frac{m_2}{m_1}, \tag{B–95}$$

the dynamic magnification factor $D = x_1 k_1/F_1$ can be written as

$$D = \frac{\sqrt{(\nu^2 - \theta^2)^2 + 4\theta^2\nu^2\zeta_2^2}}{\sqrt{\left[\mu\nu^2\theta^2 - (\theta^2 - 1)(\theta^2 - \nu^2)\right]^2 + 4\theta^2\left[\zeta_2\nu(\theta^2 + \mu\theta^2 - 1)\right]^2}}, \tag{B–96}$$

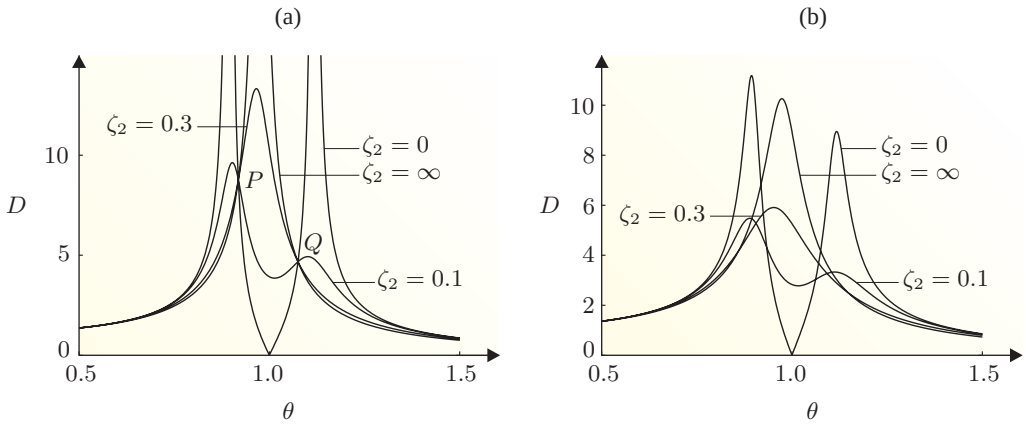

Figure B–6 Dynamic response of a 2DOF system for different values of the damping constant ζ_2, a mass ratio $\mu = 0.05$ and a tuning frequency $\nu = 1$: (a) undamped primary structure $\zeta_1 = 0$, (b) damped primary structure $\zeta_1 = 0.05$.

Fig. B–6a shows the dynamic magnification factor D as function of the input frequency θ for a mass ratio $\mu = 0.05$ and a tuning frequency $\nu = 1$. Different values of the damping ratio ζ_2 have been illustrated in Fig. B–6a. For $\zeta_2 = 0$, the amplitude of the primary structure follows a 2DOF system without viscous damping, and an SDOF system is obtained when $\zeta_2 = \infty$. It should be noted that for different values of ζ_2, the curves intersect at two points P and Q. Changing the tuning frequency ν will shift the amplitudes of the two fixed points up and down the curve with $\zeta_2 = 0$. The optimal value of the tuning frequency ν is obtained when the two points P and Q have equal amplitudes. For this optimum tuning frequency ν^{opt}, the optimum damping ratio ζ_2^{opt} can be estimated for the case where the curve has a horizontal tangent through one of two points P and Q. By doing so, the optimum tuning frequency ν^{opt} and damping ratio ζ_2^{opt} read according to Den Hartog (1984):

$$\nu^{\text{opt}} = \frac{1}{1+\mu}, \tag{B–97a}$$

$$\zeta_2^{\text{opt}} = \sqrt{\frac{3\mu}{8(1+\mu)}}. \tag{B–97b}$$

Following the same principles mentioned above for $c_1 \neq 0$, the dynamic magnification factor D reads

$$D = \frac{\sqrt{(\nu^2-\theta^2)^2 + 4\theta^2\nu^2\zeta_2^2}}{\sqrt{\left[\mu\nu^2\theta^2 - (\theta^2-1)(\theta^2-\nu^2) + 4\zeta_1\zeta_2\nu\theta^2\right]^2 + 4\theta^2\left[\zeta_2\nu(\theta^2+\mu\theta^2-1) + \zeta_1(\theta^2-\nu^2)\right]^2}}. \tag{B–98}$$

However, as indicated in Fig. B–6b, the curves of the dynamic magnification factor D for different values of the damping ratio ζ_2 do not pass through any fixed points. Hence, other methods must be considered in order to estimate optimum values of the tuning frequency ν^{opt} and damping ratio ζ_2^{opt}. According to Tsai and Lin (1994), the optimum parameters can be determined by a

numerical search for the minimum peak of the dynamic magnification factor D. In other words, for a fixed value of the tuning frequency ν, the maximum amplitudes for different values of ζ_2 are found. For this maximum amplitude, the corresponding minimum amplitude is determined. For various values of the tuning frequency ν, the procedure is repeated. Searching for the smallest minimum amplitude of the dynamic magnification factor D then provides the optimum tuning frequency ν^{opt} and damping ratio ζ_2^{opt} for a given mass ratio μ and damping ratio ζ_1.

Eigenvibration Analysis

The modal properties of the equivalent dynamic 2DOF system shown in Fig. B–5a will in the following be derived. The undamped circular eigenfrequency ω_1 for DOF 1 is used as reference frequency ω^{ref}. From Eq. (B–84a), it then follows that

$$\omega^{\text{ref}} = \omega_1 = \sqrt{\frac{k_1}{m_1}}. \tag{B–99}$$

Considering DOF 2 as a mathematical pendulum, the circular eigenfrequency ω_2 reads

$$\omega_2 = \sqrt{\frac{g}{L}}, \tag{B–100}$$

where g is the gravitational acceleration and L is the length of the pendulum. Hence, the stiffness of DOF 2 can be expressed in the following way:

$$k_2 = \frac{g m_2}{L}. \tag{B–101}$$

With a view to obtaining optimum damping of DOF 1 by means of DOF 2, Eq. (B–97a) is used. Thus, the optimum length of the pendulum can be expressed as

$$L^{\text{opt}} = g\frac{(1+\mu)^2 m_1}{k_1}. \tag{B–102}$$

In addition, Eq. (B–101) can be written as

$$k_2 = \frac{\mu}{(1+\mu)^2} k_1. \tag{B–103}$$

According to Eq. (B–85), the damping constants c_1 and c_2 can be expressed as

$$c_1 = 2\zeta_1 \omega_1 m_1, \tag{B–104a}$$

$$c_2 = 2\zeta_2 \omega_2 m_2 = 2\omega_1 m_1 \frac{\mu}{1+\mu}\zeta_2. \tag{B–104b}$$

Consequently, Eq. (B–83) for $F_1 = 0$ can be rewritten in the following way:

$$\mu m_1 \left(\mathbf{M}\ddot{\mathbf{x}} + \mathbf{C}\dot{\mathbf{x}} + \mathbf{K}\mathbf{x}\right) = \mathbf{0}, \tag{B–105a}$$

where

$$\mathbf{M} = \begin{bmatrix} \frac{1}{\mu} & 0 \\ 0 & 1 \end{bmatrix}, \tag{B–105b}$$

$$\mathbf{C} = \frac{2\omega^{\text{ref}}}{1+\mu}\begin{bmatrix} \frac{\zeta_1(1+\mu)}{\mu} + \zeta_2 & -\zeta_2 \\ -\zeta_2 & \zeta_2 \end{bmatrix}, \tag{B–105c}$$

$$\mathbf{K} = \frac{\left(\omega^{\text{ref}}\right)^2}{(1+\mu)^2}\begin{bmatrix} \frac{(1+\mu)^2}{\mu} + 1 & -1 \\ -1 & 1 \end{bmatrix}. \tag{B–105d}$$

According to Eq. (B–59), the jth undamped eigenfrequency ω_j can be expressed as

$$\omega_j = |\lambda_j| = \sqrt{\mu_j^2 + \nu_j^2}. \tag{B–106}$$

To obtain a non-trivial solution, the characteristic equation in Eq. (B–65) is used which entails a fourth order polynomial, *i.e.*

$$\Omega^4 + 2\left(\zeta_1+\zeta_2\right)\Omega^3 + \frac{1}{1+\mu}\left(4\zeta_1\zeta_2+\mu+2\right)\Omega^2 + \frac{2}{(1+\mu)^2}\zeta_2\left(\frac{\zeta_2}{\zeta_1}+1+\mu\right)\Omega + \frac{1}{(1+\mu)^2} = 0, \tag{B–107a}$$

where Ω_j is a dimensionless frequency given by

$$|\Omega_j| = \frac{|\lambda_j|}{\omega^{\text{ref}}} = \frac{\omega_j}{\omega^{\text{ref}}}. \tag{B–107b}$$

As an example, consider the following parameters:

$M_1 = 226383,$

$\mu = 0.03,$

$\omega^{\text{ref}} = 1.5520,$

$\zeta_1 = 9.5493\text{e-}004,$

$\zeta_2 = 0.4940.$

According to Eq. (B–105), the global mass, damping and stiffness matrices then become:

$$\mathbf{M} = \begin{bmatrix} 226383 & 0 \\ 0 & 6856 \end{bmatrix}, \tag{B–108a}$$

$$\mathbf{C} = \begin{bmatrix} 1.09\text{e+}004 & -1.02\text{e+}004 \\ -1.02\text{e+}004 & 1.02\text{e+}004 \end{bmatrix}, \tag{B–108b}$$

$$\mathbf{K} = \begin{bmatrix} 5.61\text{e+}005 & -1.56\text{e+}004 \\ -1.56\text{e+}004 & 1.56\text{e+}004 \end{bmatrix}. \tag{B–108c}$$

The roots in Eq. (B–107) can be determined to

$$\lambda_1 = -\mu_1 + \mathrm{i}\nu_1 = -0.03 + 1.53\mathrm{i}, \tag{B–109a}$$

$$\lambda_2 = -\mu_2 - \mathrm{i}\nu_2 = -0.03 - 1.53\mathrm{i}, \tag{B–109b}$$

$$\lambda_3 = -\mu_3 + \mathrm{i}\nu_3 = -0.74 + 1.34\mathrm{i}, \tag{B–109c}$$

$$\lambda_4 = -\mu_4 - \mathrm{i}\nu_4 = -0.74 - 1.34\mathrm{i}. \tag{B–109d}$$

As indicated, the roots in Eq. (B–107) are complex conjugated. Hence, only j=1 and j=3 need to be considered. According to Eq. (B–106), the absolute value of the eigenvalues gives the undamped circular eigenfrequency ω_j. Hence,

$$\omega_1 = \sqrt{\mu_1^2 + \nu_1^2} = 1.53, \tag{B–110a}$$

$$\omega_3 = \sqrt{\mu_3^2 + \nu_3^2} = 1.53. \tag{B–110b}$$

Using Eqs. (B–60a) and (B–17), the modal damping in terms of the logarithmic decrement δ_j is found,

$$\delta_1 = 2\pi \frac{\frac{\mu_1}{\omega_1}}{\sqrt{1 - \left(\frac{\mu_1}{\omega_1}\right)^2}} = 0.10, \tag{B–111a}$$

$$\delta_3 = 2\pi \frac{\frac{\mu_3}{\omega_3}}{\sqrt{1 - \left(\frac{\mu_3}{\omega_3}\right)^2}} = 3.49. \tag{B–111b}$$

The complex mode shapes $\boldsymbol{\Phi}^{(j)}$ are determined by Eq. (B–64). The modes shapes are normalised by setting the component $\Phi_2^{(j)} = 1$. Hence,

$$\Phi_1^{(1)} = \frac{-\left(M_{12}\lambda_1^2 + C_{12}\lambda_1 + K_{12}\right)}{\left(M_{11}\lambda_1^2 C_{11}\lambda_1 + K_{11}\right)} = -0.47 + 0.51\mathrm{i}, \tag{B–112a}$$

$$\Phi_1^{(3)} = \frac{-\left(M_{12}\lambda_3^2 + C_{12}\lambda_3 + K_{12}\right)}{\left(M_{11}\lambda_3^2 C_{11}\lambda_3 + K_{11}\right)} = -0.01 + 0.03\mathrm{i}. \tag{B–112b}$$

The complex modes shapes $\boldsymbol{\Phi}^{(1)}$ and $\boldsymbol{\Phi}^{(3)}$ then read

$$\boldsymbol{\Phi}^{(1)} = \begin{bmatrix} -0.47 + 0.51\mathrm{i} \\ 1 \end{bmatrix}, \tag{B–113a}$$

$$\boldsymbol{\Phi}^{(3)} = \begin{bmatrix} -0.01 + 0.03\mathrm{i} \\ 1 \end{bmatrix}. \tag{B–113b}$$

In order to determine the displacement of DOF 1 and DOF 2 for given initial conditions, the damped modal masses need to be determined. From Eq. (B–77) it follows that

$$m_1 = \boldsymbol{\Phi}^{(1)\top}\mathbf{C}\boldsymbol{\Phi}^{(1)} + 2\lambda_1\boldsymbol{\Phi}^{(1)\top}\mathbf{M}\boldsymbol{\Phi}^{(1)} = -3.29\text{e+}005 - 1.47\text{ie+}004, \tag{B–114a}$$

$$m_3 = \boldsymbol{\Phi}^{(3)\top}\mathbf{C}\boldsymbol{\Phi}^{(3)} + 2\lambda_3\boldsymbol{\Phi}^{(3)\top}\mathbf{M}\boldsymbol{\Phi}^{(3)} = 9.53\text{e+}002 + 1.77\text{ie+}004. \tag{B–114b}$$

Assuming the following initial conditions

$$\mathbf{x}_0 = \begin{bmatrix} 0 \\ 1 \end{bmatrix} \quad , \quad \dot{\mathbf{x}}_0 = \begin{bmatrix} 0 \\ 0 \end{bmatrix}, \tag{B–115}$$

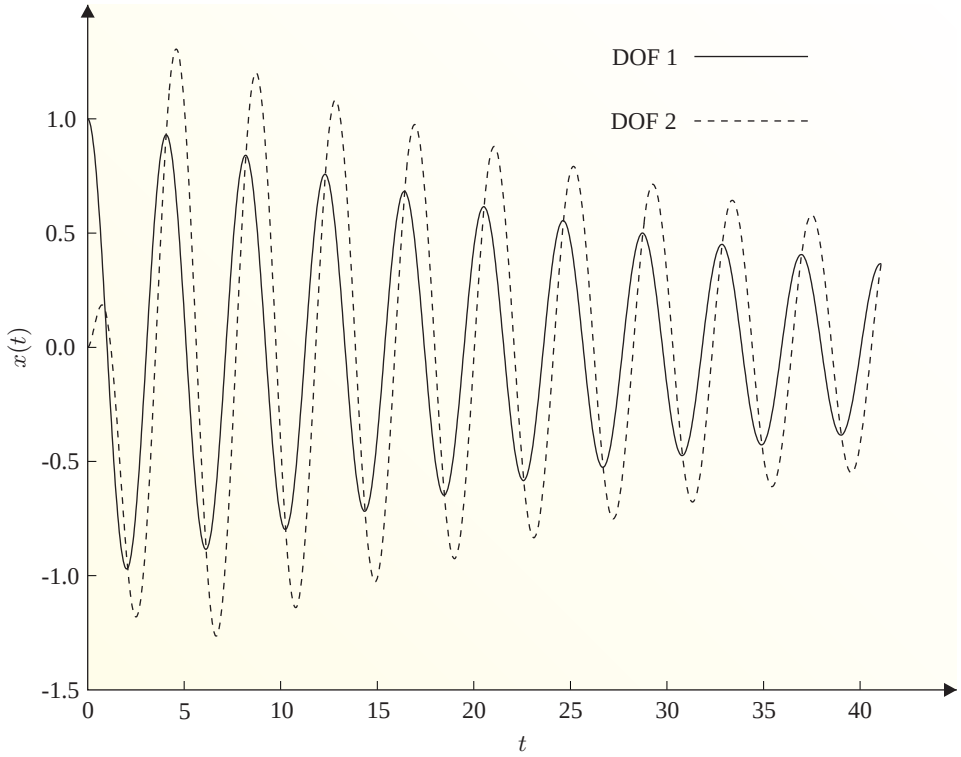

Figure B–7 Dynamic response in terms of expansion in damped eigenmodes vs. time for a dynamic 2DOF system.

the initial damped modal coordinates are given by Eq. (B–81), *i.e.*

$$q_1(0) = \frac{1}{m_1}\boldsymbol{\Phi}^{(1)\top}\left((\mathbf{C}+\lambda_1\mathbf{M})\mathbf{x}_0 + \mathbf{M}\dot{\mathbf{x}}_0\right) = 0.53 - 0.53\mathrm{i}, \tag{B–116a}$$

$$q_3(0) = \frac{1}{m_3}\boldsymbol{\Phi}^{(3)\top}\left((\mathbf{C}+\lambda_3\mathbf{M})\mathbf{x}_0 + \mathbf{M}\dot{\mathbf{x}}_0\right) = -0.53 - 0.89\mathrm{i}. \tag{B–116b}$$

Finally, the displacements of DOF 1 and DOF 2 are obtained using Eqs. (B–79) and (B–82) for $\mathbf{F}(\tau) = 0$. Fig. B–7 shows the expansion in damped eigenmodes for the considered 2DOF system with the initial conditions given by Eq. (B–115).

B.1.4 Stationary Random Process

Data analysis used for engineering practice often deals with determination of the dependency of two or more sets of data. The relationships are generally found by a correlation function or its Fourier transform, the so-called spectral density function.

Correlation Functions

Data representing a physical phenomenon do often consist of several single time histories $x_k(t)$. Each single time history is called a sample function or a sample record and will often be unique.

For that reason, the data are considered random. The collection of all possible sample functions that the random phenomenon might have produced is called a random process or a stochastic process $\{x(t)\}$. If the random process $\{x(t)\}$ consists of n sample records, the mean value of the random process can be computed at any specific time t_1,

$$\mu_x(t_1) = \lim_{n\to\infty} \frac{1}{n} \sum_{k=1}^{n} x_k(t_1). \tag{B–117}$$

In a similar manner, a correlation between the values of the random process at two different times t_1 and $t_1 + \tau$, denoted as the autocorrelation function $R_{xx}(t_1, t_1 + \tau)$, can be found,

$$R_{xx}(t_1, t_1 + \tau) = \lim_{n\to\infty} \frac{1}{n} \sum_{k=1}^{n} x_k(t_1) x_k(t_1 + \tau). \tag{B–118}$$

In case of $\mu_x(t_1)$ and $R_{xx}(t_1, t_1 + \tau)$ vary as time t_1 varies, the random process $\{x(t)\}$ is said to be nonstationary. For the special case, where $\mu_x(t_1)$ and $R_{xx}(t_1, t_1 + \tau)$ remain constant with changes in the time t_1, the data is said to be stationary, *i.e.* $\mu_x(t_1) = \mu_x$ and $R_{xx}(t_1, t_1 + \tau) = R_{xx}(\tau)$. For stationary data, the average value μ_x and the autocorrelation $R_{xx}(\tau)$ may equal the corresponding average and autocorrelation value computed over time from the single sample records. In this case, the random process $\{x(t)\}$ is said to be ergodic and results in the following expressions:

$$\mu_{x_k} = \lim_{T\to\infty} \frac{1}{T} \int_0^T x_k(t)\mathrm{d}t = \mu_x, \tag{B–119a}$$

$$R_{x_k x_k}(\tau) = \lim_{T\to\infty} \frac{1}{T} \int_0^T x_k(t) x_k(t + \tau)\mathrm{d}t = R_{xx}(\tau). \tag{B–119b}$$

The autocorrelation function $R_{x_k x_k}(\tau)$ for a stationary sample record is a measure of time-related properties in the data that are separated by fixed time delays. In other words, it contains information about how quickly random processes or random records change with respect to time. From its definition, the autocorrelation function is always an even function of τ which means $R_{x_k x_k}(-\tau) = R_{x_k x_k}(\tau)$. Fig. B–8 illustrates the autocorrelation for wide bandwidth random noise. It should be noted that the autocorrelation for $\tau = 0$ is the mean square value of the data ψ_x^2. Moreover, the autocorrelation collapses to a constant value equal to the square of the mean μ_x^2 as τ increases. In case of more than one random signal is being applied to a system, it is important to describe the relationship between the random processes. Consider two random processes $\{x(t)\}$ and $\{y(t)\}$ which are assumed to be stationary. Hence, they can be represented by individual time history records $x_k(t)$ and $y_k(t)$. By introducing a time delay τ between $x_k(t)$ and $y_k(t)$, the so-called cross-correlation function is given by

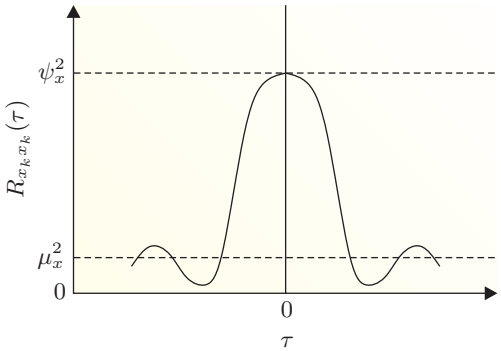

Figure B–8 The autocorrelation function for wide bandwidth random noise.

$$R_{x_k y_k}(\tau) = \lim_{T\to\infty} \frac{1}{T} \int_0^T x_k(t) y_k(t+\tau) \mathrm{d}t. \tag{B–120}$$

The discrete time formulation for estimating the cross-correlation function can be written as follows:

$$R_{x_k y_k}(t_1, t_1+\tau) = \lim_{n\to\infty} \frac{1}{n} \sum_{k=1}^{n} x_k(t_1) y_k(t_1+\tau). \tag{B–121}$$

B.1.5 Spectral Density Functions

As mentioned earlier, the spectral density function can be found by Fourier transform of a correlation function. More specific, the cross-spectral density function between two time history records $x_k(t)$ and $y_k(t)$ representing the stationary random processes $\{x(t)\}$ and $\{y(t)\}$ is determined by the Fourier transform of the cross-correlation function between those records,

$$S_{x_k y_k}(\mathrm{i}\omega) = \int_{-\infty}^{\infty} R_{x_k y_k}(\tau) \mathrm{e}^{-\mathrm{i}\omega\tau} \mathrm{d}\tau. \tag{B–122a}$$

For the special case where $y_k(t) = x_k(t)$, the autospectral density function, also denoted the power spectral density function, becomes

$$S_{x_k x_k}(\mathrm{i}\omega) = \int_{-\infty}^{\infty} R_{x_k x_k}(\tau) \mathrm{e}^{-\mathrm{i}\omega\tau} \mathrm{d}\tau. \tag{B–122b}$$

Eq. (B–122) defines the spectral density functions for all frequencies and are often denoted as two-sided spectra. From the symmetry properties of the stationary autocorrelation function, the following expressions yield for the autospectral density function:

$$S_{x_k x_k}(-\mathrm{i}\omega) = S^*_{x_k x_k}(\mathrm{i}\omega) = S_{x_k x_k}(\mathrm{i}\omega), \tag{B–123}$$

where the asterisk (*) on $S_{x_k x_k}$ indicates the complex conjugate. Another way of defining the spectral density functions is by use of Fourier transforms on the original data records. By considering a pair of sample records $x_k(t)$ and $y_k(t)$ from two stationary random processes $\{x(t)\}$ and $\{y(t)\}$, the spectral density functions can be defined for a finite time interval $0 \le t \le T$ as

$$S_{x_k x_k}(\mathrm{i}\omega, T) = \frac{1}{T} X^*_k(\mathrm{i}\omega, T) X_k(\mathrm{i}\omega, T), \tag{B–124a}$$

$$S_{x_k y_k}(\mathrm{i}\omega, T) = \frac{1}{T} X^*_k(\mathrm{i}\omega, T) Y_k(\mathrm{i}\omega, T), \tag{B–124b}$$

where $X_k(\mathrm{i}\omega, T)$ and $Y_k(\mathrm{i}\omega, T)$ represent finite Fourier transforms of $x_k(t)$ and $y_k(t)$, *i.e.*

$$X_k(\mathrm{i}\omega, T) = \int_0^T x_k(t) \mathrm{e}^{-\mathrm{i}\omega t} \mathrm{d}t, \tag{B–124c}$$

$$Y_k(\mathrm{i}\omega, T) = \int_0^T y_k(t) \mathrm{e}^{-\mathrm{i}\omega t} \mathrm{d}t. \tag{B–124d}$$

For T tending toward infinity, the estimates of $S_{xx}(\mathrm{i}\omega)$ and $S_{xy}(\mathrm{i}\omega)$ are given by

$$S_{xx}(\mathrm{i}\omega) = \lim_{T\to\infty} \mathrm{E}\left[S_{x_k x_k}(\mathrm{i}\omega, T)\right], \tag{B–125a}$$

$$S_{xy}(\mathrm{i}\omega) = \lim_{T\to\infty} \mathrm{E}\left[S_{x_k y_k}(\mathrm{i}\omega, T)\right]. \tag{B–125b}$$

In practice, it is more convenient to work with spectra defined over positive frequencies only. These are called one-sided spectral density functions and are defined as

$$G_{xx}(\mathrm{i}\omega) = 2S_{xx}(\mathrm{i}\omega), \tag{B–126a}$$

$$G_{xy}(\mathrm{i}\omega) = 2S_{xy}(\mathrm{i}\omega). \tag{B–126b}$$

By evaluating the products $\mathbf{x}(t)\mathbf{x}(t+\tau)$ and $\mathbf{f}(t)\mathbf{x}(t+\tau)$ in Eq. (B–38) and taking expected values of both sides, the autocorrelation function $\mathbf{R}_{ff}$ and cross-correlation function $\mathbf{R}_{xf}$ as function of the impulse response function $\mathbf{h}(\tau)$ can be found. Direct Fourier transformation of these correlation functions together with various algebraic steps give the important formulas for the two-sided spectral density functions $\mathbf{S}_{xx}$ and $\mathbf{S}_{xf}$ and the one-sided spectral density functions $\mathbf{G}_{xx}$ and $\mathbf{G}_{xf}$

$$\mathbf{S}_{xx} = |\mathbf{H}(\mathrm{i}\omega)|^2\, \mathbf{S}_{ff}(\mathrm{i}\omega) = \mathbf{H}^*(\mathrm{i}\omega)\mathbf{S}_{ff}(\mathrm{i}\omega)\mathbf{H}(\mathrm{i}\omega)^\top, \tag{B–127a}$$

$$\mathbf{S}_{xf} = \mathbf{H}(\mathrm{i}\omega)\mathbf{S}_{ff}(\mathrm{i}\omega), \tag{B–127b}$$

$$\mathbf{G}_{xx} = |\mathbf{H}(\mathrm{i}\omega)|^2\, \mathbf{G}_{ff}(\mathrm{i}\omega) = \mathbf{H}^*(\mathrm{i}\omega)\mathbf{G}_{ff}(\mathrm{i}\omega)\mathbf{H}(\mathrm{i}\omega)^\top, \tag{B–128a}$$

$$\mathbf{G}_{xf} = \mathbf{H}(\mathrm{i}\omega)\mathbf{G}_{ff}(\mathrm{i}\omega). \tag{B–128b}$$

B.2 Digital Data Analysis Processing

Before experimental modal analysis can be established, some specific data acquisition and processing procedures are required. In general, experimental modal analysis involves instrumentation by transducers. Transducers like accelerometers consist of a mechanical element that get stressed by accelerative forces which causes an electrical charge that is proportional to the accelerative forces. The output from the individual transducer consists of an analog signal which means that the signal is continuously variable. When dealing with data analysis, the most desirable way to store data is in a digital medium that is easily accessed by a computer. For that reason, the analog signals from the transducers must be converted into a digital format using an analog-to-digital converter. The signals will then be represented by discrete values. Fig. B–9 shows the process prior to the digital signal processing. According to Fig. B–9, the input signal is processed with an electronic anti-aliasing low-pass filter. The reason for this low-pass filter is described in the following section. The section is based on Smith (1997), Ewins (2000) and Liu and Frigaard (2001).

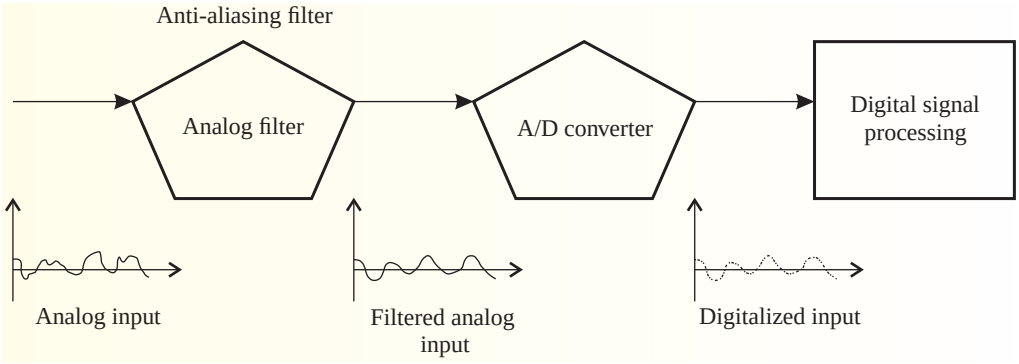

Figure B–9 Schematic diagram of an analog-to-digital conversion of analog signal.

B.2.1 Sample Frequency and Aliasing

Determination of an appropriate sampling frequency f_s is important for digital data analysis. Fig. B–10 shows two sinusoidal waves before and after digitalization. The continuous line represents the analog signal entering the analog-to-digital converter, while the dots represent the digital signal leaving the analog-to-digital converter. The sine wave in Fig. B–10a has a frequency of 0.09 of the sampling frequency f_s. Because no other sinusoid will produce the pattern of samples, the samples properly represent the analog signal. However, when the analog frequency is increased to 0.95 of the sampling frequency f_s, the samples represent a different sine wave from the one contained from the analog signal data. This is shown in Fig. B–10b. Sinusoidal signals changing frequencies during sampling is denoted as aliasing. In order to avoid this phenomenon, the Nyquist sampling theorem is used which specifies that a continuous signal can be properly sampled only if it does not contain frequency components above one-half of the sampling frequency f_s. This frequency is denoted the Nyquist frequency or the aliasing frequency and can be formulated using the sampling duration T_0 and the total number of samples n, *i.e.*

$$f_{\text{nyquist}} = f_{\frac{n-1}{2}} = \frac{\frac{n-1}{2}}{T_0} = \frac{\frac{n-1}{2}}{(n-1)\frac{1}{f_s}} = \frac{1}{2\frac{1}{f_s}} = \frac{f_s}{2}. \tag{B–129}$$

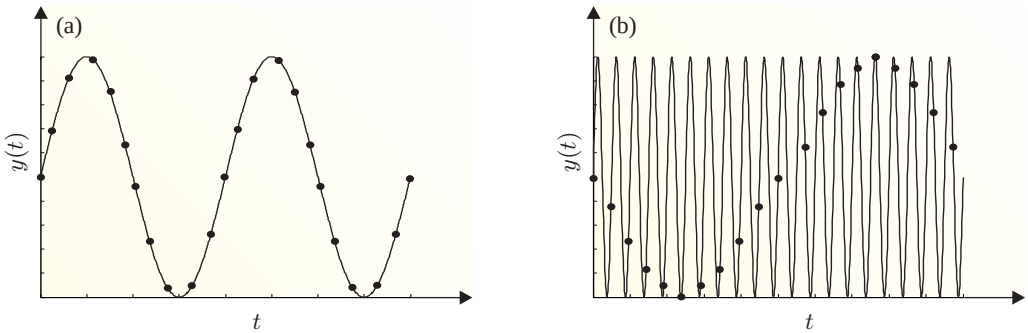

Figure B–10 Sinusoid before and after digitization: (a) proper sampling with a frequency of an analog sine wave smaller than the Nyquist frequency, (b) improper sampling with a frequency of an analog sine wave greater than the Nyquist frequency.

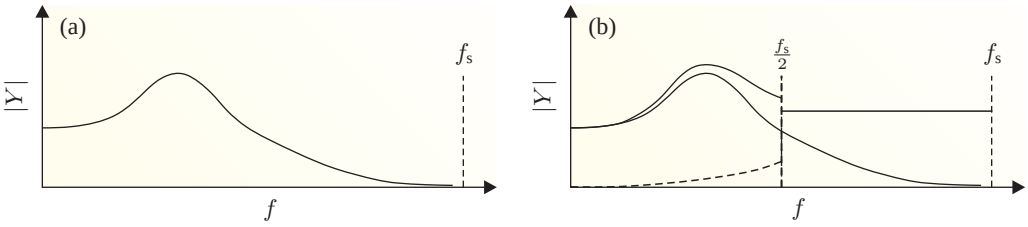

Figure B–11 Aliasing after Fourier transform: (a) true spectrum of signal, (b) indicated spectrum from FFT.

The Nyquist frequency f_{nyquist} is the highest frequency that can be defined by a sampling frequency f_s. Frequencies in the original data above f_{nyquist} will appear below f_{nyquist} and be confused with the data in this lower-frequency range. A low-pass filter is for that reason used to remove the frequency content of the original data above f_{nyquist} prior to the analog-to-digital conversion. Such a filter is referred to as an anti-aliasing filter. Because no low-pass filter has an infinitely sharp cut-off shape, the anti-aliasing filter cut-off frequency is set to approximately 80% of f_{nyquist} to assure that any data at frequencies above f_{nyquist} are strongly suppressed. The aliasing phenomenon is shown in Fig. B–11. A good rule of thumb for experimental modal analysis is that if the lowest frequency of interest is f_{min}, then the length of the time series should at least be 1000 cycles of the corresponding period. With this in mind and the above definition of an anti-aliasing filter, the following expressions can be stated:

$$t_{\text{total}} \geq \frac{x}{f_{\text{min}}}, \quad x \approx 1000, \tag{B–130a}$$

$$f_{\text{max}} \leq 0.8 f_{\text{nyquist}} \Rightarrow f_s \geq 2.5 f_{\text{max}}, \tag{B–130b}$$

where f_{max} is the highest frequency of interest.

B.2.2 Leakage Caused by Fourier Transform

Traditional experimental modal analysis is based on Fourier transform techniques. The Fourier transform of digital data is usually obtained by Fast Fourier Transformation (FFT) which can be used to provide estimates of spectral density and correlation functions. However, FFT assumes periodicity which means that the data record of finite length is assumed to repeat itself in both ends of the record. Due to the fact that digital signals in general exhibit nonperiodicity, errors will be introduced. These errors are denoted leakage and can be illustrated by Fig. B–12 in which two sinusoidal signals are represented. In Fig. B–12a, the signal is perfectly periodic in the time window T which induces a single line in the spectrum. In Fig. B–12b, the periodicity assumption is not valid. As a result, the spectrum is not represented by a single line. Instead, energy has leakage into a number of spectral lines close to the true frequency. For modal analysis, this means that the energy related to vibrations at the resonance frequencies leaks out which results in an apparent higher damping of the corresponding modes.

Windowing

A solution to minimise leakage is by windowing the data before the FFT is applied and thereby secure periodicity by multiplying the measured data by a suitable time window. However, the

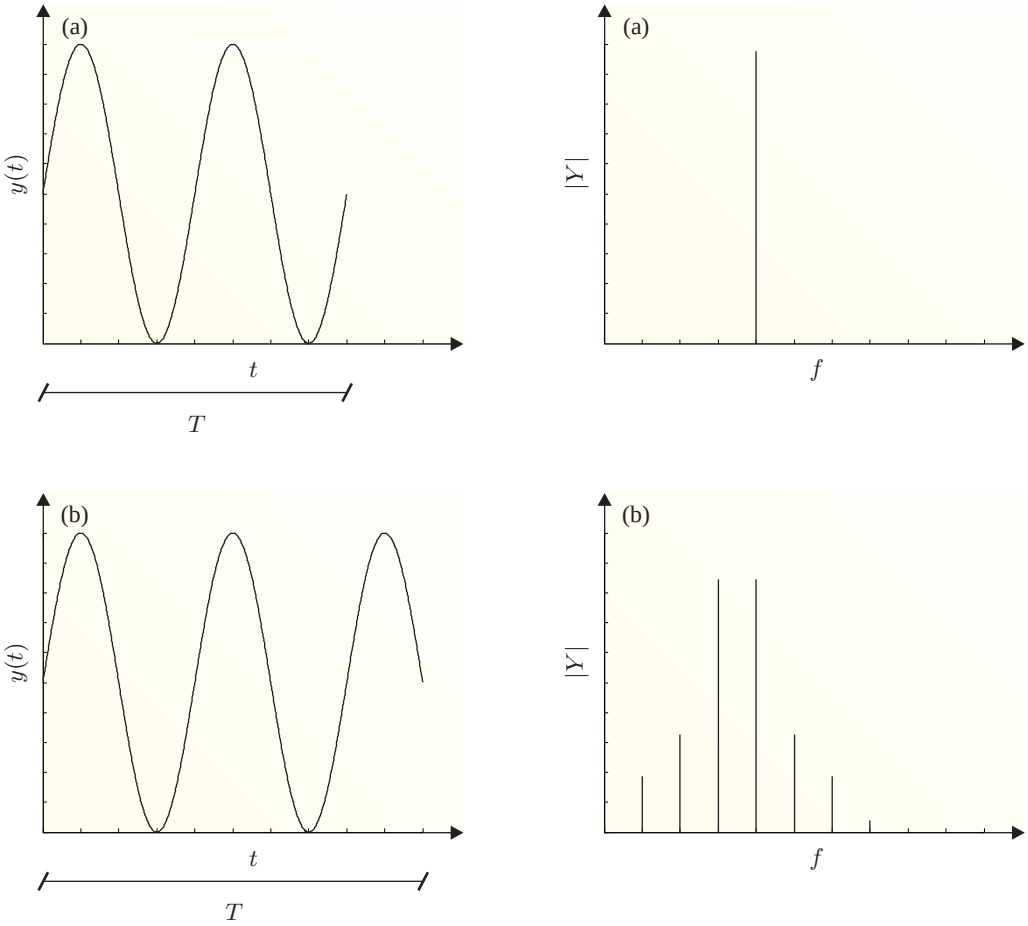

Figure B–12 Sample length and leakage of frequency spectrum: (a) ideal signal, (b) non-periodic signal.

bias cannot be completely removed and it will appear as a leakage bias in the frequency domain. Hence, the spectral peaks will be blunted and induce an unpredictable overestimation of the damping. Nevertheless, Fourier transformation is widely used within signal processing, and often the cosine-taper data window is applied to reduce the leakage given by

$$d(t) = \begin{cases} \frac{1}{2}\left(1 - \cos\frac{10\pi t}{T_0}\right) & \text{for} \quad 0 \leq t \leq \frac{T_0}{10} \\ 1.004 & \text{for} \quad \frac{T_0}{10} \leq t \leq \frac{9T_0}{10} \\ \frac{1}{2}\left(1 + \cos\frac{10\pi(t-\frac{9T_0}{10})}{T_0}\right) & \text{for} \quad \frac{9T_0}{10} \leq t \leq T_0 \end{cases} . \tag{B–131}$$

Fig. B–13 shows the cosine-taper window. In many cases, the frequency spectrum provided by an FFT analysis will be filled with noise because of insufficient information in the original data to obtain a well defined spectrum. To reduce the noise, averaging is applied. This is done by dividing the data into n multiple sub segments, multiply each of the segments with the time window and convert them into a frequency spectrum. The resulting spectrum is then found by

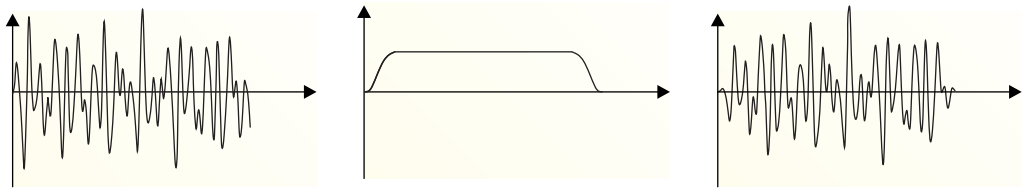

Figure B–13 Use of cosine-taper window in order to secure periodicity.

summing all the spectra from each sub segment and dividing by the number of sub segments n. Using 8 sub segments will for that reason results in a reduction of the standard deviation for each spectral from 100% to $\frac{1}{\sqrt{8}} = 35\%$. However, it should be noted that the frequency resolution will be more coarse when averaging.

B.3 Structural Assessment by Operational Modal Analysis

Since the very early days of awareness of structural vibrations, experimental modal analysis has been necessary for two major objectives:

1. Validation of numerical modal analysis through comparison of numerical results with those obtained from experimental modal analysis. This process is called modal updating.

2. After the event of a natural phenomenon such as a windstorm, experimental modal analysis is helpful to evaluate whether or not structural damage has occurred. In other words, estimates of dynamic properties of a structure during its service life can be determined by experimental modal testing.

In the traditional experimental modal technology, a set of frequency response functions at several points along the structure are estimated from the measured response divided by the measured excitation, see Eq. (B–39). A popular method of exciting structures artificially is through use of an impulse hammer. This device has the advantages of providing almost white noise, *i.e.* the spectral density function of the impulse loading is almost constant over all frequencies. It means that the output spectrum contains full information of the structure as all modes are excited equally. By moving the excitation and only measure the response in one single point, it is possible to determine the frequency response function matrix $\mathbf{H}(\omega)$. This procedure is called multi input single output (MISO). The ratio between the individual entries in the frequency response function $\mathbf{H}(\omega)$ for a frequency ω equal

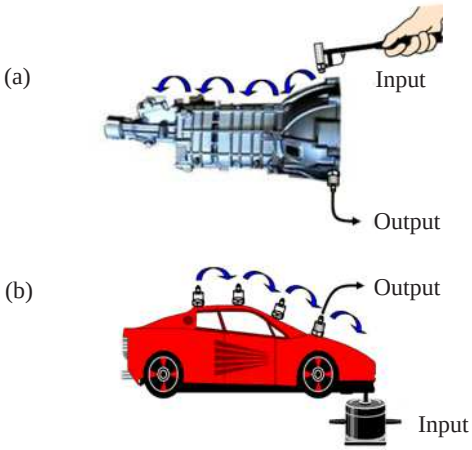

Figure B–14 Traditional modal technology: (a) hammer excitation, (b) shaker excitation.

to the resonance frequency ω_0 represents the corresponding mode shape Φ. An alternative to impulse hammers is electrodynamic shakers which are often used to excite large and complex structures like cable-stayed bridges. The shaker device is able to produce a large variety of input signals like random and multi-sine signals. Due to the possibility of applying sinusoidal forces, a direct identification of the resonance frequencies and mode shapes is easy. For this type of modal procedure, the frequency response function is found by moving accelerometers with one or more fixed accelerometers as reference and only excite the structure in one single point. This procedure is called single input multi output (SIMO). The two procedures of determining the dynamic properties of an arbitrary structure are shown in Fig. B–14. However, the main problem with forced vibration tests on large civil engineering structures is that the most significant modes of vibration in a low range of frequencies are difficult to excite. Moreover, forced excitation of such structures requires extremely heavy excitation equipment. As a consequence of the drawbacks related to traditional experimental modal analysis, operational modal identification is developed. This method allows to determine the inherent properties of a structure by measuring only the response of the structure without using an artificial excitation. In the following section, a more detailed description of operational modal analysis is given.

B.3.1 Operational Modal Identification

In many cases, large civil engineering structures are excited by natural loads that cannot easily be controlled, for instance wave loads, wind loads or traffic loads. Besides, the structures are excited by noise from environmental vibrations around the structure. Thus, a procedure to identify modal parameters based on the output response is needed. Instead of exciting the structure artificially and dealing with the natural excitation as an unwanted noise source, operational modal identification uses the natural excitation as the excitation source. This means that the dynamic properties of the structure are determined within true boundary conditions and actual force and vibration levels. Operational modal identification makes use of the multiple input multi output (MIMO) technology. Contrary to traditional experimental modal analysis, closely space modes and repeated modes are easily determined by this identification method with a high degree of accuracy. Fig. B–15 shows the principle of operational modal analysis. The unknown excitation forces are assumed to be produced by a virtual system loaded by stationary zero mean Gaussian white noise. This white noise is assumed to drive both the real structural system and the virtual loading system. It means that modes belonging to the real structural system and “modes” that belong to the virtual loading system are identified. The real structural modes are characterised as lightly damped modes, whereas the virtual loading “modes” are characterised as highly damped “modes”. In addition, identification of computational modes might be discovered because the signals are contaminated with noise. In general this means that it is of outmost importance that the structural modes are separated from the noise modes and excitation modes during the modal identification process.

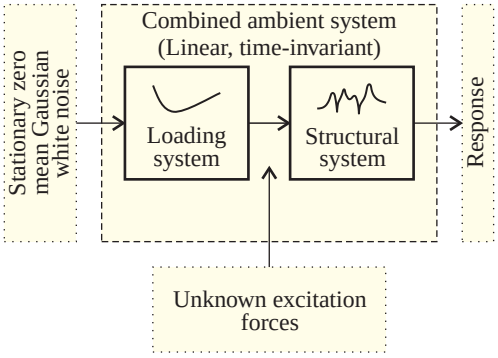

Figure B–15 Principle of operational modal analysis.

Different methods of identifying the structural modal parameters exist in operational mo-

dal analysis. Frequency Domain Decomposition (FDD) identification techniques and Stochastic Subspace Identification (SSI) are widely used. In the following, only the FDD identification technique is presented.

Frequency Domain Decomposition Technique

In order to determine the damped eigenfrequency f_d, the damping ratio ζ and the damped mode shape $\mathbf{\Phi}^{(j)}$ of a civil engineering structure, the FDD technique is useful. This section explains how the spectral density matrix for each output time series is decomposed into a set of single-degree-of-freedom (SDOF) systems and how the individual SDOF autospectral density functions are transferred back to time domain to identify the damped eigenfrequency f_d and the damping ratio ζ for each SDOF system. The section is based on Brincker *et al.* (2000), Zang *et al.* (2001) and Brincker *et al.* (2001).

Theoretical Overview of Frequency Domain Decomposition

According to Eq. (B–128a), the output spectral density matrix $\mathbf{G}_{yy}(\mathrm{i}\omega)$ is described by the input spectral density matrix $\mathbf{G}_{xx}(\mathrm{i}\omega)$ and the frequency response matrix $\mathbf{H}(\mathrm{i}\omega)$,

$$\mathbf{G}_{yy}(\mathrm{i}\omega) = \mathbf{H}^*(\mathrm{i}\omega)\mathbf{G}_{xx}(\mathrm{i}\omega)\mathbf{H}(\mathrm{i}\omega)^\top, \tag{B–132}$$

where the asterisk (*) on $\mathbf{H}$ indicates the complex conjugated, and the superscript T denotes transpose. The frequency response matrix $\mathbf{H}(\mathrm{i}\omega)$ defined by Eq. (B–39) can be written in a typical partial fraction form in terms of poles λ_k and residues $\mathbf{R}_k$,

$$\mathbf{H}(\mathrm{i}\omega) = \sum_{k=1}^{n} \frac{\mathbf{R}_k}{\mathrm{i}\omega - \lambda_k} + \frac{\mathbf{R}_k^*}{\mathrm{i}\omega - \lambda_k^*}, \tag{B–133}$$

where n is the number of modes of interest. The modal participation factor γ_k, which specify how much a given mode $\mathbf{\Phi}^{(k)}$ participates in a given direction, reads

$$\gamma_k = \frac{\mathbf{\Phi}^{(k)\top}\mathbf{M}\mathbf{U}}{\mathbf{\Phi}^{(k)\top}\mathbf{M}\mathbf{\Phi}^{(k)}}, \tag{B–134}$$

where $\mathbf{M}$ and $\mathbf{U}$ are the mass matrix and influence vector, respectively. The residue $\mathbf{R}_k$ is then given by

$$\mathbf{R}_k = \mathbf{\Phi}^{(k)}\boldsymbol{\gamma}^\top, \tag{B–135}$$

where $\boldsymbol{\gamma}$ is the modal participation vector. By assuming that the input $x(t)$ is white noise, *i.e.* the input spectral density matrix $\mathbf{G}_{xx}(\mathrm{i}\omega)$ is constant, Eq. (B–132) then becomes:

$$\mathbf{G}_{yy}(\mathrm{i}\omega) = \sum_{k=1}^{n}\sum_{s=1}^{n} \left[\frac{\mathbf{R}_k}{\mathrm{i}\omega - \lambda_k} + \frac{\mathbf{R}_k^*}{\mathrm{i}\omega - \lambda_k^*}\right] \mathbf{C} \left[\frac{\mathbf{R}_s}{\mathrm{i}\omega - \lambda_s} + \frac{\mathbf{R}_s^*}{\mathrm{i}\omega - \lambda_s^*}\right]^\mathrm{H}, \tag{B–136}$$

where $\mathbf{C}$ is the constant input spectral density matrix and the superscript H denotes the Hermitian transpose, *i.e.* the conjugate of the transpose of the matrix. Using the Heaviside partial fraction theorem and furthermore assuming a lightly damped structure and that only a limited number of

modes at a certain frequency ω contributes, the output spectral density function $\mathbf{G}_{yy}(\mathrm{i}\omega)$ can be written in the following final form:

$$\mathbf{G}_{yy}(\mathrm{i}\omega) = \sum_{k \in \mathrm{Sub}(\omega)}^{n} \frac{d_k \boldsymbol{\Phi}_k \boldsymbol{\Phi}_k^{\top}}{\mathrm{i}\omega - \lambda_k} + \frac{d_k^* \boldsymbol{\Phi}_k^* \boldsymbol{\Phi}_k^{*\top}}{\mathrm{i}\omega - \lambda_k^*}, \tag{B–137}$$

where d_k is a scalar constant and $k \in \mathrm{Sub}(\omega)$ is the set of modes that contribute at the particular frequency.

Identification Procedure

The FDD method is an extension of the well-known frequency domain approach, also referred to as the peak picking approach which is based on mode estimation directly from the autospectral density matrix at the peak. Four main steps are needed in order to find the damped eigenfrequency f_d and the damping ratio ζ by use of the FDD technique:

1 A Discrete Fourier Transform (DFT) is performed on the raw output time data $y(t)$ in order to obtain the spectral density matrix $\mathbf{G}_{yy}(\mathrm{i}\omega)$ known at discrete frequencies.

2 Estimation of each output spectral density matrix is decomposed by taking the Singular Value Decomposition (SVD) of the matrix, *i.e.* a unitary matrix holding singular vectors and a diagonal matrix holding scalar singular values are defined.

3 Near a peak corresponding to the kth mode in the spectrum, the first singular vector is an estimate of the mode shape and the corresponding singular value is the autospectral density function corresponding to an SDOF system. This function is identified using the Modal Assurance Criterion (MAC).

4 Using Inverse Fourier Transform (IFFT) on the autospectral density function, the damped eigenfrequency f_d and the damping ratio ζ are estimated from the correlation function.

Basically, the dynamic deflection $\mathbf{y}(t)$ of a damped MDOF system is a linear combination of the mode shapes $\boldsymbol{\Phi}^{(j)}$ and the modal coordinates $\mathbf{q}(t)$ according to Eq. (B–50),

$$\mathbf{y}(t) = \boldsymbol{\Phi}\mathbf{q}(t) = \sum_{j=1}^{n} \boldsymbol{\Phi}^{(j)} q_j(t). \tag{B–138}$$

Eq. (B–138) is illustrated graphically in Fig. B–16.

According to Eq. (B–118), the correlation function of the system response $\mathbf{y}(t)$ then reads

$$\mathbf{R}_{yy}(\tau) = \mathrm{E}\left[\mathbf{y}(t+\tau)\mathbf{y}(t)^{\top}\right] = \mathrm{E}\left[\boldsymbol{\Phi}\mathbf{q}(t+\tau)\mathbf{q}(t)^{\mathrm{H}}\boldsymbol{\Phi}^{\mathrm{H}}\right] = \boldsymbol{\Phi}\mathbf{R}_{qq}(\tau)\boldsymbol{\Phi}^{\mathrm{H}}. \tag{B–139}$$

Using Fourier transformation, the spectral density functions can be obtained,

$$\mathbf{G}_{yy}(\mathrm{i}\omega) = \boldsymbol{\Phi}\mathbf{G}_{qq}(\mathrm{i}\omega)\boldsymbol{\Phi}^{\mathrm{H}}. \tag{B–140}$$

As mentioned earlier, the first step in the FDD technique is to determine the output spectral density matrix for each frequency using the DFT. In general, the size of each spectral density matrix is $n \times n$, where n is the number of transducers. Each element of the matrices is a spectral

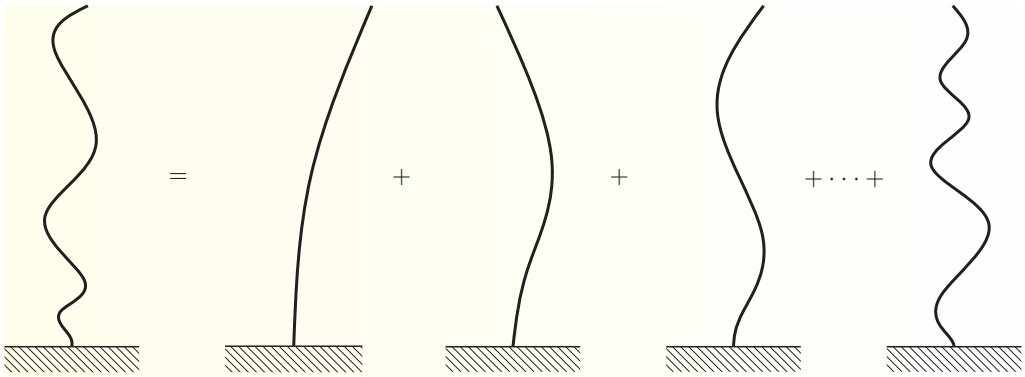

Figure B–16 System response $\mathbf{y}(t)$ as a linear combination of the mode shapes $\mathbf{\Phi}^{(j)}$ and the modal coordinates $q_j(t)$.

density function. The diagonal elements of the matrices are the real-valued spectral densities between a response and itself, *i.e.* the autospectral density. The off-diagonal elements are the complex cross-spectral densities between two different responses. It is important to notice that the spectral density matrix is Hermitian which means that it is equal to the Hermitian of itself, *i.e.* symmetric in the real part and antisymmetric in the imaginary part, see Section B.1.5. To avoid too much redundant information when estimating the spectral densities, a proper choice of projection channels are used. Often many row and columns in the spectral density matrix are linear combinations of the others. In case of a single test set-up, the projection channels are found by determining the correlation coefficient of the measured data. The idea is to find the channel that correlates most with other channels. This channel most likely contains maximum physical information, *i.e.*

$$w_i = \sum_{j=1}^{n} = |C_{ij}|\,, \quad i = 1, 2, \ldots, n, \quad \text{Find max}\left([w_1, w_2, \ldots, w_n]\right), \tag{B–141}$$

where n is the number of channels and $j \neq i$. The remaining number of requested projection channels are found by similar search of the correlation coefficient matrix as channels that correlate the least with all previous found projection channels. These channels bring most new information.

According to the theory of the FDD technique, the Hermitian spectral density matrix known at discrete frequencies $\omega = \omega_j$ is decomposed by taking the SVD of the matrix, *i.e.*

$$\mathbf{G}_{yy}(\mathrm{i}\omega_i) = \mathbf{U}_i \mathbf{S}_i \mathbf{U}_i^{\mathrm{H}}, \tag{B–142}$$

where the matrix $\mathbf{U}_i = [\mathbf{u}_{i1}\mathbf{u}_{i2} \cdots \mathbf{u}_{in}]$ is a unitary matrix containing n singular vectors $\mathbf{u}_{ij}$ that are orthogonal to each other and $\mathbf{S}_i$ is a singular value diagonal matrix holding the singular values s_{ij}. The singular values s_{ij} and the singular vectors $\mathbf{u}_{ij}$ are ordered in singular value descending order, *i.e.* the first singular value is the largest. Comparing Eq. (B–140) with Eq. (B–142), it can be understood that the singular vectors $\mathbf{u}_{ij}$ serve as estimations of the mode shapes, and the corresponding singular values s_{ij} present the response of each of the modes (SDOF

system) expressed by the spectrum of each modal coordinate. It is then assumed that $\mathbf{G}_{qq}(\mathrm{i}\omega)$ is a diagonal matrix and the modes shapes $\mathbf{\Phi}^{(j)}$ are orthogonal. If only the kth mode is dominating, Eq. (B–137) only consists of one term and for that reason the first singular vector $\mathbf{u}_{ij}$ is an estimate of the mode shape. The corresponding first singular value s_{ij} is the autospectral density function of the corresponding SDOF system. If more than one time record is performed, the singular value for each time record is averaged. It means that the picking is based on the average singular values. Fig. B–17 shows the singular values of the output spectral density matrix. In the FFD technique, only the resonance frequency is estimated of the picked modes which results in a damping ratio equal to zero. The Enhanced Frequency Domain Decomposition (EFDD) technique is an extension to the FDD technique. Compared to FDD, the EFDD technique gives an improved estimate of both the natural frequencies and the mode shapes and also includes damping. The basic of the method follows below.

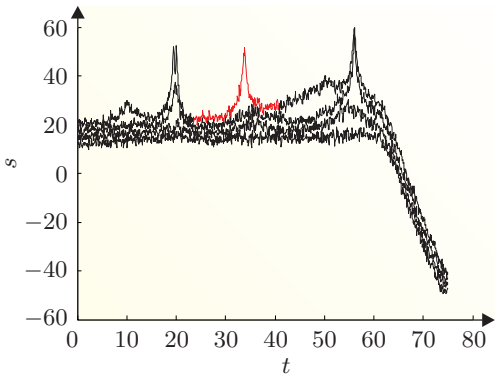

Figure B–17 Example of singular values of the spectral density matrix.

In order to identify the SDOF autospectral density function at a peak, the mode estimate $\hat{\mathbf{\Phi}}$ is compared with the singular vectors $\mathbf{u}_{ij}$ for the frequencies around the mode. In this way, an SDOF autospectral bell function can be found from which the damped eigenfrequency f_d and the damping ratio ζ can be estimated, see Fig. B–17. On both sides of the peak, a MAC value between the mode estimate $\hat{\mathbf{\Phi}}$ and the singular vector at a given frequency near the peak is calculated. As long as the MAC value is above a specified MAC rejection level, the corresponding singular value belongs to the SDOF autospectral bell. It is important to notice that the lower the MAC rejection level is, the larger the number of singular values included in the identification of the SDOF autospectral bell function will be. However, this also means that a larger deviation from the mode estimate $\hat{\mathbf{\Phi}}$ is allowed. For that reason, an often used MAC rejection level is 0.8. The MAC (Modal Assurance Criterion) reads

$$\mathrm{MAC}\left(\hat{\mathbf{\Phi}}, \mathbf{\Phi}_i\right) = \frac{\left(\hat{\mathbf{\Phi}}^\mathrm{H}\mathbf{\Phi}_i\right)^2}{\left(\hat{\mathbf{\Phi}}^\mathrm{H}\hat{\mathbf{\Phi}}\right)\left(\mathbf{\Phi}_i^\mathrm{H}\mathbf{\Phi}_i\right)} \geq 0.8. \tag{B–143}$$

To improve the estimated mode shape $\hat{\mathbf{\Phi}}$, the singular vectors that correspond to the singular values in the SDOF spectral bell function are averaged together. The average is weighted by multiplying the singular vectors with their corresponding singular value, *i.e.* singular vectors close to the peak of the SDOF spectral bell have a large influence on the mode shape estimate. The improved mode shape estimation from a weighted sum $\mathbf{\Phi}_\mathrm{weight}$ reads

$$\mathbf{\Phi}_\mathrm{weight} = \sum_{i=1}^{n} \mathbf{\Phi}_i s_i, \tag{B–144}$$

where n denotes the number of singular values in the SDOF spectral bell function. From the SDOF autospectral bell function, the damped eigenfrequency f_d and the damping ratio ζ are

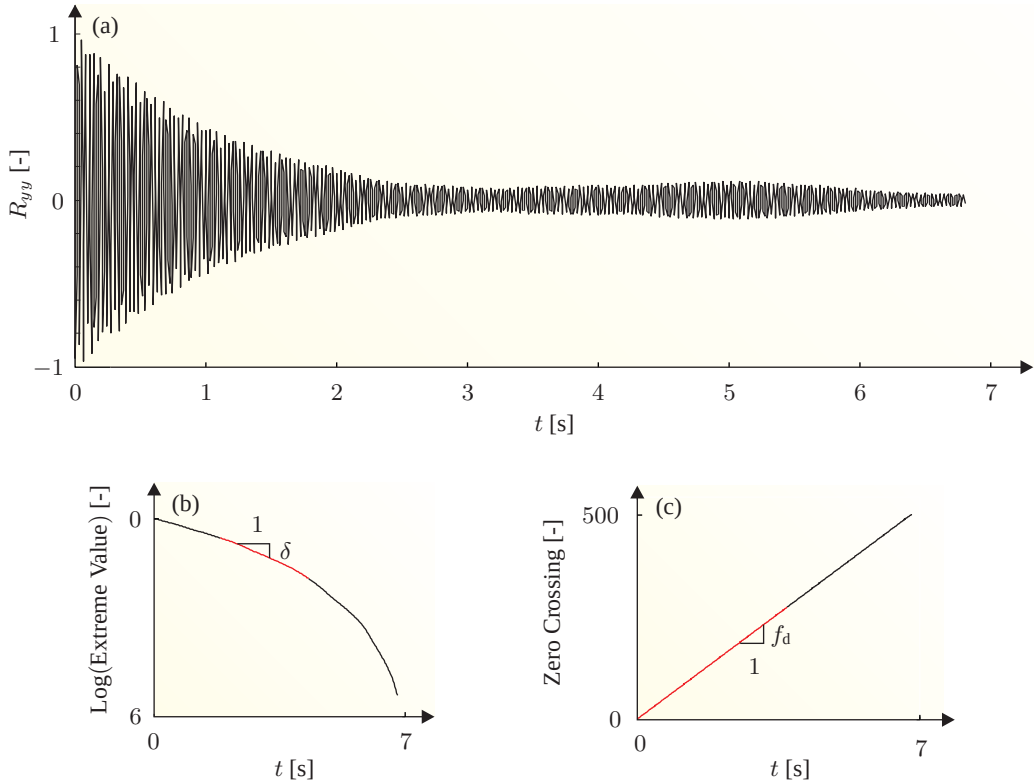

Figure B–18 Estimation of dynamic properties: (a) normalized correlation function obtained by inverse fast Fourier transformation, (b) linear regression on correlation extremes for estimation of damping, (c) linear regression on correlation crossing times for estimating the frequency.

obtained by transforming the spectral density function to time domain by IFFT. An SDOF autocorrelation function is then found, and by identification of the positive and negative extremes of this function, the logarithmic decrement δ is estimated according to Eq. (B–18). The damping ratio ζ is then found by Eq. (B–17). Due to broad-banded noise and nonlinearities, the beginning and the end of the curve may not be straight and for that reason these parts should not be included in the regression. The damped eigenfrequency f_d is found in a similar manner. By a linear regression on the time crossings of the autocorrelation function, the damped eigenfrequency ω_d is estimated as one-half of the slope of the line. Fig. B–18a shows the normalized correlation function for the mode specified in Fig. B–17. In addition, the corresponding estimations of the damped eigenfrequency f_d and the logarithmic decrement δ are shown in Fig. B–18b and Fig. B–18c, respectively.

APPENDIX C
Cross-Wind Modal Properties of Offshore Wind Turbines Identified by Full Scale Testing

Paper 1

The paper presented in this appendix is published in *Journal of Wind Engineering and Industrial Aerodynamics*, Volume 116, August 2013, Pages 94–108, DOI: 10.1016/j.jweia.2013.03.003.

ELSEVIER

APPENDIX D
Damping Estimation of a Prototype Bucket Foundation for Offshore Wind Turbines Identified by Full Scale Testing

Paper 2

The paper presented in this appendix is published in *5th International Operational Modal Analysis Conference*, May 2013, Guimarães, Portugal, Pages 1–11.

APPENDIX E
Assessment of Dynamic Substructuring of a Wind Turbine Foundation Applicable for Aeroelastic Simulations

Paper 3

The paper presented in this appendix is published in *Wind Energy*, May 2014, Early view, DOI: 10.1002/we.1763.

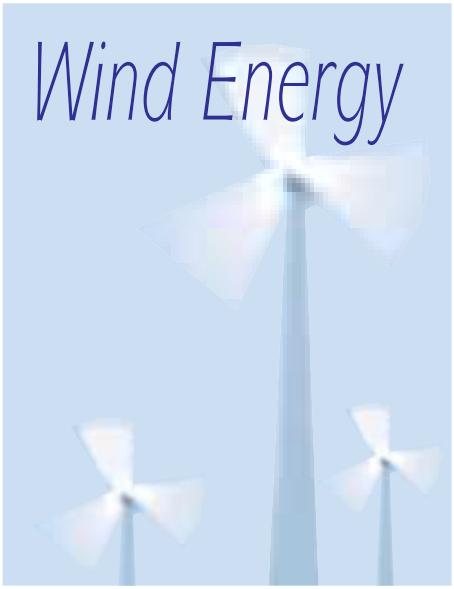

APPENDIX F
Computationally Efficient Modelling of Dynamic Soil–Structure Interaction of Offshore Wind Turbines on Gravity Footings

Paper 4

The paper presented in this appendix is published in *Renewable Energy*, Volume 68, August 2014, Pages 289–303, DOI: 10.1016/j. renene.2014.02.008.

ELSEVIER

APPENDIX G
Effects of Soil–Structure Interaction on Real Time Dynamic Response of Offshore Wind Turbines on Monopiles

Paper 5

The paper presented in this appendix is published in *Engineering Structures*, Volume 75, September 2014, Pages 388–401, DOI: 10. 1016/j.engstruct.2014.06.006.

ELSEVIER

APPENDIX H

Dynamic Response Sensitivity of an Offshore Wind Turbine: A Fully Coupled Time-Domain Approach for Varying Subsoil Conditions

Paper 6

The paper presented in this appendix is submitted to *Ocean Engineering*, January 2014, In review.

ELSEVIER

APPENDIX I

A Probabilistic Analysis of the Dynamic Response of Monopile Foundations: Soil Variability and its Consequences

Paper 7

The paper presented in this appendix is submitted to *Probabilistic Engineering Mechanics*, May 2014, In review.

ELSEVIER